Spring 5-5-2018

Functional Signature Ontology-Based Identification and Validation of Novel Therapeutic Targets and Natural Products for the Treatment of Cancer

Beth Neilsen
University of Nebraska Medical Center

Functional Signature Ontology-Based Identification and Validation of Novel Therapeutic Targets and Natural Products for the Treatment of Cancer

By

Beth K. Neilsen

A DISSERTATION

Presented to the Faculty of
the University of Nebraska Graduate College
in Partial Fulfillment of the Requirements
for the Degree of Doctor of Philosophy

Cancer Research Graduate Program

Under the Supervision of Professor Robert E. Lewis

University of Nebraska Medical Center
Omaha, Nebraska

May 2018

Supervisory Committee:

Jennifer Black, Ph.D.

Jing (Jenny) Wang, Ph.D.

Allison Cushman-Vokoun, M.D./Ph.D.

Juan Cui, Ph.D.

To my parents, Dr. and Mrs. Mitchell and Rebecca Neilsen,

For always encouraging me to think critically,

pushing me to be the best version of me,

for giving me the space to think for myself,

teaching me compassion, and most importantly,

for molding me into the person I am today.

To my sisters, Anne and Stephanie,

for always being my best friends and teammates.

Thank you for putting up with all my antics and

serving as my fellow competitors in life.

To my friends and family,

you have made the happy moments brighter and the sad moments lighter.

Without you, none of this would have been possible.

Acknowledgements

This work would not be possible without the support, guidance, and assistance of many people. I owe my deepest gratitude to my mentor, Rob Lewis. Thank you for giving me the opportunity to grow as a researcher and as a person under your guidance. You allowed me to utilize my past experiences, while allowing me room to make mistakes and pushing me to develop in new areas. You challenged me to think in new ways about new problems. I cannot thank you enough for your constant support and guidance even when I was too stubborn or not insightful enough to ask for it.

I would like to thank current and former members of the Lewis Lab for both challenging and supporting me. Thank you Drew Gehring and Rob Livergood for teaching me and welcoming me when I first joined the lab. I am grateful for the friendship and dedication to the lab Lili Guo and Deandra Smith showed. I cannot say how much I appreciate your support and discussions on our projects, science overall, and life in general. Binita, without your mentorship, I would not be the scientist I am today. I joined the lab knowing next to nothing about wet lab research, and your patience and never-ending willingness to answer my questions molded me into the researcher I am today. Thank you, Eyerusalem, for allowing me to mentor you. I hope I was able to teach you half as much as you taught me. You will never know how much you challenged me and pushed me to be better at science and research. Jamie, thank you for making me the researcher I am today. You taught me more about science, both in technical lab skills and thinking critically about biological questions, than I ever could have hoped for or imagined. You provided friendship and mentorship when I needed it most, and for that I will be forever grateful. Kurt, I cannot say how much I appreciated your presence in the lab during my last year of graduate school. You helped me to focus and find perspective in my research. Diane, you have been the heart of the Lewis lab. Your dedication and unwavering commitment to supporting all of us is unrivaled. No matter the request, you went above and beyond and made sure we had what we needed to do our

experiments. You will never know how much I appreciated having someone to talk to and commiserate with when experiments were not going well. To Danielle, I cannot tell you how much I value you as a friend and colleague. I am constantly amazed by your dedication and enthusiasm for research. I cannot wait to see the researcher you become, and I am so thankful I was blessed with you as a lab mate. Thank you for listening to all my ramblings, my unending, short list of experiments that were needed to finish a project, and my efforts to "get my life together" without judgement and with unwavering support. I appreciate your help finishing all of the experiments I planned on "big days." I could not have done it without you. I would like to thank my supervisory committee for your insightful comments and mentorship. Without your guidance and suggestions, both my research and my individual development could not have advanced as much as it did over these four years. You helped me to grow and learn more, about science and myself, than I thought was possible. You pushed me think about science differently and find new ways to solve problems and answer questions. You have changed the way I think about science, which has provided me with a new perspective and solid foundation that I will rely on for the rest of my career.

To all Lewis lab members, CRGP students and faculty, past and present, I could not have asked for a better group of individuals to work with each and every day. You make coming to lab a pleasure. Your probing questions, enlightening comments, collaborative nature, and our lively discussions have been the highlight of my time as a graduate student. Thank you.

Functional Signature Ontology-Based Identification and Validation of Novel Therapeutic Targets and Natural Products for the Treatment of Cancer

Beth K. Neilsen, Ph.D.

University of Nebraska Medical Center, 2018

Supervisor: Robert E. Lewis, Ph.D.

Multiple studies have revealed that Ras-driven tumors acquire vulnerabilities by adapting cellular mechanisms that promote uncontrolled proliferation and suppress apoptosis. Kinase Suppressor of Ras 1 (KSR1) modulates ERK activation downstream of oncogenic Ras, and knockdown of KSR1 selectively kills malignant, Ras-driven cancer cells, but does not kill immortalized, non-transformed human colon epithelial cells (HCECs). $KSR1^{-/-}$ mice are fertile and phenotypically normal, but resistant to Ras-driven tumor formation suggesting KSR1 represents a vulnerability in cancer cells.

To identify additional vulnerabilities in cancer, a screening approach termed Functional Signature Ontology (FUSION) was used to screen 14,355 genes and 1,200 natural product fractions in K-Ras-mutant HCT116 colon cancer cells for functional similarity to KSR1 and a selective requirement in colon cancer cells. FUSION identified numerous targets including TIMELESS, WDR5, and an AMPK inhibitor, 5'-hydroxy-staurosporine.

Downstream of oncogenic signaling, TIMELESS is constitutively overexpressed in multiple types of cancer and required for increased cancer cell proliferation. TIMELESS depletion increases γH2AX, a marker of DNA damage, and triggers downstream G2/M arrest via increased CHK1 and CDK1 phosphorylation. Wee1 or CHK1 inhibition in combination with TIMELESS depletion demonstrates at least additive effects suggesting this combination may be efficacious for the treatment of cancer.

WDR5 is overexpressed, and WDR5 depletion reduces cell viability in colon cancer cells by reducing H3K4Me3 and increasing γH2AX, which further sensitizes cells to radiation-induced

DNA damage. WDR5 inhibition also reduces colon cancer cell viability, but less so than WDR5 depletion.

The catalytic, kinase-containing α2 subunit isoform of AMPK is expressed at variable levels in colon cancer cells and is selectively required for colon cancer cell survival suggesting that AMPK kinase inhibition may be a useful component of cancer therapeutic strategies. FUSION identified 5´-hydroxy-staurosporine as a competitive inhibitor of AMPK that is selectively toxic to colon cancer cells.

Our results demonstrate the ability of FUSION to reveal functional similarities between genes, identify novel inhibitors, and expose oncogene-induced changes in cancer that promote proliferation and survival, but may also leave cancer cells vulnerable to targeted therapies.

Table of Contents

List of Figures

List of Tables

List of Abbreviations

5-FU	5-Fluorouracil
5-OH-S	5'-hydroxy-staurosporine
ACSL5	Acyl-CoA Synthetase Long-Chain Family Member 5
ALDOC	Aldolase C
AML	Acute Myeloid Leukemia
AMPK	AMP-activated protein kinase
ATAC	Ada Two-A Containing
ATCC	American
BNIP3	BCL2/Adenovirus E1B 19 kDa Interacting Protein 3
BNIP3L	BCL2/Adenovirus E1B 19 kDa Interacting Protein 3-Like
CA1-CA5	Conserved Area 1-5
CFSE	Carboxyfluorescein succinimidyl ester
COMPASS	SET/MLL COMplex of Proteins ASsociated with Set1
COSMIC	Catalogue of Somatic Mutations in Cancer
CSA	Common Seed Analysis
DAVID	Database for Annotation, Visualization, and Integrated Discovery
DDR	DNA-damage response
DMEM	Dulbecco's Modified Eagle's Medium
EBV	Epstein-Barr Virus
ED	Euclidean Distance
EMT	Epithelial Mesenchymal Transition
FBS	Fetal Bovine Serum
FUSION	Functional Signature Ontology
GESS	Genome-wide enrichment of Seed Sequences
GSEA	Gene Set Enrichment Analysis
γH2AX	Phosphorylated form of H2A.X (S139)
H3K4	Histone 3 Lysine 4
H3K4Me1-3	mono-, di-, or tri-methylation of Histone 3 Lysine 4
H3K27Me3	Tri-methylation of Histone 3 Lysine 27
HCECs	Human Colon Epithelial Cells
HPRT	Hypoxanthine-guanine phosphoribosyltransferase
HPV	Human papillomavirus
HSV	Herpes Simplex Virus
KSR	Kinase Suppressor of Ras
IQGAP1	IQ motif-containing GTPase activating protein 1
IR	Ionizing Radiation
LOXL2	Lysyl Oxidase-Like 2
MEF	Mouse Embryo Fibroblasts

MG132	Z-Leu-Leu-Leu-al
MMC	Mitomycin C
MOF	Males Absent On
MP1	MEK partner 1
MSigDB	Molecular Signatures Database
NDRG1	N-Myc Downstream Regulated 1
NLS	Nuclear Localization Signal
OXAL	Oxaliplatin
PC	Pearson Correlation
PI	Propidium Iodide
polyHEMA	Poly-2-hydroxyethyl methacrylate
PPIB	Cyclophilin B
RNAi	RNA interference
SAM	Sterile-α-motif
SD	Standard deviation
TCGA	The Cancer Genome Atlas
TCGA Datasets:	
BRCA	Breast Invasive Carcinoma
COAD	Colon Adenocarcinoma
LUAD	Lung Adenocarcinoma
LUSC	Lung Squamous Cell Carcinoma
GBM	Glioblastoma
PRAD	Prostate Adenocarcinoma
PAAD	Pancreatic Ductal Adenocarcinoma
SARC	Sarcoma
OV	Ovarian Serious Cystadenocarcinoma
CESC	Cervical Squamous Cell Carcinoma
TIMELESS/TIM	TIMELESS Circadian Clock
WDR5	WD-40 Repeat Containing Protein 5
WRAD	WDR5, RBBP5, ASH2L, and DPY30

Chapter 1: Introduction

Portions of the content covered in this chapter are the subject of a published review article in *Expert Opinion on Therapeutic Targets* by Neilsen BK *et al*.[2]

Cancer

In 2018, the American Cancer Society estimates that more than 1.7 million people will be diagnosed with cancer for the first time, and just over 600,000 people will die from cancer in the United States [4]. Cancer is the second leading cause of death among Americans with only heart disease causing more deaths [5]. Colon cancer is the third most common cancer in men and women with projections that more than 140,000 individuals will be diagnosed with this disease in 2018. Even though colon cancer has a high survival rate if caught in early stages, it remains the third most lethal type of cancer and is projected to kill more than 50,000 individuals in 2018 [4]. Patients with early stage or only locally advanced disease can be treated with multiple modalities including surgical resection and radiation therapy with the potential for curative outcomes. However, the only real treatment option for patients with any type of advanced or metastatic cancer are systemic therapies that include chemotherapy, hormone therapy, immune-based therapy, and/or targeted therapy. Most chemotherapeutics are often not curative, not selective (target all rapidly dividing cells), and not effective after resistance develops. Hormone therapies are highly efficacious in tumors that are reliant on hormone receptors for growth (e.g. breast and prostate cancers), but not all tumors rely on these receptors and those that do, often evolve so they are no longer susceptible to these therapies. Immune-based therapies (a.k.a immunotherapies) represent a new, promising category of therapeutics, but very few of these therapies have been developed and tested such that they are ready for clinical use. Studies have shown that immunotherapy is particularly effective in tumors with high mutational burdens (e.g. melanoma) or in tumors that have mechanisms promoting immune escape (e.g. increased PD-L1 expression in lung cancer), which has limited the approval of immunotherapies for use in specific tumor types with these characteristics. While often very effective and without significant side effects, very few targeted therapies exist and those that do are commonly specific for one type of cancer (e.g. imatinib targeting BCR-ABL in CML). Therefore, developing novel therapeutic strategies to target and kill cancer cells, preferably with little or no harm to normal tissues, is vital. Specific

targeting of cancer cells can be achieved by targeting the vulnerabilities that develop in tumors as a result of driving mutations altering normal cellular mechanisms to promote uncontrolled growth and suppress apoptosis. Specifically, oncogenic Ras mutations have been shown to induce changes in cancers that introduce targetable vulnerabilities in cancer cells that are not present or significantly diminished in normal cells.

Ras Mutations in Cancer and Therapeutic Targeting of Ras

Oncogenic Ras mutations are a common trait of more than one third of all tumors [6]. There are three isoforms of Ras: K-Ras, H-Ras, and N-Ras. K-Ras mutations, the most commonly mutated isoform of the Ras gene, are present in 25%-30% of all human cancers [6]. Mutations in H-Ras and N-Ras are present in 3% and 8% of all tumors, respectively [7,8]. Ras mutations are also present at much higher frequencies in certain types of cancers. Approximately one fifth of lung cancers, one third of colon cancers, and more than two thirds of pancreatic cancers have oncogenic Ras mutations [8].

Based on its prevalence, substantial efforts have been directed towards developing a targeted Ras inhibitor; however, despite these efforts, very few efficacious therapies have been developed that specifically target Ras. Based on our understanding of Ras, inhibition could be achieved by decreasing the amount of activated, GTP-bound Ras, disrupting the interaction between Ras and its downstream effectors, stabilizing non-active protein complexes, or preventing Ras membrane localization [9]. Despite substantial understanding of Ras regulation and function, inhibiting Ras has been problematic. This is due, at least in part, to difficulty interfering with the nucleotide-binding pocket of the protein, which is much more difficult than blocking the ATP-binding pocket of kinases. This is likely due to the incredibly high affinity of Ras for GTP, which is in the picomolar range [10]. Instead of inhibiting nucleotide binding, the possibility of inhibiting the guanine exchange factor SOS, which catalyzes the conversion of GDP-bound Ras (inactive) to GTP-bound Ras (active), has been explored. Compounds have been identified that

bind to Ras and interfere with SOS binding [11-13]; however, it is unclear if this interference will be clinically efficacious or if drugs with a high enough affinity to substantially displace SOS can be developed from the recently identified starting compounds. Recently, a drug specifically targeting the G12C mutant isoform of Ras (Ras^{G12C}), but not wildtype Ras has been identified. This compound specifically binds to Ras^{G12C} because it binds to a pocket that is only exposed on the Ras^{G12C} mutant and alters its nucleotide preference such that it favors GDP over GTP thereby suppressing mutant Ras signaling [12]. More recently, another group has identified an inhibitor that preferentially binds to Ras^{G12D} that demonstrated some efficacy in xenograft models re-opening the possibility of directly targeting Ras [14].

Alternatively, instead of targeting Ras GTP binding, groups have attempted to inhibit Ras by interfering with its localization to the cell membrane, which is required for Ras activation and is dependent upon post-translational lipid modifications. Initial attempts to block Ras farnesylation, demonstrated some efficacy, but, surprisingly, were only effective at inhibiting H-Ras localization and activation. Subsequent studies revealed that in addition to farnesylation, K-Ras and N-Ras can also undergo lipid modifications by geranylgeranyltransferases effectively circumventing their dependency on farnesyltransferases for cell membrane localization and activation [15,16].

Since targeting Ras directly has proven difficult and complicated, several inhibitors of proteins downstream of Ras have been developed. An attempt to interfere with the interaction between Ras and Raf was made, but the identified compound that reduced this interaction demonstrated low efficacy in preclinical models [17]. Some success has been achieved through the development of Raf and MEK inhibitors, yet efficacy is still highly variable in tumors. Additionally, resistance to Raf and MEK inhibitors often develops and is characterized by reestablishment of ERK signaling suggesting that more robust disruption of Ras signaling is still likely to be efficacious [18].

Kinase Suppressor of Ras

Kinase Suppressor of Ras (KSR) proteins were identified more than twenty years ago in *Drosophila melanogaster* (Drosophila) (KSR) and *C. elegans* (KSR1 and KSR2) and shown to modulate Ras-mediated signaling [19-21]. It was immediately recognized that KSR had a larger effect on signaling from mutant Ras than wildtype Ras. This result was counterintuitive as the more robust signal from constitutively active Ras was thought to be more difficult to repress than signals from wildtype Ras. This is intriguing as it opens the possibility of selectively targeting Ras-mutated tumors through KSR [22]. In Drosophila, heterozygous mutations in KSR reverted the phenotype of a mutant, constitutively active form of Ras (Ras^{G12V}), which demonstrates the ability of KSR to suppress mutant Ras signaling [21]. Several groups have shown that KSR acts downstream of Ras as a molecular scaffold for the Raf/MEK/ERK kinase cascade to promote downstream Ras signaling unless KSR is significantly overexpressed [23-37]. Therefore, the name Kinase Suppressor of Ras is a misnomer as endogenous levels of KSR promote Ras signaling, while only substantial overexpression of KSR serves to suppress Ras signaling. Therefore, KSR plays a role in regulating several cellular mechanisms to promote cell proliferation and survival including increasing the metabolic capacity, cell cycle re-initiation following DNA damage repair, and translational regulation of key mediators that promote the transformation such as MYC [3,33,38-42]. However, the mechanisms behind these effects have not been fully elucidated.

Phenotypic analysis of KSR genetic inactivation

KSR proteins have been studied by genetic inactivation in several model systems. In Drosophila, there is only one KSR protein and homozygous inactivating or truncating mutations are lethal [21]. In contrast, in a genetic screen to identify modifiers of Ras signaling, it was discovered that heterozygous loss of *ksr* suppresses Ras^{G12V} signaling and prevented the roughening of the eye that is seen with increased Ras signaling in Drosophila [21]. In comparison, two KSR proteins (KSR1 and KSR2) are present in *C. elegans*, as well as in mammals. KSR1 and

KSR2 have different expression profiles in mammals and both unique and overlapping functions [43]. KSR2 is largely expressed in the brain including the pituitary. While KSR1 is also highly expressed in the brain, it is also expressed at relatively low levels in most other tissues and has been shown to be overexpressed in tumors [3]. In all cases, KSR proteins contribute positively to ERK phosphorylation and activation downstream of Ras [19-21]; however, either due to their distinct functions or varied expression profiles, animals lacking KSR1 or KSR2 have different phenotypes.

Apart from a few minor defects, *ksr1*$^{-/-}$ knockout mice are fertile and otherwise phenotypically and developmentally normal (Fig. 1.1). *Ksr1*$^{-/-}$ mice have hair follicle defects similar to the phenotype of *egfr*$^{-/-}$ mice reinforcing the idea these proteins are within the same pathway [24,44,45]. As a result of reduced ERK signaling, *ksr1*$^{-/-}$ mice have a marginally impaired immunological response, particularly in regards to T-cell activation [24,34,46,47]. Most importantly, *ksr1*$^{-/-}$ mice are resistant to Ras-driven tumor formation [24]. This fact is demonstrated by the reduced mammary tumor burden in *ksr1*$^{-/-}$ mice with transgenic expression of polyomavirus Middle T-Antigen [24]. Induction of skin tumors with v-Ha-Ras was also completely lost in *ksr1*$^{-/-}$ mice [45]. These observations demonstrate that KSR1 modulates Ras signaling *in vivo*, but it is largely dispensable for normal cell survival. This selective requirement for KSR1 in Ras-driven tumor formation makes it an attractive target for therapeutic intervention.

In contrast to the mild phenotype of *ksr1*$^{-/-}$ mice, *ksr2*$^{-/-}$ mice have reduced fertility and become spontaneously obese [48-51] (Fig. 1.1). Although *ksr2*$^{-/-}$ mice have not been assessed for their resistance to tumor formation, there is *in vitro* evidence for a role of KSR2 in promoting tumor formation. In *ksr1*$^{-/-}$ mouse embryo fibroblasts (MEFs), ectopic expression of KSR2 restored ERK1/2 activation and mutant Ras-dependent anchorage-independent growth [52]. KSR2 is expressed in a mouse neuroendocrine cell line (Min-6) and mouse neuroblastoma/rat glioma hybrid cell line (NG108-15) and shRNA-mediated depletion of KSR2 in these cell lines reduced proliferation and anchorage-independent growth [52]. Consistent with observations from the *ksr2*

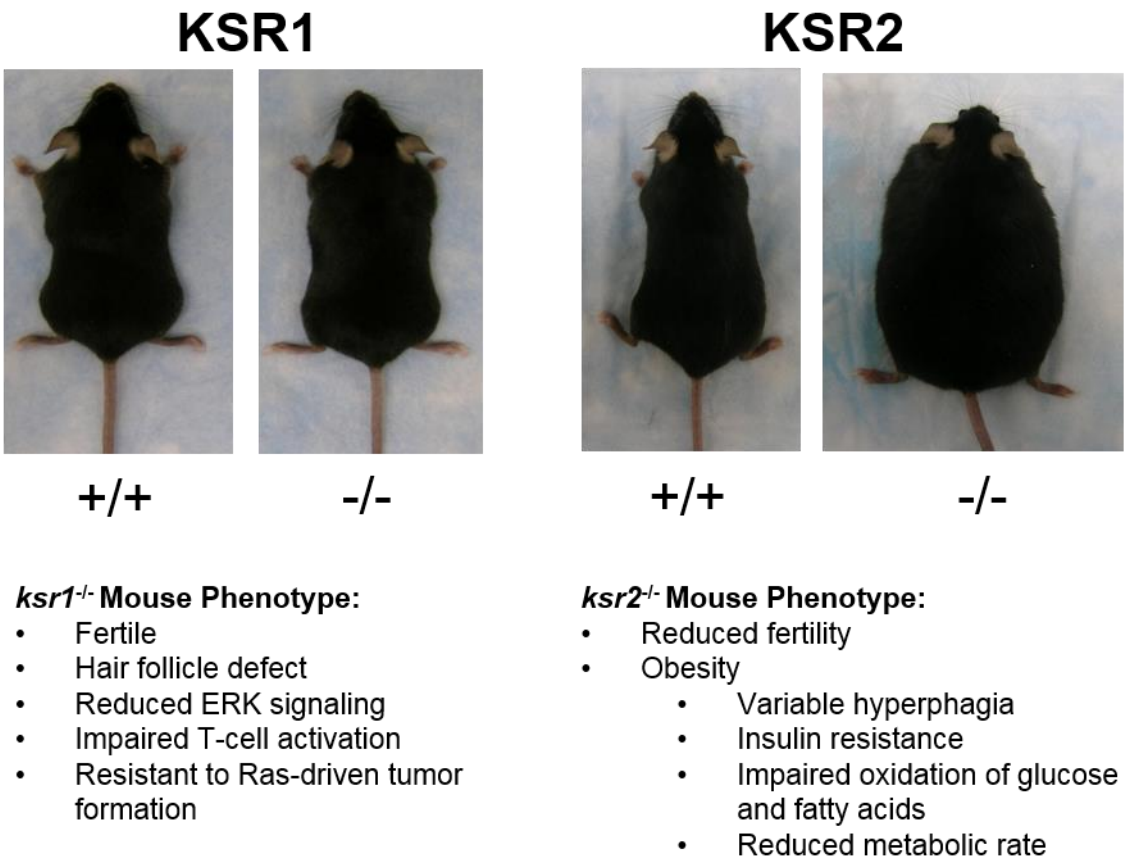

Fig. 1.1: KSR Knockout Mice. Ksr1$^{-/-}$ mice are largely developmentally and phenotypically normal, yet resistant to Ras-driven transformation. Ksr2$^{-/-}$ mice have an abnormal metabolic profile and become obese. (Images of KSR1 and KSR2 knockout mice were taken by Diane Costanzo-Garvey. This figure has been previously published in [2]).

knockout mice, RNAi-mediated depletion of KSR2 in insulinoma cell lines showed decreased ERK1/2 and AMPK activation leading to reduced metabolic activity. Therefore, while the role of KSR2 in human cancers has not been defined, substantial evidence suggests a potential, pro-tumorigenic role for KSR2 in cancer. However, thus far, KSR2 has not been shown to be significantly expressed and required in any type of tumor, suggesting that while KSR2 may possess oncogenic capabilities, its contribution in cancer may be limited due to its restricted tissue-specific expression [52,53]. Additionally, the profound differences in the phenotype of *ksr1*$^{-/-}$ and *ksr2*$^{-/-}$ mice demonstrate that while there is likely significant overlap in their functions, KSR1 and KSR2 must have unique and distinct physiological roles and therefore may contribute differently to tumorigenesis.

The role of KSR in cancer

KSR1 has been extensively implicated as playing a key role in Ras-driven cancers [3,24,29,32,38,41,42,45,52,54-56]. Consistent with its role as a molecular scaffold for the Raf/MEK/ERK cascade, KSR1 interacts with each kinase in this cascade [31,32,57], and increasing levels of KSR1 enhance Ras signaling to a maximum point [32]. As predicted of a scaffold, exceeding the optimal cellular KSR1 expression disrupts ERK signaling and inhibits Ras transformation likely by separating and sequestering the members of the kinase cascade from one another [32,56]. Comparing KSR1 expression in a panel of colon cancer cell lines to non-transformed human colon epithelial cells demonstrated that colon cancer cells have increased KSR1 expression, which suggests that enhanced ERK signaling may be accomplished, at least in part, through upregulation of KSR1 in colorectal cancer [3]. *Ksr1*$^{-/-}$ mouse embryo fibroblasts that exogenously express Ras^{G12V} are resistant to Ras-driven transformation, maintain contact inhibition, and fail to form colonies in soft agar [32]. In preclinical, mechanistic studies, stable depletion of KSR1 using multiple shRNA sequences reduces the ability of colon cancer cells expressing mutant K-Ras to grow in an in vitro soft agar assay as well as in an in vivo xenograft mouse model [3]. Finally, RNAi-mediated

depletion of KSR1 robustly induces cell death in the Ras-mutated colon cancer cell line HCT116 cells, but not in non-transformed human colon epithelial cells [3]. Taken together, these results support the conclusion that KSR1 is required for mutant Ras to promote the development and maintenance of cancer such that targeting KSR1 is likely to be selectively toxic to Ras-driven cancers with relatively little toxicity to the patient.

Structural analysis of KSR proteins

KSR is highly conserved from invertebrates to mammals. However, Drosophila express only one KSR protein, while *C. elegans* and mammals encode two members, KSR1 and KSR2 [21,31]. KSR proteins are structurally related to Raf proteins; however, they have diverged to obtain significant structural and functional differences (Fig. 1.2). KSR proteins are highly homologous, containing five conserved areas (CA1-CA5) [21]. The first conserved region on the N-terminus end is CA1. B-Raf binding to KSR1 requires a 40 amino acid sequence within CA1 and prior MEK binding via the CA5 area of KSR1 [28,58,59]. Within the CA1 domain, amino acids 25-170, termed CA1α, contain a coiled coil and sterile-α-motif (SAM), which promotes KSR1 membrane association that is essential for its effects on MAPK signaling [60]. The CA2 is a proline-rich region with an unknown function. CA3 is a cysteine-rich atypical C1 motif that mediates the membrane localization of KSR by recruiting phospholipids and is largely homologous with the CR1 cysteine-rich region in Raf [61,62]. Studies on the cysteine-rich region of KSR, in contrast to C1 regions in Raf and PKCγ, have demonstrated that the KSR1 C1 domain is structurally unique, particularly within the ligand binding region, such that KSR does not react to phorbol esters or ceramide and does not directly interact with Ras [62]. CA4 is a serine/threonine rich region containing a FXFP motif that mediates interaction with ERK [28,63,64] and is similar to the CR2 region in Raf proteins. Interaction of KSR1 with ERK is not constitutive and requires Ras activation [65,66]. The CA5 domain in KSR proteins encodes a kinase domain highly homologous to Raf family CR3 kinase domains [20,21]. While CA5 contains a putative kinase domain, there are

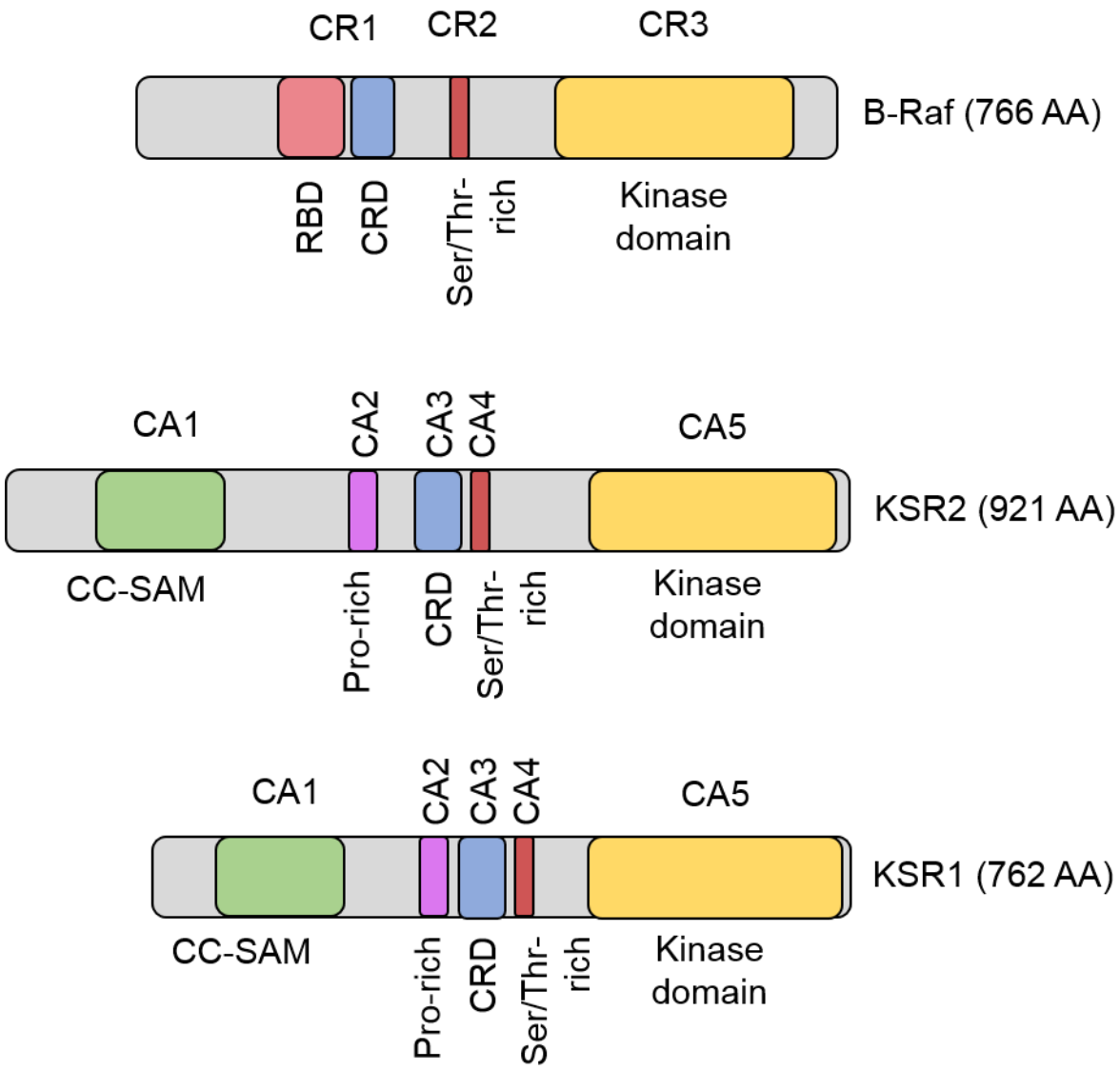

Fig. 1.2: KSR Structure. KSR proteins are structurally similar to Raf proteins with the CA3, CA4, and CA5 regions in KSR sharing significant homology with the CR1, CR2, and CR3 regions in Raf respectively. (This figure has been previously published in [2]).

CR1-3: Conserved Regions 1-3
RBD: Ras-binding domain
CRD: Cysteine-rich domain
Ser/Thr-rich: Serine/Threonine-rich domain
CA1-5: Conserved Areas 1-5
CC-SAM: Coiled coil-sterile alpha motif domain
Pro-rich: Proline-rich domain

multiple mutations within this domain including an important lysine to arginine exchange in a lysine residue that is generally required for kinase activity (Table 1.1) [21,28]. Substantial effort has been exerted to clarify if KSR can or does phosphorylate any substrates within cells, and if so whether this activity contributes to the downstream effects of KSR. The general consensus currently is that KSR is not likely to have any biologically relevant kinase activity and instead exerts its effects through protein-protein interactions and altered subcellular localization.

MEK1/2 bind to the CA5 region of KSR proteins and the interaction is constitutive in both quiescent and cells activated with growth factors [57,65,66]. Mutations within the CA5 region that abrogate binding of KSR to MEK also reduce ERK signaling (Table 1.1) [19-21,57,66]. However, due to the location of these mutations either within or near the ATP binding domain, they potentially also interfere with ATP binding or other KSR functions that may be independent of interaction with MEK (Table 1.1). Mutation C809Y within the C terminal tail of KSR1, and distal to the ATP binding domain, also disrupts MEK binding to KSR, yet allows for increased Ras-mediated ERK signaling (Table 1.1) [56]. These data suggest that the interaction between KSR and MEK is dispensable for Ras-induced ERK signaling and raises the possibility that this interaction reflects a negative regulatory role for KSR1 that controls the timing and spatial location of MEK activation. The CA5 domain is also required for KSR to bind to Raf, but the mechanism is incompletely understood [58]. Another region has been identified in KSR2 between CA2 and CA3 that is required for the interaction between KSR proteins and AMPK. Mutations in this and nearby regions reduced the binding of AMPK to KSR (Table 1.1) [50,53,59,67]. Tissue-specific splice variants have also been identified. B-KSR1 is a splice variant of murine KSR1 that is preferentially expressed in neural tissues that largely acts like KSR1 in regards to Raf/MEK/ERK interactions and signaling regulation, but specifically plays a role in cells within the central nervous system [66]. A truncated version of KSR2 (T-KSR2) was found in mouse testes, which may play a role in male fertility [68].

Mutation	Effects	Location	Species	References
W255X, R277H	Decrease constitutively active Ras-mediated signaling	CA3	*C. elegans*	[19]
G549E, P696L, Q733X	Decrease constitutively active Ras-mediated signaling	CA5	*C. elegans*	[19]
G484E	Decrease constitutively active Ras-mediated signaling	CA5, ATP-binding region	*C. elegans*	[20]
R531H	Decrease constitutively active Ras-mediated signaling	CA5	*C. elegans*	[20]
G494E	Decrease constitutively active Ras-mediated signaling	CA5	*C. elegans*	[20]
P630S, P630L	Decrease constitutively active Ras-mediated signaling	CA5	*C. elegans*	[19,20]
Intron 12 Change G→A generating a stop codon following G678	Decrease constitutively active Ras-mediated signaling	CA5	*C. elegans*	[20]
C727Y	Decrease constitutively active Ras-mediated signaling	CA5	*C. elegans*	[20]
A696V	Decrease constitutively active Ras-mediated signaling	CA5	Drosophila	[21]
A703T	Decrease constitutively active Ras-mediated signaling	CA5	Drosophila	[21]
S721+10bp in N727 → frameshift	Decrease constitutively active Ras-mediated signaling	CA5	Drosophila	[21]
S548+4bp→ L50G, R51S	Weak disruption of constitutively active Ras-mediated signaling	N-terminus	Drosophila	[21]
C359S and C362S (CRM-KSR1)	Prevented the enhanced Ras^{V12}-mediated signaling seen with the expression of exogenous WT KSR1, but did not disrupt Ras^{V12}-mediated maturation Loss of KSR1 membrane localization	CA3	*Xenopus* oocyte meiotic maturation assays using exogenous mouse KSR1	[61]
CA3 domain (amino acids 319–390)	Augments Ras signaling	CA3-Only	Mouse KSR1	[61]
CRM CA3 domain	Abolished augmented Ras signaling	CA3	Mouse KSR1	[61]
Myristylated N-Terminus KSR1 (Myr-KSR)	Constitutively localized to the plasma membrane Accelerates Ras^{V12}-induced maturation Expression of Myr-KSR alone was unable to promote oocyte maturation	N-terminus	*Xenopus* oocyte meiotic maturation assays using exogenous mouse KSR1	[61]
CRM Myr-KSR	Abolished the positive effect of Myr-KSR on Ras signaling	CA3, N-terminus	Mouse KSR1	[61]
R589M, R589L	Inactivates kinase domain and blocks MEK binding	CA5, ATP-binding site	Mouse KSR1	[69,70]
G580V and A587T	Decreased MEK:KSR association Decreased ERK activation	CA5	Mouse	[69]
S190, T256, T274, S297, S320, T411, S429, S434, S518	KSR phosphorylation sites confirmed with mutagenesis	N-Terminus to the CA5 domain	Mouse	[70]
C540	Suppressed ERK and MEK activation Interacts with MEK1 Decreased Ras signaling (suppressed Xenopus oocyte maturation, cellular transformation, and Drosophila eye development)	Truncated C-terminus, kinase domain preserved	Mouse	[55,63,69,70]
N539	No effect on the activation of ERK Fails to interact with MEK1 Unable to bind B-Raf Interacts with ERK2	Truncated N-terminus	Mouse	[55,58,63,69,70]

C809Y	Lacks KSR:MEK interaction Unable to bind B-Raf Increased Ras signaling	CA5 MEK docking site	Mouse	56-58,66,69
FSFP/AAAP **DEF docking motif for activated ERK (FxFP)** **(AxAP- KSR1)**	Lacks KSR:ERK interaction Decreased Ras signaling (decreased Ras^{G12V}-induced senescence associated β-galactosidase activity) Required for Ras-induced senescence Decreased proliferative rate with activated Ras Increased binding to endogenous B-Raf	FXFP Motif ERK docking site CA4	Mouse	56,58,64,71
S392A, S392A/S297A	Defective 14-3-3 binding Enhanced growth-factor mediated binding to B-Raf Increased plasma membrane localization even without growth factor stimulation Accelerates Ras-induced oocyte maturation Unable to promote oocyte maturation without activated Ras Promotes ERK activation and cell cycle progression following growth factor treatment	CA3	*Xenopus* oocyte meiotic maturation assays using exogenous mouse KSR1	38,65,72,73
L360A/R363A (KR/AA) **L360Q/R363G (KR/QG)**	Abolished CK2 binding No decrease in MEK, ERK, or 14-3-3 binding Decreased Ras-mediated MEK and ERK activation	CA3	*Xenopus* oocyte meiotic matu- ration assay	74
S518A **(CK2 phosphorylation site)**	No apparent effects on Ras signaling Biological effect is unknown	CA5	Mouse	74
L56G and R57S	Disrupted binding of mammalian KSR1 to endogenous B-Raf.	CA1	Mouse	58
T260A/T274A/S320A/S443A **(FBm-KSR1)** **ERK-dependent S/TP sites mutated to alanine**	Increased/Prolonged plasma membrane localization Increased association with B-Raf Increased Ras signaling	CA5	Mouse	58,65
Loss of CA3 **Frameshift mutations and nonsense mutation that disrupt the kinase domain** **E667V, A373T**	Disrupt or reduce AMPK binding to KSR2	CA3 Region between CA2 and CA3	Mouse Human	50,53,67
Asp-529A **DEVA mutant**	Inhibition of caspase cleavage Reduced apoptotic signaling in response to tumor necrosis factor and cycloheximide treatment due to decreased caspase cleaved C-terminal KSR fragments	CA5 C-Terminus DEVD site for caspase-mediated cleavage	Mouse	75
C-terminal KSR1 fragment (CTF-KSR1) **Result of caspase cleavage during apoptosis**	Reduced ERK activation and enhanced apoptotic signaling	C-Terminus	Mouse	75

Table 1.1: KSR Mutations and Associated Characteristics
(This table has been previously published in [2]).

KSR proteins are molecular scaffolds of the Raf/MEK/ERK kinase cascade

Substantial evidence has demonstrated that KSR proteins act as molecular scaffolds for the Raf/MEK/ERK kinase cascade [23-37,76]. KSR promotes Raf phosphorylation of MEK [26,61,63] and is required for maximal Ras-mediated ERK phosphorylation and activation by MEK [21,24,31,32,38,63]. Prior to experiments that controlled the level of KSR1 expression, publications reported a conflicting role for KSR overexpression, suggesting that KSR1 could both promote and inhibit Ras signaling [19-21,32,55,61,63,65,69,77,78]. These data were consistent with the idea that KSR1 acts as a scaffold for the Raf/MEK/ERK kinase cascade as increasing this scaffold to an optimum level increases signaling; however, once the optimal level is exceeded, models predict that the scaffold will dilute and sequester the individual signaling components and disrupt signaling. This dose-dependent action of KSR1 was demonstrated in *ksr1*$^{-/-}$ mouse embryo fibroblasts expressing various levels of a transgene KSR1 [32]. ERK signaling and proliferation, as well as KSR1 interaction with Raf, MEK, and ERK, all increased with increasing KSR1 expression until KSR1 was approximately 14-fold higher than endogenous levels in wild type mouse embryo fibroblast cells. ERK signaling and cell proliferation then dramatically decreased, while the interaction of Raf, MEK and ERK with KSR1 plateaued when KSR1 was further increased to a level 20-fold higher than endogenous levels [32]. When excessively high levels of KSR inhibits signaling of the MAPK cascade, these inhibitory effects can be abrogated by overexpressing additional components of the MAPK pathway. This was elegantly demonstrated in Drosophila S2 cells where the overexpression of Raf and MEK in conjunction with KSR overexpression still demonstrates robust MEK phosphorylation by Raf even with levels of KSR that would normally interfere with MEK phosphorylation [31]. These characteristics are consistent with the defining features of scaffolding proteins [79,80]. Furthermore, the scaffolding activity of KSR is both temporally and spatial regulated allowing for additional levels of regulation of the Ras pathway. In resting conditions, KSR1 is bound to MEK and an autocatalytic ubiquitin ligase, IMP, and is sequestered in the cytoplasm as a result of C-TAK1 phosphorylating KSR1 at S392, which

promotes 14-3-3 binding [57,58,65,69,72,77,81] (Fig. 1.3A). The crystal structure of KSR2 kinase domain bound to MEK demonstrated that these proteins interact at two primary locations: the activation segments within their kinase domains and the alpha G helixes on the C-terminal lobe of each protein [26], and mutations within the alpha G helix of MEK [58], or mutations that either disrupt the secondary structure of or are within the alpha G helix of KSR inhibits the binding of KSR to MEK (Table 1.1) [26]. Of note, when KSR is bound to MEK, the activation segments of both proteins are constrained. MEK cannot be phosphorylated and activated, and KSR is in an inactive conformation [26]. This inactive state may reflect KSR1:MEK heterodimers in the cytoplasm of quiescent cells. Upon Ras activation, Raf is phosphorylated, and PP2A dephosphorylates KSR1 at S392, such that 14-3-3 no longer binds [82] (Fig. 1.3B). IMP dissociates simultaneously from KSR1, interacts with GTP-bound Ras, autoubiquitinates, and is targeted to the proteasome for degradation [81] (Fig. 1.3B). KSR1 is then free to move to the plasma membrane with MEK in tow [23,31,32] (Fig. 1.3C). The localization of KSR1 to the plasma membrane is dependent upon its interaction with Caveolin-1 and is required for KSR1-mediated ERK activation and Ras-driven transformation [36]. Once KSR1 localizes to the plasma membrane, MEK is phosphorylated by activated Raf [23,31,32,61,83]. Based on the observation that KSR1 bearing C809Y mutations fails to interact with MEK and promotes ERK activation better than wildtype KSR1, MEK is predicted to phosphorylate ERK when it is dissociated from KSR1 (Table 1.1). Once phosphorylated by MEK, ERK interacts with KSR1, and this interaction is required for normal ERK signaling [56,58] (Fig. 1.3D). The sustained and coordinated activation of ERK ultimately promotes the transformation, survival, and proliferation of Ras-driven cancer cells [24,32,39,45]. The activation of ERK also controls a negative feedback loop, in which activated ERK when bound to KSR1 phosphorylates and inhibits both KSR1 and B-Raf [58,84]. This phosphorylation by ERK causes KSR1 and B-Raf to dissociate from the plasma membrane and halts additional ERK activation.

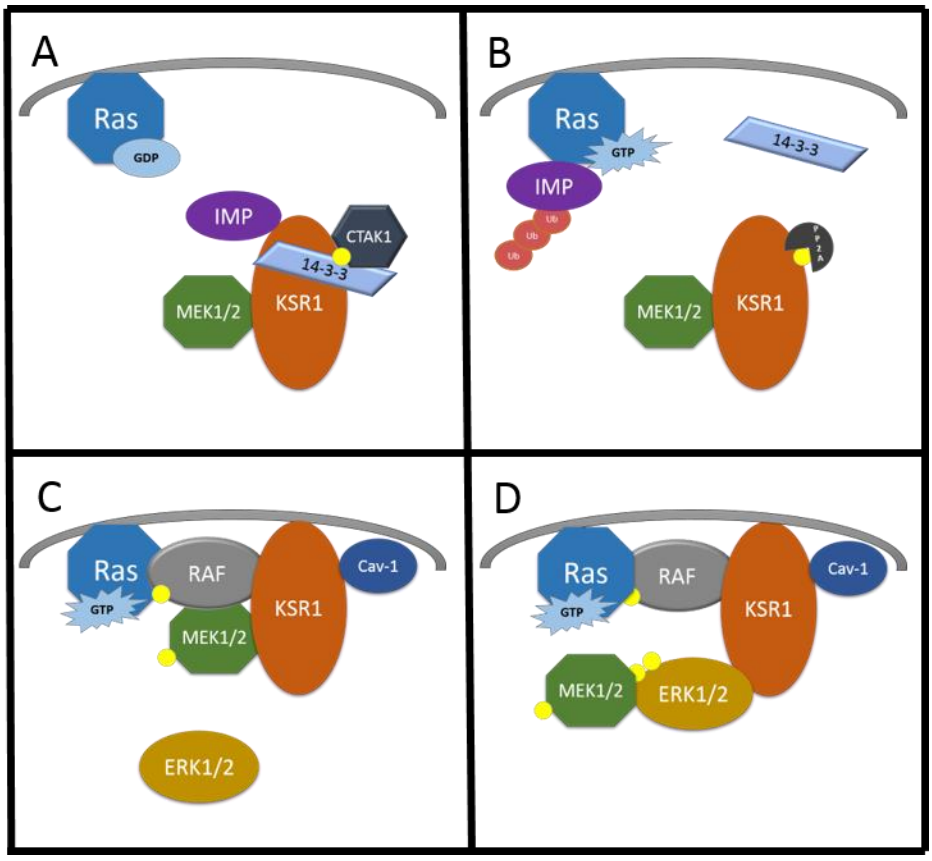

Fig. 1.3: KSR1 as a scaffold for the Raf/MEK/ERK kinase cascade. (A) When Ras is bound to GDP and inactive, KSR1 is constitutively bound to MEK1/2 and IMP and is phosphorylated (yellow circle) at S392 by C-TAK1 allowing for 14-3-3 binding and cytoplasmic sequestration. (B) Upon Ras activation, PP2A dephosphorylates KSR1 at S392 causing 14-3-3 and IMP to dissociate and IMP to autoubiquitinate and be degraded. (C) Through interaction with caveolin-1, KSR1 and MEK1/2 then move to the plasma membrane where Raf activates MEK1/2 by phosphorylation at S217/S221. (D) MEK1/2 then dissociates from KSR1 and activates ERK1/2 through phosphorylation at T202/Y204 and T185/Y187. Activated ERK1/2 then associates with KSR1, which allows ERK1/2 to phosphorylate KSR1 and Raf and initiate a negative feedback loop. (This figure has been previously published in [2]).

KSR proteins form heterodimers with Raf proteins to regulate MEK and ERK activation

Dimerization of Raf proteins is thought to be crucial for wildtype Raf activation. This dimerization is not unique to Raf proteins within the MAPK pathway as both Ras and ERK have also been shown to form dimers [85-89]. The similarity between KSR and Raf proteins is specifically conserved within the region required for Raf dimerization, and KSR has been shown to form heterodimers with Raf, particularly B-Raf [26,54,83]. This dimerization regulates an allosteric conformational change in KSR that allows for the phosphorylation of MEK [26]. Specifically, when KSR forms a dimer with a Raf protein (cis interaction), the conformational change in KSR facilitates the exposure of the activation site on MEK and allows for its phosphorylation. However, the dimerization of KSR and Raf orients the Raf protein such that the catalytic site of Raf is not in proximity to its phosphorylation target site on MEK [26]. Therefore, this phosphorylation must be completed by another Raf protein (trans interaction) [26]. More recently, it has been shown that KSR2 is also able to homodimerize through a side-to-side interface that is specifically dependent upon Arg718 [26]. In a genetic screen, mutations at this site were previously shown to suppress Ras signaling, suggesting that dimerization of KSR proteins is required to promote Ras signaling [19-21]. This is consistent with results demonstrating that mutations that inhibit the KSR-Raf heterodimerization decrease Raf activity (Table 1.1) [83]; however, the functional role of KSR homodimers is still incompletely understood.

The effects of Raf kinase inhibitors on KSR and Raf dimerization

Raf kinase inhibitors were developed in the hopes they would be able to suppress Ras signaling even in the presence of oncogenic, activating Ras or Raf mutations. Unfortunately, while these inhibitors were shown to strongly antagonize Raf activity in Raf^{V600E} mutant cells, paradoxical increases in Raf activity and downstream signaling were often seen in cells with Ras or Raf mutations following treatment with Raf kinase inhibitors [90-92]. Several follow-up studies demonstrated that this effect was due to increased Raf dimerization and subsequent activation [90,92-94]. This led to several studies that revealed there are multiple classes of Raf mutations

including highly activating mutations (e.g. V600E) that resulted in constitutively-activated, monomeric Raf, in addition to mutations that only weakly improved the catalytic activity of Raf or even decreased it, yet promoted Raf dimer formation and therefore increased subsequent Raf activation [90,92]. Initial Raf kinase inhibitors targeted kinase activity and therefore were largely only functional against the highly activating Raf mutations [92]. It is important to note, that Raf inhibitor binding also demonstrated inverse cooperativity as binding of the inhibitor to one Raf protein in a Raf protein dimer, decreased the affinity of the other Raf protein to inhibitor binding [95,96]. The initial Raf inhibitors also promoted increased dimer formation, such that the use of Raf inhibitors could cause paradoxical Raf activation by promoting Raf activation through dimerization, while only inhibiting one Raf protein within the dimer and leaving the other catalytically active.

Raf inhibitors also promote KSR1-B-Raf heterodimer formation [27]. In this manner, KSR1 can compete with other Raf proteins (C-Raf) for inhibitor-induced dimerization to B-Raf. The dimerization between C-Raf and B-Raf promotes ERK signaling; however, complex formation of KSR and B-Raf actually limits ERK activation [27]. This suggests that high KSR expression in cells being treated with Raf kinase inhibitors may actually limit paradoxical, rebound ERK activation downstream of inhibitor-induced Raf dimerization and activation. While dimerization of B-Raf with KSR2 has been shown to allosterically alter the orientation of KSR2 into a more catalytically active conformation, KSR expression reduced Raf inhibitor-induced paradoxical ERK signaling, which suggests that the overall effects of KSR in this scenario are not likely to be a result of its kinase activity, but instead are a consequence of its interaction with B-Raf [27].

Non-Canonical Functions of KSR Proteins

Recent work has demonstrated additional functions for KSR that are either independent of or downstream of its role as a scaffold for the Raf/MEK/ERK kinase cascade. Both KSR1 and KSR2 have been shown to promote AMPK expression or activity [3,34,50,52]. While the role of AMPK in cancer is still controversial, multiple groups have shown that after transformation,

AMPK can promote tumor cell survival by mediating an increase in the overall metabolic capacity allowing the cells to survive in stressful conditions. One mechanism by which this occurs is through the upregulation of PGC1β and its transcriptional partner ERRα [3,41]. An additional KSR-regulated mechanism promoting the expression of PGC1β has recently been described where KSR1 promotes ERK activation in colon cancer cells, which is required for increased MYC translation. MYC then acts as a transcription factor and increases PGC1β transcript levels [42]. KSR proteins also play a role as overall metabolic regulators in cells by regulating glucose metabolism [40] and adipogenesis [33]. The scaffold function of KSR1 promotes adipogenesis by coordinating the timing and intensity of ERK-dependent p90 RSK activation with the expression of its key adipogenic substrate C/EBPβ. Defective adipogenesis *in vitro* caused by loss of KSR1 can be rescued by adding back low levels of KSR1. Increasing KSR1 levels above the optimal level inhibits adipogenesis through sustained ERK signaling while inducing the phosphorylation and inhibition of the key adipogenic transcription factor PPARγ [33].

The presence of a kinase domain within the CA5 region of KSR has led numerous groups to examine the potential of KSR to act as a kinase. Initial reports suggested KSR was a ceramide-activated kinase [97] even though amino acids critical for phosphotransferase activity, including the lysine involved in exchange of the gamma phosphate of ATP with a substrate, are not conserved within the kinase domain of KSR proteins [21,43,66]. More recently, a crystal structure of the kinase domain of KSR2 and MEK1 with ATP bound within the catalytic site combined with *in vitro* assays and chemical genetics data suggested KSR2 has the potential to phosphorylate MEK [26]. However, the evidence supporting a role for KSR as a kinase has shown very low levels of substrate phosphorylation *in vitro* (low stoichiometry), has demonstrated phosphorylation on sites different than those required to activate MEK, has largely been based on experiments performed outside of cellular systems, and may be a consequence of co-precipitating kinases as many subsequent experiments have demonstrated KSR1 lacks catalytic activity [61,70]. This raises the

question as to whether any residual intrinsic kinase activity, if present, within KSR proteins has biological relevance. Expression of the isolated kinase domain of KSR inhibited ERK signaling and suppressed Ras-dependent *Xenopus* oocyte maturation, cellular transformation, and Drosophila eye development [63]. This supports the role of KSR proteins as molecular scaffolds, where the isolated expression of the CA5 domain, which could only bind and sequester MEK, but not regulate its cellular localization or coordinate interactions with Raf, would be expected to antagonize MAPK signaling [57,63,69]. In contrast, the conservation of the binding site residues for ATP within KSR and the prevalence of mutations within the ATP binding pocket in loss-of-function KSR mutants do suggest that ATP binding itself may play an important role in KSR activity (Table 1.1) [20,21,63]. Thus, KSR proteins have largely been considered pseudokinases.

KSR1 has been shown to travel through the nucleus when in complex with MEK [98]. The functional significance of this subcellular localization is unknown, but may facilitate activity of ERK toward nuclear substrates. Further investigation may provide additional understanding of the complex role KSR plays in modulating ERK signaling as well as other processes. These and additional undiscovered pathways could reveal novel approaches for targeting of KSR-dependent actions specific to tumor cell maintenance.

KSR as a Target for Therapy

Based on the role KSR1 plays in modulating signaling through the Raf/MEK/ERK kinase cascade, and the fact that *ksr1*$^{-/-}$ mice are largely phenotypically normal, inhibiting KSR1 in Ras-driven cancers appears to be a reasonable approach to selectively target cancer cells without subjecting patients to the side effects that normally accompany chemotherapeutics. Supporting this strategy, RNAi approaches depleting cancer cells of KSR both within *in vitro* and *in vivo* models demonstrated a decrease in tumor growth [3]. Further, a continuous infusion of phosphorothioate antisense oligonucleotides that inhibited KSR1 expression caused regression of established tumors and inhibited metastases without overt toxicity in Ras-driven PANC-1 pancreatic and A549 non-small cell lung cancer xenografts in nude mice [99].

Recent studies have attempted to target KSR proteins directly for therapy. The small molecule APS-2-79 is able to bind and stabilize KSR in an inactive state, interfere with KSR:Raf heterodimerization, and inhibit oncogenic Ras signaling [54]. Based on the finding that mutations in KSR that suppress oncogenic Ras signaling largely mapped to a region adjacent to the ATP-binding pocket, it was hypothesized that a small molecule that bound KSR within the ATP-binding pocket could interfere with Ras signaling. APS-2-79 blocks heterodimerization with Raf and conformationally biases KSR towards an inactive state [54] similar to the conformation of the KSR2 kinase domain bound to MEK1 and ATP [26]. In this conformational state, MEK cannot be phosphorylated because the active segments of both MEK and KSR2 interact directly with additional stabilization provided by interactions between the alpha G helices on the C-terminal lobe of each protein [26].

The efficacy of APS-2-79 has been demonstrated with a simplified cell-based reconstitution system that monitored KSR-dependent MEK and ERK signaling. KSR enhanced MEK phosphorylation at Ser218/Ser222 by Raf in a dose-dependent manner. This increased phosphorylation was inhibited by APS-2-79, but not a similar small molecule that due to small modifications was no longer able to bind to KSR2. The effect of APS-2-79 was also lost when KSR was mutated within the active site (A690F) such that KSR can promote MEK phosphorylation even in the absence of ATP binding. APS-2-79 had no ability to affect MEK phosphorylation in the absence of KSR, suggesting that the effect of APS-2-79 on ERK signaling is dependent on KSR, and APS-2-79 does not inhibit MEK phosphorylation by interacting directly with Raf proteins even though Raf shares a high degree of homology with KSR1 and KSR2 [54]. Unfortunately, APS-2-79 was only modestly able to decrease cell viability in two Ras-mutated cancer cell lines (HCT116 and A549) and did not affect Raf-mutated cancer cells (A375 and SK-MEL-293) [54]. In contrast to APS-2-79 treatment, in HCT116 cells, transient siRNA-mediated depletion of KSR1 dramatically reduced viability *in vitro* and stable shRNA-mediated depletion of KSR1 reduced tumor growth *in vivo* [3]. There are several reasons that may explain the

discrepancy between APS-2-79 treatment and RNAi-induced protein loss. The ability of APS-2-79 to bind and directly inhibit KSR1 has not yet been demonstrated, and therefore it may not bind and inhibit KSR1 as well as it binds to KSR2, potentially limiting its efficacy in cancer cell lines that express high levels of KSR1. The limited efficacy of APS-2-79 could also result from compensation by alternative MAPK pathway scaffolds. Several scaffolds have been shown to allow for increased Ras-mediated signaling such as IQ motif-containing GTPase activating protein 1 (IQGAP1), Sef, dystroglycan, β-arrestin, MEK partner 1 (MP1), and Paxillin [29,79,80,85,86,100]. However, this possibility is less likely as the RNAi-mediated depletion of KSR1 robustly disrupts Ras signaling even with potential compensation by other scaffolds. It is also possible that APS-2-79 only inhibits a subset of KSR-dependent signaling events and therefore is less effective than RNAi-mediated depletion of KSR1. Interestingly, APS-2-79 treatment shows substantial synergy with the MEK inhibitor trametinib in Ras-mutated, but not Raf-mutated, cancer cells. This observation suggests that robustly inhibiting Ras-mediated ERK signaling in conjunction with inhibition of non-canonical components of KSR1-dependent signaling is efficacious though the exact mechanism behind this combinatory effect is not known [54]. Demonstrating the ability of APS-2-79 to bind and inhibit KSR1, as it was only tested against KSR2, and evaluating its ability to suppress both canonical and non-canonical KSR1-dependent effects will be important moving forward.

Alternative Approach to Identify Novel Effectors of Ras-driven Tumorigenesis

Despite being identified more than 20 years ago, the functions of KSR proteins and the mechanisms by which they modulate Ras signaling and promote cancer cell survival are still not fully understood. It is well established that KSR acts as a scaffold for the Raf/MEK/ERK kinase cascade and promotes phosphorylation and activation of Ras downstream effectors through protein:protein interactions and subcellular trafficking. However, fully understanding the dynamics of these interactions, the regulatory mechanisms controlling KSR subcellular

localization, and the regulation of KSR expression in cells is vital because KSR has the potential to both promote and inhibit ERK signaling. This behavior is consistent with KSR acting as a scaffold protein and suggests that since KSR modulates Ras signaling in normal cells, KSR itself must be tightly regulated. These regulatory mechanisms, while likely still at play in cancer cells, are at least somewhat disrupted as evidenced by increased KSR1 protein expression. This increased expression in cancer and selective requirement for KSR1 for cancer cell survival, but not normal cell survival, suggests that KSR1 would be a selective, efficacious therapeutic target in pancreatic, colon, and lung cancers where Ras mutations are commonly required for tumor growth and survival.

Recent work has further characterized KSR proteins, and several new functional and physical interactions have been identified. The introduction of Raf inhibitors has expanded the understanding of KSR:B-Raf heterodimerization and the mechanisms behind Raf activation. The recent publication by Dhawan *et al.* demonstrated the possibility of targeting KSR proteins with a small molecular inhibitor that stabilizes KSR in an inactive state to effectively limit Ras signaling. The limited efficacy of APS-2-79 as monotherapy against Ras- and Raf-mutated cancer cells is disappointing; however, more selective targeting of KSR1 may substantially improve its effectiveness and is still a viable therapeutic approach based on the promising signaling studies. However, studies on Raf inhibitors has also highlighted the complex nature of these signaling pathways and the potential for paradoxical re-activation of Raf, which may complicate the targeting of KSR as well. Thus, it will be important to examine the effects of KSR inhibition in a global context, particularly in light of the potential for side effects given the obesity phenotype seen in KSR2 knockout mice and evidence that KSR expression antagonizes Raf kinase inhibitor-induced Raf dimerization and paradoxical activation.

Therefore, identifying additional targets that represent selective vulnerabilities that are only present in cancer cells provides the opportunity for the development of novel therapeutics that would possess a large therapeutic index with the potential to dramatically improve both

patient outcomes and quality of life while undergoing treatment. To identify additional genetic targets that, like KSR1, are selectively required in cancer cells, but not in normal cells, KSR1 was applied as a positive control to a functionality-based genome-scale screen termed Functional Signature Ontology (FUSION). FUSION identified numerous potential therapeutic targets based on Euclidean distance and Pearson correlation similarity metrics, which were further filtered and prioritized based on bioinformatic analysis. Biological validation of the prioritized hits demonstrated an increased requirement for these targets in cancer cells as compared to normal cells. Targets were further evaluated to elucidate their mechanisms of action in cancer and evaluate their potential to serve as therapeutic targets either independently or in combination with current therapies for the treatment of cancer.

Chapter 2: Materials and Methods

FUSION Analysis

Only abbreviated methods describing the experimental completion of the FUSION screen that are required to understand the computational and bioinformatic analysis that is the topic of Chapter 3: FUSION are included as the genome-scale screen was previously completed by Dr. Kurt Fisher and its methods are fully described in his dissertation and published manuscripts [3,42,101].

FUSION Screen Experimental Details

Gene expression for genes within the KSR1-depletion genes expression-based signature (BNIP3, NDRG1, ACSL5, ALDOC, and BNIP3L) and control genes (PPIB and HPRT) was measured using the Affymetrix Quantigene 2.0 Multiplex assay. This assay captures and amplifies the signal using branched DNA, such that the gene expression can be easily quantified by measuring fluorescence using a Luminex instrument following the addition of streptavidin phycoerythrin.

The screen used siRNA pools from the Dharmacon siGenome library that were predicted to target a single genetic target to individually knockdown 14,355 unique genetic targets. This was robotically performed simultaneously in biologic triplicate on three 384-well plates. The plates were processed in the following groups: #1: 1-5, 20-22; #2 6-13; #3: 14-19, 23, 24; #4: 25-32; #5: 33-40; #6: 41-44; #7: 66-67.

Data Preprocessing

Data preprocessing consisted of acquiring all the original data files and ensuring they were formatted consistently so they could be processed in an automated fashion. R scripts were used to read and integrate the data. Then the data was reformatted and scrubbed so that it could be computationally analyzed. Once the data was fully integrated and formatted, the values were background subtracted using “blank” wells (40 μl of water and 30 μl of hybridization solution), and geometric mean normalized to the housekeeping genes (PPIB and HPRT). Negative numbers

were set to the probe minimum on each plate. All processing was completed for each biological replicate individually and on the average of the three biological replicates. At each stage, intermediate data files were generated and saved for future review if needed.

Outlier Detection

Control wells were excluded if their raw PPIB value was less than 1000. Outliers from the repeated wells (*i.e.*, control and KSR1 depleted wells) were identified using the grubbs.test algorithm in R. Minimum number for control wells per plate was set to 6 and for KSR1-depleted targets per group was set to 20. Outlier wells for all individual gene depletions were identified based on variability between replicates and excluded from results based on the biological replicate precision filter described in Chapter 3: FUSION.

Accuracy, Precision, and Scalability

To assess the validity of the screen algorithms, three measures were used: accuracy, precision, and scalability. To measure the accuracy, the previously biologically validated hits was used. Since these have already been validated and been shown to be KSR1-like, they are expected to be in the top results (cutoff was top 5% of results). To measure precision, the ability for siKSR1 replicates to cluster was evaluated visually by plotting the siKSR1 positive control values by Euclidean distance and Pearson correlation similarity metrics. Scalability refers to the consistency between results regardless of the number of plates used. For example, the results should be relatively consistent if 25%, 50% of all the plates are included in the analysis. This was evaluated by plotting the Euclidean distance similarity metric for the data from the kinome plates for each normalization method after processing and normalizing the data using only the three plates from the kinome or the entire genome-scale dataset. The correlation between the results from the kinome-only processing/normalization compared to the results from the genome-scale dataset processing/normalization was calculated.

Normalization

Each normalization method was completed and evaluated on a per plate, group, or whole assay basis. Normalization was completed based on the reporter median, plate position, or negative controls. Normalization to reporter median is completed by finding the median value for each individual gene within the KSR1-depletion signature from each plate, group, or across the whole assay. Each gene reading is then divided by the median value for that given gene. For plate position normalization, the same method is employed, but the median is determined for each row, column, or both (if more than one plate is being evaluated). Normalization to negative controls is performed by finding the median value for each gene within the KSR1-depletion signature from the negative control (non-targeting siRNA/siControl) wells. After normalization, the data underwent log base 2 transformation.

Calculate Similarity

The positive control (siKSR1) target was the average of the KSR1-depleted wells from each experimental group/batch after outliers were excluded. Euclidean distance and Pearson correlation metrics were calculated using the rdist and cor functions in R.

Calculate Viability Filter

The viability filter is based on the decrease in PPIB with a given gene depletion relative to the average PPIB in the control wells. Based on the geomean normalized values for each replicate individually and for the average of the three replicates, the PPIB decrease was calculated as follows:

$$\text{PPIB Decr}_i = 1 - \text{PPIB}_i/\text{PPIB}_{CONT}$$

Cell Culture

Colorectal cancer cell lines HCT116, LoVo, RKO, HCT15, SW480, SW620, T84, and Caco2 were purchased from American Type Culture Collection (ATCC). Cells were grown in Dulbecco's Modified Eagle's Medium (DMEM) containing high glucose and L-glutamine with

10% or 20% (Caco2) fetal bovine serum (FBS). All colorectal cancer cells were grown at 37°C with ambient O_2 and 5% CO_2. Immortalized non-transformed human colonic epithelial cell lines (HCEC) and HCEC exogenously expressing G12V mutant H-Ras (HCECs + Ras) were a gift from J. Shay (UT Southwestern) [102]. HCECs and HCECs + Ras were grown in medium composed of 4 parts DMEM to 1 part media 199 (Sigma-Aldrich) with 2% cosmic calf serum (GE Healthcare), 25 ng/mL EGF, 1 μg/mL hydrocortisone, 10 μg/mL insulin, 2 μg/mL transferrin, and 5 nM sodium selenite. HCECs were grown in a hypoxia chamber with 2% O_2 and 5% CO_2 at 37°C. In some cases, additional supplementation with l-glutamine/gluta-max (1%), non-essential amino acids (1%), penicillin-streptomycin (1%), gentamicin (final concentration of 50 μg/mL), and/or Fungizone (amphotericin B solution final concentration of 0.25-2.5 μg/mL) was used. When used the additional reagent and concentration used are specified in the respective methods sections.

siRNA Reverse Transfections

Pooled or individual (Table D.1) ON-TARGET plus siRNAs (DharmaconGE) were introduced into the cell lines listed above following the Lipofectamine RNAiMAX (Invitrogen) reverse transfection protocol and as described: 5 μL of RNAiMax was added to 2 mL of cells in normal culture media (150,000 cells/mL), 500 μL Opti-MEM media in 6-well plates with a final RNAi concentration of 40 nM. HCECs were transfected following the RNAiMax reverse transfection protocol using 5 μL RNAiMax transfection reagent per 3-5 mL of media and 100,000 cells/mL with a final RNAi concentration of 20 nM in 6 cm plates (Corning™, Primaria™) or on 6-well plates. After a 72-hour transfection, cells were lysed in RIPA lysis buffer with protease and phosphatase inhibitors as described in the Western Blot Analyses section.

cDNA Forward Transfections

200,000-500,000 cells were plated on 6-well plates with one well for each forward

transfection or experimental condition. When cells were 50-90% confluent (usually 24 hours after plating) depending on your experiment/timeline, add transfection reagents. Transfection reagents are made in two parts, first 2.5-10 μg of plasmid is added to OptiMem to a final volume of 250 μL. Second, 5-12.5 μL of Lipofectamine 2000 is added to OptiMem again to a final volume of 250 μL. The contents of the first tube (containing plasmid) was added to the second tube (Lipofectamine 2000 and OptiMem) and were inverted 3 times to mix and incubated for 5 minutes. The entire 500 μL mixture was added dropwise to the cells on the 6-well plate. Cells were collected 24-72 hours after transfection.

Circadian Rhythm Cell Synchronization

Cells were circadianly synchronized by treating with 50% horse serum for 2 hours, 10 μM forskolin for 30 minutes, or 100 nM dexamethasone for 30 minutes. Cells were then collected at the end of the treatment (0 hr) and every four hours for the next 24-48 hours. For each collection, the media was collected, cells trypsinized and pelleted. The cell pellet was rinsed with PBS and repelleted. The pellet was then snap frozen in liquid nitrogen and stored at -80C until all samples could be lysed in RIPA lysis buffer with protease and phosphatase inhibitors (described in Western Blot Analysis section) and analyzed by western blot.

Anchorage-independent growth on poly-2-hydroxyethyl methacrylate (polyHEMA)-coated plates

10 mg/ml polyHEMA stock solution was made by dissolving polyHEMA in 95% ethanol and shaking at 37°C until fully dissolved (6 hours to overnight). 96-well plates were coated with polyHEMA by evaporating 100-200 μl of the 10 mg/ml stock polyHEMA solution in each well. Cells were plated in complete medium on polyHEMA-coated wells at a concentration of 1.5-2 x 10^4 cells/100 μl 48 hours post-transfection (as described above). Cell viability was measured per the manufacturer's protocol using the CellTiter-Glo® Luminescent Cell Viability Assay (Promega). Specifically, this was done by adding 90 μl of CellTiter-Glo® reagent, shaking for

two minutes to lyse the cells, incubating at room temperature for 10 minutes, and measuring luminescence (POLARstar OPTIMA).

Cell growth assay

5,000-10,000 (HCEC, LoVo, T84, Caco2) cells/well were transfected on white or clear 96-well plates. Transfections were done as described above but at a ratio of 1:25 for all of the reagents. At 72 or 96 (start with half as many cells) hours post-transfection, 10 μL of alamarBlue® (ThermoFisher Scientific) was added to each well (100 μL) or 100 μL of alamarBlue® was added per mL of media and media was removed from the 96-well plate and replaced with the alamarBlue®/media mixture. Plates were incubated at 37°C for 1-3 hours and fluorescence was measured (POLARstar OPTIMA). Results were background subtracted (well with media + alamarBlue® without any cells) and normalized with the control being set to 1. In other instances, cell viability was measured per the manufacturer's protocol using the CellTiter-Glo® Luminescent Cell Viability Assay (Promega). Specifically, this was done by adding 90 μl of CellTiter-Glo® reagent, shaking for two minutes to lyse the cells, incubating at room temperature for 10 minutes, and measuring luminescence (POLARstar OPTIMA).

Cell Count

Adherent cells were counted by removing the media, washing the cells gently with PBS, and trypsinizing the cells. The total volume of trypsin and media cells were resuspended in was kept consistent across samples and noted for total cell number calculations. At each time point, cells were then counted either manually using a hemocytometer or using a Coulter Counter to obtain a concentration of cells. This was then multiplied by the total volume of suspended cell mixture to obtain a total cell count.

Sensitization Studies with IR or 5-FU

2,500 (or 5,000 for slower growing cell lines: HCEC, LoVo, T84, Caco2) cells/well were

plated or transfected on white or clear 96-well plates or 200,000 cells were plated/transfected on 6-well plates. Transfections were done as described above but at a ratio of 1:25 for 96-well plates. At 24 hours, drug was added if included in the experiment. At 48 hours, 3-5 Gy gamma IR was applied to the cells in a single dose (RS-2000 Irradiator). At 96 hours after plating, alamarBlue® (ThermoFisher Scientific) was added to each well (100 µL alamarBlue/1 mL media) or cells were collected for western blot analysis. Plates were incubated at 37°C for 1-3 hours and fluorescence was measured (POLARstar OPTIMA).

Colony Forming Assay

250-500 (HCEC, LoVo, T84, Caco2) cells were plated on 12-well or 24-well plates. Drug was added 24 hours later and replaced as needed. Media containing Fungizone (Amphotericin B – 2.5 µg/mL final conc.) and gentamicin (50 µg/mL final conc.) was used. 10-14 days later, cells were rinsed with PBS, and methanol for 20 minutes to fix the cells. Cells were rinsed with water and incubated in Giemsa Stain (diluted 1:10-1:20) for 5 minutes. Cells were washed with gently running water. Plates were laid upside down and dried overnight. Images were taken of the colonies using the LI-COR Odyssey imager. Cell colony number and size were quantified using an ImageJ macro and the built-in analyze particles function.

Carboxyfluorescein succinimidyl ester (CFSE) Cell Proliferation/Division Assay

Cells were stained with CFSE by resuspending 2 million HCT116 or SW480 cells in 10 µM CFSE in PBS (1 mL total volume) in a 1.5 mL Eppendorf tube. Resuspended cells were incubated at 37°C in the hot water bath for 15 minutes, washed once with 5 mL media, and resuspended in 13 mL media. Two mL of cells/media (approximately 300,000 cells/well) were added to each well on a 6-well plate on top of the siRNA transfection reagents as described previously. After 96 hours, cells were trypsinized, pelleted, and resuspended in PBS for flow cytometry analysis to measure CFSE staining. Remaining cells, after flow cytometry analysis,

were used in western blot evaluation to confirm target gene depletion.

Propidium Iodide

Cells were assessed for apoptosis using the sub-G1 peak and percent of cells in each phase of the cell cycle as measured by flow cytometry following propidium iodide (PI) staining. Prior to staining, all media in the sample well was collected and placed in a 12 x 75 mm round bottom polystyrene tube (BD Falcon, 352054). Cells were washed once with PBS, the PBS was saved, and cells were subsequently treated with 0.25% trypsin for 5 minutes. Media was then used to resuspend the trypsin-treated cells, which were collected and placed in the polystyrene tube. Cells were pelleted by centrifugation for 5 minutes at 2800 RPM using an Immunofuge II. The media was aspirated, and the cells were fixed in 1 mL of ice cold 70% ethanol overnight at -20°C. Cells were then warmed to room temperature (~15 minutes on bench), pelleted by centrifugation for 5 minutes, then rehydrated in 1 mL of room temperature PBS and incubated at 37°C for 15 minutes. Cells were then pelleted, the PBS aspirated, and the cells were resuspended in PI stain overnight. Data was acquired using a Becton-Dickinson FACSCalibur flow cytometer and analyzed using FlowJo Cell Cycle analysis to detect the percentage of cells in the sub-G1 peak, 2N peak/G1 phase, S phase, and 4N peak/G2 phase.

RT-qPCR

RNA was harvested using 1 mL TriReagent (MRC, TR118) and stored at -80°C until extraction. RNA was extracted per manufacturer's protocol and final RNA was eluted with nuclease-free water. RNA was quantified using the NanoDrop 2000 (Thermo Scientific). Reverse transcription was performed using iScript™ Reverse Transcription Supermix for RT-qPCR (Bio-Rad, 170-8840) with 1 µg of total RNA per 20 µL reaction. RT-qPCR was performed using the primers and conditions listed in Table 2. All targets were amplified using SsoAdvanced™ Universal SYBR Green Supermix (Bio-Rad) with 40 cycles of a 2-step program (95°C x 5 sec,

T_m x 45 sec). Primer sequences used are specified in Table D.2.

TCGA

mRNA expression was analyzed based on the FPKM-UQ normalized RNASeq values of normal solid tissue samples and primary tumors from within The Cancer Genome Atlas (TCGA) Breast Invasive Carcinoma (BRCA)(Number of Samples from Normal N=113 and Primary Tumor N=1102), Colon Adenocarcinoma (COAD) (N=41 and N=478 samples with 456 unique patients), Lung Adenocarcinoma (LUAD)(N=59 and N=533), Lung Squamous Cell Carcinoma (LUSC)(N=49 and N=502), Glioblastoma (GBM)(N=5 and N=156), Prostate Adenocarcinoma (PRAD)(N=93 and N=498), Pancreatic Ductal Adenocarcinoma (PAAD)(N=4 and N=177), Sarcoma (SARC)(N=2 and N=259) datasets and primary tumors only from Ovarian Serous Cystadenocarcinoma (OV)(N=374) and Cervical Squamous Cell Carcinoma (CESC)(N=304) datasets. Results were analyzed for statistical significance using unpaired (unmatched samples) and paired (patient-matched samples) Student's *t* tests.

Western Blot Analysis

Whole cell lysate extracts were prepared in radioimmunoprecipitation assay (RIPA) buffer comprised of 50 mM Tris-HCl, 1% NP-40, 0.5% Na deoxycholate, 0.1% Na dodecyl sulfate, 150 mM NaCl, 2mM EDTA, 50 mM NaF, 10 μg/mL aprotinin, 10 μg/mL leupeptin, 2 mM EDTA, 1 mM PMSF. Nuclear and Cytoplasmic lysates were obtained using the ThermoFisher NE-PER Nuclear and Cytoplasmic Extraction Reagents Kit (78835, ThermoFisher Scientific) based on the manufacturer's protocol and the 100X Halt Protease and Phosphatase Inhibitor Cocktail (ThermoFisher Scientific 78440). Protein concentration was determined using the Promega BCA protein assay. SDS-PAGE was performed, membranes were blocked in Odyssey PBS blocking buffer (LI-COR Biosciences, 927-40000), and incubated in primary antibody (listed below) overnight at 4°C. LI-COR secondary antibodies (IRDye 800CW, 680LT,

or 680RD) were diluted 1:10,000-1:50,000 in 0.1% TBS-Tween (for nitrocellulose). Membranes were imaged using the LI-COR Odyssey.

In vitro kinase assay

AMPK assays were performed by diluting 20 ng of AMPKα1β1γ1and 60 ng of AMPKα2β1γ1 in 5 µl of 10 mM MOPS (pH 7.2), 5 mM β-glycerophosphate, 10 mM $MgCl_2$, 2 mM EGTA, 0.8 mM EDTA and 0.1 mM DTT, 80 ng/µl BSA and 8% glycerol and placing them on ice. 5 µl of AMP (480 µM final in water), drug or DMSO diluted in water (1:10,000 nM final), 1 mg/ml SAMS substrate (in water) and α-^{32}P-ATP (40-500 µM final dilution in 25 mM MOPS pH 7.2, 12.5 mM β-glycerophosphate, 25 mM $MgCl_2$, 5 mM EDTA, 2 mM EGTA and 0.25 mM DTT) was added. Standard assay included a 50 µM final ATP concentration. Samples were mixed and incubated in 30°C water bath for 15 minutes with gentle rocking and then returned to ice. 20 µl of samples were spotted on P81 paper and allowed to dry. Papers were washed three times each with 200 ml 0.1% phosphoric acid, allowed to dry, placed in a vial with scintillation cocktail, and counted. One sample without enzyme was used to correct for non-specific binding to the P81, which was determined to be equal to using no SAMS peptide in a mock assay.

Anchorage-independent growth in soft agar

Cells were seeded at 5 x 10^3 cells/35 mm dish in 1 ml of top agarose consisting of Iscoves's Dulbecco Modified Growth Medium (DMEM) mixed with 0.4% NuSieve GTG agarose, 4 mM L-Glut, 1% NEAA and 1% penicillin/streptomycin suspended over a bottom layer consisting of 2 ml of DMEM with 0.8% Nu-Sieve GTG agarose, 4 mM L-Glut, 1% NEAA and 1% penicillin/streptomycin. DMSO or 5-OH-S was placed in both top and bottom layers at a concentration of 10 µM. Colonies over 100 microns were counted and representative photomicrographs were taken after 14 days of incubation in 37°C and 5% CO_2.

Antibodies

Primary antibodies were diluted as follows:

P-4EBP1 (T70 9455, Cell Signaling) 1:1000; T-4EBP1 (53H11, 9644, Cell Signaling) 1:1000; pACC (#3661, Cell Signaling) 1:2000; tACC (#3676, Cell Signaling) 1:2000; B-Actin (C-4, 47778, Santa Cruz) 1:2000; pAKT S473 (9271, Cell Signaling) 1:1000; pAKT T308 (9275, Cell Signaling) 1:1000; tAKT (9272, Cell Signaling) 1:1000; pAMPKα1α2 (#2531, Cell Signaling) 1:1000; AMPKα1α2 (#2532, Cell Signaling) 1:1000; AMPKα2 (#AF2850, R&D systems) 1:1000, and AMPKα1 (#2795, Cell Signaling) 1:1000; AMPKβ1 (#12063, #4182, Cell Signaling) 1:1000, and AMPKβ2 (#4148, Cell Signaling) 1:1000; AMPKγ1 (#ab32382, Abcam) 1:2000; Beclin 1 (3495, Cell Signaling) 1:1000; CDC25C (4688, Cell Signaling) 1:1000; P-CDC25C (S216, 9528, Cell Signaling) 1:1000; P-CDC25C (T48, 9527, Cell Signaling) 1:1000; P-CDK1 (Y15, 9111, Cell Signaling) 1:1000; T-CDK1 (77055 and 9112, Cell Signaling) 1:1000; P-CHK1 S345 (2348, Cell Signaling) 1:1000; T-CHK1 (G-4, 8408, Santa Cruz) 1:1000; eIF4A (C32B4, 2013, Cell Signaling) 1:1000; eIF4E (9742, Cell Signaling) 1:1000; peIF4E (S209, 9741, Cell Signaling) 1:1000; pERK (9106, Cell Signaling) 1:1000; ERK (9102, Cell Signaling) 1:1000; ERRa (V-19, 32971, Santa Cruz) 1:1000; P-GSK3B (S9, cs-55585, Cell Signaling) 1:1000; Phospho-Histone H2A.X (Ser139)(2577, Cell Signaling) 1:1000; H2A.X (2595, Cell Signaling) 1:1000; H3K4Me3 (ab8580, Abcam) 1:1000; H3K4Me1 (ab8895, Abcam) 1:1000, Histone 3 (ab1791, Abcam) 1:2500; HDAC2 (ab7029, Abcam) 1:5000; KSR1 (H-70, Santa Cruz) 1:1000; pMEK (4694, Cell Signaling) 1:1000; MEK (9122, Cell Signaling) 1:1000; MYC (5605, Cell Signaling) 1:1000; MDM2 (sc-965, Santa Cruz) 1:500; p53 (6243, Santa Cruz) 1:1000; P21 (ab7903, Abcam) 1:1000; PARP (9542, Cell Signaling) 1:1000; PDCD4 (D29C6, #9535, Cell Signaling) 1:1000; PP2ACa/B (1D6, sc-80665, Santa Cruz) 1:1000; PUMA (3041, ProSci, gift from Xu Luo lab) 1:1000; pRAPTOR (#2083, Cell Signaling) 1:1000; tRAPTOR (#2280, Cell Signaling) 1:1000; RBBP5 (A300-109A, Bethyl) 1:1000; P-RSK (S380, cs-9341, Cell Signaling) 1:1000; T-RSK (601225, BD Biosciences) 1:1000; TIMELESS (A300-

961A, Bethyl) 1:5000; α-tubulin (B-5-1-2, Santa Cruz) 1:2500; ULK1 (#4773, Cell Signaling) 1:1000; P-ULK1 (S317, #12753, Cell Signaling) 1:1000; WDR5 (ab22512, Abcam) 1:1000, and P-Wee1 (S642) (4910, Cell Signaling) 1:1000. The PGC1β antibody was a generous gift from Dr. Ching-Yi Chang and Dr. Donald McDonell (Duke University) and was used at 1:5000 dilutions.

Anti-mouse, and anti-rabbit secondary antibodies conjugated to Alexa Fluor 680 (Invitrogen, Carlsbad, CA) or IRDye800, and IRDye680LT were used at 1:5000-1:10,000 dilutions.

Reagents

Additional reagents included recombinant AMPKα1β1γ1 (#P47-10H, SignalChem) and AMPKα2β1γ1 (#P48-10H, SignalChem), SAMS peptide (S07-58, Cquential Solutions), and radioactive α-^{32}P-ATP (64014, MPBIo). Poly-2-hydroxyethyl methacrylate (polyHEMA, P3932), cycloheximide (CHX, C7698), Wright-Giemsa stain (WG16), the MYC inhibitor 10058-F4 (F3680), and propidium iodide (PI, P4170) were purchased from Sigma-Aldrich. OICR-9429 was purchased from Caymen Chemical (1801787-56-3). WDR5-C47 was purchased from Xcessbio (M60118-2). The RSK inhibitor BI-D 1870 was purchased from Axon MedChem (1528). The mTOR inhibitor AZD8055 (HY_10422), Wee1 inhibitor MK-1775 (HY-10993) and CHK1 inhibitor AZD-7762 (HY-10992) were purchased from MedChem Express. The ERK inhibitor SCH772984 was purchased from SelleckChem (S7101). Z-Leu-Leu-Leu-al (MG132, S2619) and 5-flurouracil (5-FU, AC228440010) were purchased from Fisher. The AKT inhibitor MK2206 was a gift from the Black Lab.

Constructs purchased from Addgene include: pcDNA4-Flag-TIM (22887, Addgene) and WDR5 plasmid (#15552). Other constructs include an GIPZ WDR5 shRNA (Thermofisher RHS4531-EG11091), pTRIPZ inducible WDR5 shRNA (Dharmacon/Fisher RHS4696-200696686 Clone: V2THS-140181), and pTRIPZ inducible TIMELESS shRNA (Dharmacon/Fisher RHS-4696-200685318 Clone: V2THS-47526).

STR PCR Profiling for Cell Line Validation

The DNA Forensic Lab Core Facility within MMI was utilized to verify cells lines using STR PCR Profiling. A PBS washed cell pellet (can be frozen) is needed to perform the analysis. The results were evaluated using the ATCC tool: https://www.atcc.org/STR%20Database.aspx

Statistical Analyses

P values were calculated using Prism Software (GraphPad, La Jolla, CA). A P value of less than 0.05 was considered statistically significant. Values presented as bar plots are shown as mean +/- standard deviation (SD) unless otherwise noted.

Chapter 3: Evaluation of a Functional Signature Ontology genome-scale screen to identify novel targets in cancer

Introduction

Tumors acquire vulnerabilities due to oncogene-driven changes in cell signaling pathways, which promote uncontrolled proliferation and suppress apoptosis. These vulnerabilities provide opportunities to develop selective cancer therapeutics that lack the side effects accompanying current therapies. Previously, Kinase Suppressor of Ras 1 (KSR1), a scaffold for the Raf/MEK/ERK kinase cascade, has been shown to be required for maximal ERK activation and Ras-driven transformation [3,24,32,38,41,56]. Depletion of KSR1 by RNA interference (RNAi) kills malignant, Ras-driven cancer cells, but not immortalized, non-transformed human colon epithelial cells (HCECs) [3]. Additionally, KSR1$^{-/-}$ mice are viable and fertile [24] suggesting KSR1 is not required for normal cell survival making it a prime therapeutic target; however, drug development targeting KSR1 has had limited success.

Using screening approaches to identify KSR1-like targets that are selectively required for cancer cell survival has proven fruitful. In fact, Gene Set Enrichment Analysis (GSEA) of gene expression alterations discovered through microarray analysis in HCT116 colon cancer cells with and without KSR1 led to the discovery that PGC1β and ERRα were key downstream effectors of KSR1 in cancer [3]. Further analysis revealed that PGC1β and ERRα were overexpressed in cancer and required for cancer cell survival as shown in both cell line-based and tumor xenograft studies. These findings led us to hypothesize that novel vulnerabilities in cancer could be identified using an unbiased genetic depletion screen.

RNA interference (RNAi) screens can be performed using multiple techniques. The two most common techniques involve using either a pooled gene depletion method or an arrayed single gene depletion method (Fig. 3.1). In pooled approaches, an entire library of shRNA (RNAi) or sgRNA (CRISPR-based screens) is added to a single dish of cells. This method is typically performed for longer periods of time, which allows a few cells with the desired phenotype to outgrow other cells and become overrepresented at the end of the study. Cells can

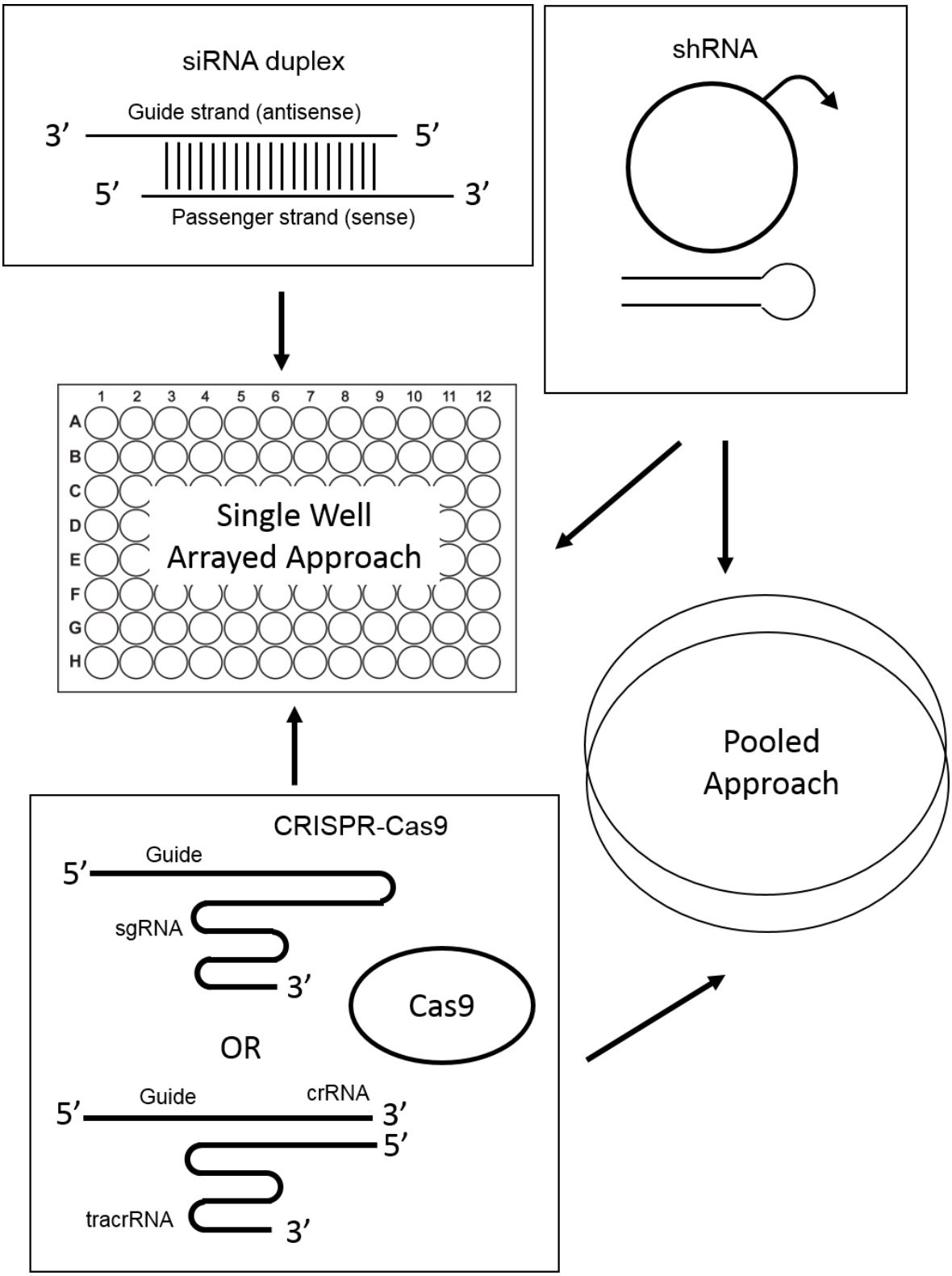

Fig. 3.1: RNAi-mediated screening overview. High-throughput screening can be completed by applying siRNA, shRNA, or CRISPR-Cas9 to alter gene expression or genetically manipulate cells in either an arrayed or pooled approach.

then be examined for the presence of shRNA barcodes or genetic mutations through sequencing to determine the genetic alteration that induced the phenotype of interest or is overrepresented in a population. Recently, several groups have utilized the pooled method to perform CRISPR-based screens seeking to identify mechanisms of drug resistance. In these instances, a pool of sgRNA targeting the entire genome are added to cells stably expressing Cas9 that are sensitive to a given therapy. Shortly after the addition of sgRNA, the drug of interest is added and clones that develop drug resistance to the therapy survive. These are then evaluated by sequencing to determine the genetic alterations that were responsible for the development of resistance. In the arrayed, single well screen, siRNA or shRNA targeting a single gene is added to each well. The result of the individual gene depletion is then evaluated in each well typically using high content microscopy, cell viability, or other reporter assays such that each gene depletion examined in the screen yields a quantifiable effect. One vital aspect in arrayed screening is identifying the optimal readout. Assessing cell viability is cheap and informative; however, it is a crude approach and does not distinguish between numerous downstream effects of gene depletion. This approach was therefore not sensitive enough for this study since the goal was to identify genetic targets that are functionally similarly to KSR1 such that they are selectively required only in cancer cells. Other common readout assays evaluate the state or effect of individual gene depletions on a specific downstream target of interest. KSR1 promotes phosphorylation of ERK, therefore, evaluating the phosphorylation status of ERK with each gene depletion could have been applied as the screen readout. However, this approach suffers from a significant weakness in that it would fail to detect targets that acted either downstream or tangentially to ERK. Additionally, the activation of ERK has been well-studied and using phosphorylation of ERK would be likely to just reinforce the already identified interactions without revealing significant novel effectors in cancer. Recent studies have also demonstrated that it is likely KSR1 has functions that are independent of its effects on ERK, further necessitating the use of a different readout for this function-based screen.

In 2004, Stegmaier *et al.* published a study describing the successful implementation of

gene expression-based high-throughput screening to identify chemical compounds that induce differentiation of acute myeloid leukemia cells. This method used a gene expression-based signature as a marker for the differentiation phenotype, which can be quantifiably compared between known differentiating agents and the tested compounds. In this implementation, they screened 1,739 compounds using RNA extraction, RT-PCR, then performing mass spectrometry to assess gene expression of five genes that demonstrated altered expression following cell differentiation. This screen ultimately identified eight compounds that induced the differentiation signature and demonstrated morphological and functional evidence of differentiation upon follow-up analysis [103]. This study definitively demonstrated that a gene expression-based signature could be used as a proxy for a phenotype of interest such that one could effectively assess the functional effect of a chemical or genetic perturbation without having to examine or even knowing all the intermediate steps allowing for an unbiased, rapid identification of novel potential therapeutic targets in cancer.

Therefore, a gene expression-based screening approach termed Functional Signature Ontology (FUSION) [3] was utilized to identify other genes that are functionally similar to KSR1, such that they are required for colon cancer survival, but not normal colonic epithelial cell survival. To do this, a gene signature representing the downstream effects of KSR1 depletion in HCT116 colon cancer cells was established. This was based on gene expression changes in HCT116 cells with and without KSR1 measured using a microarray. Based on this analysis, six reporter probes (BNIP3, NDRG1, ALDOC, LOXL2, ACSL5, BNIP3L), which decreased in expression following KSR1 depletion were chosen for the KSR1-depletion gene expression-based signature (Table 3.1). Since these six genes demonstrated consistent downregulation upon KSR1 depletion, their expression was measured following individual gene depletions to identify genes that had a similar effect on their expression, and, theoretically, the same overall effect on cancer cells (Fig. 3.2). Two additional reporters, cyclophilin B (PPIB) and hypoxanthine-guanine phosphoribosyltransferase (HPRT) that did not change with KSR1-depletion were included as

Gene	Gene Details
BNIP3	BCL2/Adenovirus E1B 19 kDa Interacting Protein 3: Encodes a mitochondrial protein with a BH3 domain, pro-apoptotic
NDRG1	N-Myc Downstream Regulated 1: alpha/beta hydrolase superfamily, involved in stress response, hormone response, cell growth and differentiation
ALDOC	Aldolase C: Fructose-bisphosphate:Glycolytic enzyme that catalyzes F1,6BP and F1P → DHAP, G-3-P
LOXL2	Lysyl Oxidase-Like 2:Biogenesis of connective tissues, crosslinkage of collagen and elastin
BNIP3L	BCL2/Adenovirus E1B 19 kDa Interacting Protein 3-Like: Protein with a BH3 domain, binds Bcl-2, pro-apoptotic
ACSL5	Acyl-CoA Synthetase Long-Chain Family Member 5: Converts free fatty acids into fatty acyl-CoA esters → lipid biosynthesis and fatty acid degradation

Table 3.1: Genes comprising the KSR1 depletion gene expression-based signature.

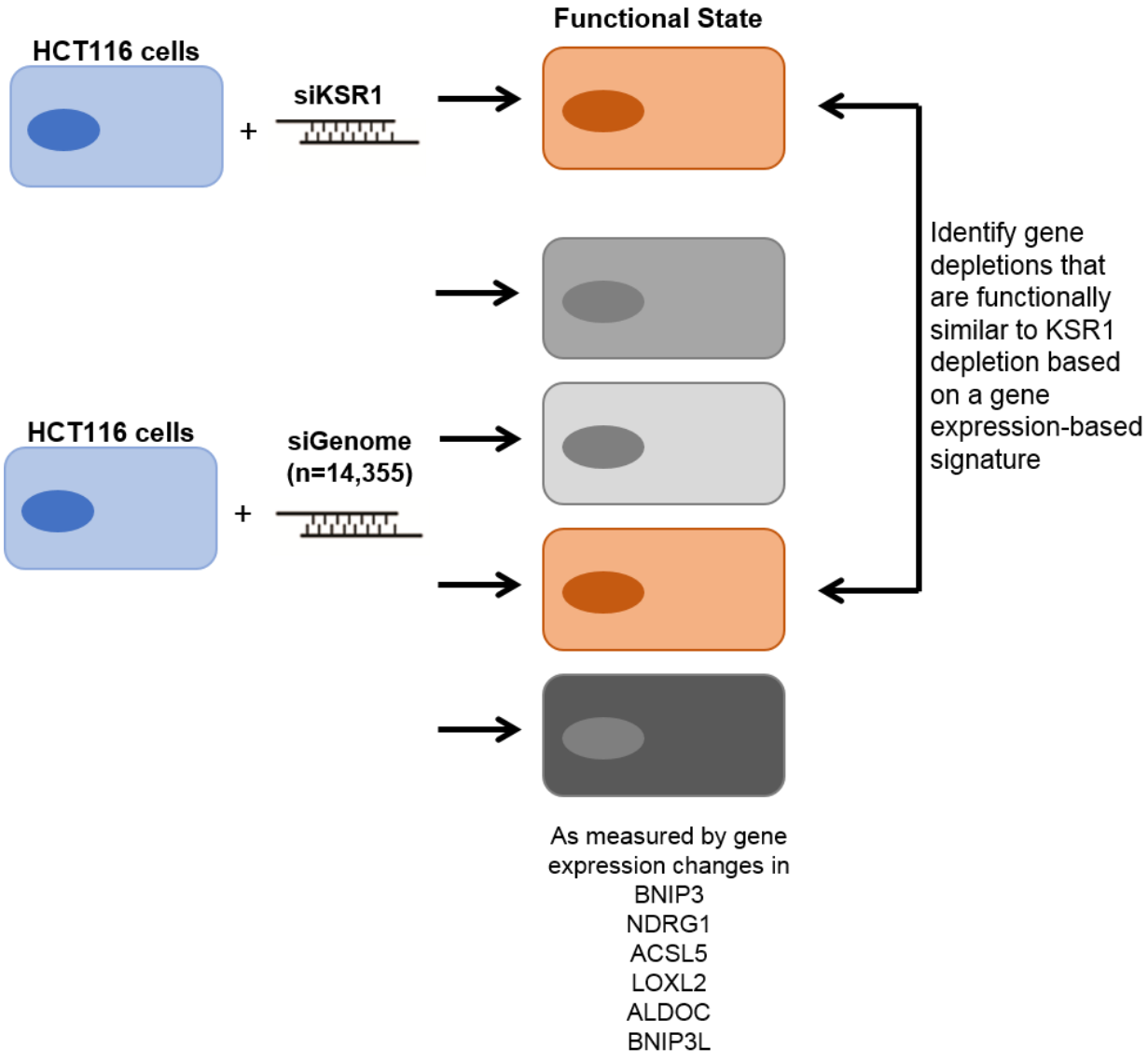

Fig. 3.2: Representative diagram of the FUSION analysis.

control reporters and were used to account for well-to-well cell number variation. This allowed for the relative change in gene expression to be evaluated without being confounded by cell proliferation or viability changes. In contrast to the study performed by Stegmaier *et al.* that measured gene expression using RT-PCR followed by mass spectrometry, the gene expression-based signature was measured using the Affymetrix Quantigene 2.0 Multiplex assay. This allowed for a much easier evaluation of gene expression during high throughput screening as gene expression was easily quantified for each gene in the KSR1-depletion signature by measuring fluorescence. The identification of the KSR1-depletion gene expression signature (BNIP3, NDRG1, ALDOC, LOXL2, ACSL5, BNIP3L) and validation of the Affymetrix Quantigene 2.0 Multiplex assay laid the foundation for the preliminary kinome (791 kinases, phosphatases, and related genes) screen, which was robotically performed simultaneously in biologic triplicate on three 384-well plates. Each gene within the kinome portion of the siGenome library (Dharmacon) was individually knocked down using pooled siRNA sequences and gene expression of BNIP3, NDRG1, ACSL5, ALDOC, BNIP3L, PPIB, and HPRT were measured (Fig. 3.3). Data underwent quality control and data preprocessing (see Chapter 2: Materials and Methods), then was normalized based on the median gene expression for each of the six genes in the KSR1-depletion signature (Fig. 3.3). Positive control outliers (siKSR1 wells) were identified using Grubbs algorithm as described in Chapter 2: Materials and Methods. The positive control target was the average of all remaining siKSR1 wells. Euclidean Distance and Pearson Correlation similarity metrics were used to evaluate the effects on the gene expression-based signature following each individual gene depletion. Five (AMPKγ1, EPHB4, ERK5, DYRK1A, and LATS1) of the top ten hits from the kinome screen were biologically validated with three of these hits (AMPKγ1, EPHB4, DYRK1A) being examined extensively and two being the subject of published manuscripts from the Lewis lab [3,42] (Fig. 3.4).

The current work expands upon this early success with FUSION and applies this analysis to the full genome-scale RNAi screen that interrogated 14,355 genes (siGenome library from

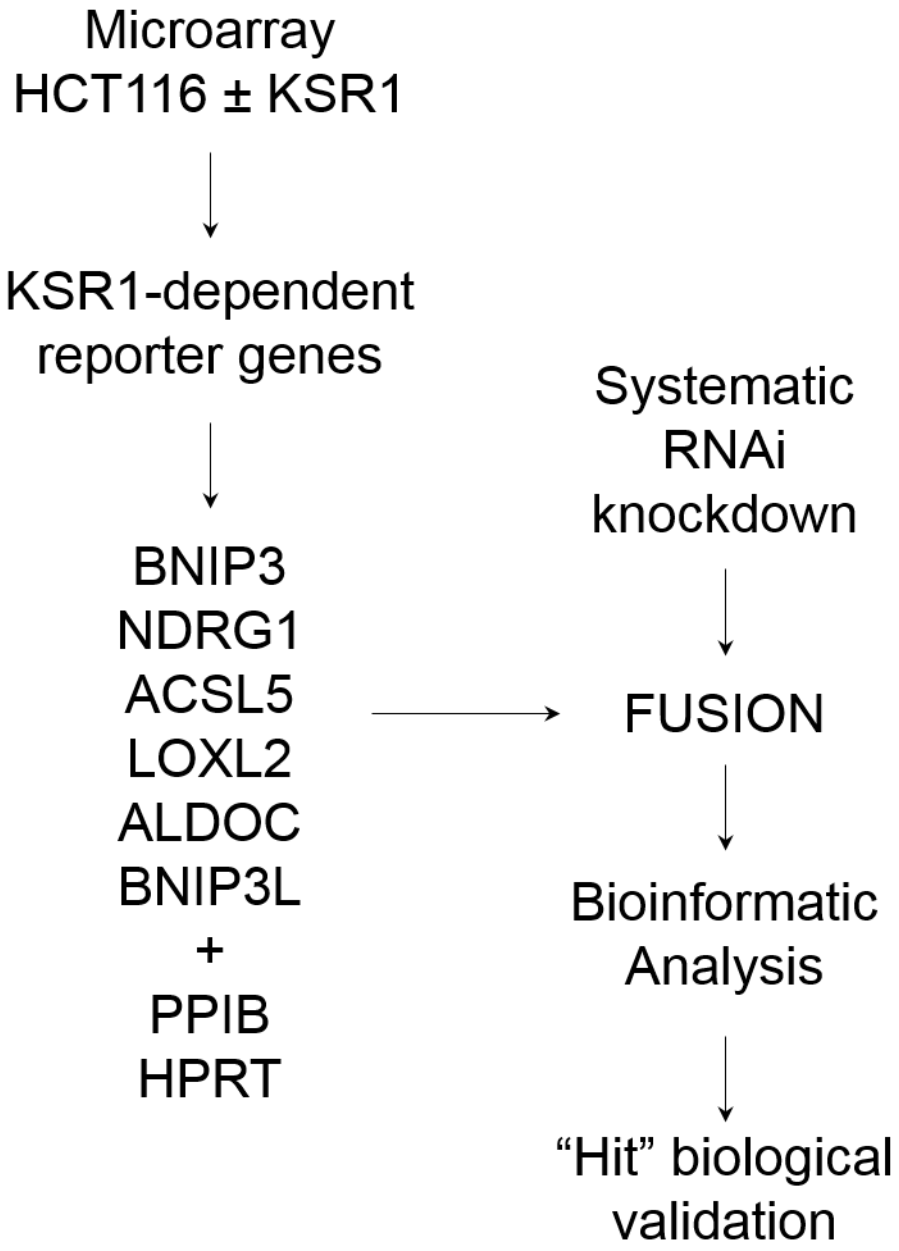

Fig. 3.3: FUSION relies on the identified KSR1 depletion gene expression-based signature to evaluate the functional similarity between KSR1 and other genes.

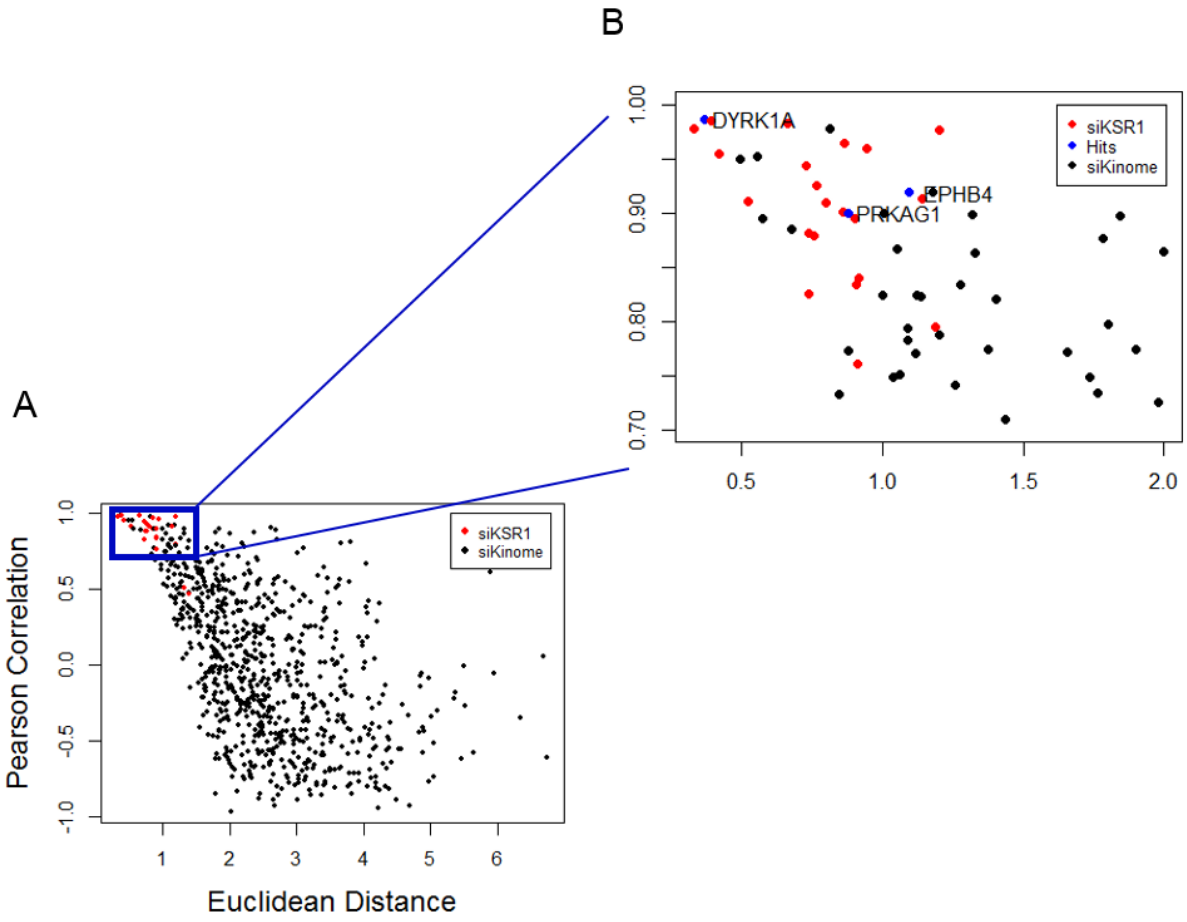

C

Biologically Validated Hit	Pearson Correlation	Euclidean Distance
DYRK1A	0.987	0.281
EPHB4	0.966	0.852
PRKAG1/AMPKγ1	0.895	0.843

Fig. 3.4: Biologically validated hits from the preliminary kinome screen. (A) Scatter plot of the kinome screen results based on Euclidean distance and Pearson correlation. KSR1-depleted wells are shown in red and the remaining gene depletions from the kinome library are shown in black. (B) Expanded view of the Euclidean distance and Pearson correlation metrics for each gene depletion. KSR1-depleted wells are shown in red, validated hits in blue, and the remaining gene depletions in black. (C) Table of validated hits with Pearson correlation and Euclidean distance metrics.

Dharmacon) and was adapted to evaluate 1,200 natural product fractions in the K-Ras^{G13D}-driven human colorectal cancer cell line HCT116. However, the scale of the expanded experiment dramatically increased the experimental and computational complexity required to elucidate promising targets while limiting false positives. First, the size of the genome-scale screen forced it to be processed in batches. This caused a certain degree of unavoidable variability between individual runs that must be accounted for in order to preserve the unbiased nature of the screen. These batch-wise variances need to be identified and accounted for prior to analysis. This was completed through normalization of the data. Additionally, in any experiment with more than 50,000 measurements there is bound to be a certain number of faulty wells that generate outliers in the data that should be excluded from analysis. Following the data preprocessing and normalization, the functional similarity between KSR1 and each gene screened was quantified in the same manner that was employed in the kinome screen using Euclidean distance and Pearson correlation similarity metrics. However, this led to the identification of nearly 800 potential target genes. To prioritize the identified hits, filters were applied to the 788 identified genes and bioinformatic analyses were performed to identify common pathways or related proteins that were identified in an attempt to limit false positives and prioritize the identified targets.

Results

FUSION Screen: Experimental Background

Each 384-well plate consists of 24 vertical columns and 16 horizontal rows. On every plate, 10 control wells with non-targeting siRNA (siCont) and 10 wells containing siRNA targeting KSR1 (siKSR1) are split evenly between columns 3 and 22 along with other control gene depletions (PPIB and PLK1) in the same columns above and below the siCont and siKSR1 wells as shown in the plate layout diagram (Fig. 3.5). The screen was performed in experimental batches because of the limitations in the size of the incubating shaker such that only eight plates could be processed at a time.

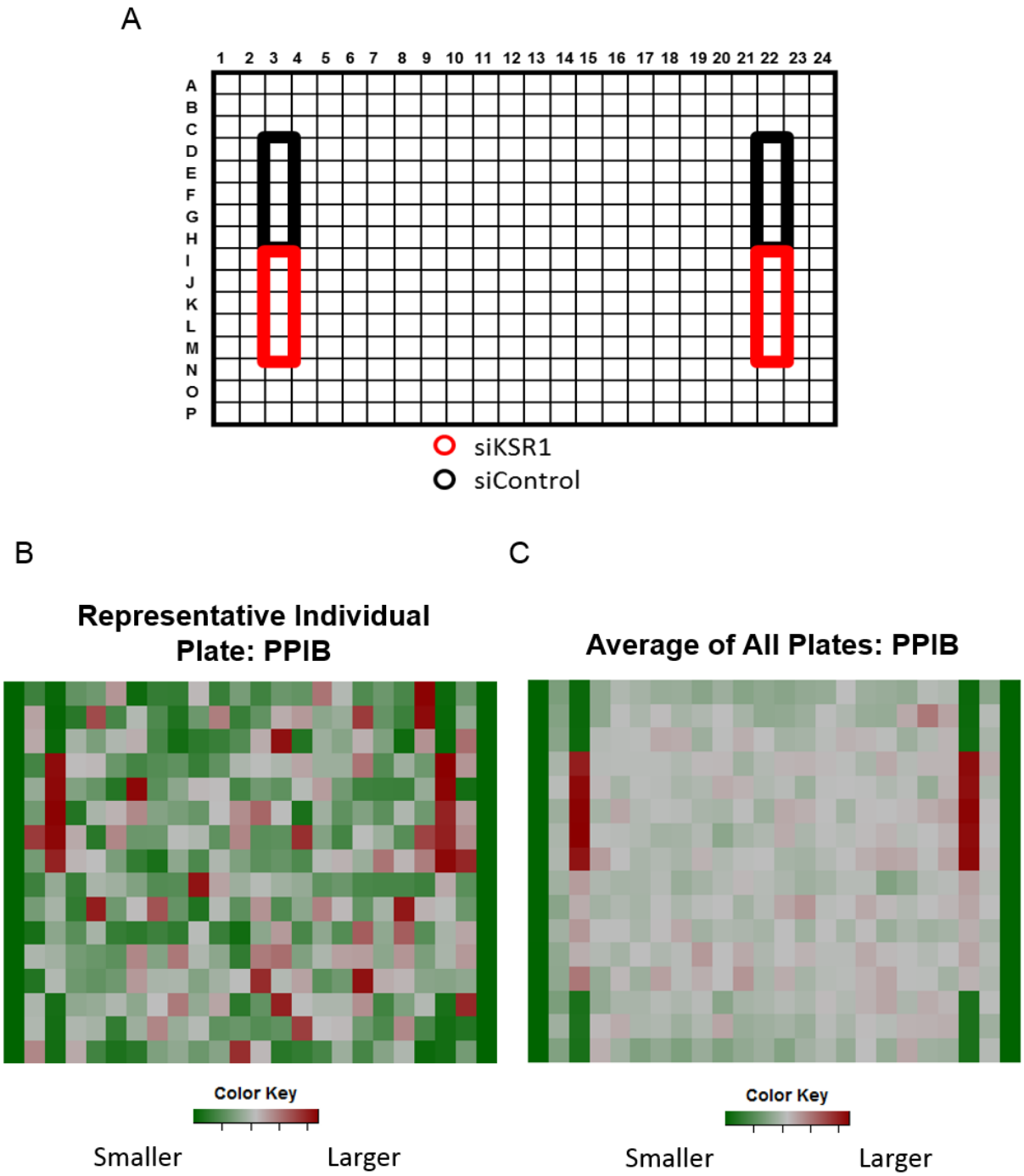

Fig. 3.5: FUSION screen 384-well plate layout. (A) Plate layout with control and KSR1-depleted wells in columns 3 and 22 shown in black and red, respectively. (B and C) Plate diagram heatmap with PPIB values from a representative individual plate (B) and average of all plates (C).

Quality Control: Probe Correlations

Ideally, the probes included in the gene expression-based signature will move independently and will not co-vary. To evaluate the covariation of probes, a pairwise comparison between each of the probes was performed. BNIP3 and NDRG1 had a correlation value of 0.84, while the remaining pairwise comparisons demonstrated correlations less than 0.7 (Fig. 3.6).

Quality Control: Experimental Consistency

Experimental variability was examined and visualized using the raw HPRT and PPIB gene expression. Replicate and plate consistency were evaluated using PPIB expression (Fig. 3.7). There was a high level of correlation between replicates (Fig. 3.7). Interestingly even though the same number of cells were plated in each experiment, there was significant variation between the PPIB ranges on different plates particularly between experimental batches (Fig. 3.7B). These differences were consistent between the three replicates (Fig. 3.7B). These effects are seen in the expression of all of the genes examined, but to differing degrees (Fig. 3.8). This could be due to different gene depletions being placed on each plate; however, this is highly unlikely as non-targeting siRNA and lethal controls appear on every plate and a large number of unique gene depletions are found on each plate. Examining the raw PPIB gene expression relative to the well type clearly demonstrates the ranges for the PPIB values fluctuate between plates and batches (Fig. 3.9). Reassuringly, background control wells and lethal controls have minimum PPIB values, while the non-targeting siRNA negative controls consistently have some of the highest PPIB levels. The positive control, KSR1-depleted wells sit between these two groups and demonstrate intermediate PPIB values and are intermixed within the other screened gene depletions (Fig. 3.9). Other possibilities that could explain the different PPIB ranges include the experimental cell growth being altered or probe signal intensity varying between plates or processing groups. Follow-up analysis demonstrated that the PPIB value was highly variable depending on the confluency or density of the cells on the stock plate prior to plating for the experiment. This suggests that the confluency of the cells was affecting whether the cells were in

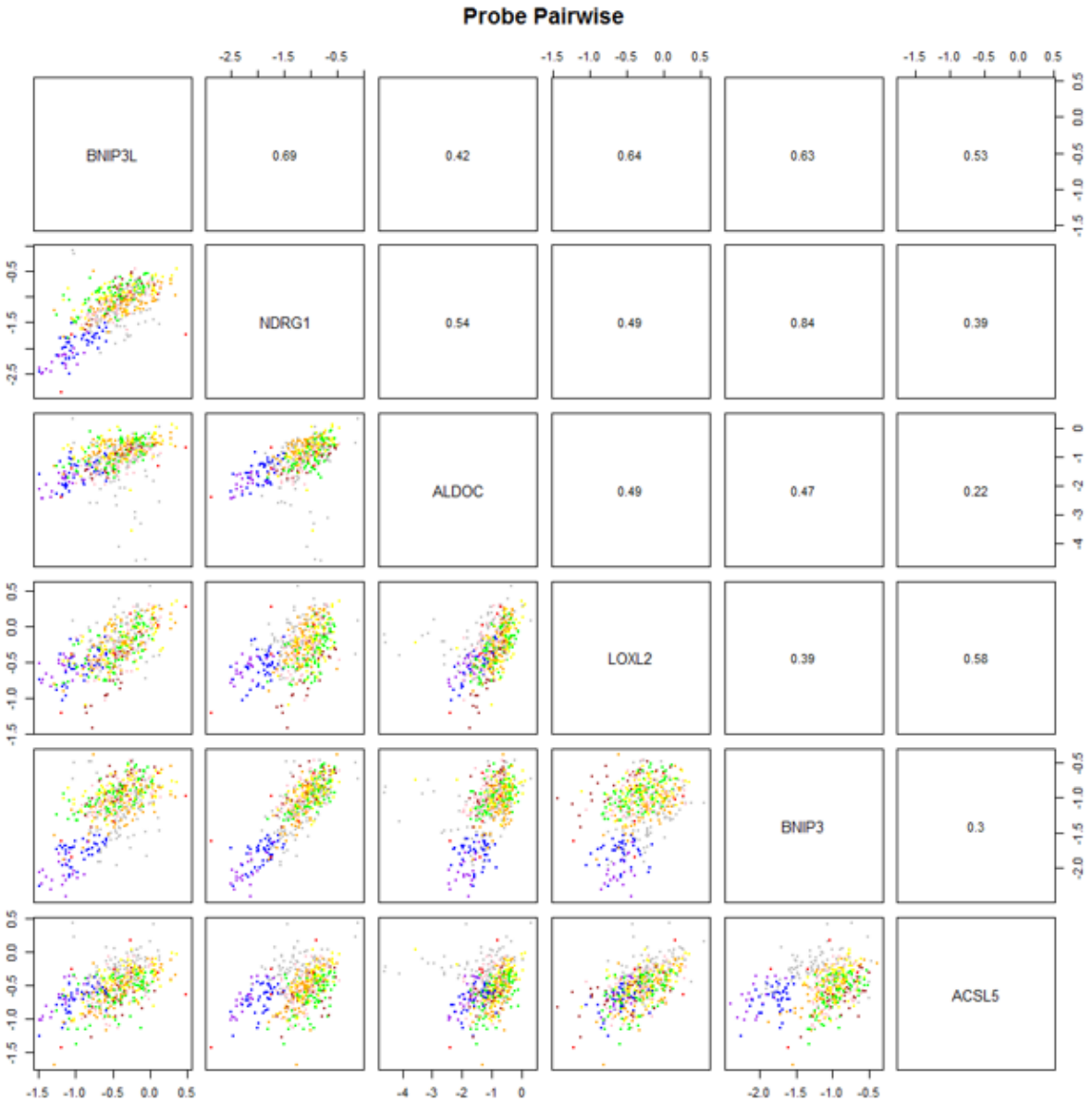

Fig. 3.6: Pairwise evaluation of gene expression-based signature probes. Correlation between gene expression for the six genes within the KSR1-depletion reporter genes BNIP3L, NDRG1, ALDOC, LOXL2, BNIP3, and ACSL5. Correlation values are designated in the top/right half above the diagonal and plots comparing the values are shown one the bottom/left half below the diagonal. Dot colors within the correlation plots represent the experimental group or batch.

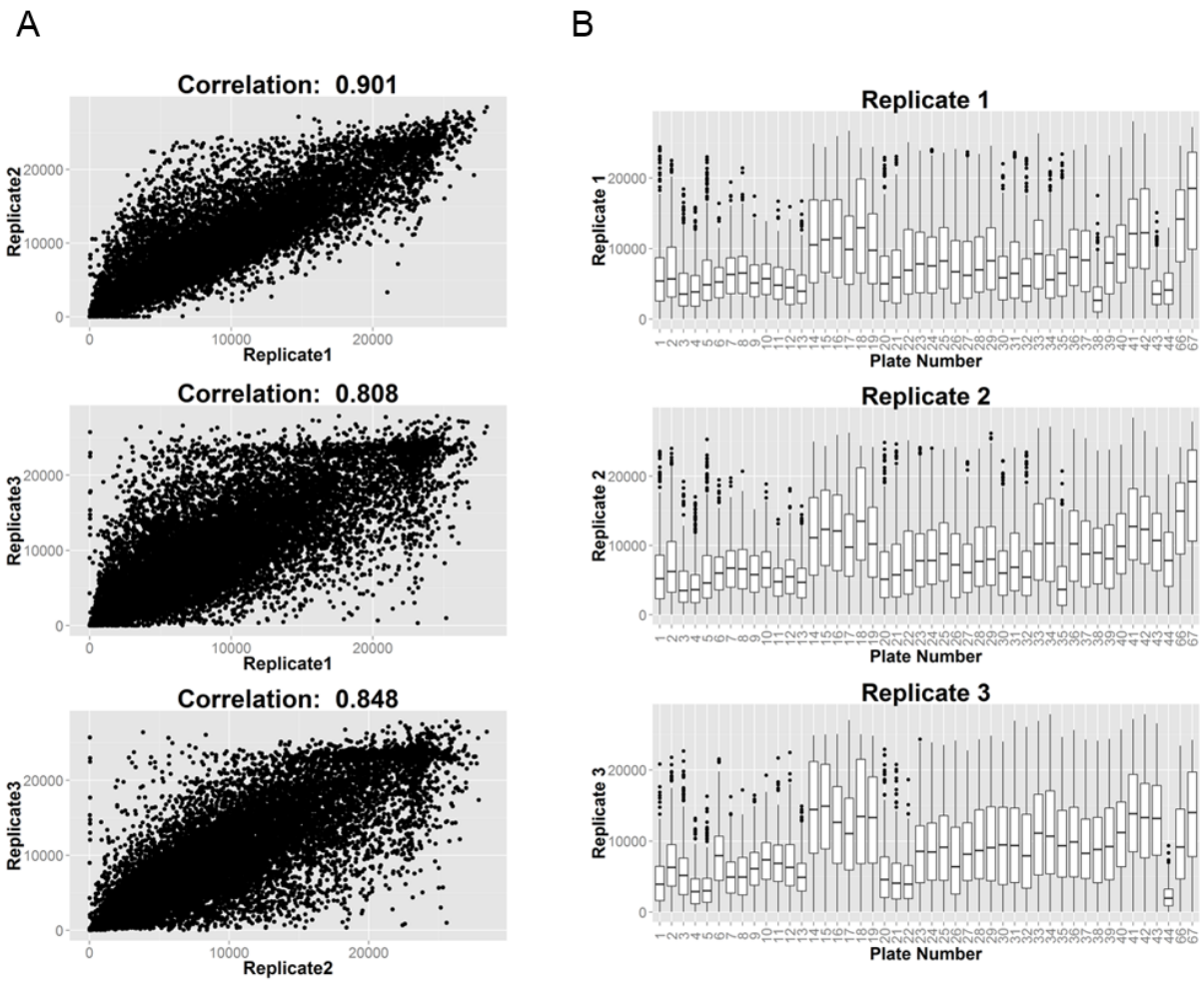

Fig. 3.7: Replicate and Plate Consistency. (A) Scatter plot and correlation between biological replicates. (B) Raw PPIB values for each replicate by plate.

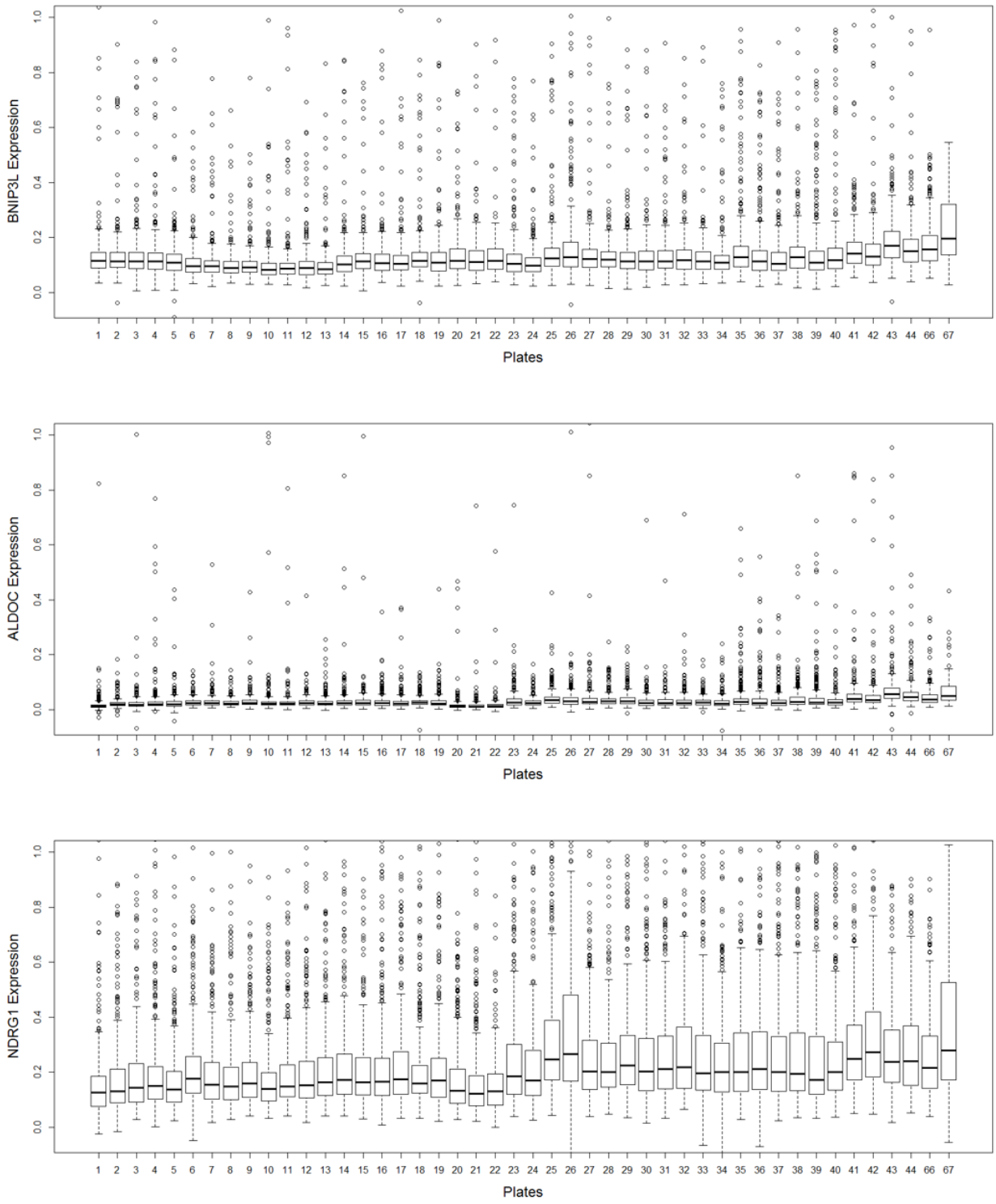

Fig. 3.8: Probe consistency across plates. Boxplot of BNIP3L, NDRG1, ALDOC, LOXL2, BNIP3, ACSL5, HPRT, and PPIB expression represented by plate. (Continued on the following pages).

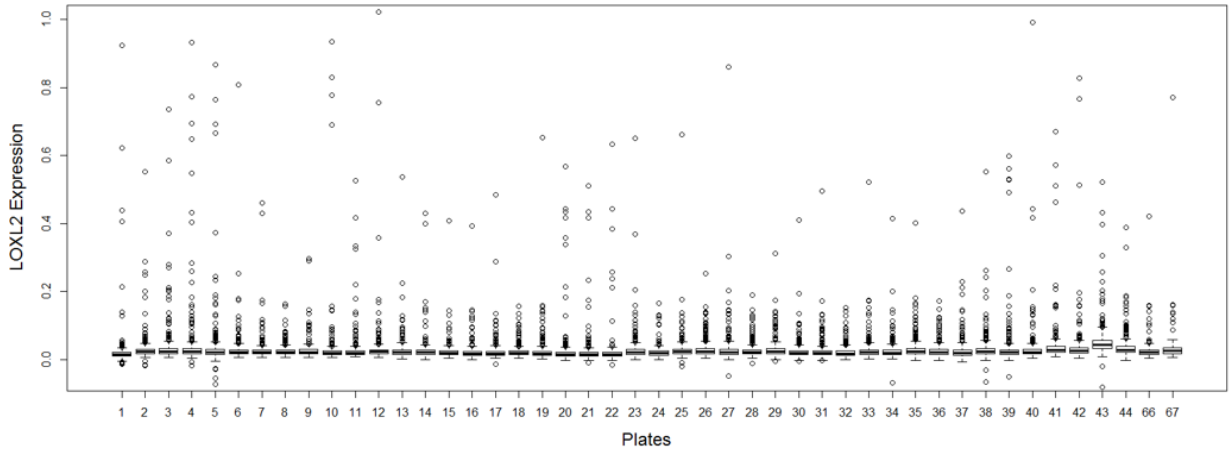

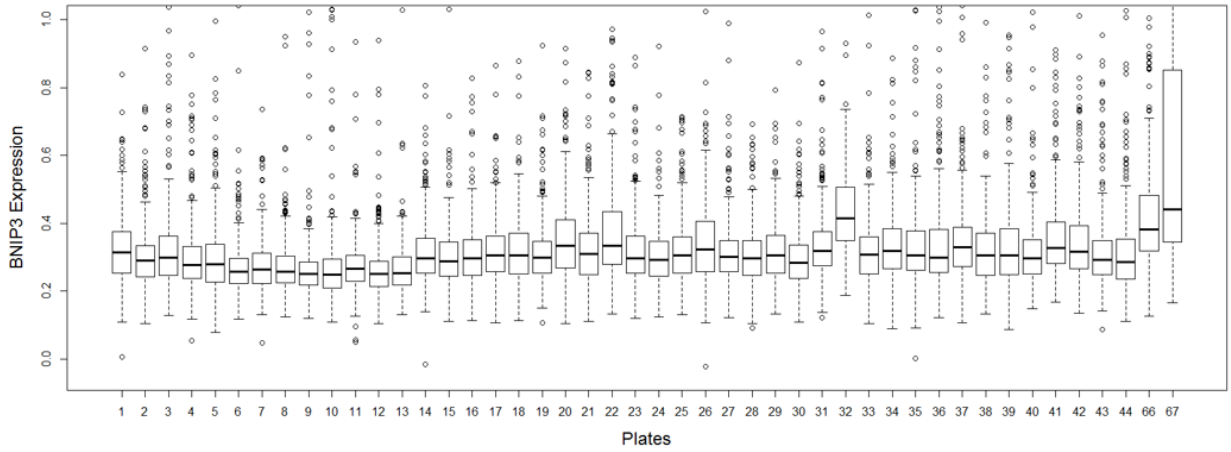

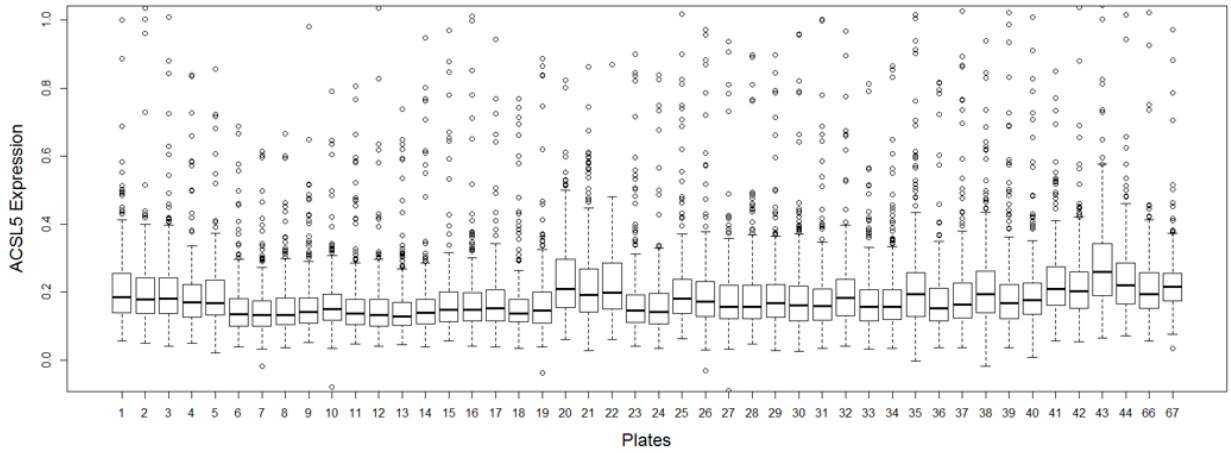

Fig. 3.8 Continued: Probe consistency across plates.

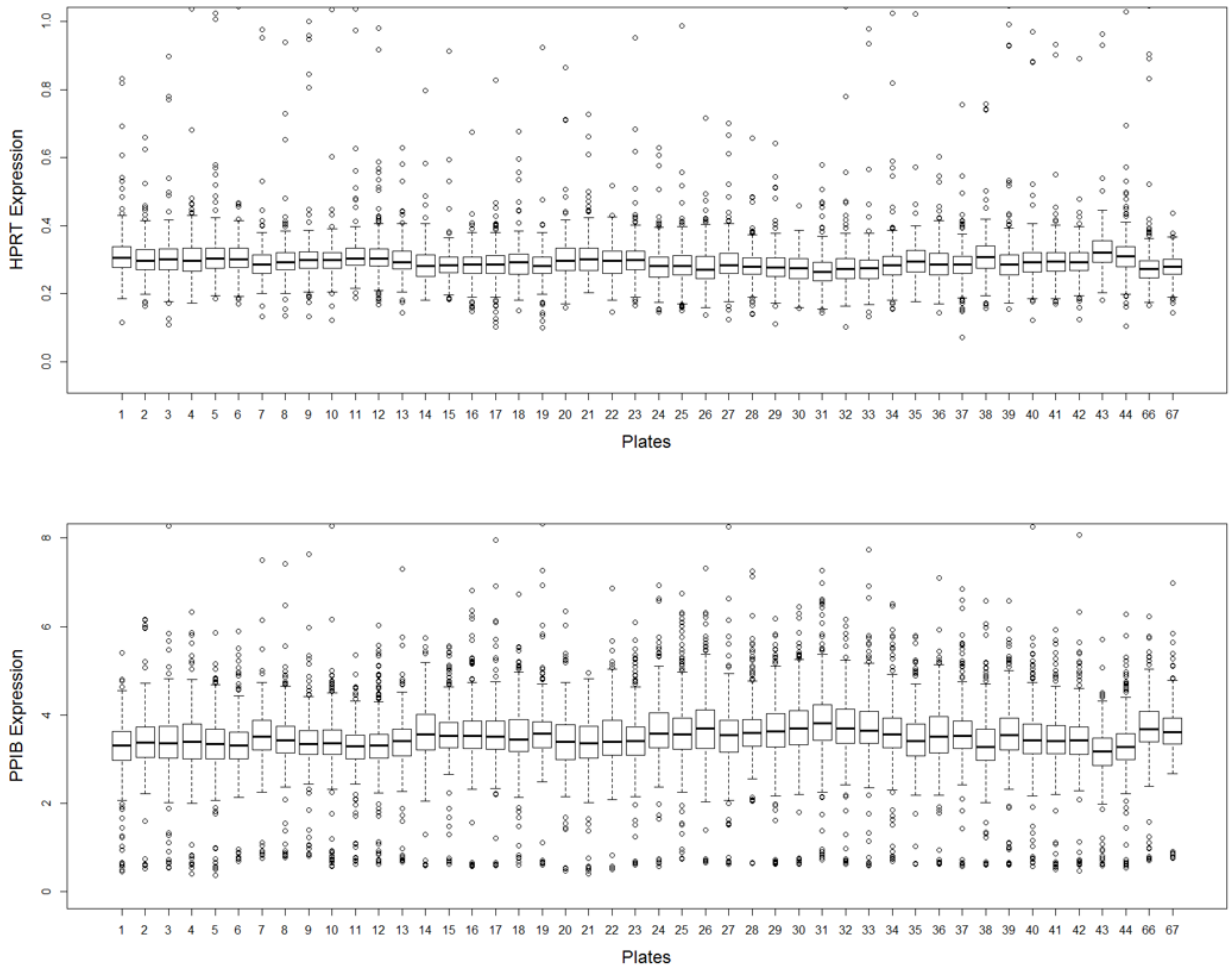

Fig. 3.8 Continued: Probe consistency across plates.

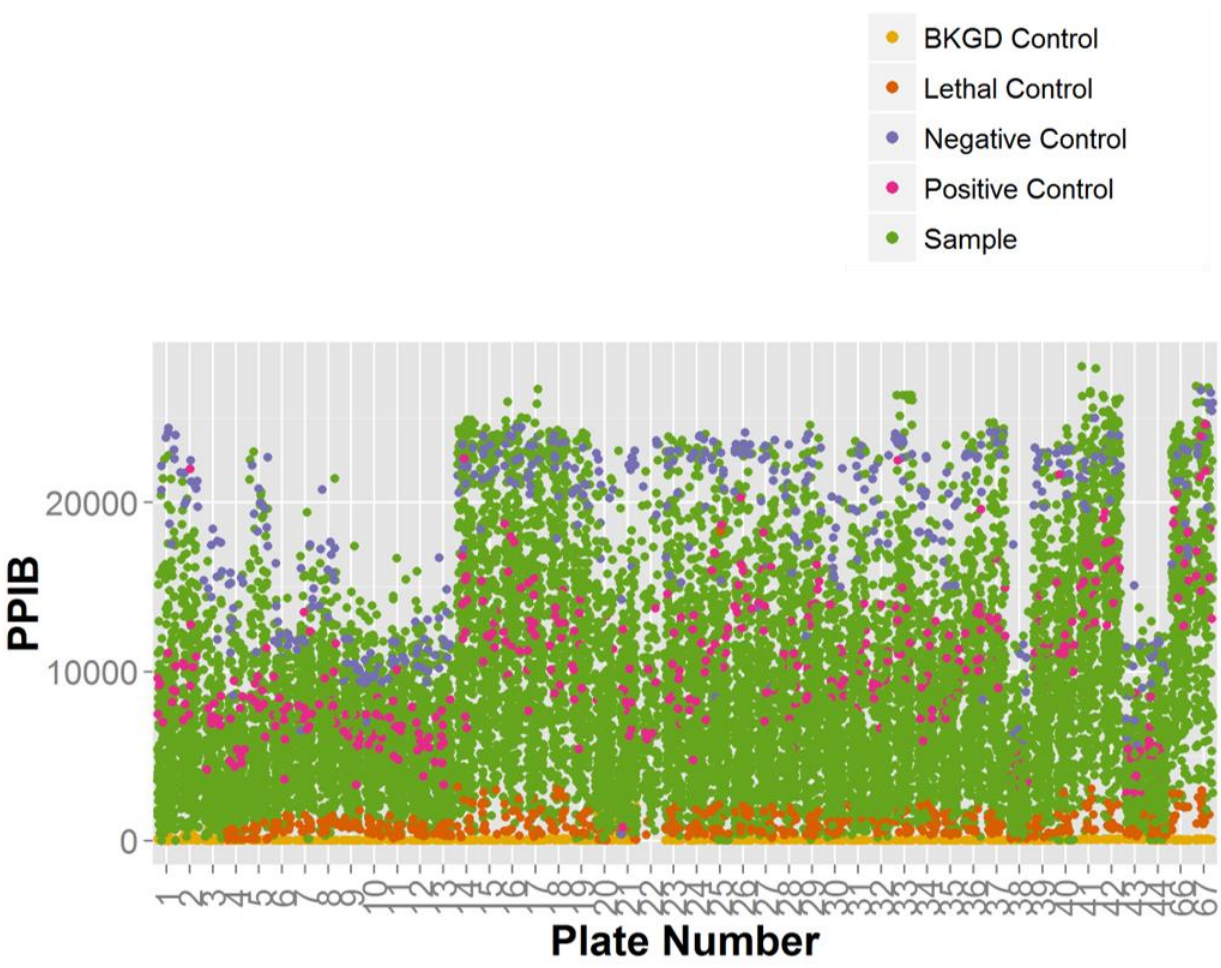

Fig. 3.9: Scatterplot of Raw PPIB values by well type. Average raw PPIB for the three biological replicates. Dot color represents the well type: BKGD control in yellow; Lethal control in orange; Negative control (non-targeting siRNA) in blue; positive control (KSR1-depleted) in pink; and siRNA library gene depletion in green.

a log growth phase or becoming senescent and highlights the importance of careful replication of all aspects of the experiment particularly when completing large-scale screens. Additionally, the reporters within the Quantigene system reported differently with different types of serum, which unfortunately was changed between groups of experimental plates.

The potential effect of plate position (*i.e.* plate row and column) was evaluated. PPIB showed a slight trend for increased values on edge rows and HPRT demonstrated an offsetting slight decrease in these rows resulting in no differences being seen in gene expression for any of the genes within the KSR1-depleted signature panel after PPIB- and HPRT-based geomean normalization (Fig. 3.10). More dramatic effects were seen in gene expression based on column (Fig. 3.11). Columns 1 and 24 were excluded from this analysis because they only contained background controls (Fig. 3.5 and Chapter 2: Materials and Methods). Columns 3 and 22 have lower readings in PPIB, NDRG1, and ACSL5, as well as a substantially increased range of values for BNIP3 (Fig. 3.11). This can be attributed to the effect of non-random plating in these columns (Fig. 3.5) as these two columns contained five non-targeting negative control wells, five KSR1-depleted wells, and six additional lethal controls.

Quality Control: Outlier Detection

Outliers were identified among the positive control (KSR1-depleted) wells and negative control (non-targeting siRNA-treated) wells (Fig. 3.12 and Fig. 3.13). Prior to algorithmic identification of outliers, visual examination of the PPIB expression in negative and positive control wells demonstrated a cluster with PPIB values less than 1000 on plates 20 and 21 (Fig. 3.12). This led to further examination of these wells, which revealed that they were blank wells and not negative or positive control wells despite being labeled as such. These wells were therefore no longer included as positive and negative controls. Algorithmic identification of outliers was performed for each plate individually for the negative controls and across each experimental batch for the positive control, KSR1-depleted wells using a Grubbs algorithm

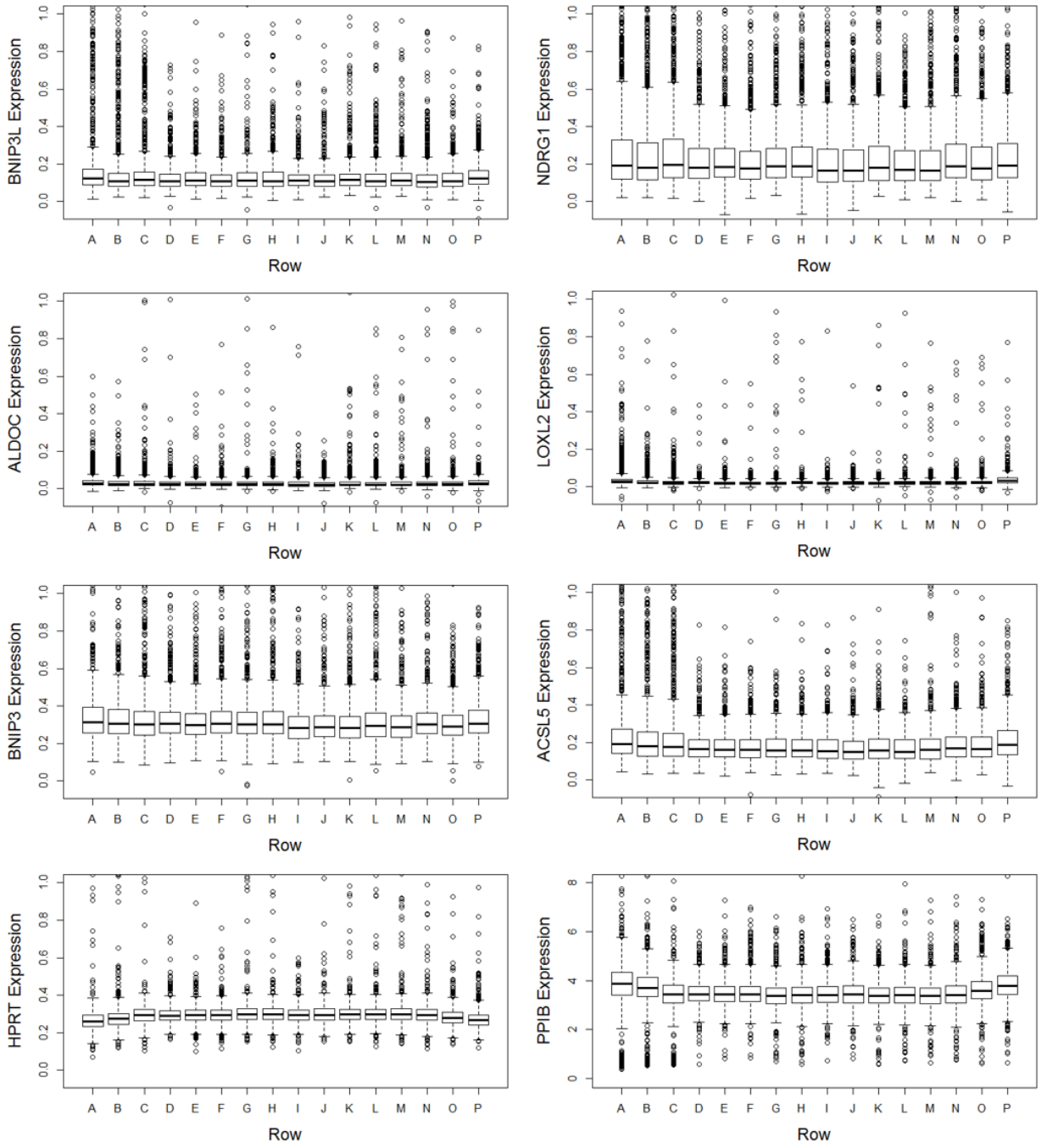

Fig. 3.10: Plate position effects evaluated by row. Boxplots of BNIP3L, NDRG1, ALDOC, LOXL2, BNIP3, ACSL5, HPRT, and PPIB expression represented by row.

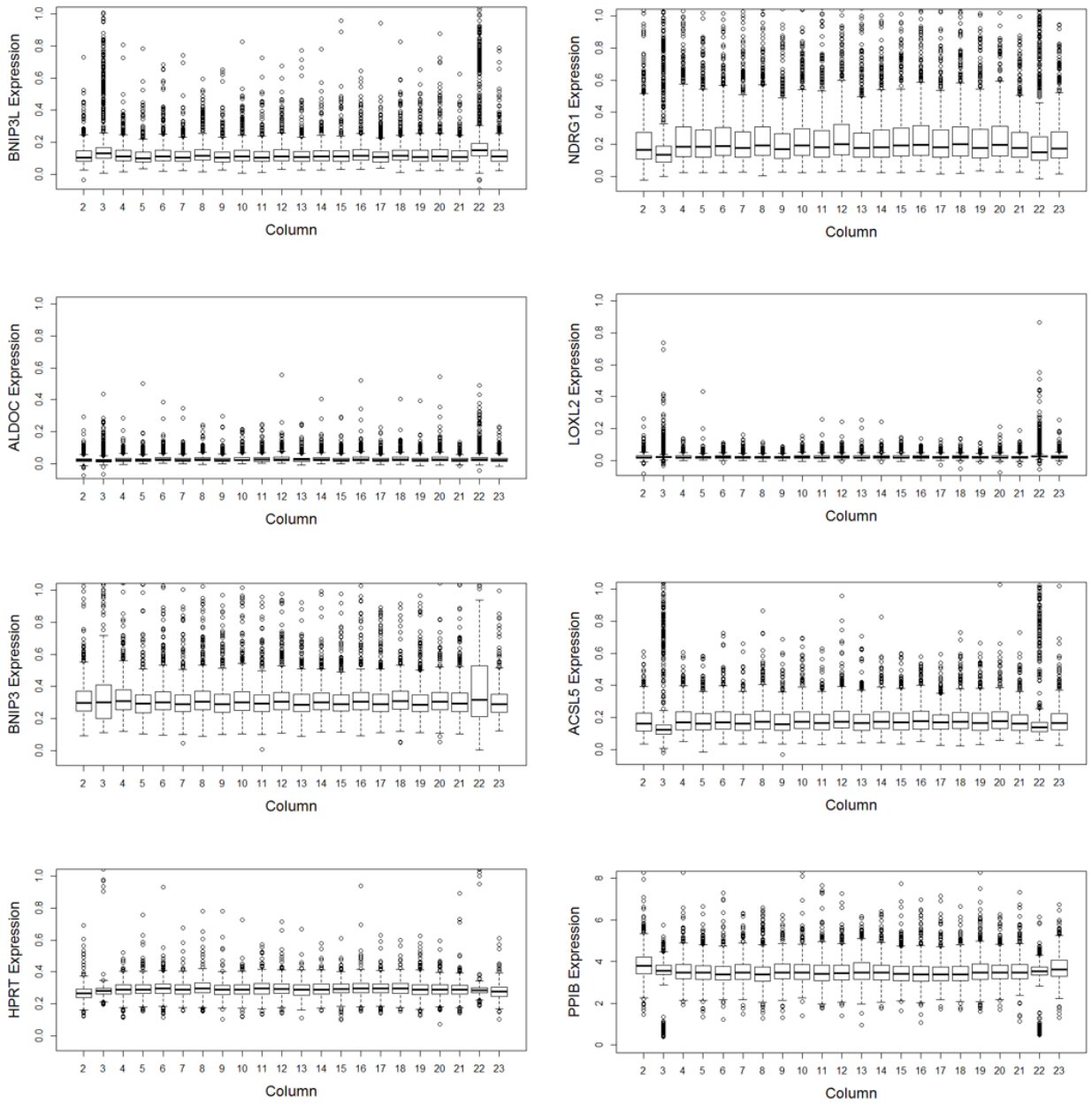

Fig. 3.11: Plate position effects evaluated by column. Boxplots of BNIP3L, NDRG1, ALDOC, LOXL2, BNIP3, ACSL5, HPRT, and PPIB expression represented by column.

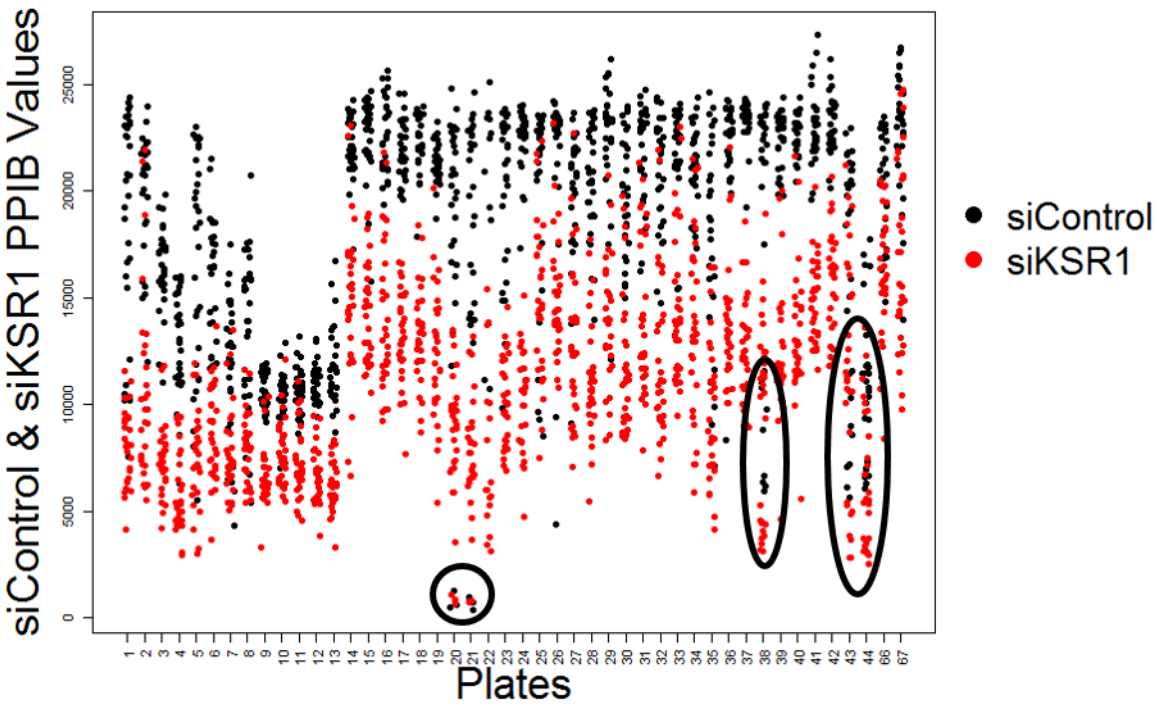

Fig. 3.12: Relationship between raw PPIB values of negative control (siControl) and positive control (siKSR1) wells by plate. Negative control wells are shown in black and positive control wells are shown in red. Circles designate outliers in plates 20 and 21 and a highly variable third biological replicate in plates 38, 43, and 44.

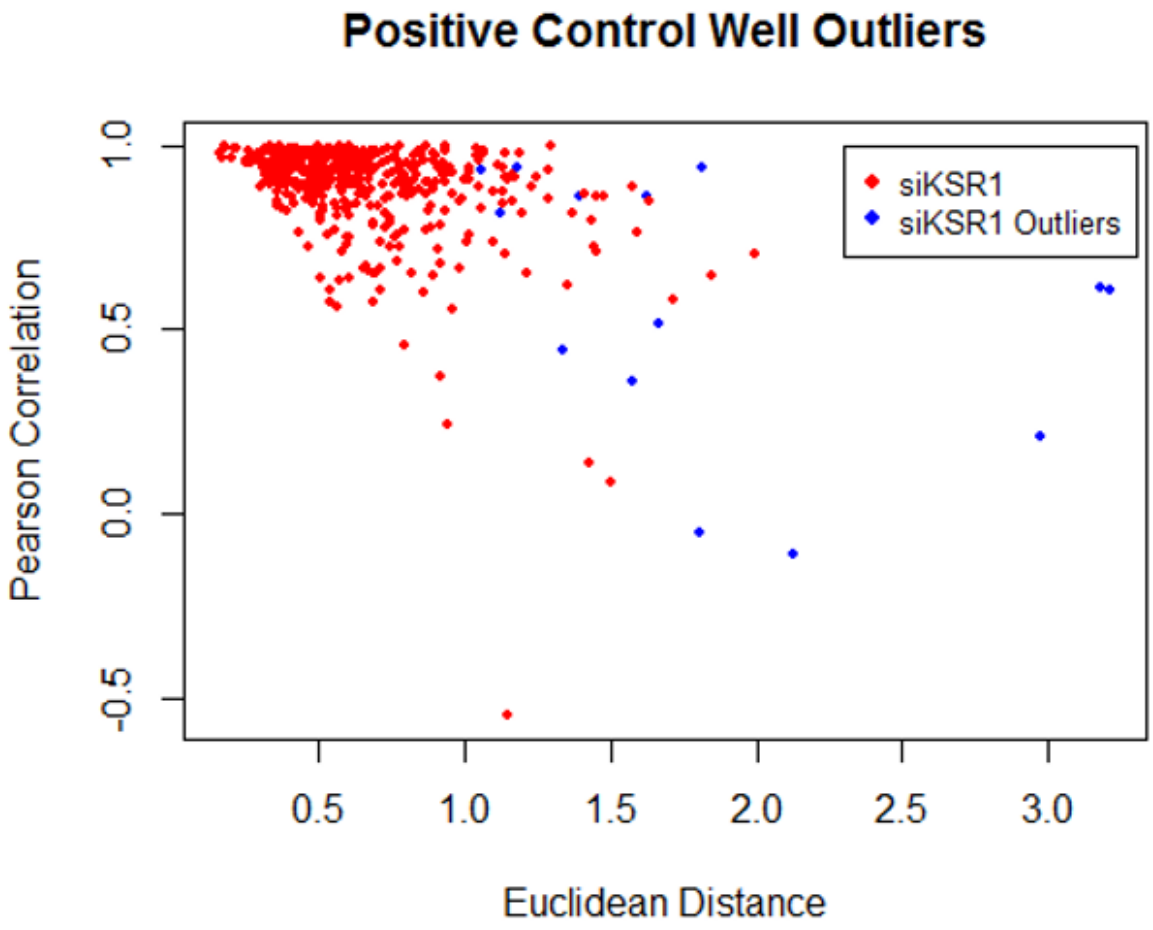

Fig. 3.13: Outliers identified in positive control wells using the Grubbs algorithm.

(described in Chapter 2: Materials and Methods). The Grubbs algorithm is based on minimizing the distance between samples, therefore, outliers were preferentially excluded if they had a higher Euclidean distance more so than a reduced level of correlation (Fig. 3.13).

Seventy-five outliers in control wells that were transfected with non-targeting siRNA were identified out of a total 452 negative control wells. Fifteen outliers were identified from the average of the three biological replicates for the KSR1-depleted wells. Examining each biological replicate individually, 30, 25, and 31 outliers were identified for the first, second, and third biological replicate respectively. This is out of a total 456 KSR1-depleted wells on 46 plates, such that each plate averages less than one KSR1-depleted well outlier and represents a 7% or less outlier detection rate for these repeated wells.

Outliers for each individual RNAi-mediated gene depletion were visualized based the standard deviation between the three biological replicates using a heatmap shown by plate position (Fig. 3.14). These were not immediately excluded from further analysis, but their presence identified the need for a filter based on consistency in results between the three biological replicates.

FUSION Normalization

The genome-scale screen represented a substantial increase in complexity over the original kinome-only screen, and the original method of normalization was not designed to handle this complex, variable data set. Therefore, over 100 algorithmic variations following the same general pattern of data validation and initial processing, normalization, outlier identification of non-targeting control and KSR1-depleted wells and removal, generation of the siKSR1 target, and similarity evaluation were evaluated. Several of these steps could be completed across all of the data, by experimental batch, or on a plate-by-plate basis, which contributed to the high number of algorithmic variations evaluated.

Normalization methods typically include normalizing to the mean/median of all samples for a given probe based on the Z-score or variation of this method, normalizing to plate position,

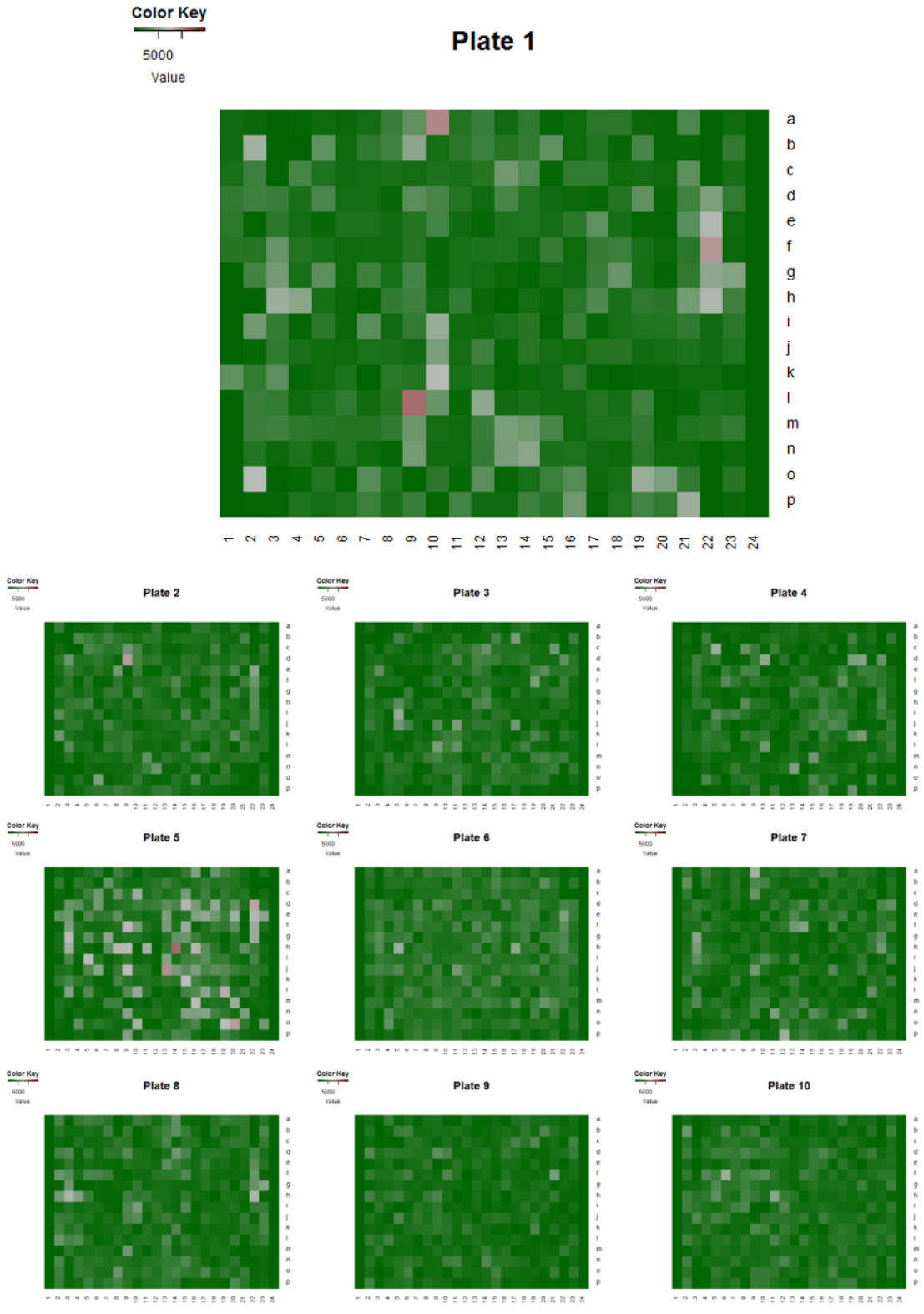

Fig. 3.14: Identification of outliers was performed by evaluating the standard deviation between the PPIB values on the three biological replicate plates. Plate layout heatmap representing the standard deviation for each knockdown between the three biological replicates. Green depicts a lower standard deviation and red depicts a larger standard deviation. (Continued on the next pages).

Fig. 3.14 Continued: Identification of outliers was performed by evaluating the standard deviation between the PPIB values on the three biological replicate plates.

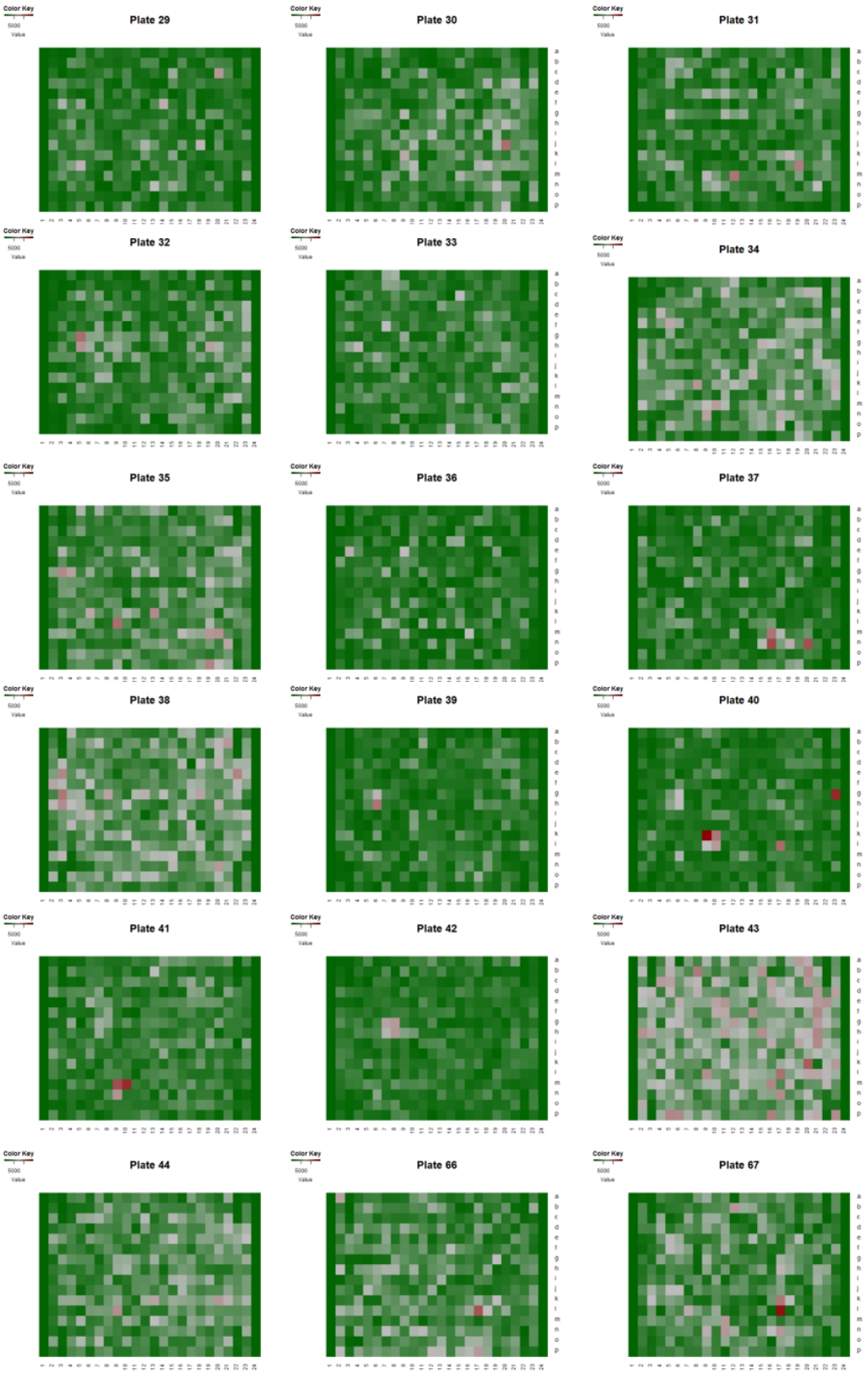

Fig. 3.14 Continued: Identification of outliers was performed by evaluating the standard deviation between the PPIB values on the three biological replicate plates.

or normalizing to positive or negative controls. Each of these methods has pros and cons and should be selected for utilization based on the specific biologic question being asked and the experimental design being employed. The methods of normalization that were examined included normalizing based on plate median values, by plate position, or to control wells all with log base 2 transformation. Each of these methods were evaluated using the ranking of the previously validated kinome hits (accuracy), evaluating the effects of analyzing the kinome vs the entire genome-scale screen (scalability), and confirming the KSR1 depletion wells demonstrated high similarity based on Euclidean distance and Pearson correlation similarity measures (precision).

FUSION Normalization: Reporter Median

First, normalization to reporter median was evaluated (Fig. 3.15). This was the method originally used to analyze the pilot kinome screen data that successfully identified multiple genes that were biologically validated and shown to be selectively required for colon cancer cell survival. To assess the validity of the screen algorithms, three measures were used: accuracy, precision, and scalability, which are fully described in Chapter 2: Materials and Methods. Unfortunately, the previously validated hits dropped dramatically demonstrating a low accuracy (Fig. 3.15A). To measure precision, the ability for siKSR1 replicates to cluster was evaluated, which in this algorithm was satisfactory (Fig. 3.15B). Last, scalability was examined. In this case, the scalability is low because the analysis depends on all plates being on the same range and assumes the median on each plate is and should be the same (Fig. 3.15C). However, based on the experimental setup (non-random plate assignments based on the siGenome library), there is no expectation that all of the plates should be the same (i.e. the median on one plate could be the minimum or max for another). Based on the poor performance of this normalization method, additional methods were evaluated.

FUSION Normalization: Plate Position

Our collaborators initially chose to pursue normalization based on plate position based on

A

Accuracy

Biologically Validated Hits (Original Rank in Kinome)	Dist. Rank	Corr. Rank	Euc. Dist.	Pearson Corr.
DYRK1A (#1)	4272	949	1.690	0.673
PRKAG1 (#10)	5700	781	1.878	0.703
EPHB4 (#7)	1278	860	1.221	0.689

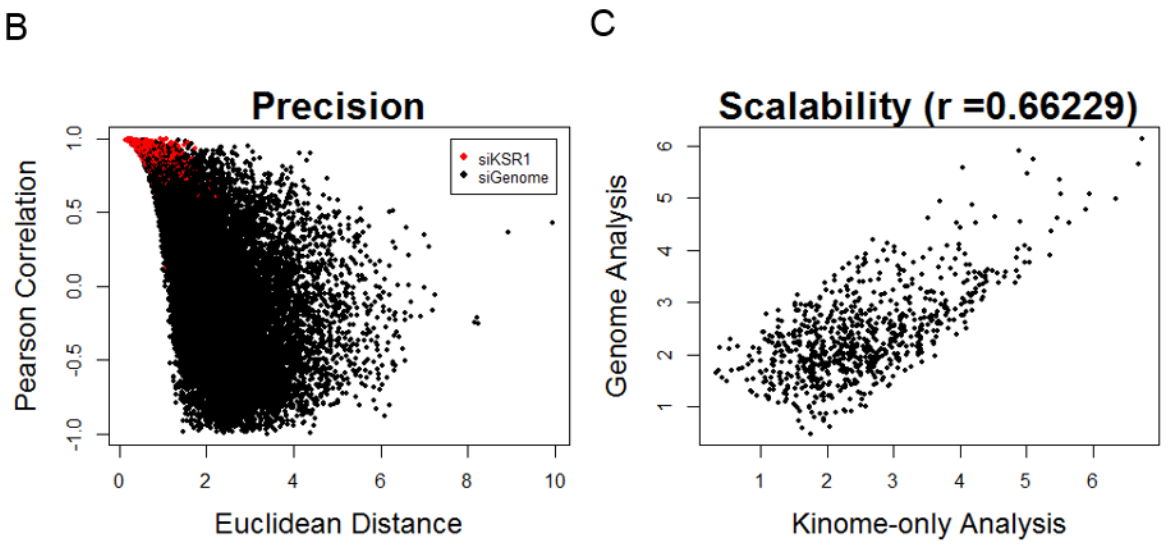

Fig. 3.15: Evaluation of median reporter normalization based on accuracy, precision, and scalability. (A) Table containing the Euclidean distance and Pearson correlation rank and values for three previously biologically validated hits: DYRK1A, PRKAG1 (AMPKγ1), and EPHB4. (B) Scatterplot of positive control (KSR1-depleted) wells shown in red and individual gene depletions from the siGenome library shown in black based on Euclidean distance and Pearson correlation similarity metrics. (C) Scatterplot and correlation of the Euclidean distance metrics for the kinome data after normalizing only the kinome or analyzing the entire genome.

the plate positional effects they were seeing particularly in regard to the column assignment. This was prior to the recognition that these effects could largely be attributed to the non-random plating (i.e. control wells being assigned to the same column on each plate) (Fig. 3.5). Unfortunately, this normalization method also demonstrated very low accuracy (Fig. 3.16A) and almost no precision (i.e. there was no correlation between the KSR1-depleted wells) (Fig. 3.16B), which was very concerning as the identification of hits is predicated upon their similarity to KSR1-depleted wells. If the repeated KSR1-depleted wells were not similar to each other, it would be very difficult, if not impossible, to identify additional genes that could be described as KSR1-like. In retrospect, the distribution of KSR1-depleted wells could have been predicted based on this normalization scheme in conjunction with the knowledge that the KSR1-depleted wells all reside in one column. Therefore, normalizing in any way based on column position, forces these wells to be evenly assigned across a normal distribution, which pushes them to have very little similarity with each other. This method does have nearly perfect scalability between the kinome- and genome-scale screens. This is expected as normalization based on plate position for each individual plate, is not affected or altered by the addition of more plates resulting in the outcomes from each plate being completely independent from the other plates analyzed resulting in perfect scalability (Fig. 3.16C).

FUSION Normalization: Normalize to Controls

Finally, the method of normalizing to control wells was evaluated (Fig. 3.17). This method intuitively makes sense in the context of the biological experiments because it is consistent with how the reporters were initially chosen (represents a difference between an siControl well and siKSR1 or other individual gene knockdown), it takes into account experimental differences (plate to plate or group to group), and it does not require any assumptions be made about randomness of plating. Normalization based on the median of the negative control (non-targeting siRNA) wells for each individual plate demonstrated high accuracy, precision, and scalability (Fig. 3.17). Therefore, it was selected for future analysis.

A

Accuracy

Biologically Validated Hits (Original Rank in Kinome)	Dist. Rank	Corr. Rank	Euc. Dist.	Pearson Corr.
DYRK1A (#1)	10029	787	1.645	0.762
PRKAG1 (#10)	4200	6225	1.028	0.138
EPHB4 (#7)	3896	98	0.996	0.927

B

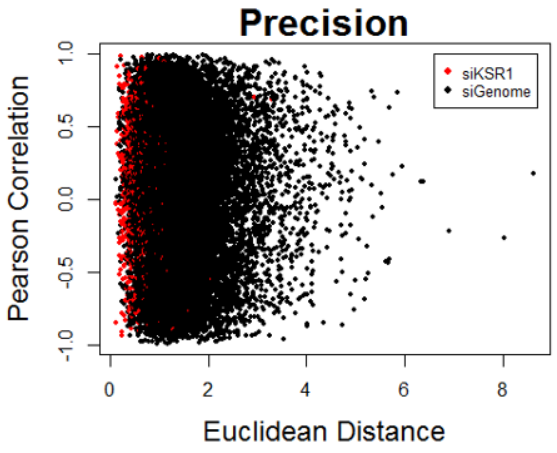

C

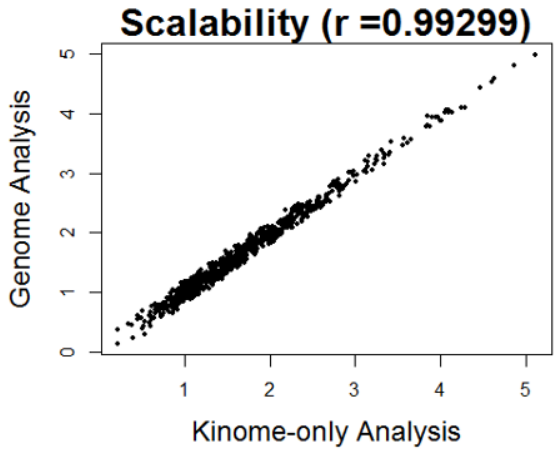

Fig. 3.16: Evaluation of plate position normalization based on accuracy, precision, and scalability. (A) Table containing the Euclidean distance and Pearson correlation rank and values for three previously biologically validated hits: DYRK1A, PRKAG1 (AMPKγ1), and EPHB4. (B) Scatterplot of positive control (KSR1-depleted) wells shown in red and individual gene depletions from the siGenome library shown in black based on Euclidean distance and Pearson correlation similarity metrics. (C) Scatterplot and correlation of the Euclidean distance metrics for the kinome data after normalizing only the kinome or analyzing the entire genome.

A

Accuracy

Biologically Validated Hits (Original Rank in Kinome)	Dist. Rank	Corr. Rank	Euc. Dist.	Pearson Corr.
DYRK1A (#1)	1	1	0.280	0.987
PRKAG1 (#10)	200	107	0.843	0.895
EPHB4 (#7)	211	20	0.852	0.966

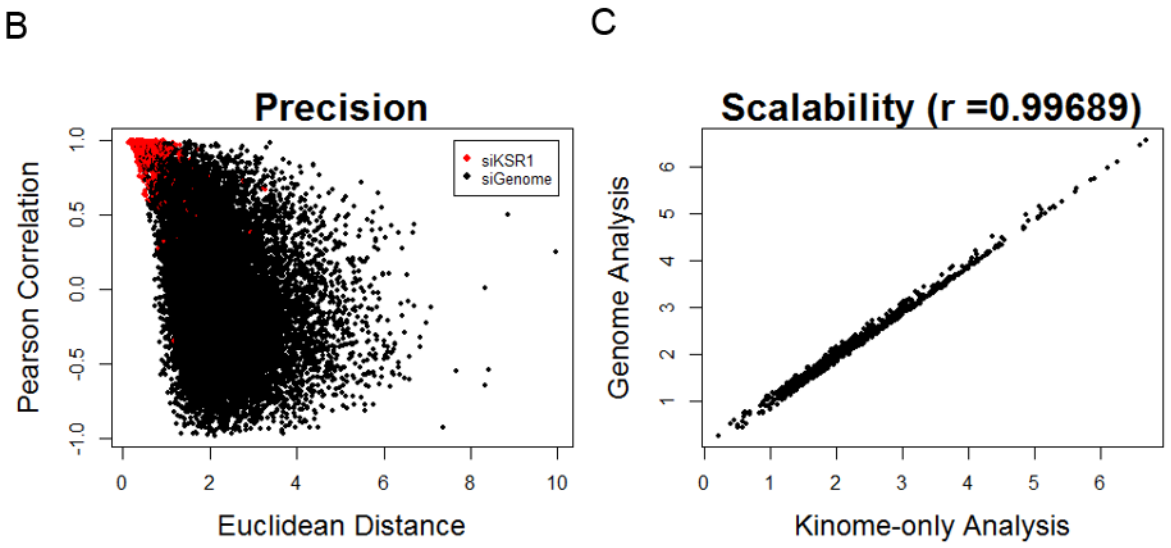

Fig. 3.17: Evaluation of negative control normalization based on accuracy, precision, and scalability. (A) Table containing the Euclidean distance and Pearson correlation rank and values for three previously biologically validated hits: DYRK1A, PRKAG1 (AMPKγ1), and EPHB4. (B) Scatterplot of positive control (KSR1-depleted) wells shown in red and individual gene depletions from the siGenome library shown in black based on Euclidean distance and Pearson correlation similarity metrics. (C) Scatterplot and correlation of the Euclidean distance metrics for the kinome data after normalizing only the kinome or analyzing the entire genome.

FUSION Output

The positive control target was established by averaging the positive control (KSR1-depleted) wells after the exclusion of outliers. Based on this target, the FUSION analysis provides a ranked list of genes based on two similarity metrics, Euclidean Distance (ED) and Pearson Correlation (PC). Empirically, other targets with both a high correlation and a low distance were the most likely to validate. Therefore, linear regression analysis was used to establish a cutoff (PC > 0.25 X ED + 0.5) for KSR1 similarity based on the ED and PC values of KSR1- positive controls (Fig. 3.18A). Using this linear regression cutoff, 788 hits were identified from the genome-scale screen (Fig. 3.18B). Unfortunately, this is too many for follow-up biological validation (Table 3.2). One approach that could have been employed would have been to complete a follow-up screen comparing viability changes in HCEC and HCT116 cells with genetic knockdown using individual oligos. This would have limited off-target effects because the effect could be confirmed for multiple siRNAs as well as evaluating the selective toxicity to cancer as compared to normal cells. This approach, while commonly practiced and effective, is also very expensive and likely would still yield numerous promising targets. Instead, further bioinformatic analysis was applied to limit the hits.

Bioinformatic Analysis

In this screen, eliminating false positives was prioritized over reducing false negatives leading to a high degree of specificity, but lower sensitivity. Stringent criteria were established in an attempt to reduce wasted time and resources following up on false positives. To do this, the following factors were used as limiting criteria: viability (hits remaining = 662), precision (189), seed sequence off-target potential (157), and target expression level in HCT116 cells (81) and colon adenocarcinoma samples within The Cancer Genome Atlas (40) (Fig. 3.19). This was paired with gene set enrichment analysis (GSEA), Database for Annotation, Visualization, and Integrated Discovery (DAVID)-based KEGG pathway and GO term association, and Cytoscape pathway analysis.

A

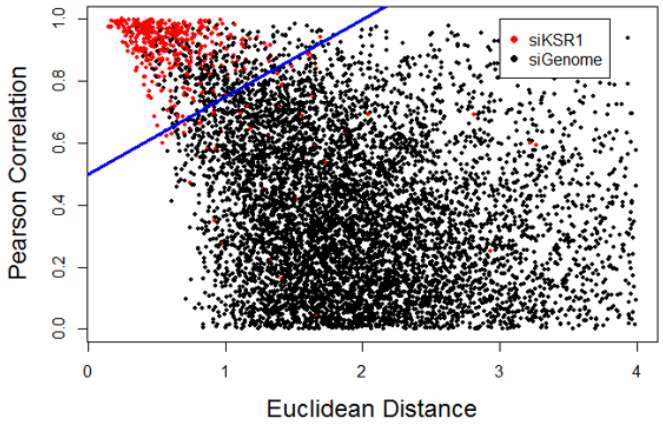

B

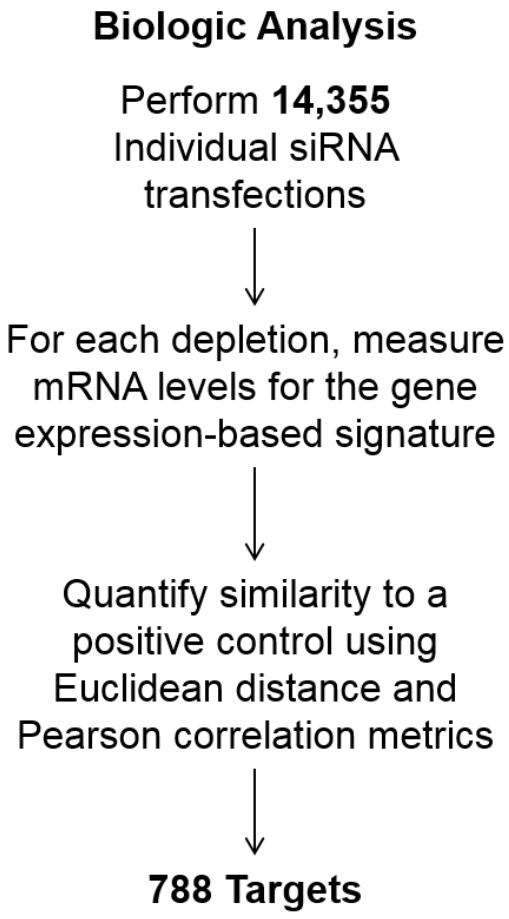

Fig. 3.18: FUSION identified 788 targets. (A) Scatterplot of positive control (KSR1-depleted) wells shown in red and individual gene depletions from the siGenome library shown in black based on Euclidean distance and Pearson correlation similarity metrics. The linear regression-based cutoff to specify hits based on Euclidean distance and Pearson correlation metrics is shown as a line in blue. (B) Flow chart of the FUSION screen that identified 788 targets.

NCOR2	UBASH3B	NPEPL1	NPL	ABTB2	KIAA0100	FPR1	APOL6
PPT1	DACH2	TEN1-CDK3	MYCBPAP	CHRNA5	ZCCHC9	ADRA1D	TXK
TACR3	CHCHD2	RAB21	HSPA9	NAP1L1	PTPN4	TCHH	CLPB
RGS19	ADIPOR1	CPB2	IFFO1	ZC3H14	CISH	ATP2A3	SPNS1
STK32A	PIP4K2C	NIM1K	HIAN2	GLIPR1L1	LPAR3	ABHD1	PODXL
SEMA7A	S100B	SFSWAP	CADM3	RNASEH2C	HCRT	TH	TMPRSS13
RGS12	CDH1	DEDD	TRO	ACAD11	PTCD2	DNAJC5	ST5
GPRC5B	PIGL	GIPC1	DLX3	PIK3CG	PLA2G12B	TMEM204	OR2B2
WDR5B	LPAR4	PPP1R16B	MRPL38	CSRNP2	THAP2	MRGPRX3	GLIPR1
TAS2R13	BAZ2B	JAM3	HSPH1	RGS4	ZBTB37	ATP5G2	HLA-DMA
LDOC1L	SRCT1	AKAP6	MYH9	ETV6	NFYA	CCDC136	PRODH
PAIP2	VN1R2	FYCO1	ADGRL3	NEK3	LDHC	PRR5L	IRX1
FAM172A	C15orf48	DYM	FLJ13105	PPP4R1L	AHNAK	OR51B4	KIN
LGALS2	RBM5	LPO	PI4K2A	FOSL2	NOS3	OR10H2	SELE
OR1E2	EVA1A	C19orf44	RGS2	ACSS3	CHIA	FGFBP2	P2RY8
LINC01547	NUDT4	ADGRE5	NSUN7	FOS	KRT84	FIBP	SH3D21
AADAC	PDCD2L	EPHB4	ADORA2B	TKTL2	RNASE7	MMAA	TMEM126A
PTGFR	VWA7	C4orf17	RNF128	HTR5A	TATDN1	CELSR2	AMELX
ACADM	ADGRL1	NKTR	HNF1A	ZBTB45	SIPA1	OR2C1	NPY5R
ZNF385D	TCFL5	ACKR4	APOC1	LPAR5	RHOH	AFTPH	VN1R1
TXNDC2	DLX6	NTNG2	RIOK3	MYH14	FGF9	EN2	NPIPA1
ZNF566	CNTNAP4	OR51E2	LRIG2	EFCAB1	SIGLEC11	ADO	SOD2
TAAR9	OR52A1	LPAR1	CCDC183	DMWD	AKIRIN2	BDKRB1	HK1
GPR183	PINK1	FKSG17	CCDC142	RHOXF2	ACYP2	PAX1	MARVELD1
FAR1	ZRANB3	OR1J2	DCAKD	RAB34	FAM136A	HOXC11	ANG
TNS1	GPR143	ATG12	MAS1L	OR2T1	ZNF394	ATP8B4	FRY
CARS2	LRRC27	EIF4EBP2	ADRA2B	OR3A2	ZNF541	MAGI1	MMP19
PTGER1	VIP	RHBDD1	SH3GL2	NPY2R	ZMYND8	TIMELESS	FAM167B
ADGRG1	MAF1	RIN1	IP6K1	NPVF	HSP90AA1	SYP	PLXNC1
PSG7	IL22RA1	JRKL	TCF19	OR7A17	FAM207A	TMEM156	APOPT1
ECE2	SDPR	ACTR10	MUC2	PCNA	NR3C1	CXCL8	KLF16
OPRM1	SEPP1	AARS	LRRC19	NEK6	SDCBP	COG8	CARD11
ZGPAT	SYT15	TAAR1	3-Sep	DHRS9	GABBR2	CLPTM1L	RPE65
MC1R	CERS1	VPS25	H3F3B	ZNF702P	RBM48	GPR162	CYSLTR2
TTTY5	NUDT16L1	SLC35G5	GNB1	OTX1	LGR5	MSMO1	KDM2B
CRIP1	RGP1	C14orf151	DDB2	ZMYND15	TAS2R4	UGT1A3	ESYT3
HTATIP2	OR2H1	NUBPL	GPR75	CDC42BPB	CLEC11A	FRMPD3	SEPT1
ENDOU	C12orf49	ARHGAP10	MEX3B	OR5V1	OR3A1	ARHGAP11A	HAS2
CSF3R	ASCL1	NRP1	DDX47	PDE1C	NEURL1	YIPF4	GABARAP
OR51E1	PRKAG1	BAALC	ALDH18A1	TCF7L2	APLNR	HBZ	GADD45B
TPM2	PTPRT	FYTTD1	NFIC	SLC7A6	GZMA	HNRNPD	TXNDC15
DUSP2	CYORF15B	HOXD1	PRDM13	RHOBTB1	MAP4K4	ETV4	PCDHB12
MAPK10	DYRK1A	APLF	PRSS27	BAD	OXTR	ALLC	ABLIM3
OR5P3	CRY1	GRWD1	TOMM40L	PPP1R14D	FARP1	RHNO1	FUBP3
OR2W1	MFSD7	CXorf36	ELAVL3	SLC25A2	ARFGAP2	KIAA1024	GLI1
PCDH17	TMEM222	TAAR8	SOCS1	CRHR1	DMXL1	SCO2	CKS1B
MC2R	FRS3	ZNF28	OR2A4	BACH1	DGAT1	RASL11B	RSPH6A
CDKN1A	TTLL2	PKN3	CIRBP	PARM1	MTCH1	TAAR2	ADRA1B
CDH19	VCAM1	ITIH5	MND1	ZNF557	SYTL1	RFK	C3orf20
TRPM7	MTNR1A	CXCL13	MAP2K7	SPIC	TAS2R14	ZSWIM5	DRD4

Table 3.2: List of 788 hits from FUSION.

OR13A1	PSENEN	TCERG1	NPPB	TBRG1	ITGA10	GATAD2B	CPSF7
ERLIN1	SPATC1L	BATF	RAB27B	TFB2M	TBX22	GTF2I	ABCC4
TBX2	HN1L	GRM2	PCOLCE	TUSC3	FGFBP1	RPRM	PRLHR
TPK1	SPINK7	GUCA2B	ZNF559	NLRP12	GPR1	CELF1	HORMAD1
ZNF528	HIST1H2AC	FGFR1	MMEL1	PEBP1	ANGPTL6	CTC1	SVEP1
NONO	DNAJC9	LGALS13	VIPR1	ARF6	ANKRD20A1	ADGRE1	EZR
LATS1	PIK3C2G	ABCG4	FAM126A	IL1B	ALKBH5	SND1-IT1	SLC35E2
PLCB4	PDZD7	GRK1	PCDHA3	SNED1	ZNF484	SNTA1	CD3E
NPTX2	FAM167A-AS1	PTP4A1	C7orf50	FSCB	C9orf78	SCD5	AMD1
NME3	RAB33B	GPR61	VBP1	CPT1B	KLHL22	GPR101	TM2D1
ADCYAP1R1	HPCAL1	PRH2	ABCG8	ADGRF3	SRY	TESK2	TAZ
DLX2	SNX2	C10orf76	POF1B	CDR2L	PTDSS2	FLJ10246	MEST
STXBP3	NMBR	PRSS1	ADRM1	SYCP1	FOXC2	ITFG3	KIRREL2
FOXP3	ARMC2	IGSF9	TMEM43	PTH1R	PROZ	CLMP	PNKP
FAAP100	MVK	PROP1	LGALS3BP	SLC22A16	LY6G5C	STAG3L4	CNFN
DLX1	LHCGR	HIST1H4I	RNF208	OR8B8	VGLL4	MS4A2	FGF13
FOXD1	HPR	PARD6G	MAPK8IP2	ASB13	CDKN1B	BTRC	EFNA2
SSBP1	TAS2R46	TAX1BP1	TMEM25	TNNC2	UBA5	GMPPA	WDR78
MON1A	IMMP2L	KRTAP9-3	CDKN3	MUS81	LRRTM4	SORT1	GTF2A1L
CFAP69	OXER1	BMP4	IGFBP5	KRCC1	ZDHHC8	ACTRT3	USP48
FER	RASGRF2	KLF13	PSG9	ECHDC3	KLK10	NFATC3	TNIP1
CMSS1	HOOK3	CHD6	ULK4	TSPYL5	SRSF4	FNDC1	NPFFR2
SLITRK2	RGS5	ZNF382	GSK3A	LRRC8D	MORN1	SLC10A7	TMEM185A
RALB	BMP2	TEAD3	CHKA	ARL3	LRRC37A2	PUM1	SPIRE2
METTL25	PIK3CG	DDA1	DDHD1	TAS2R16	HSPA1B	PAPD5	IFNG
PRKY	SHC1	ZNF397	PI4KA	ITPKB	C1orf115	LTBP2	CYP2A13
GARNL3	MAGT1	FLJ12595	CHRM1	TAS2R39	TEC	PKD2	PTGDR
ADIPOQ	RAP1A	ADGRA2	HSPB8	GRK7	GPR17	SPINK1	LUM
MT4	LY6K	SPATA16	TGM2	PDE4B	GCGR	FCAMR	CCNL1
B3GNT9	TNNI2	AATK	DRP2	WDR24	PHC2	HNF1B	GABRG1
HFE	FSCN2	QDPR	GNAZ	TEKT2	GPR6	EMC6	TBCK
MAPK7	TSEN2	TRAF7	GNG11	PRICKLE3	CHST15	VRK1	FZD1
BCO2	RGS9	S1PR5	RGS1	TSN	PAQR8	MDS1	IRX3
GNRH1	FAM155B	HKDC1	EIF4G2	ARPP19	RPP30	DEFB4A	CDH5
MATK	ZNF395	NODAL	HSH2D	LRRC61	CD40	KCNIP3	ADORA3
SPIRE1	MRI1	RASD1	ZFYVE21	CCR4	FRMD8	ZNF124	GFI1B
ZNF84	RFXANK	CDK20	PECR	FAM184A	C10orf2	MFSD5	FLJ14054
OR3A3	PIK3R1	L3MBTL3	HAND1	GPR82	GP2	MEFV	PSD2
KLHL1	RHOBTB2	ZXDC	MPV17L2	ACSF2	SPARC	FAM134B	
NUDT2	TBL1XR1	SSTR4	SCTR	FAM167A	RPL7A	POLR3GL	
TRABD	NR1D1	CDC2L2	QRICH2	EGR4	SPATA9	LPAR2	
OR6A2	ENTPD7	GFM2	IL17RB	PTPRJ	STRN	GABPA	
CHCHD5	BBC3	ADORA3	NEK4	ADGRB2	KISS1R	MICA	
IQCG	FZD10	ARSJ	PAX5	ROM1	AMIGO1	MACC1	
XCL2	TAAR6	GPR160	MYH11	DRC7	PCDHB10	MMRN2	
GARS	PLEKHA1	ZNF182	UQCR10	CXCL3	NR4A2	IL27RA	
SCN9A	AMMECR1L	NTSR1	LY6H	ZBTB22	SLC46A2	MINA	
GNG3	MRGPRX4	PKN1	MTERF2	POLE	NPHS1	TNFSF15	
DRD1	FAM118B	CSTF3	C11orf63	PPP1R14C	BMX	INPP5E	
GPR55	P2RY14	TMEM11	GNAI3	LAT1-3TM	PQLC1	RAC1	

Table 3.2 Continued: List of 788 hits from FUSION.

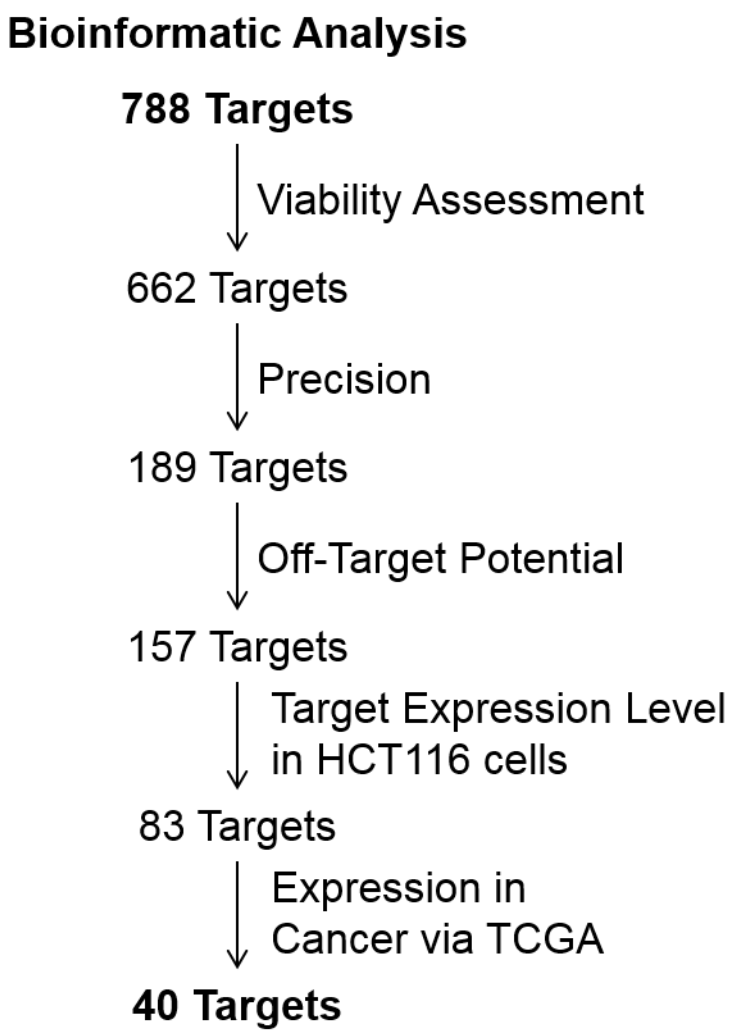

Fig. 3.19: Flow chart of prioritizing targets using bioinformatic filters that limited the FUSION-identified 788 to 40 hits.

This approach was based on the idea that the FUSION analysis suggests these genes relate, so gene set enrichment analysis or the evaluation of pathways and functionally related genes that are enriched at the top of the results allows us to focus on the most promising hits.

Bioinformatic Analysis: Filtering the Results

The viability filter cutoff was a PPIB decrease of greater than 20% in the average of the replicates. This reduced the number of hits approximately 15% or from 788 to 662. Based on the earlier identification that in a few cases significant variability occurred between the three biological replicates within the screen (Fig. 3.14), precision, or consistency of results was added as a metric to filter out potentially false positive results. The criteria used that the maximum difference between the three biological replicates of an identified hit must be less than 0.6 for Euclidean distance and 0.2 for Pearson correlation to be considered further. This reduced the number of hits dramatically from 662 to 189.

The results were then evaluated for the presence of enrichment of certain seed sequences within the siRNAs targeting the top results from the screen (Fig. 3.20). This was completed using two independent algorithms: Common seed analysis (CSA)[104] and Genome-wide enrichment of seed sequences (GESS)[105]. Criteria were imposed such that results that were identified using either method as potentially being hits due to seed sequence effects were excluded. This reduced the number of hits from 189 to 157.

Finally, the expression of the identified hits was evaluated in HCT116 cells based on microarray analysis and in colon tumors based on TCGA. To pass the microarray expression filter, the gene had to be designated as being “Present”. The TCGA-based filter required that genes had greater than 150 RSEM expression. These cutoffs reduced the number of hits to 83 and then to 40, respectively (Table 3.2).

Bioinformatic Analysis: Gene Set Enrichment Analysis (GSEA)

The Gene Set Enrichment Analysis (GSEA)[106-108], maintained by the Broad Institute of

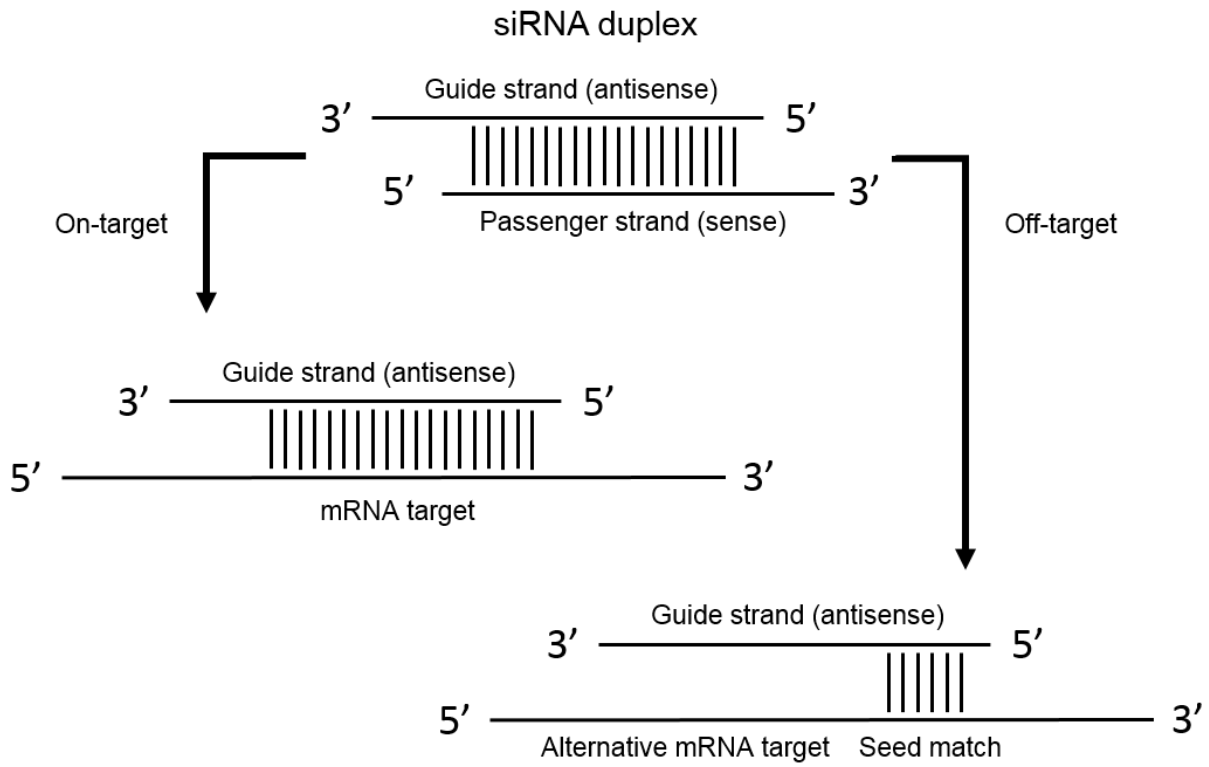

Fig. 3.20: Seed sequence off-target effect diagram.

Symbol	Gene Name
PPT1	palmitoyl-protein thioesterase 1 [HGNC:9325]
ECE2	endothelin converting enzyme 2 [HGNC:13275]
CRIP1	cysteine-rich protein 1 (intestinal) [HGNC:2360]
TPM2	tropomyosin 2 (beta) [HGNC:12011]
CHCHD2	coiled-coil-helix-coiled-coil-helix domain containing 2 [HGNC:21645]
TCFL5	transcription factor-like 5 (basic helix-loop-helix) [HGNC:11646]
DEDD	death effector domain containing [HGNC:2755]
EPHB4	EPH receptor B4 [HGNC:3395]
ACTR10	actin-related protein 10 homolog (S. cerevisiae) [HGNC:17372]
AARS	alanyl-tRNA synthetase [HGNC:20]
GRWD1	glutamate-rich WD repeat containing 1 [HGNC:21270]
HSPH1	heat shock 105kDa/110kDa protein 1 [HGNC:16969]
TCF19	transcription factor 19 [HGNC:11629]
GNB1	guanine nucleotide binding protein (G protein), beta polypeptide 1 [HGNC:4396]
CIRBP	cold inducible RNA binding protein [HGNC:1982]
MAP2K7	mitogen-activated protein kinase kinase 7 [HGNC:6847]
NEK3	NIMA-related kinase 3 [HGNC:7746]
KIAA0100	KIAA0100 [HGNC:28960]
SDCBP	syndecan binding protein (syntenin) [HGNC:10662]
MAP4K4	mitogen-activated protein kinase kinase kinase kinase 4 [HGNC:6866]
ATP5G2	ATP synthase, H+ transporting, mitochondrial Fo complex, subunit C2 (subunit 9) [HGNC:842]
TIMELESS	timeless circadian clock [HGNC:11813]
PODXL	podocalyxin-like [HGNC:9171]
NONO	non-POU domain containing, octamer-binding [HGNC:7871]
GARS	glycyl-tRNA synthetase [HGNC:4162]
ZNF395	zinc finger protein 395 [HGNC:18737]
TAX1BP1	Tax1 (human T-cell leukemia virus type I) binding protein 1 [HGNC:11575]
ZNF397	zinc finger protein 397 [HGNC:18818]
ADGRA2	adhesion G protein-coupled receptor A2 [HGNC:17849]
TRAF7	TNF receptor-associated factor 7, E3 ubiquitin protein ligase [HGNC:20456]
GPR160	G protein-coupled receptor 160 [HGNC:23693]
LGALS3BP	lectin, galactoside-binding, soluble, 3 binding protein [HGNC:6564]
HSPB8	heat shock 22kDa protein 8 [HGNC:30171]
HSH2D	hematopoietic SH2 domain containing [HGNC:24920]
ASB13	ankyrin repeat and SOCS box containing 13 [HGNC:19765]
PQLC1	PQ loop repeat containing 1 [HGNC:26188]
GMPPA	GDP-mannose pyrophosphorylase A [HGNC:22923]
LTBP2	latent transforming growth factor beta binding protein 2 [HGNC:6715]
MMRN2	multimerin 2 [HGNC:19888]
TAZ	tafazzin [HGNC:11577]

Table 3.3: List of 40 FUSION-identified hits after bioinformatic filtering.

MIT and Harvard, is a tool developed to look for the presence of the selective enrichment of genes at the top of a result set compared to the rest of the data based on the annotated gene sets in the Molecular Signatures Database (MSigDB) [106,108]. This analysis demonstrates if any of the known gene sets have more members ranking higher than they would if their members were distributed randomly throughout the results, and if any sets are likely to represent a common pathway or function that is required for survival in HCT116 cells. Even though GSEA is limited by the gene sets that are already known, it still has the potential to identify known gene sets that have a previously unrecognized role in Ras-driven, KSR1-dependent tumorigenesis.

A ranked list of genes based on the Pearson correlation similarity metric was used as the input and compared against the Hallmark Gene Sets and identified multiple gene sets whose members were enriched in the top results with a nominal p-value less than 5% and a false discovery rate of less than 25%. Enriched Hallmark gene sets included KRAS_Signaling_Up, PI3K_AKT_MTOR_Signaling, UV_Response_UP, P53_Pathway, Hypoxia, IL2_Stat5_Signaling, IL6_JAK_STAT3_Signaling, Interfereon_Gamma_Response, Inflammatory Response, TNFA_Signaling_Via_NFKB, and Adipogenesis (Fig. 3.21).

Bioinformatic Analysis: Database for Annotation, Visualization, and Integrated Discovery (DAVID)

Instead of analyzing a ranked list of genes from the FUSION analysis for enrichment of gene sets within the top results, DAVID analysis provides gene annotation and assignment to functional groups or pathway mapping for a list of hits. Therefore, the 788 hits identified from FUSION analysis were supplied to DAVID for GO term annotation (biological processes and molecular function) and KEGG pathway mapping. Of the 788 hits that were supplied for DAVID analysis using Entrez IDs, 779 were identified and included in the results. The missing IDs were 83459 (DKFZP761H1710/NM_031297), 79765 (HIAN2/NM_024711), 84234 (DKFZP547F072/NM_032274), 55104 (FLJ10246/NM_018038), 80068 (FLJ13105/XM_376325), 57413 (AD026/NM_020683), 985 (CDC2L2/NM_024011), and

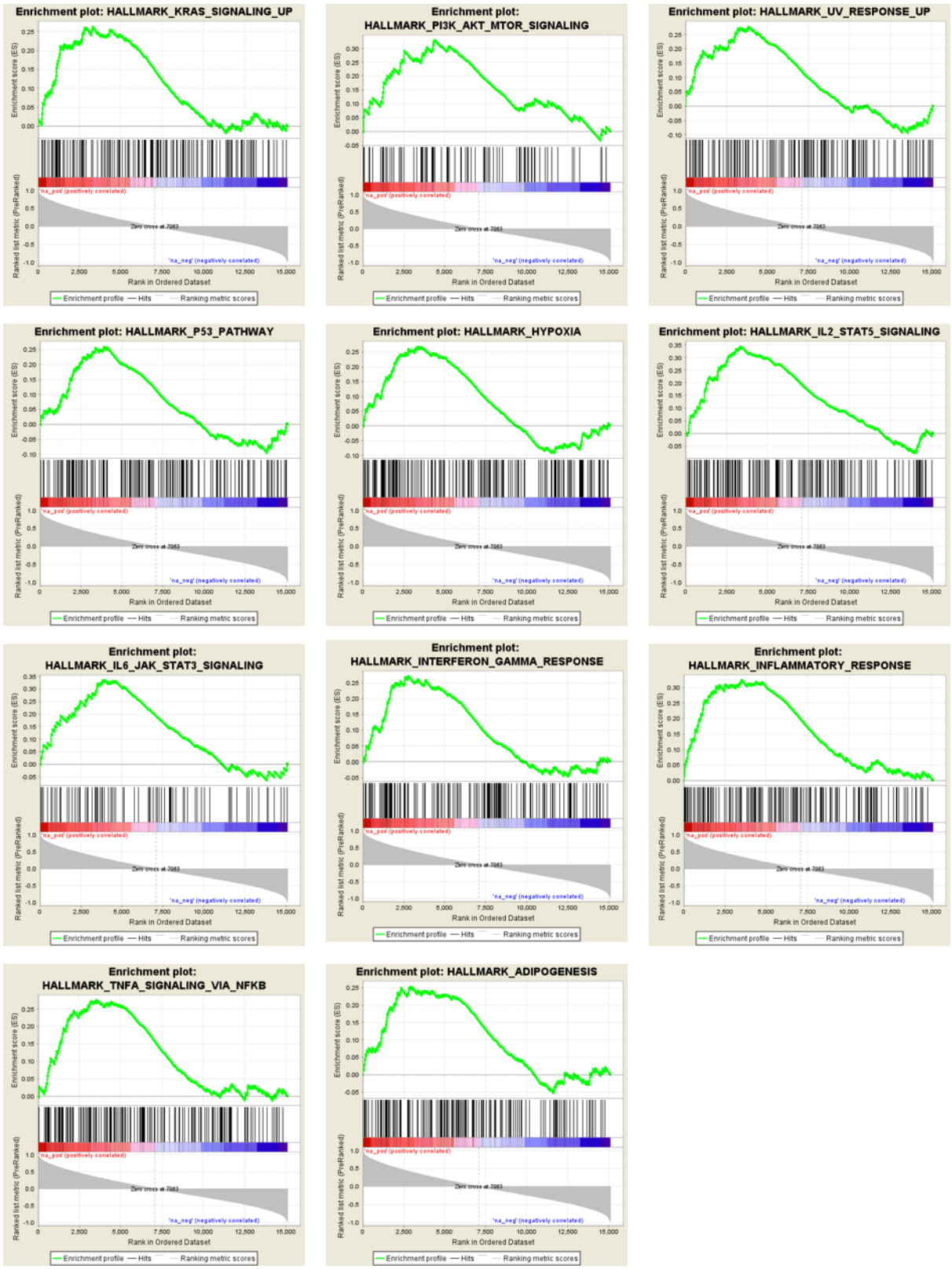

Fig. 3.21: Gene Set Enrichment Analysis (GSEA) Hallmark Gene Sets positively associated with hits from FUSION.

84800 (C14orf151/NM_032714). KEGG pathway mapping identified neuroactive ligand-receptor interaction, calcium signaling pathway, taste transduction, chemokine signaling pathway, leukocyte transendothelial migration, inositol phosphate metabolism, colorectal cancer, and melanoma terms were identified with a p-value of less than 0.1. Identified GO terms for molecular function included G-Protein coupled receptor activity, transmembrane receptor activity, signal transducer activity, receptor activity, peptide receptor activity, G-protein coupled, peptide receptor activity, neuropeptide receptor activity, neuropeptide binding, and kinase activity with a Bonferroni corrected p-value of less than 0.01 and FDR < 5%. Identified GO terms for biological processes included G-protein coupled receptor protein signaling pathway, cell surface receptor linked signal transduction, signal transduction, regulation of cellular process, regulation of biological process, biological regulation, second-messenger-mediated signaling, cyclic-nucleotide-mediated signaling, intracellular signaling cascade, regulation of cyclic nucleotide metabolic process, G-protein signaling, coupled to cyclic nucleotide second messenger, regulation of nucleotide metabolic process, regulation of nucleotide biosynthetic process, regulation of cyclic nucleotide biosynthetic process, MAPKKK cascade, regulation of catalytic activity, regulation of cAMP metabolic process with a Bonferroni corrected p-value of less than 0.01 and FDR <5%. The presence of a large number of GO terms surrounding GPCR signaling, signal transduction, kinase activity, and MAPKKK cascade were reassuring; however, the list of KEGG pathways and GO terms that were found to be associated with the FUSION hits were difficult to interpret and did not reveal new information as was anticipated. Therefore, additional methods including graphical representations of the associated cellular functions were employed.

Bioinformatic Analysis: Cytoscape App Reactome and Reactome Pathway Browser

In collaboration with Dr. Nicholas Woods, evaluation using hits that had a PC greater than 0.7 and an ED less than 1 (197 targets queried, 47 returned) using the Reactome Cytoscape App [109,110] demonstrated pathway enrichment of GPCR ligand binding (CX3CR1, ADCYAP1R1, LPAR4, CXCL13, TAS2R4, P2RY14, TAS2R13, HTR5A, MTNR1A, MC1R, ADORA2B,

GNRH1), neuroactive ligand-receptor interaction (ADCYAP1R1, LPAR4, TAAR8, P2RY14, HTR5A, MTNR1A, MC1R, ADORA2B), Rap1 signaling (RAP1A, YWHAZ, SIPA1), Calcineurin-regulated NFAT-dependent transcription in lymphocytes (EGR4, NFATC3, FOS, RNF128), Heterotrimeric G-protein signaling pathway $G_i\alpha$ and $G_s\alpha$ mediated pathway (RGS19, GNG3, RAP1A, HTR5A, MTNR1A, ADORA2B), Neurotrophic factor-mediated Trk receptor signaling (TGS19, RAP1A, FRS3, GIPC1), PDGFRβ signaling pathway (RAP1A, FOS, YWHAZ, MAPK10, SIPA1), and Circadian Rhythm pathway (TIMELESS, NR1D1, CRY1) with an FDR < 1% (Fig. 3.22). One of our previously validated hits, AMPKγ1 was integrated in this figure clustering with the circadian rhythm pathway, which led us to investigate these three targets further. Only one of the three circadian rhythm pathway genes, TIMELESS, also passed all of the bioinformatic filters making it a prioritized hit for further evaluation.

Conclusions

Using a gene expression-based signature as a proxy or readout for our phenotype of interest (effect of KSR1 depletion in cancer cells), Functional Signature Ontology (FUSION) was applied to a genome-scale genetic depletion screen to identify genes that are selectively required in colon cancer cells, but dispensable in normal cells. Hits that were biologically shown to be preferentially required in colon cancer cells represent cancer-specific vulnerabilities that can often be tied back to driving oncogenic signaling, reinforcing the idea that oncogenes corrupt or hijack certain cellular pathways or functions to promote tumorigenesis. This, however, can leave the cells susceptible or vulnerable to targeted therapies that disrupt the required downstream effectors.

The scale of this screen dramatically increased the complexity for computational analysis as compared to the preliminary kinome screen. The sheer size of the data being analyzed made it difficult to perform initial quality control checks on the data as issues were not readily apparent until R scripts were written to aid in data visualization. Additionally, experimental limitations

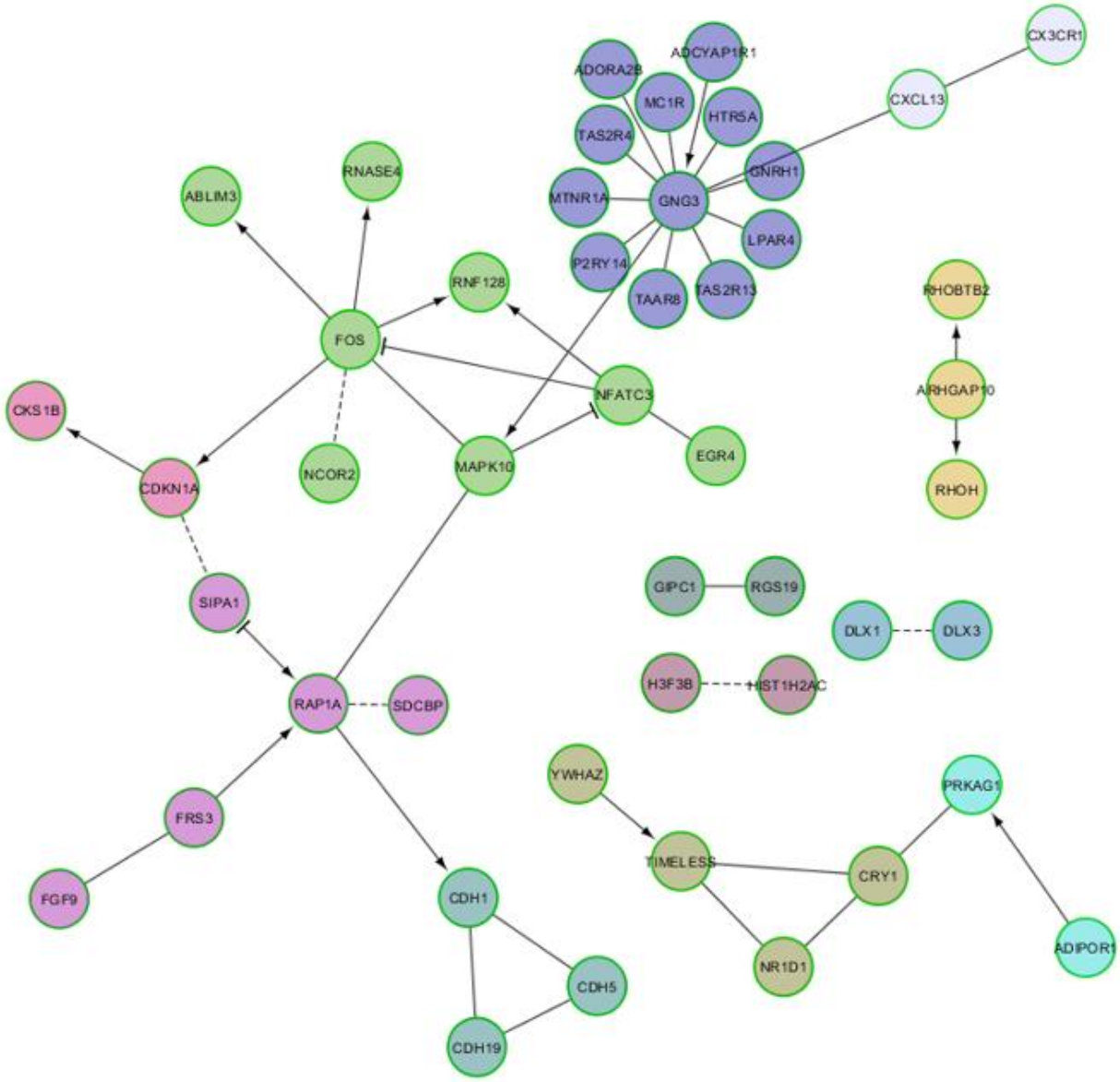

Fig. 3.22: Pathway enrichment analysis performed using the Reactome Cytoscape App. Functionally related genes are grouped by color.

forced the screen to be performed in batches further compounding the biological variability between plates. The batched processing also created a lapse in time between when the initial and last plates were processed. Unfortunately, only rudimentary quality control checks were evaluated as each plate was completed, such that additional issues were painstakingly identified and corrected after all of the data was generated and was being compiled.

Another confounding issue that arose was the lack of random plating both due to control wells being plated in the same two columns on each plate as well as the functionally grouped library being assayed in the groups assigned by the manufacturer. This eliminated the possibility of normalizing the results based on plate position or median probe value as either technique would experience confounding due to the non-random plating.

After these issues were identified, they were addressed using multiple computational approaches. R scripts were generated to take the raw reads that were manually validated, complete the geomean normalization, and integrate the data for further analysis. Negative and missing values were set to the plate minimums for each probe. Outliers were identified and excluded in an attempt to eliminate variability in the positive and negative controls due to faulty wells. Numerous methods of normalization were considered and evaluated with a normalization method based on the negative control wells (treated with non-targeting siRNA) outperforming the other methods based on accuracy, precision, and the potential for scalability. In retrospect, it is logical that this method would be preferable when the experimental conditions are considered. It is vital that experimental conditions be considered when performing the quality control evaluation and computational processing of biologic experimental data. A robust understanding of how the screen was performed prior to computational processing could have reduced the amount of time required and limited wasted efforts to computationally process the screen data. For this to occur, strong collaborations must be formed between the individuals performing the biologic assay and the individuals performing the computational analysis such that both of these groups can work closely together to ensure the experiments are performed in a robust manner that will allow for

direct computational-mediated assessment after completion. This requires both biologists and computer or data scientists to learn about the other field at least to an extent such that they can effectively communicate.

Several modifications or additions could be employed to improve upon the current computational analysis of FUSION. Further evaluation of the six genes within the KSR1-depleted gene signature to delineate those that preferentially identified hits that were biologically validated could lead to a refinement of the KSR1-depletion signature gene set. This could then lead to dropping one or more probes from the signature or weighting the probes to give more discriminatory power to certain probes. Since the dynamic ranges of the probes varied, the genes within the gene expression signature were inherently given different levels of impact on the similarity metrics used to identify other KSR1-like genes. This effect is much more pronounced on Euclidean distance, but is seen to a lesser extent on the Pearson correlation similarity metric.

A FUSION screen was also performed on a library of microRNA, natural products, and commercially available drugs. The results from the microRNA screen were computationally and biologically validated by our collaborators in Dr. Michael White's lab at UT Southwestern [101]. Genetic targets and natural product compounds identified at multiple time points during the computational analysis of FUSION are the subject of the subsequent chapters contained herein. These include TIMELESS (Chapter 4), a circadian gene that was identified in the 40 hits listed in Table 3.3, WDR5B/WDR5 (Chapter 5), a highly ranking gene within the 788 initially identified hits listed in Table 3.2, and AMPKγ1/5-OH-S [1] (Chapter 6), a genetic target initially identified in the preliminary kinome screen depicted in Fig. 3.4 and a compound that inhibits AMPK that was identified in the natural product screen. Preliminary biological validation data is also provided for ECE2 (Table 3.3), HAS2, DYRK1A, and BMP4 (Table 3.2) in Appendix A.

Out of the prioritized 40 hits (Table 3.3), other targets that are of particular interest include MAP2K7 and MAP4K4, two highly druggable kinases that share JNK as a direct downstream target, and two heat shock proteins, HSPH1 and HSPB8.

Chapter 4: TIMELESS promotes colon cancer cell proliferation by limiting the accumulation of DNA damage

Portions of the material covered in this chapter are the subject of a manuscript submitted for publication by Neilsen BK *et al*.

Introduction

Data indicate that the FUSION screen provides a platform for identifying novel therapeutic targets and demonstrates the potential to identify oncogene-specific vulnerabilities in an unbiased manner. Based on the similarity between gene expression signatures, Timeless Circadian Clock (TIMELESS) was identified as being KSR1-like and a potential therapeutic target in cancer (Fig. 4.1).

TIMELESS Protein Structure

Mammalian TIMELESS is a protein that was named for its similarity to the TIMELESS protein in Drosophila with which it shares four homologous regions, nuclear localization signals (NLS), short stretches of glutamate-rich regions, and a conserved DEDD sequence on the C-terminus [111,112] (Fig. 4.2). However, later studies revealed that a different gene in Drosophila, TIMEOUT, shares greater sequence similarity to mammalian TIMELESS [113]. TIMELESS is also a member of an evolutionarily conserved family of orthologs that are conserved all the way back to yeast and are implicated in DNA synthesis, S-phase dependent checkpoint activation, and chromosome cohesion [114,115]. Mammalian TIMELESS is highly conserved, as mouse and human TIMELESS share greater than 80% identity in both the nucleotide and amino acid sequences [111,116]. The human form of TIMELESS contains a TIMELESS domain on the N-terminus, which is required for homodimerization and interactions with TIPIN, CHK1, and CRY1 proteins [111,112,116,117]. On the C-terminus, TIMELESS has the TIMELESS C-terminal domain that is predicted to be required for nuclear localization. Between these two regions, is the glutamic acid-rich region and a region predicted to contribute to DNA binding (Fig. 4.2).

Circadian Rhythm

TIMELESS was initially identified in Drosophila where TIMELESS is a circadian gene that serves as a negative circadian regulator. Initial studies of TIMELESS function in mice, failed to demonstrate circadian expression or function [118]; however, several mouse strains have been

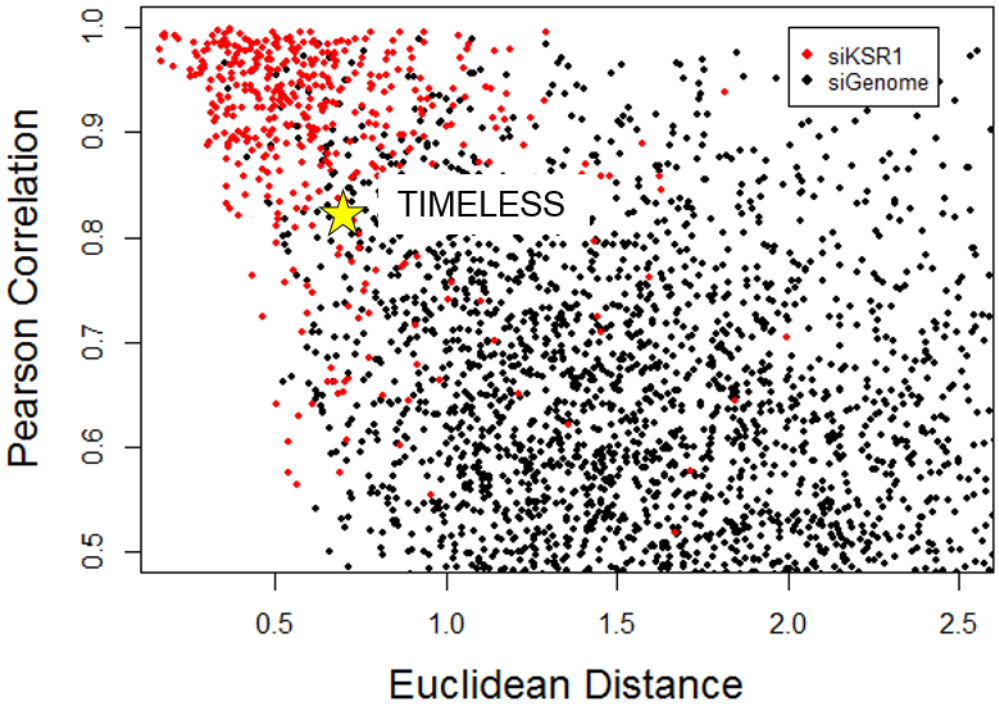

Fig. 4.1: FUSION identified TIMELESS as a functional analogue of KSR1 based on Pearson correlation and Euclidean distance similarity metrics.

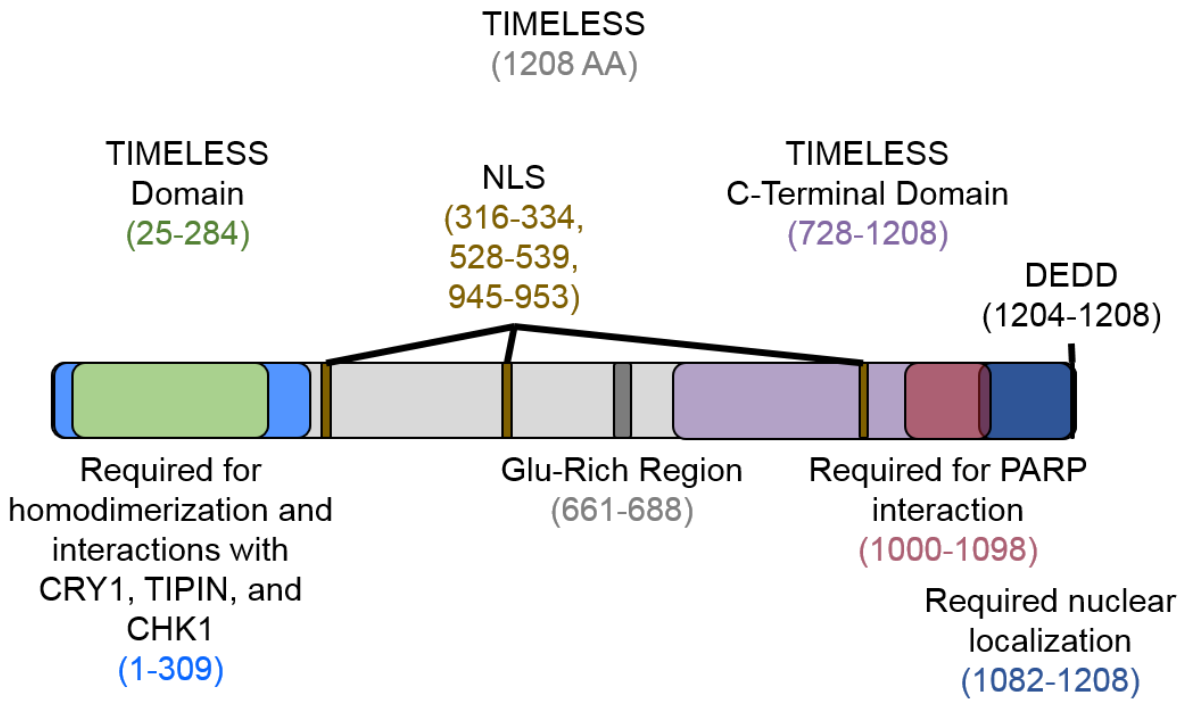

Fig. 4.2: TIMELESS protein structure diagram.

shown to have abnormal circadian rhythms, which casts some doubt as to the applicability of these findings to human TIMELESS. In early studies, TIMELESS mRNA did not oscillate in the suprachiasmatic nucleus (SCN) or the retina and was not altered with light exposure at night in mice [111,112,116]. However, soon thereafter another group demonstrated constitutive, high expression of TIMELESS in the SCN, but oscillatory expression of TIMELESS in the retina with light/dark cycles [119]. Further studies using a different probe against TIMELESS observed diurnal variation of TIMELESS mRNA in the SCN with peak levels at the day-to-night transition in light-entrained animals and demonstrated light pulse-induced elevation in TIMELESS mRNA in mice [120]. In rat models, TIMELESS expression demonstrated clear 24-hour oscillations and physically interacted with the PERIOD circadian proteins (PER1/2/3). Conditional knockout of TIMELESS in the SCN disrupted SCN neuronal activity rhythms and altered levels of other known core clock genes [121], which provided strong evidence for a role for TIMELESS in the mammalian circadian clock.

Canonical circadian signaling is driven by CLOCK:CYCLE/BMAL1 binding to E-boxes (CACGTG sequences) within promoters thereby initiating transcriptional activation of circadian genes, including PER and TIMELESS [122]. PER and TIMELESS then inhibit CLOCK:CYCLE/BMAL1 activity forming a negative feedback loop. Mutations of the canonical E-box sequence of TIMELESS reduces mRNA cycling and circadian locomotor activity rhythms demonstrating the necessity of the E-box sequences and the transcriptional regulation of circadian cycles [122,123].

In both Drosophila and mammalian models, TIMELESS has been shown to interact with other circadian genes, most notably the family of PERIOD proteins. This interaction promotes protein stability and nuclear localization of both interacting partners [111,119,124-128]. When the PER:TIMELESS complex is in the nucleus, it inhibits CLOCK:CYCLE/BMAL1 DNA binding at E-boxes, which dramatically decreases circadian gene transcription (including PER and TIMELESS transcription), without affecting CLOCK:CYCLE/BMAL1 heterodimer formation [122,129-133]. In addition, complex formation between PER:TIMELESS and

CLOCK:CYCLE/BMAL1 induces hyperphosphorylation of CLOCK by DBT/CK1 leading to CLOCK degradation [133]. TIMELESS has also been shown to interact with CRY proteins. While CRY proteins support light-dependent degradation of TIMELESS in Drosophila, CRY1/2 inhibits CLOCK:CYCLE/BMAL1 and interacts with PER1/2 and TIMELESS in a light-independent manner in mice [134].

An additional layer of regulation exists through post-translational modifications. Phosphorylation of PER by DBT/CK1 targets PER for degradation, and phosphorylation of TIMELESS by Sgg/GSK3 promotes the PER:TIMELESS complex translocation to the nucleus, both of which significantly alter the circadian period [135-144]. Additionally, GSK3-mediated phosphorylation of PER-bound TIMELESS initiates a CK2-mediated phosphorylation cascade. Mutations in TIMELESS that block this phosphorylation cascade delay its nuclear accumulation and affect rhythmic behavior [145]. Data suggest that PER:TIMELESS complex formation prevents PER phosphorylation and subsequent degradation revealing the mechanism by which TIMELESS promotes PER stability [136,146].

TIMELESS is rapidly degraded through a ubiquitin-proteasome mechanism that is preceded by tyrosine phosphorylation and generally triggered in response to light. This contributes to light-mediated circadian cycle entrainment [127,128,130,147-151]. Alternative mechanisms do exist to maintain the circadian rhythms in the absence of light as evidenced by the continued phosphorylation and degradation of TIMELESS through a ubiquitin-proteasome mechanism even in the absence of light. However, this mechanism is mediated by different kinases than those that promote light-induced degradation [152]. Specific kinases have been identified that regulate the stability of mammalian TIMELESS including multiple individual Src-family tyrosine kinases that direct the degradation (Fyn or Hck) or protection of TIMELESS (c-Src and c-Yes) based through changes to phosphorylation-dependent ubiquitylation [153]. Recent screens have also revealed several protein phosphatases that alter the circadian cycle suggesting possible additional mechanisms by which the circadian rhythm is regulated through phosphorylation changes [154].

Development

TIMELESS is essential for development [118,155-157] and has been shown to be highly expressed in the developing lung, liver, kidney, and neuroepithelium [156,158]. The definitive requirement for TIMELESS has been shown as TIMELESS depletion causes defects in kidney development and evidence suggests TIMELESS may be an immediate early gene that is required for kidney morphogenesis [156], lung development [157], and neural development [158]. Further, mouse embryonic stem cells lacking TIMELESS formed embryoid bodies that failed to cavitate due to a lack of programmed cell death and differentiation, which ultimately arrested development [159].

DNA synthesis

During normal DNA replication, TIMELESS depletion decreased DNA replication efficiency and caused genomic instability demonstrated by increased γH2AX, Rad51, and Rad52 foci formation [114,160]. TIMELESS localized to replication forks and limited ssDNA accumulation as well as fork rotation during DNA replication to prevent DNA damage and chromosomal instability [114 161-164]. This is particularly important at sites of physical barriers including centromeres, telomeres, ribosomal DNA repeats, and termination sites [165]. Specifically at telomeres, TIMELESS promoted efficient DNA replication, and TIMELESS depletion caused telomere shortening independent of telomerase, increased DNA damage leading to telomere aberrations, and slowed telomere replication [166]. As a component of the replication fork barrier, TIMELESS also coordinated transcription and S-phase DNA replication thereby reducing DNA damage [167].

TIMELESS interacted with DNA helicases [168-170] and stimulated their unwinding activity by enhancing DNA binding [171]. Additionally, TIMELESS coupled the replicative helicase complex to DNA polymerases for efficient DNA synthesis [172]. TIMELESS also stimulated the activity of DNA polymerases α, δ, and ε [169], and without TIMELESS, replication fork progression was dramatically decreased [171,173]. TIMELESS promoted chromosome cohesion, and

TIMELESS depletion caused a 100-fold increase in sister chromatid discohesion and induced significant chromosome fragmentation [114,163,165,174,175].

These combined mechanisms demonstrate how TIMELESS promotes high fidelity, efficient DNA synthesis. These mechanisms also likely contribute to the maintenance of viral genomes as TIMELESS has been shown to promote viral episome maintenance in two cancer-associated viruses: Herpes Simplex virus (HSV, Kaposi's sarcoma) and Epstein-Barr virus (EBV, Burkitt's lymphoma)[176,177].

Cell Cycle

The cell cycle is under circadian regulation [178-181], and TIMELESS could be the mediator that coordinates this connection [182]. TIMELESS expression is regulated both by the circadian rhythm and cell cycle with the highest expression occurring at night and during S and G2 phases in normal human fibroblasts, respectively [182]. TIMELESS depletion has been shown to limit the ability of cells to trigger DNA damage-associated checkpoint arrest at intra-S checkpoints and the G2/M checkpoints [173,182,183], which further sensitized cells to DNA damaging agents [183]. Loss of TIMELESS caused defects in mitotic progression [163,165] because TIMELESS synchronizes replication termination and subsequent mitotic kinase (CDK1, Auroras A and B, PLK1) activation [165].

DNA Damage

Further, in addition to causing genomic instability, DNA damage, and subsequent checkpoint activation, TIMELESS is involved in the DNA damage signaling cascade, DNA damage repair, and cell cycle arrest [114,173].

RPA binds to ssDNA during replication fork advancement and intermediate ssDNA that is created during homologous recombination following double stranded breaks and chewing back of the ends. RPA binding recruits the ATR-ATRIP complex, which then phosphorylates and activates CHK1 at S345. Activated CHK1 prevents CDK1 activation and mitotic entry, thereby

triggering the G2/M DNA damage checkpoint [184,185]. In this pathway, TIMELESS, along with its binding partner TIPIN (Timeless interacting protein) physically interacts with RPA, claspin, and CHK1 and mediates both ATR- and claspin-mediated phosphorylation of CHK1 [114,168,173,182,186-190]. Independent of ATR, CHK1 and TIMELESS are also required for efficient PCNA ubiquitination after DNA damage [191,192].

Similar to other synthetically lethal combinations in DNA damage repair pathways, TIMELESS depletion increased reliance on homologous recombination for continued DNA synthesis [160], and TIMELESS depletion dramatically increased cell sensitivity to ATR depletion. Cells deficient in ATR and TIMELESS have dramatically reduced nucleotide incorporation in S phase and experience replication failure as a result of synergistic increases in γH2AX and DNA double stranded breaks [162]. TIMELESS has also been shown to be required for ATM-mediated CHK2 activation following DNA double strand breaks [183].

TIMELESS physically interacts with PARP-1 [193,194] and this interaction is required for TIMELESS to accumulate at sites of DNA damage [193,194]. TIMELESS does not affect PARP-1 enzyme activity [193,194], but is required for recruitment of other complex components to sites of DNA damage [194]. Loss of TIMELESS reduces homologous recombination[193] as well as DNA double strand break repair [194] suggesting a role for TIMELESS in DNA damage repair. PARP inhibition prevents DNA damage repair by trapping PARP-1 at sites of DNA damage [193]. PARP inhibitors also trap TIMELESS at sites of DNA damage, but the effect of the sequestration of TIMELESS is unknown [193].

Cancer

Significant evidence now suggests that cancer may be a circadian-related disorder as several studies have demonstrated circadian rhythms are dysregulated in cancer cells [195,196]. Concerningly, large studies have correlated a substantial history of shift work and jet lag or altered sleep/wake patterns with increased cancer incidence and higher mortality rate [197-201]. This suggests circadian rhythm dysregulation is not merely a downstream effect of oncogenic

signaling, but also plays a pro-tumorigenic role. Recent work has started to elucidate the relationship between the development of cancer and circadian rhythm dysregulation as well as demonstrate the functional benefits of circadian dysregulation in cancer cells.

Oncogenes can drive the expression of certain circadian genes effectively hijacking the circadian cycle, such as when MYC drives the expression of REV-ERBα, which decreases BMAL1 expression thereby releasing the cell from its tumor suppressive effects and alters cell metabolism [202]. Recent work has also shown that restoring circadian rhythmicity *in vitro* decreased proliferation of cancer cells and circadian dosing of certain chemotherapeutics increased their efficacy [203].

TIMELESS was not mutated in cancer [204], but was significantly overexpressed in both patient tumors and cancer cell lines relative to normal adjacent tissue and normal cell lines, respectively in multiple cancer types including acute lymphocytic leukemia, breast, cervical, hepatocellular, and lung cancer (both non-small cell lung cancer and small cell lung cancer) [204-210].

Generally, TIMELESS has been shown to promote proliferation and metastasis in cancer cells [204,207,208]; however, the demonstrated mechanisms have varied greatly. In breast cancer, TIMELESS upregulated the expression and activity of MYC, and inhibition of MYC blocked the effects of TIMELESS [207]. In hepatocellular carcinoma, TIMELESS depletion decreased cell viability via increased apoptosis and G2 arrest following CHK2, but not CHK1, phosphorylation and reduced ribosomal protein biosynthesis by decreasing EEF1A2 levels [208]. TIMELESS conferred cisplatin resistance in nasopharyngeal carcinoma by activating the Wnt/β-catenin signaling pathway and promoting epithelial-mesenchymal transition [211]. Increased TIMELESS expression also correlated with tamoxifen resistance in breast cancer [212], and subsequent analysis demonstrated that 17β-estradiol promoted TIMELESS expression *in vitro* in cells sensitive to tamoxifen, but in tamoxifen-resistant cells, TIMELESS expression was independent of 17β-estradiol [212]. Clinically, increased TIMELESS expression was associated with a poorer prognosis

in breast, cervical, bladder, and lung cancer [204-207,210,212,213]. This suggests that TIMELESS likely has a conserved, protumorigenic role that is present in many types of cancer. Determining the mechanism behind its overexpression and further elucidating its functional role in tumorigenesis is likely to increase our understanding of cancer and may reveal opportunities for the development of new therapeutics.

Results

Preliminary biological validation of TIMELESS

Initial biological validation of targets identified using FUSION was performed by assessing cancer cell growth or viability in anchorage-independent conditions following RNAi-mediated target depletion by measuring cell ATP levels on polyHEMA-coated plates [214,215] using CellTiter-Glo® Luminescent Cell Viability Assay, as previously described [3]. The smartPool of four siRNA oligos (Dharmacon) targeting KSR1 or TIMELESS was used to deplete cells of the target. Growth in anchorage-independent conditions was reduced substantially with KSR1 or TIMELESS depletion in HCT116 colon cancer cells (Fig. 4.3A).

Immortalized, yet non-transformed human colon epithelial cells (HCECs)[102] are unable to proliferate in an anchorage-independent environment and were therefore not assayed in anchorage-independent culture conditions. To compare the effects of TIMELESS depletion in colon cancer cells to immortalized, yet non-transformed HCECs, RNAi-mediated depletion of TIMELESS was completed under normal plating conditions and viability was measured using alamarBlue. TIMELESS depletion for 72 hours reduced viability in HCT116 cells, but not HCECs (Fig. 4.3B). TIMELESS depletion was validated by western blot in HCECs and HCT116 cells (Fig. 4.3C).

TIMELESS is overexpressed in cancer

TIMELESS is upregulated at the RNA level in several types of tumors compared to solid normal tissue (TCGA) (Fig. 4.4A) and is upregulated at the mRNA (Fig. 4.4B) and protein level

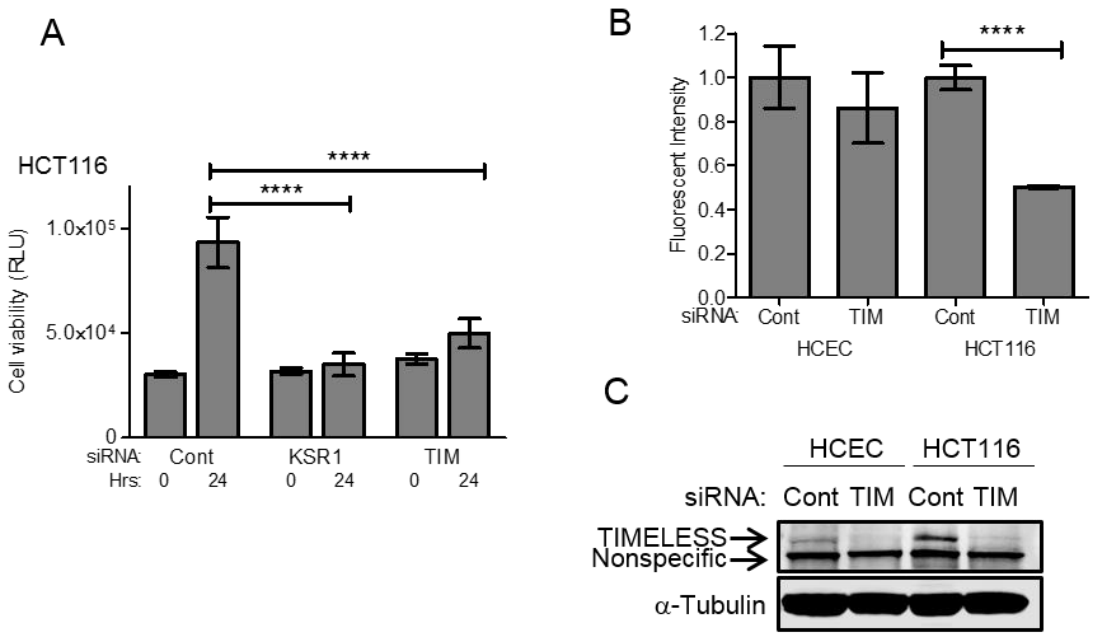

Fig. 4.3: Preliminary biological validation of TIMELESS. (A) Viability of HCT116 colon cancer cells measured using CellTiter-Glo® following RNAi of KSR1 or TIMELESS that were replated on polyHEMA-coated plates 48 hours following transfection to simulate anchorage-independent conditions. Cell viability is measured immediately after replating (Hrs: 0) and 24 hours later. (N=6). (B) Viability of HCECs and HCT116 cells measured using alamarBlue® following RNAi-mediated TIMELESS depletion for 72 hours in normal culture conditions. (N=6) (C) Immunoblot confirmation of TIMELESS depletion from B. Data are shown as mean ± SD.

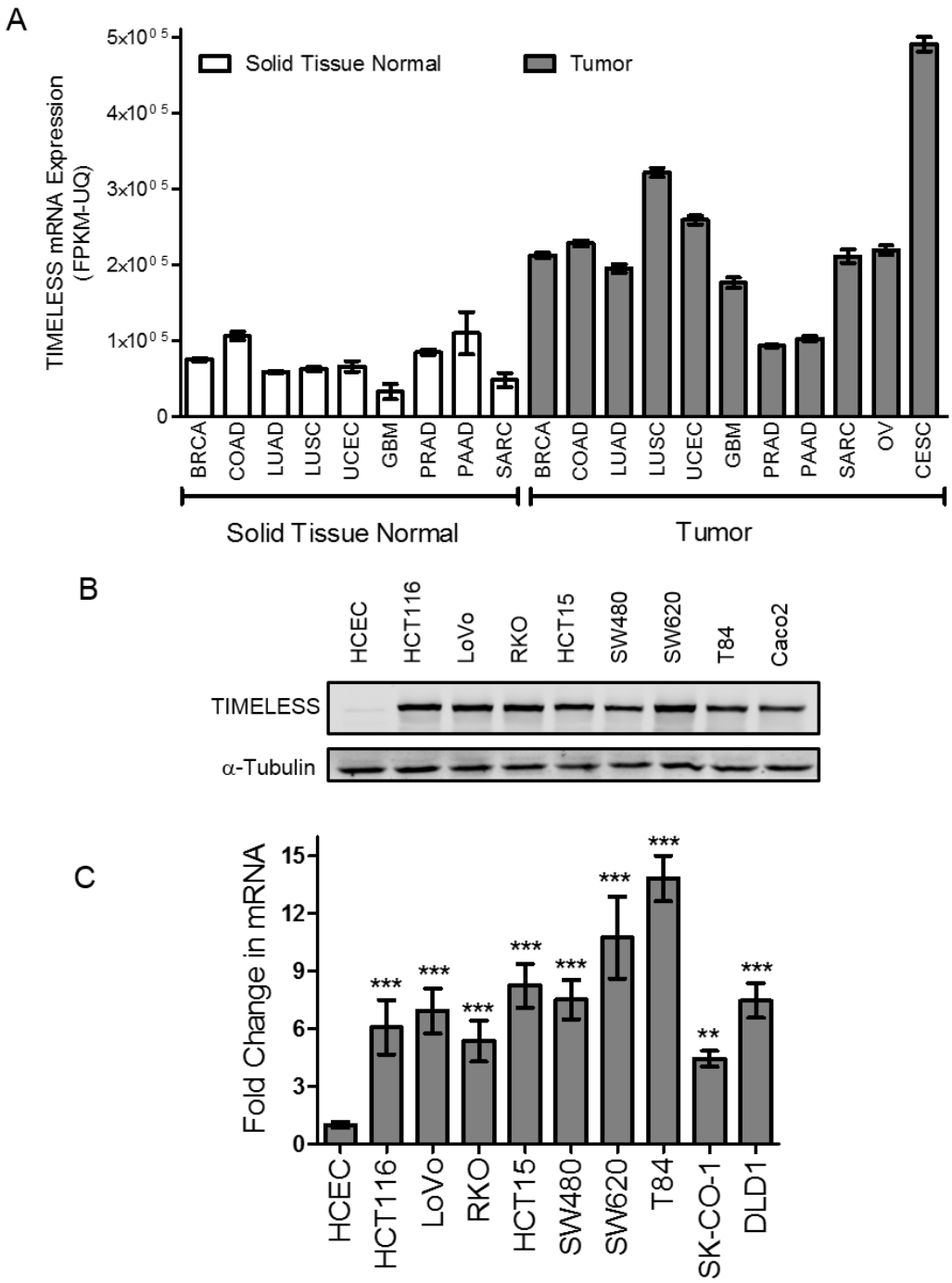

Fig. 4.4: TIMELESS is overexpressed in cancer. (A) TIMELESS gene expression (RNASeq) data from TCGA for unpaired primary colon tumors and normal solid tissue samples. The results published here are in whole or part based upon data generated by the TCGA Research Network: http://cancergenome.nih.gov/. (B) Immunoblot and (C) RT-qPCR of TIMELESS levels in a panel of colon tumor cell lines and immortalized, non-transformed HCECs. RT-qPCR data is shown as mean ± SD. (N=3) (Experiment 4.4C was completed in collaboration with Jamie McCall and Danielle Frodyma).

(Fig. 4.4C) in a panel of human colon cancer cell line (HCT116, LoVo, RKO, HCT15, SW480, SW620, T84, and Caco2) compared to HCECs.

Previous reports suggested altered promoter methylation on circadian genes was associated with their altered expression in cancer [216]. Specifically, TIMELESS promoter hypomethylation was present with TIMELESS overexpression in breast cancer [217]. Examining the Beta value of TIMELESS-associated sites included on the Illumina Infinium Human DNA Methylation 27 and Illumina Infinium Human DNA Methylation 450 beadchips from solid tissue normal and primary tumor samples from the TCGA COAD dataset revealed the methylation of TIMELESS is nearly identical between normal and colon tumor samples (Fig. 4.5A and B). Comparing TIMELESS methylation state in HCECs as compared to HCT116s demonstrated no difference in methylation (Fig. 4.5C) suggesting promoter hypomethylation is not contributing to TIMELESS overexpression in colon cancer.

TIMELESS loses circadian expression in cancer.

In normal cells and tissues, TIMELESS expression has a circadian pattern [119-121]. However, TIMELESS demonstrated a loss of circadian rhythmicity in protein expression in colon cancer cell lines. Following 50% horse serum shock for two hours, HCECs demonstrate cyclical expression of TIMELESS over a 24-hour period that is consistent with a normal circadian pattern with the highest level of expression being seen approximately 16-18 hours following serum shock (Fig. 4.6A). Conversely, in HCT116 colon cancer cells, TIMELESS is constitutively expressed at a high level, with very little cyclic alterations in expression (Fig. 4.6B). TIMELESS also demonstrated circadian expression, with an earlier peak in expression, ~ 12 hours, following cell synchronization by forskolin treatment (Fig. 4.6C).

Mutant Ras through downstream ERK signaling contributes to TIMELESS expression

To evaluate if oncogenic Ras contributes to increased TIMELESS expression in colon cancer, TIMELESS expression was examined in HCECs following exogenous expression of

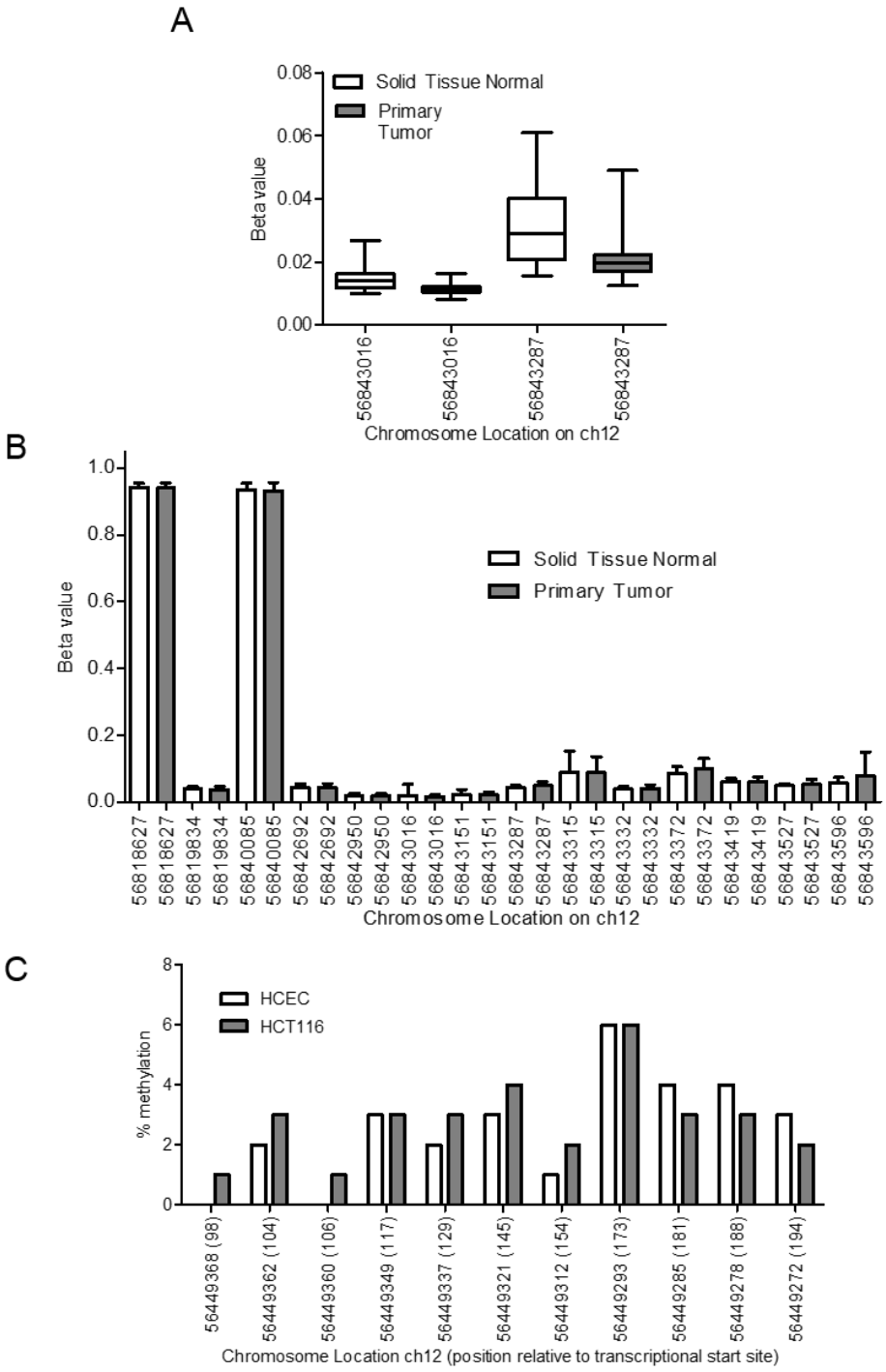

Fig. 4.5: TIMELESS overexpression is not due to methylation changes at the promoter. (A and B) TIMELESS methylation data from Illumina Infinium Human DNA Methylation 27 (A) and Illumina Infinium Human DNA Methylation 450 (B) beadchips data from TCGA for unpaired primary colon tumors and normal solid tissue samples. The results published here are in whole or part based upon data generated by the TCGA Research Network: http://cancergenome.nih.gov/. (C) Percent methylation for CpG sites near or within the TIMELESS DNA sequence in HCECs and HCT116 cells. (Experiment 4.5C was completed in collaboration with Dr. Dave Klinkebiel and the Epigenomics Core).

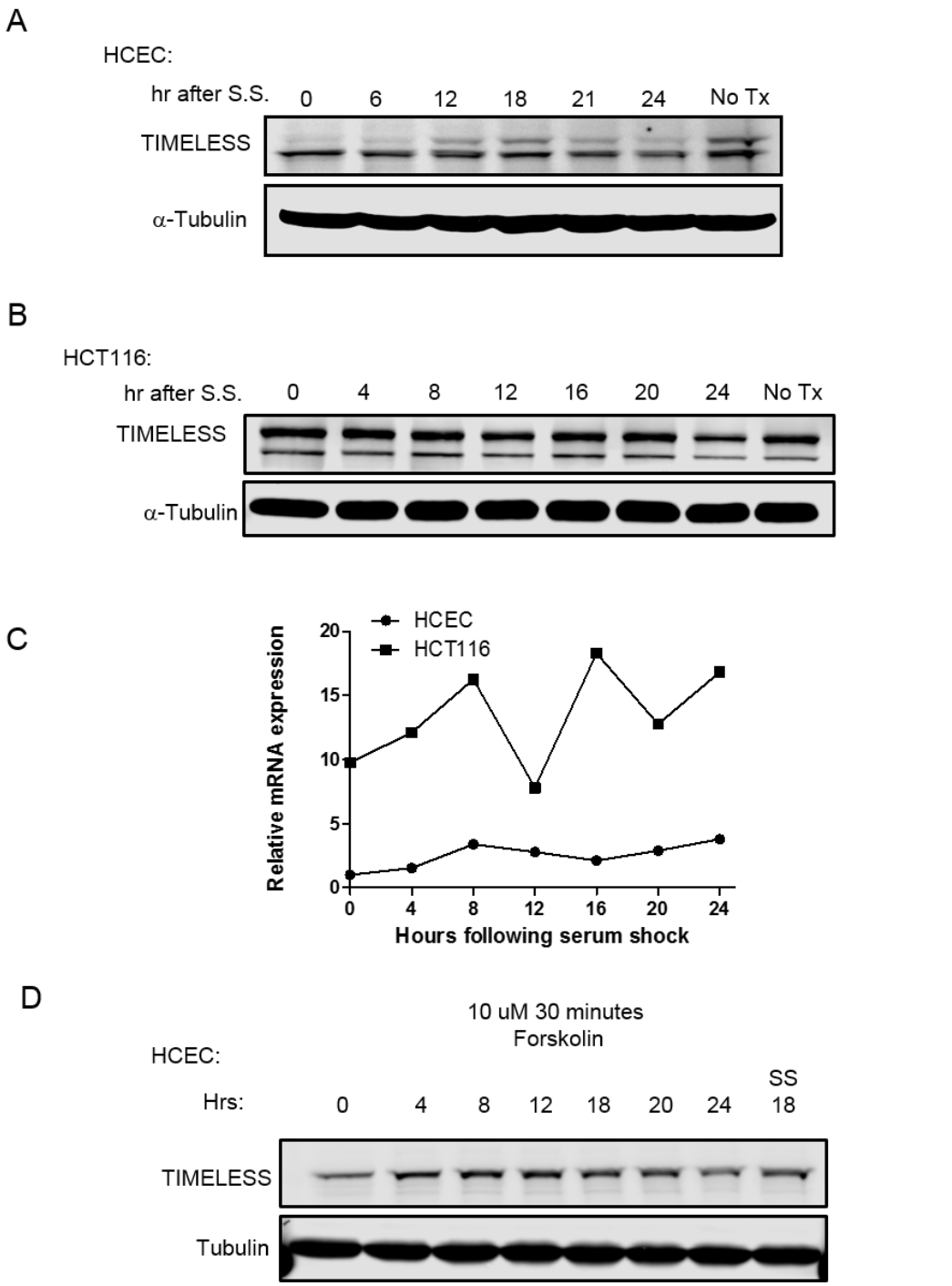

Fig. 4.6: TIMELESS is circadianly-expressed in HCECs, but constitutively overexpressed in HCT116 colon cancer cells. (A and B) Immunoblot of TIMELESS expression over 24 hours following circadian synchronization via 2 hour 50% horse serum treatment in HCECs (A) and HCT116 cells (B). (C) TIMELESS mRNA expression over 24 hours following circadian synchronization via 2 hour 50% hourse serum treatment in HCEC and HCT116 measured with RT-qPCR. (N=1). (D) Immunoblot of TIMELESS expression over 24 hours following circadian synchronization via 30 minute 10 μM foskolin treatment. (Experiment 4.6C-D were completed in collaboration with Danielle Frodyma).

mutant Ras and in HCT116 cells following ERK inhibition or RNAi-mediated ERK1/2 depletion. HCECs expressing exogenous Ras^{G12V} have increased TIMELESS expression relative to HCECs albeit not to the levels seen in the colon cancer cell lines tested. Following serum shock-induced cell synchronization, HCECs with Ras maintain circadian expression of TIMELESS, but at an increased level of expression (Fig. 4.7A). Comparing TIMELESS expression 16 hours following serum shock in HCECs with Ras to HCECs (far right lane) demonstrates Ras^{G12V} promoted TIMELESS expression. This increase in expression was abrogated with ERK inhibition with 1μM SCH772984 (Fig. 4.7B). In asynchronous HCECs, HCECs exogenously expressing Ras^{G12V}, and HCT116 colon cancer cells, ERK inhibition with 1 μM SCH772984 decreased TIMELESS expression (Fig. 4.8A) demonstrating the vital role ERK activation plays downstream of activated Ras to promote TIMELESS expression. RNAi-mediated depletion of ERK demonstrates a similar effect, but to a lesser degree (Fig. 4.8B). ERK inhibition for 24 hours prior to cell synchronization by serum shock and collection over the next 24 hours demonstrated partial restoration of the circadian expression of TIMELESS; however, the levels of TIMELESS remain elevated as compared to the non-transformed HCECs (Fig. 4.9).

In HCECs, TIMELESS expression decreases with increasing cell confluency (Fig. 4.10A). In HCT116 cells, TIMELESS expression is constitutively high regardless of cell confluency (Fig. 4.10A). However, changing the HCEC media daily dramatically reduces this decrease in TIMELESS expression. This maintained TIMELESS expression occurs coordinately with maintained levels of ERK phosphorylation and activation suggesting the possibility that replacing the media daily refreshes the EGF levels (a normal additive in the HCEC as described in Chapter 2: Materials and Methods), which then promotes ERK activation.

To evaluate how consistently ERK signaling promotes TIMELESS expression in colon cancer, multiple colon cancer cell lines were treated with 1 μM SCH772984 for 48 hours and assessed for cell viability with alamarBlue and TIMELESS expression via immunoblot. ERK inhibition decreased cell viability and TIMELESS expression in HCT116 and SK-Co-1 cancer

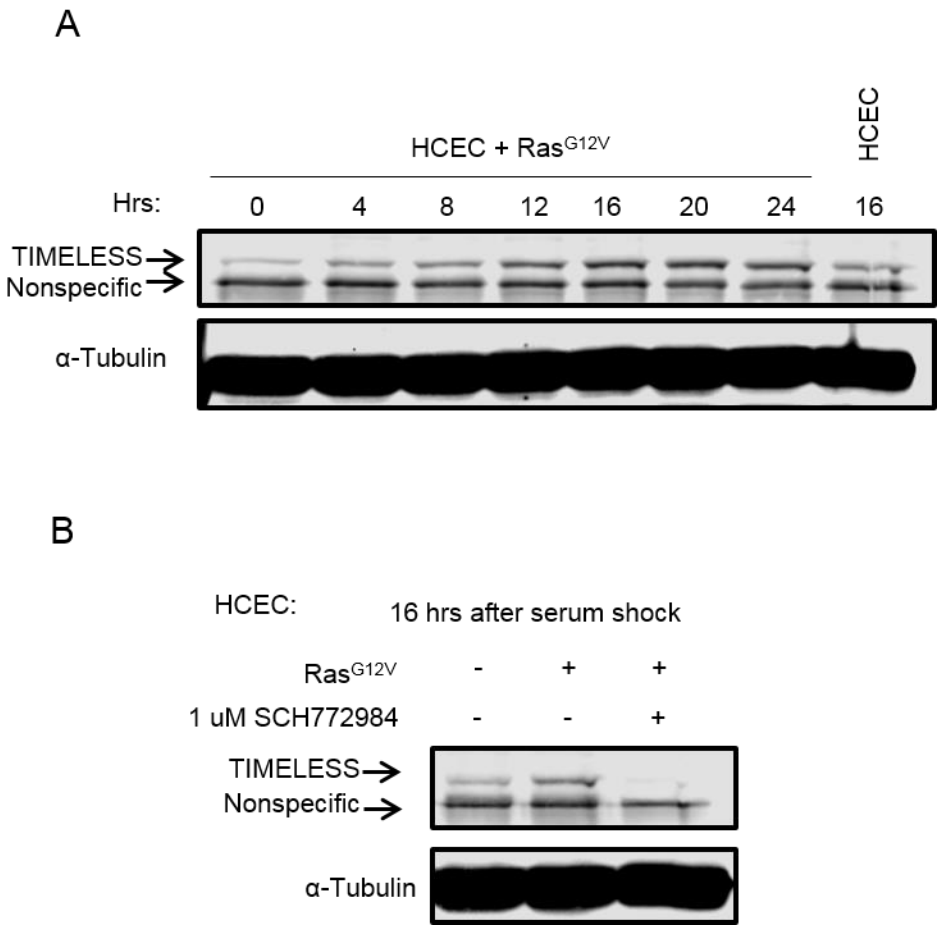

Fig. 4.7: HCECs expressing mutant RasG12V have increased, but circadianly regulated TIMELESS expression. (A) Immunoblot of TIMELESS expression over 24 hours following circadian synchronization via 2 hour 50% horse serum treatment in HCEC with Ras^{G12V}. Lysates from HCECs 16 hours after 50% horse serum shock is included for reference. (B) Immunoblot of TIMELESS in HCECs, HCECs with Ras^{G12V}, and HCECs with Ras^{G12V} treated with 1 μM SCH772984 (ERK inhibitor) 24 hours prior to synchronization with 50% horse serum shock and for the 16 hours after serum shock prior to collection.

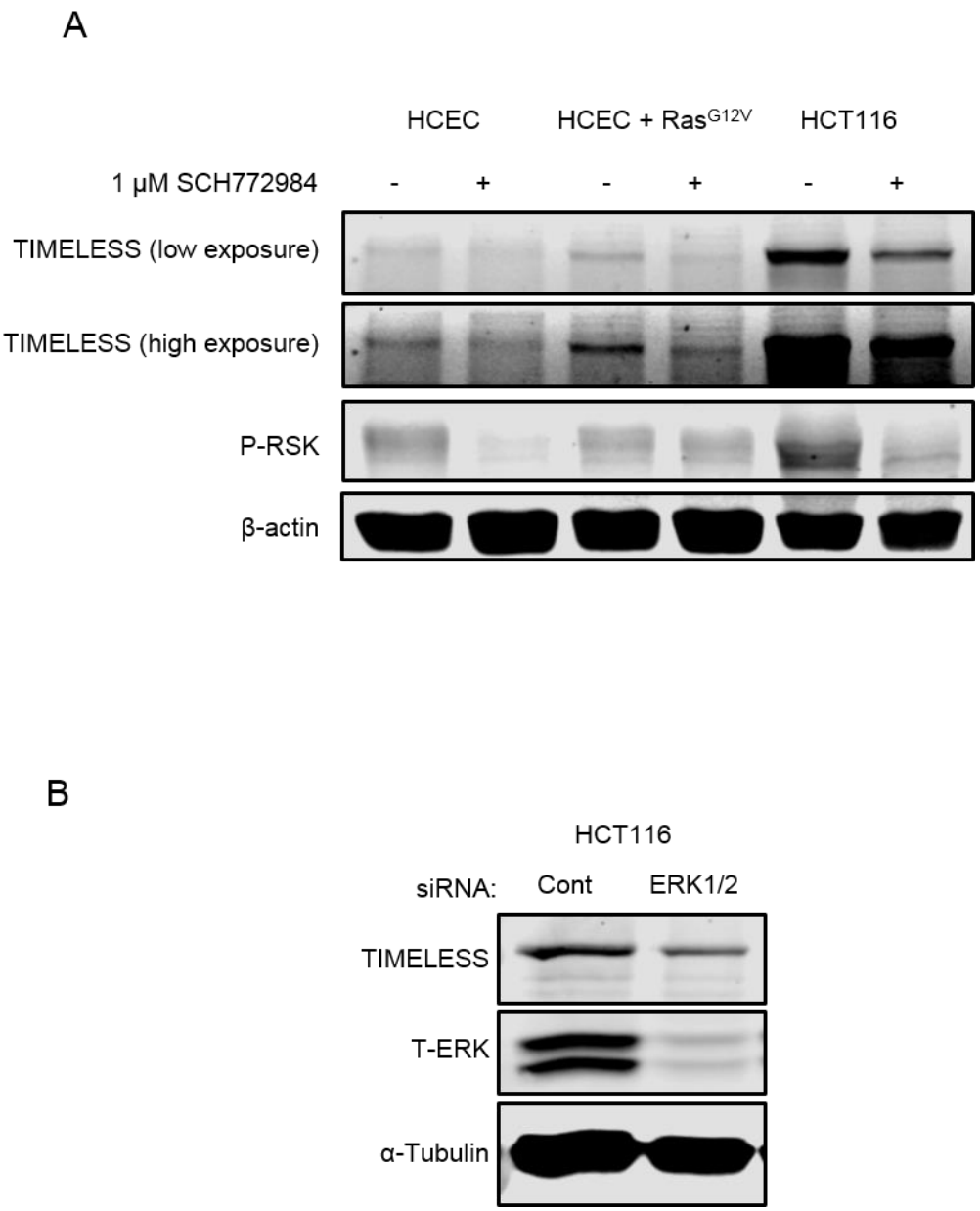

Fig. 4.8: Activated ERK promotes TIMELESS expression. (A) Western blot of TIMELESS in HCECs, HCECs that stably express H-Ras^{G12V}, and HCT116 colon cancer cells with and without 1 μM SCH772984 (ERK inhibitor) treatment for 48 hours. (B) Western blot of TIMELESS following RNAi-mediated ERK1/2 depletion for 72 hours in HCT116 cells. (Experiment 4.8B was done in collaboration with Clara Rich)

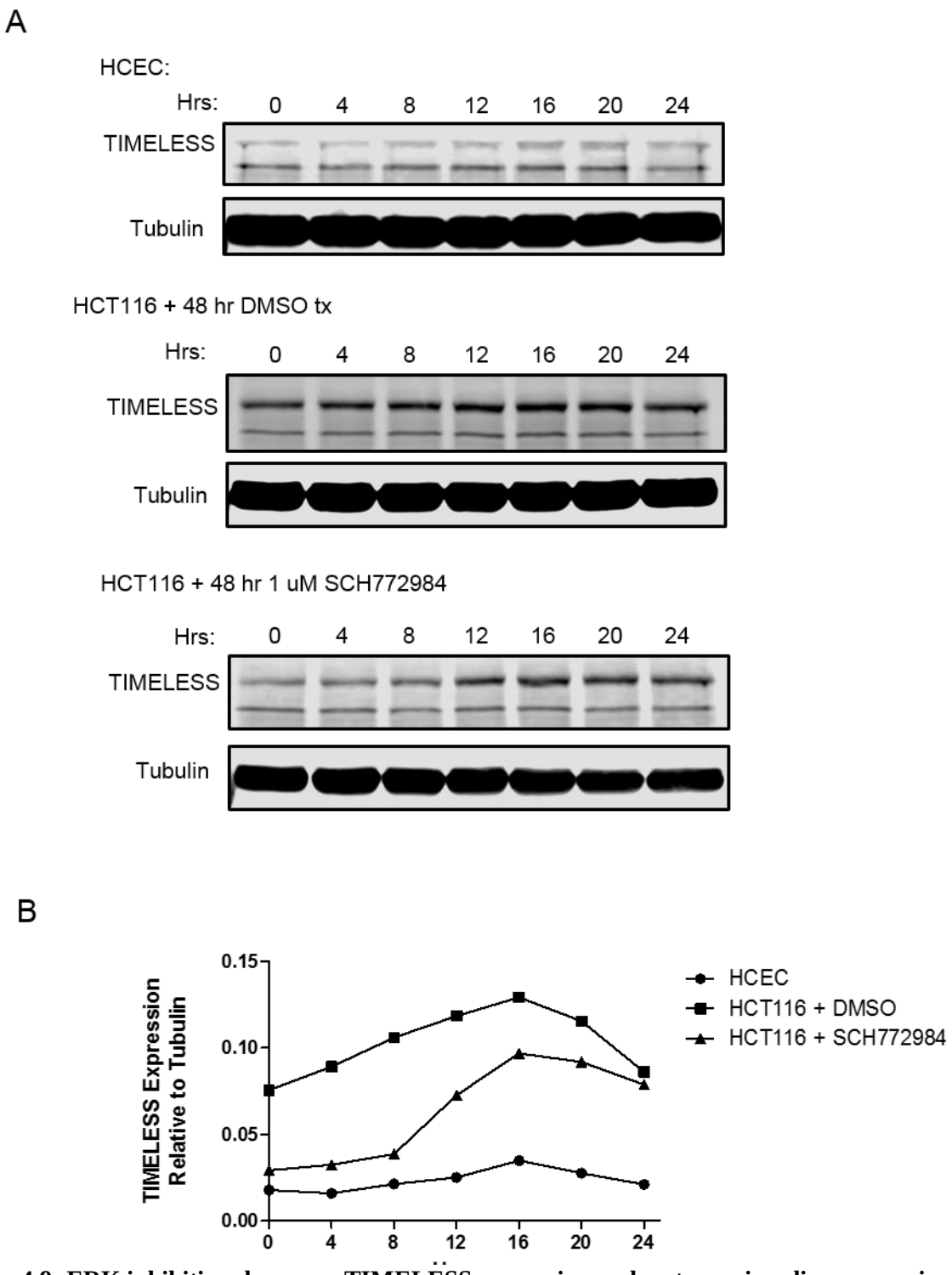

Fig. 4.9: ERK inhibition decreases TIMELESS expression and restores circadian expression of TIMELESS in HCT116 cells. (A) Immunoblot of TIMELESS expression over 24 hours following circadian synchronization via 2 hour 50% horse serum treatment in HCECs (top), HCT116 treated with DMSO (middle), and HCT116 cells treated with 1 μM SCH772984 (ERK inhibitor) (bottom) for 24 hours prior to synchronization and following synchronization throughout the time course until collection. (B) Densitometry quantification of TIMELESS levels in A. (N=1).

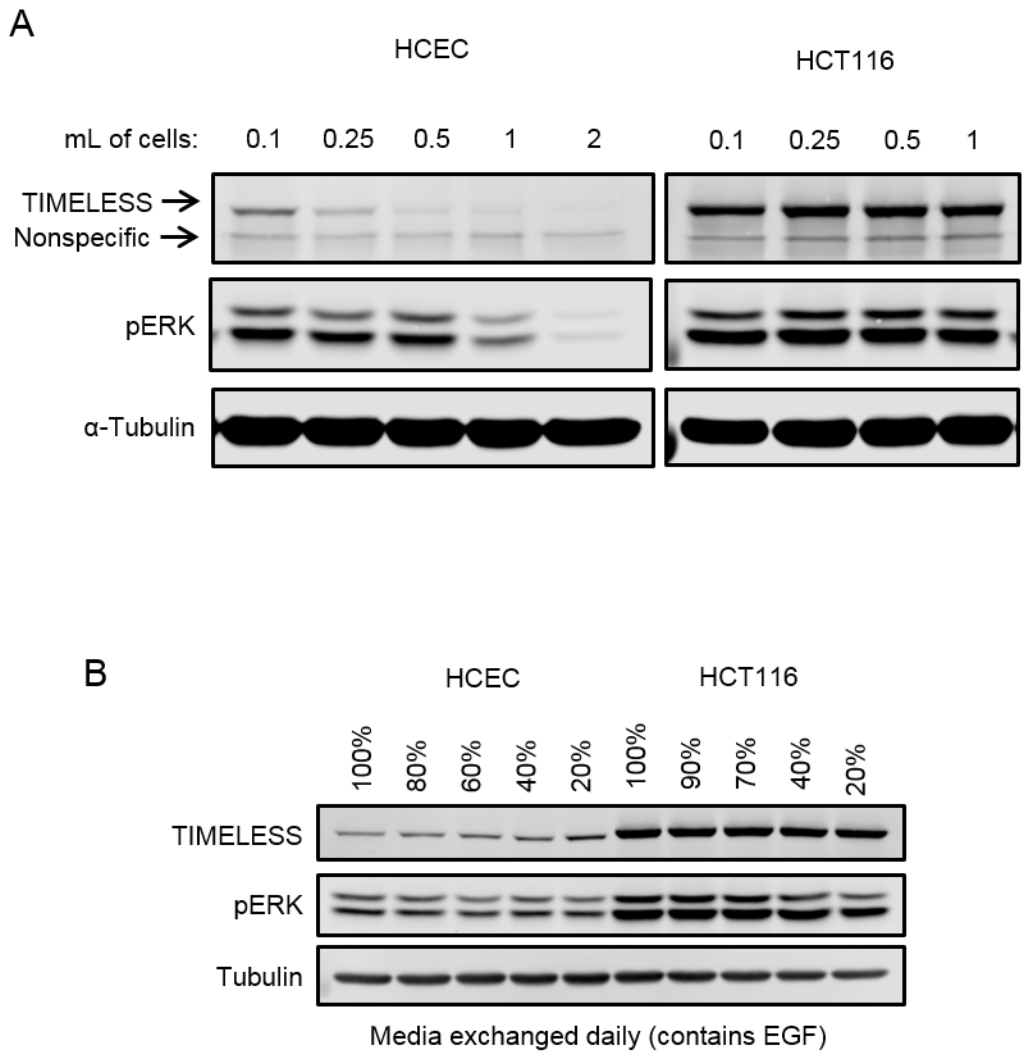

Fig. 4.10: TIMELESS expression correlates with phospho-ERK and is higher in less confluent cells. (A and B) Immunoblot of TIMELESS expression and phosho-ERK in HCEC and HCT116 cells at different stages of confluency without changing media daily (A) or changing media daily (B). Note: In both figures, the lysates from both cell lines were run on single blot and are shown at the same intensities.

cell lines, but did not affect viability or TIMELESS levels in HCT15 and FET cancer cell lines (Fig. 4.11).

TIMELESS is known to be degraded via the ubiquitin-proteosome system. ERK inhibition by 1 μM SCH772984 or MEK inhibition by 1 μM PD0325901 decreases TIMELESS expression, which was not rescued by 6-hour treatment with MG132 (Fig. 4.12A). Unfortunately, the half-life of TIMELESS appears to be extended in cancer such that a 6-hour treatment with MG132 may not have been long enough for TIMELESS expression to be rescued. Conversely, TIMELESS mRNA levels were not affected by ERK inhibition suggesting that ERK is not affecting TIMELESS transcription or mRNA stability (Fig. 4.12B).

ERK inhibition decreases cell viability and TIMELESS expression in HCT116 and SK-Co-1 cells, but not HCT15 or FET cells (Fig. 4.11). In a similar pattern, ERK inhibition reduces MYC expression in HCT116 and SK-Co-1 cells, but not in HCT15 and FET cells (Fig. 4.13A). In normal cells, protein translation is largely regulated by PI3K and mTOR signaling, but recently it has been shown that in some colon cancer cell lines PI3K and mTOR does not regulate MYC translation [218]. This led to the hypothesis that ERK may be regulating translation in these cell lines. Previous work has shown that KSR1 regulates MYC expression in HCT116 cells by promoting its translation via regulation of P-4EBP1 (T70) and PDCD4 [42]. Similarly, ERK inhibition regulates P-4EBP1 (T70) and PDCD4 in HCT116 and SK-Co-1 cells, but not HCT15 and FET cells. This opens the possibility that ERK regulates TIMELESS expression via translation in HCT116 and SK-Co-1 cells. To ascertain if the cell lines that are not affected by ERK inhibition are instead dependent on mTOR signaling for increased translation, the effect of mTOR inhibition on PDCD4, P-4EBP1 (T70), and TIMELESS was examined. mTOR inhibition with 1 μM AZD8055 decreased TIMELESS expression in HCT15 and FET cells, while TIMELESS expression in RKO and SW480 cells decreased with ERK or mTOR inhibition (Fig. 4.13B). P-4EBP1 (T70) decreased in all four colon cancer cell lines tested following mTOR inhibition, with a slight decrease in expression following ERK inhibition in HCT116 cells. ERK

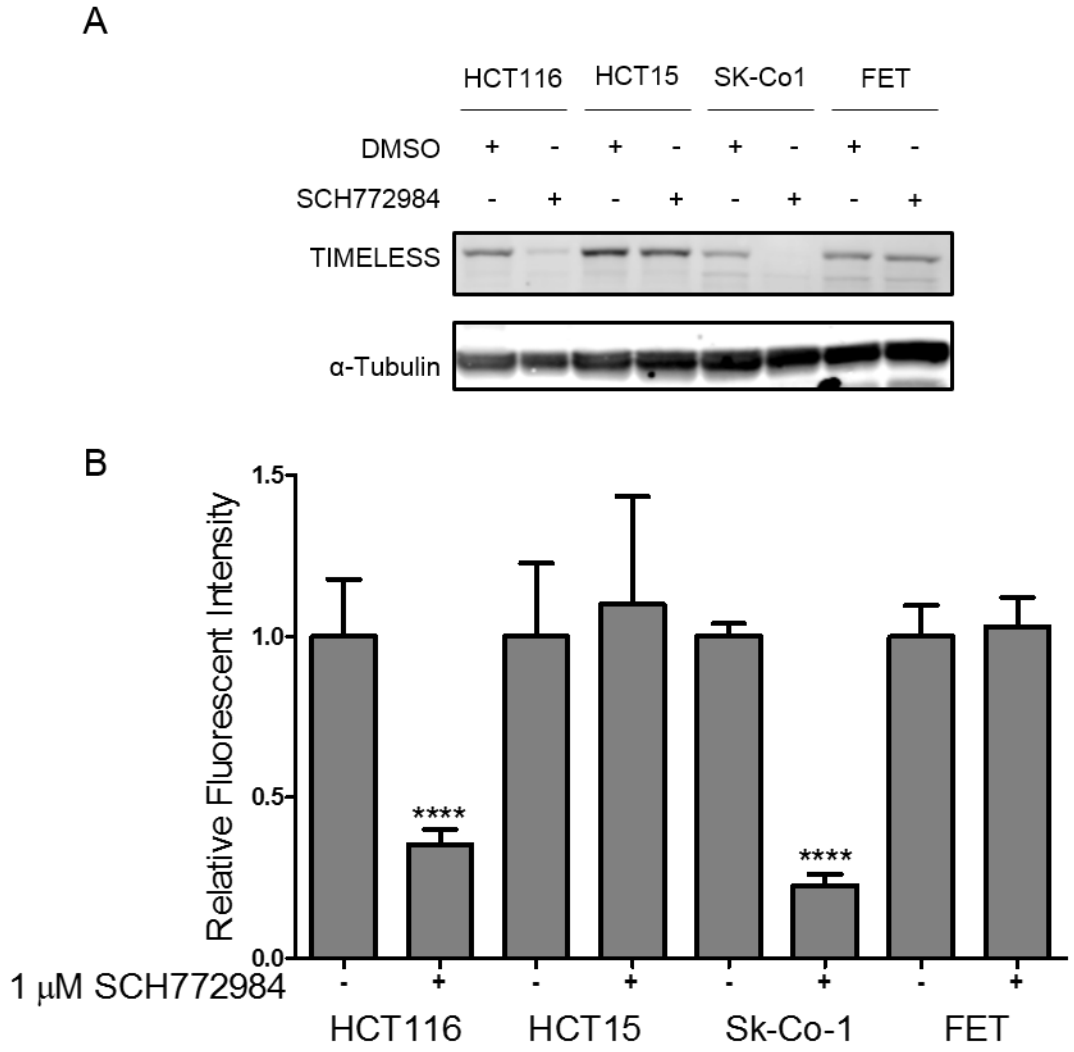

Fig. 4.11: ERK inhibition decreases TIMELESS expression in colon cancer cell lines that are sensitive to ERK inhibition. (A and B) Viability (A) and paired immunoblot analysis of TIMELESS expression (B) following treatment with 1 uM SCH772984 for 48 hours in a panel of colon cancer cells. (N=6). (Experiment 4.11A-B was done in collaboration with Danielle Frodyma)

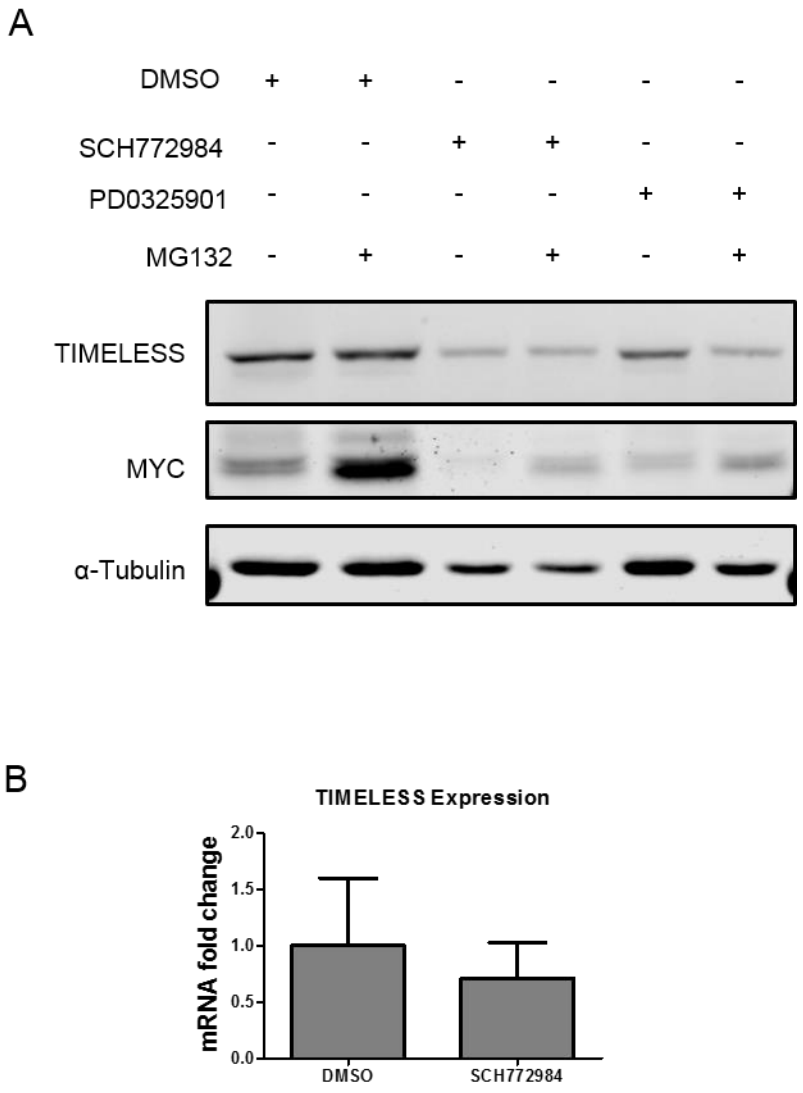

Fig. 4.12: ERK does not promote TIMELESS expression by increasing its protein stability or mRNA levels. (A) Immunoblot of TIMELESS and MYC levels (MG132 rescue control) following treatment with 1 µM SCH772984 (ERK inhibitor), or 1 µM PD0325901 (MEK inhibitor) with and without 10 µM MG132 treatment for 6 hours. (B) TIMELESS mRNA following 48 hour ERK inhibition with 1 µM SCH772984. (N=3). (Experiment 4.12B was performed in collaboration with Jamie McCall).

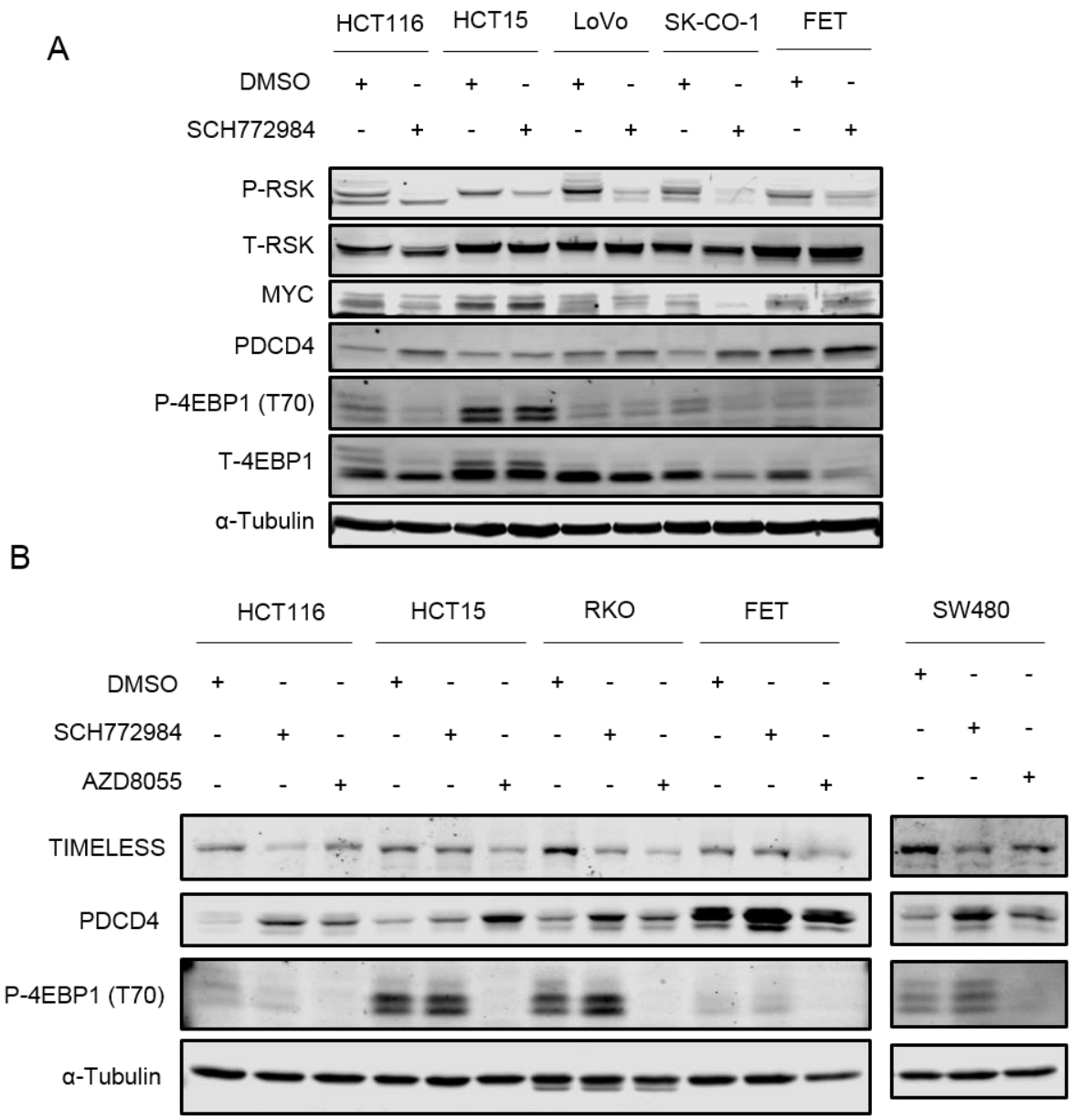

Fig. 4.13: ERK and mTOR inhibition regulates inhibitors of translation in a subset of colon cancer cell lines. (A) Immunoblot of downstream ERK targets (phospho- and total-RSK) regulators of translation (PDCD4, phospho- and total-4EBP1), and MYC following ERK inhibition with 1 μM SCH772984 for 48 hours in HCT116, HCT15, LoVo, SK-CO-1, and FET cells. (B) Immunoblot of PDCD4 and P-4EBP1 (T70) following ERK or mTOR inhibition with 1 μM SCH772984 or AZD8055 for 24 hours in HCT116, HCT15, RKO, FET, and SW480 cells.

inhibition increased PDCD4 expression in the cell lines tested, but this effect was modest in HCT15 and FET cells (Fig. 4.13B).

Using polysome profiling, the translational efficiency of TIMELESS was examined following ERK or mTOR inhibition in HCT116 and HCT15 colon cancer cells, respectively. Translational efficiency is defined as the ratio of polysome-bound mRNA to total mRNA. Total TIMELESS mRNA was unchanged, but polysome-bound TIMELESS mRNA was significantly decreased following ERK inhibition with 1 μM SCH772984 in HCT116 cells or mTOR inhibition with 1 μM AZD8055 in HCT15 cells for 24 hours resulting in an overall decrease in TIMELESS translational efficiency (Fig. 4.14).

To further evaluate the requirement for ERK or mTOR in colon cancer cells, cell viability was examined following single agent treatment with either 1 μM SCH772984 or 1 μM AZD8055 as well as combination treatment with both SCH772984 and AZD8055 either 500 nM or 1 μM doses for 48 hours. Consistent with previous results, HCT116, SW480, and RKO cells were sensitive to both the ERK inhibitor and mTOR inhibitor and underwent a substantial decrease in cell viability with either individual treatment; however, no additional effects were seen with inhibition of both ERK and mTOR together (Fig. 4.15). HCT15 and FET cells were more sensitive to mTOR inhibition than ERK inhibition, but also demonstrated very little additional effect of treating with both inhibitors simultaneously (Fig. 4.15).

The mechanism by which ERK or mTOR regulates translation is thought to be at least in part through RSK; however, RSK inhibition via 1 μM BI-D 1870 treatment only reduced TIMELESS expression in HCT15 cells, but not HCT116 or RKO cells (Fig. 4.16). RSK inhibition in HCT15 cells did not affect PDCD4 levels; however, the effect of RSK inhibition on P-4EBP1 (T70) in these cells is still unknown and could still be mediating an effect of RSK on TIMELESS translation. Additionally, the interpretation of these results is limited by the lack of positive controls that demonstrate the effects of the inhibitors on downstream targets of ERK, mTOR, and RSK. Regardless, the preliminary evidence that RSK may not be mediating the effect

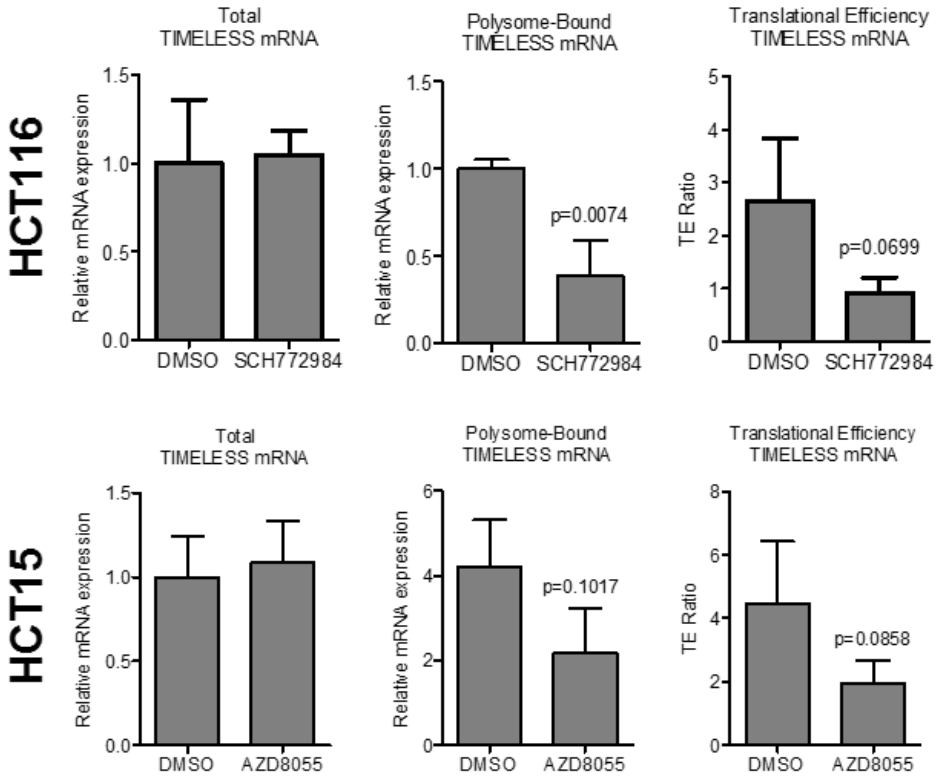

Fig. 4.14: Translation of TIMELESS is decreased following ERK inhibition in HCT116 cells and mTOR inhibition in HCT15 cells. Translational efficiency (TE) of TIMELESS in HCT116 cells (top) following ERK inhibition with 1 μM SCH772984 and in HCT15 cells (bottom) following mTOR inhibition with 1 μM AZD8055 for 24 hours. (N=3). (Experiment 4.14 was completed by Eyerusalem Lemma and Danielle Frodyma.).

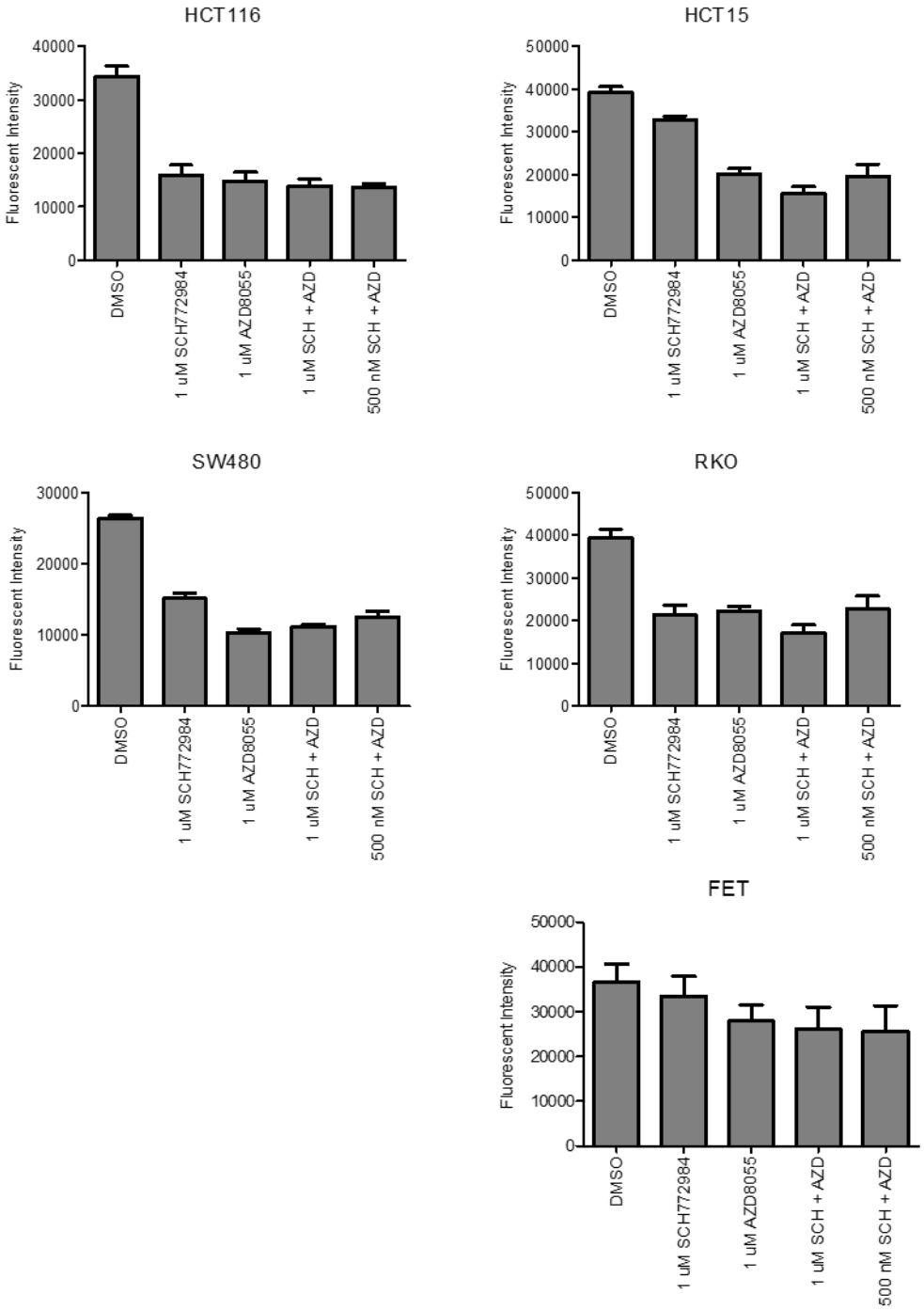

Fig. 4.15: Effects of ERK and mTOR inhibition on cell viability in a panel of colon cancer cell lines. (N=6).

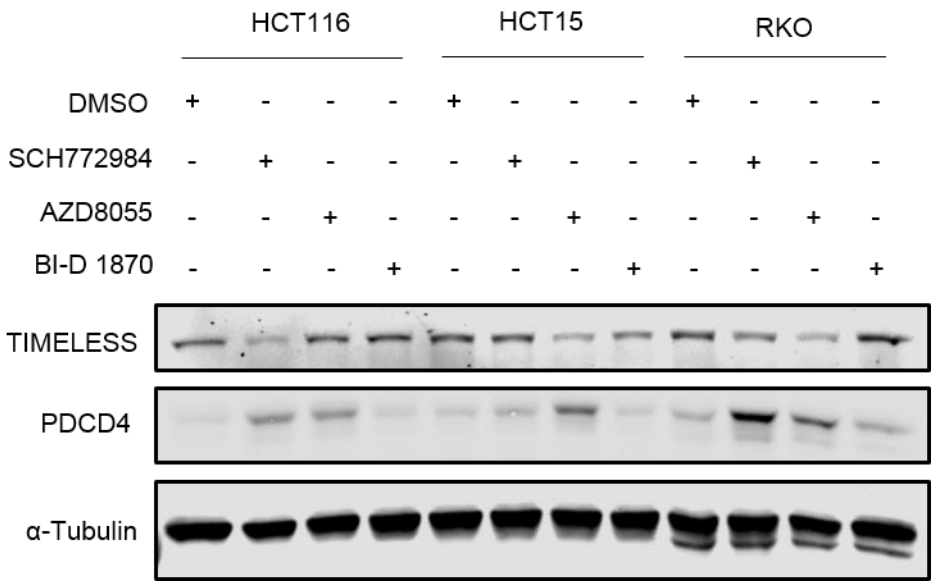

Fig. 4.16: RSK does not mediate the effect of ERK on TIMELESS. Western blot of TIMELESS and PDCD4 following ERK, mTOR, or RSK inhibition for 24 hours with 1 μM of SCH772984, AZD8055, or BI-D 1870 treatment, respectively.

of ERK on TIMELESS expression raises questions about whether this interaction is truly mediated through changes in translation.

TIMELESS is required for cancer cell proliferation

Preliminary biological validation demonstrated that HCT116 colon cancer cells were substantially more sensitive to TIMELESS depletion than HCECs (Fig. 4.3). To determine the prevalence of the requirement for TIMELESS in colon cancer cells, cell viability was measured in a panel of colon cancer cell lines following RNAi-mediated TIMELESS depletion for 96 hours using alamarBlue®. TIMELESS depletion decreased cell viability by more than 20% in HCT116, SW480, SW620, and RKO colon cancer cells (Fig. 4.17A). HCT15 colon cancer cells were not sensitive to TIMELESS depletion (Fig. 4.17A). To determine if this decrease in cancer cell viability was a result of cells undergoing apoptosis, PARP cleavage following TIMELESS depletion for 72 hours was assessed by western blot. TIMELESS depletion induced only a very slight increase in PARP cleavage in HCT116, SW480, and SW620 colon cancer cells and did not affect PARP cleavage in HCT15 or RKO cells (Fig. 4.17B). Therefore, the effect of TIMELESS depletion on cell viability cannot be attributed to an increase in apoptosis.

Comparing the effect of TIMELESS depletion on PARP cleavage in HCECs and HCT116 cells confirmed that TIMELESS depletion induces a small amount of PARP cleavage in HCT116 cells; however, TIMELESS depletion reduced levels of PARP in HCECs without increasing PARP cleavage (Fig. 4.18). Previous reports have clearly demonstrated that TIMELESS physically interacts with PARP [193,194]. This interaction was not required for PARP enzymatic activity, but loss of this interaction reduced the level of DNA damage repair suggesting a functional role for the TIMELESS PARP interaction. This data suggests the possibility that TIMELESS could promote PARP stability.

TIMELESS depletion induces G2/M arrest

A previous study demonstrated that TIMELESS knockdown in HCT116 cells did not

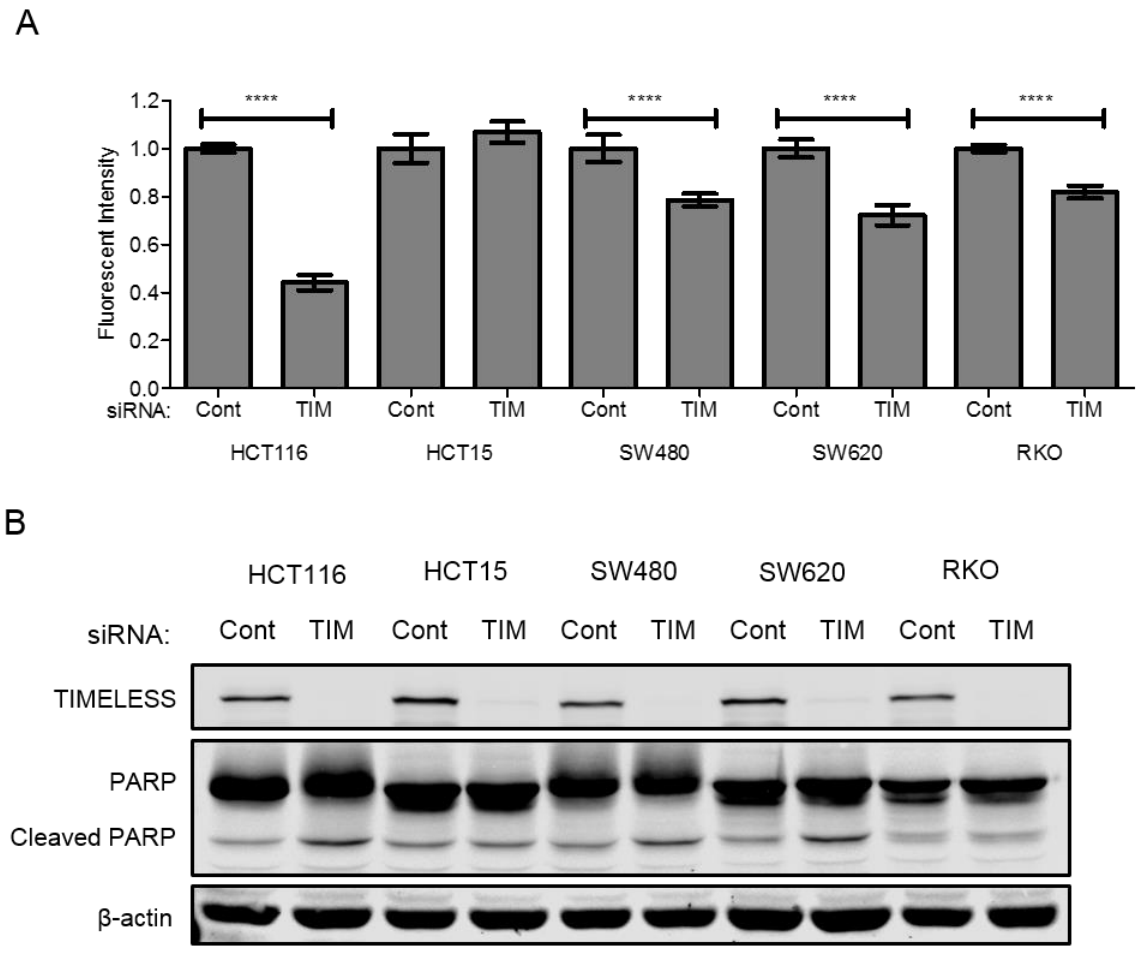

Fig. 4.17: TIMELESS is required for colon cancer cell viability, but does not induce cell death. (A) Cell viability in a panel of colon cancer cells following RNAi-mediated depletion of TIMELESS. Viability was measured by alamarBlue® assays 96 hours after transfection. (N=6). (B) Western blot of TIMELESS and PARP following RNAi-mediated TIMELESS depletion for 72 hours in HCT116, HCT15, SW480, SW620, and RKO colon cancer cells. Data are shown as mean ± SD. * $p < 0.05$, ** $p < 0.01$, *** $p < 0.001$, **** $p < 0.0001$

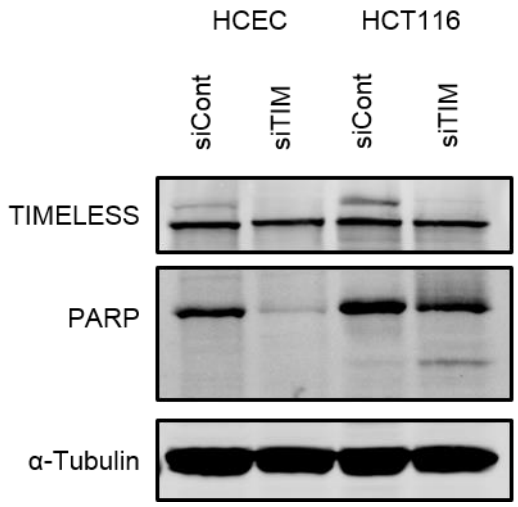

Fig. 4.18: TIMELESS depletion selectively induces low levels of cleaved PARP in HCT116 cells, but not HCECs. Immunoblot of TIMELESS and PARP following RNAi-mediated TIMELESS depletion for 72 hours in HCECs and HCT116 cells.

affect the cell cycle [183]. However, in a panel of colon cancer cell lines, TIMELESS depletion reduced metabolic capacity based on the alamarBlue® viability assay, but did not increase apoptosis based on very little, if any, increase in PARP cleavage (Fig. 4.17B). Additionally, TIMELESS has been shown to play a role in triggering cell cycle checkpoints [163,165,173,182,183]. Therefore, cell cycle analysis was performed using propidium iodide staining and flow cytometry evaluation. In HCT116, SW620, and SW480 colon cancer cell lines a very small increase in sub-G1 peak was induced with TIMELESS depletion (Fig. 4.19). This is consistent with the very minor induction of PARP cleavage in these cell lines following TIMELESS depletion (Fig. 4.17B). All five colon cancer cell lines underwent a decrease in percent of cells within G1 and an increase in percent of cells within G2 (Fig. 4.19).

TIMELESS depletion reduces cancer cell proliferation

To confirm that TIMELESS depletion reduced cell proliferation, or specifically cell division, a carboxyfluorescein succinimidyl ester (CFSE) assay was completed. CFSE is a cell-permeable, fluorescent dye that covalently binds to intracellular molecules, particularly lysine and other amine-containing molecules. The covalent integration of CFSE is highly stable such that the fluorescence is sustained for long periods of time, and the dye is not leached to other cells. With each cell division, approximately half of the integrated CFSE is passed on to each daughter cell, such that the degree of CFSE staining can be used as a marker for cell division. Therefore, HCT116 and SW480 cancer cells were stained with CFSE dye prior to RNAi-mediated TIMELESS depletion for 96 hours. Flow cytometry analysis was then employed to measure CFSE fluorescence levels (Fig. 4.20). Both HCT116 and SW480 cancer cells that lacked TIMELESS had increased mean levels of CFSE demonstrating they underwent fewer cell divisions (Fig. 4.20).

TIMELESS depletion does not affect ERK activation or MYC expression

One previous study demonstrated TIMELESS supports cancer cells by increasing MYC

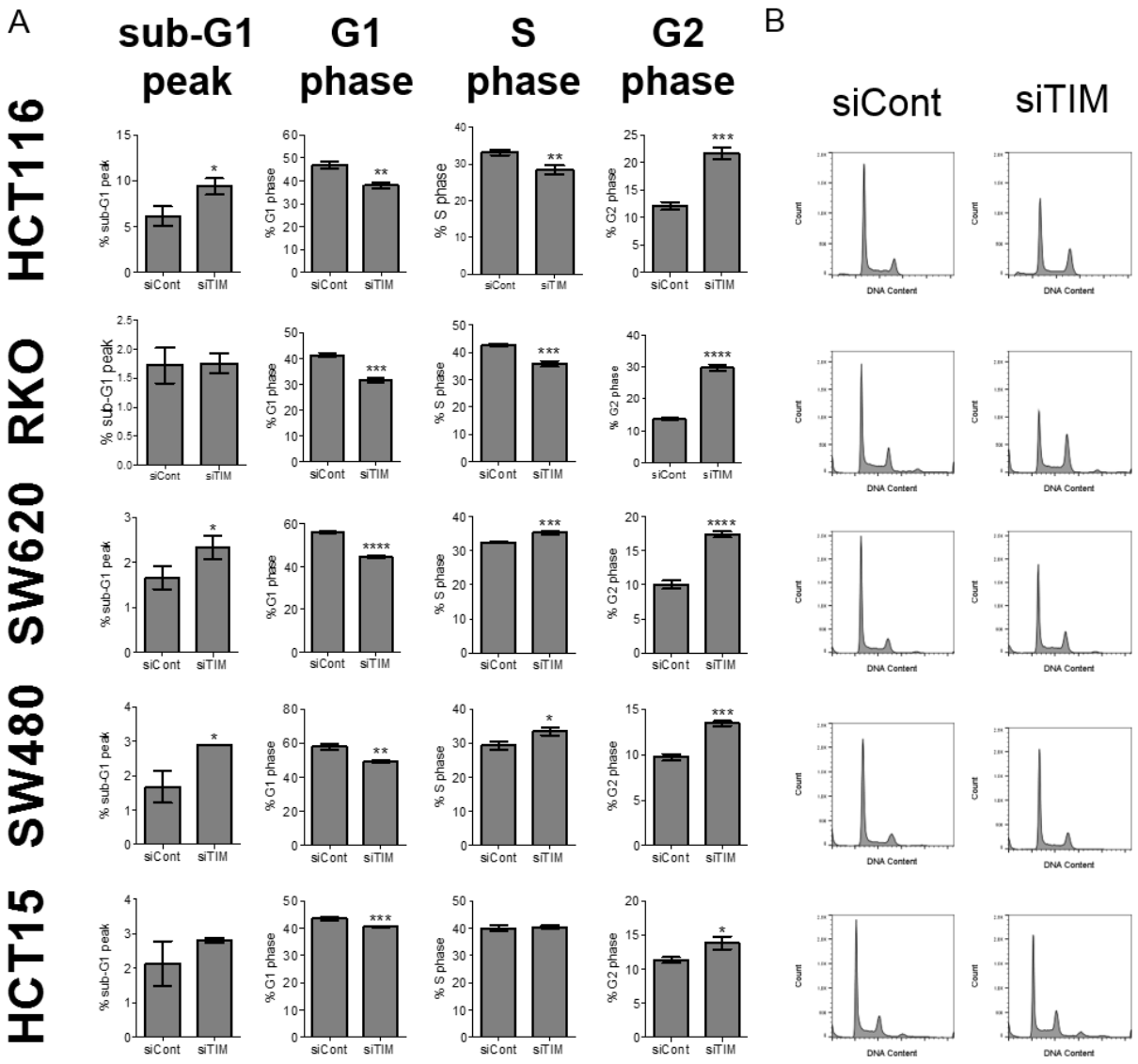

Fig. 4.19: TIMELESS depletion induces a G2/M arrest in a panel of colon cancer cells. (A) Quantification of the percent of cells in each phase of the cell cycle following RNAi-mediated TIMELESS depletion in HCT116, HCT15, SW480, SW620, and RKO colon cancer cells from 3 biological replicates. Apoptosis (% of cells in the sub-G1 peak) and cell cycle were evaluated using propidium iodide staining followed by flow cytometry analysis. (N=3). (B) Representative cell cycle histograms from (A). Data are shown as mean ± SD. * $p < 0.05$, ** $p < 0.01$, *** $p < 0.001$, **** $p < 0.0001$

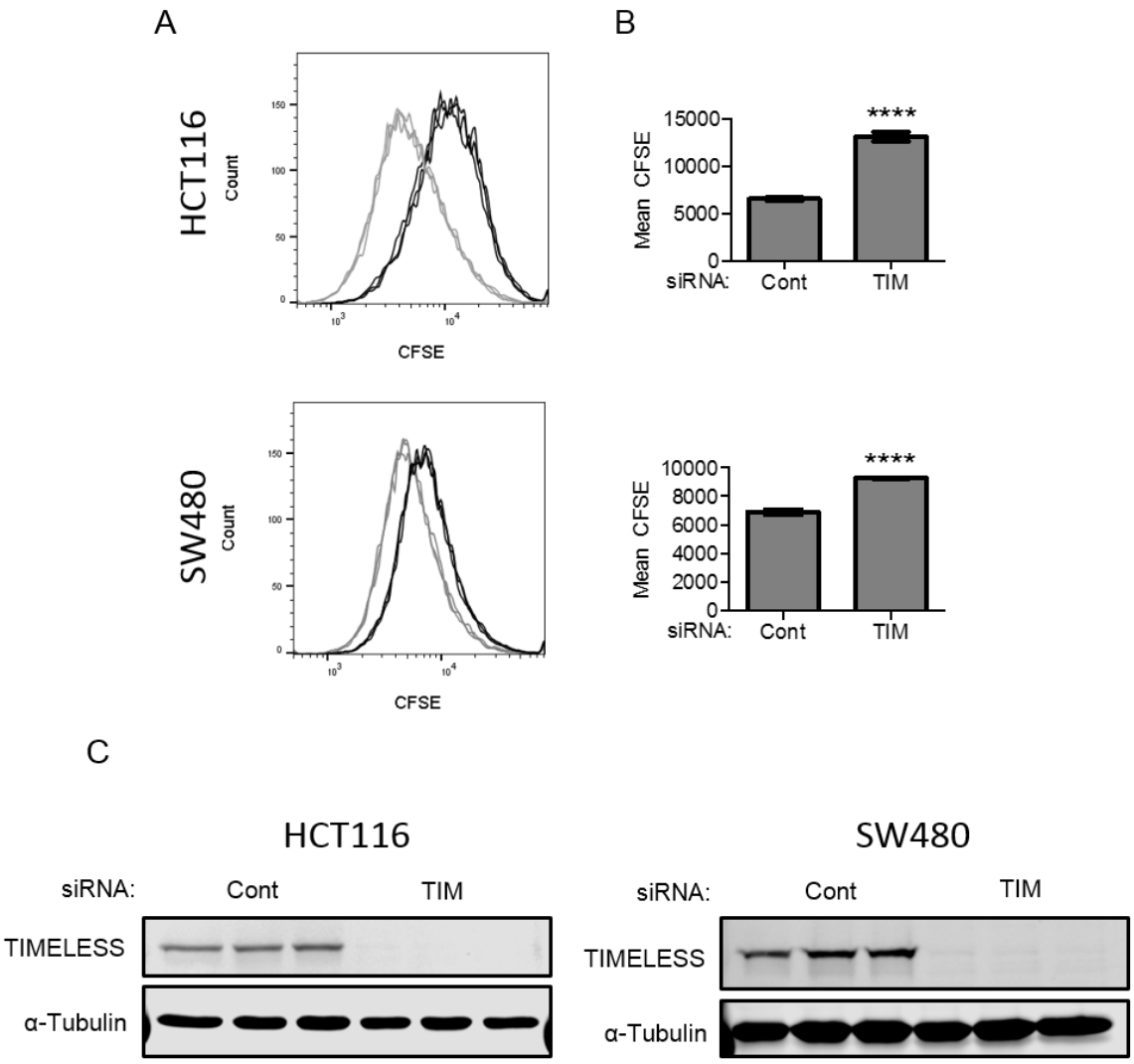

Fig. 4.20: TIMELESS depletion decreases cell proliferation. (A) Overlay histogram for three biological replicates of flow cytometry analysis of CFSE staining following RNAi-mediated TIMELESS depletion in CFSE-stained HCT116 (top) and SW480 (bottom) cells for 96 hours. Control replicates are shown in gray, and TIMELESS-depleted replicates are shown in black. (N=3). (B) Quantification of mean CFSE staining from (A). (C) Western blot confirming TIMELESS depletion in all three biological replicates of CFSE-stained cells from (A). **** $p < 0.0001$

expression and activity [207]. Another report proposed that TIMELESS could support cancer by supporting Ras signaling as Ras mRNA expression was downregulated following TIMELESS depletion [205]. Therefore, the potential for TIMELESS to support Ras or MYC to promote cell cycle advancement and proliferation was evaluated by examining the effects of TIMELESS depletion on MYC expression and ERK activation/phosphorylation. RNAi-mediated TIMELESS depletion for 72 hours did not affect ERK phosphorylation in HCEC or HCT116 cells (Fig. 4.21A) or MYC expression in HCT116 cells (Fig. 4.21B). However, serum shock (50% horse serum for 2 hours) reduced phosphorylation of ERK and induced MYC expression (Fig. 4.21B), which could be contributing to or confounding the results from the *in vitro* examination of the circadian expression of TIMELESS (Fig. 4.6).

TIMELESS depletion decreases AKT phosphorylation

Preliminary experiments demonstrated that TIMELESS reduced AKT phosphorylation and activation (Fig. 4.22). Several previous studies have demonstrated the strong role AKT plays in cell cycle advancement and have shown that expression of activated AKT can drive cells through the G2/M checkpoint via AKT phosphorylation and inactivation of Wee1. When Wee1 is active, it phosphorylates and inactivates CDK1. Therefore AKT-mediated inactivation of Wee1 releases its inhibition of CDK1 thereby preventing G2/M arrest [219,220].

AKT does not mediate the effect of TIMELESS on the cell cycle

Based on this information, the ability of exogenous expression of a mutant, constitutively active form of AKT that had S473 and T308 replaced with aspartic acid (D), which was denoted AKT^{DD}, to rescue the G2/M arrest caused by TIMELESS depletion in HCT116 cells was evaluated. Overall, TIMELESS depletion still induced a small increase in the sub-G1 peak, decreased the number of cells in the G1 phase, and increased the number of cells in the G2 phase in cells transfected with the control eGFP or the eGFP-AKT^{DD} (Fig. 4.23A). However, separating the cells that received the eGFP-AKT^{DD} construct with and without TIMELESS depletion based

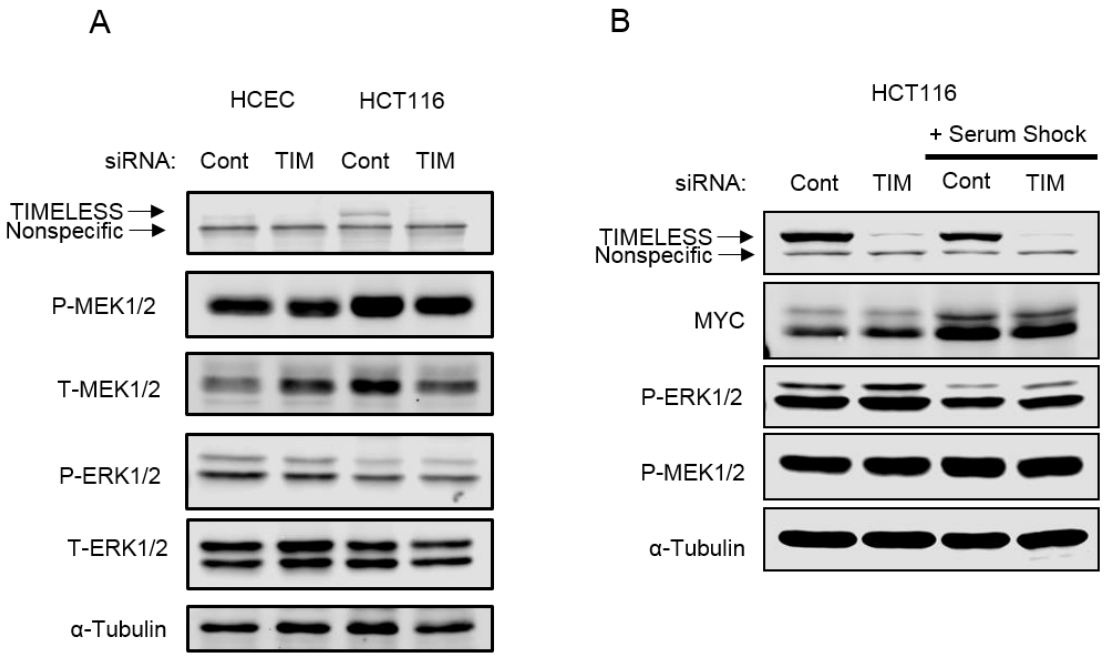

Fig. 4.21: TIMELESS depletion does not affect ERK activation or MYC levels, but serum shock decreases P-ERK and induces MYC expression. (A) Western blot of TIMELESS, phospho- and total-MEK, phospho- and total-ERK following RNAi-mediated TIMELESS depletion for 72 hours in HCECs and HCT116 cells. (B) Immunoblot of TIMELESS, MYC, phospho-ERK, and phospho-MEK following RNAi-mediated TIMELESS depletion with and without 50% horse serum shock for two hours in HCT116 cells.

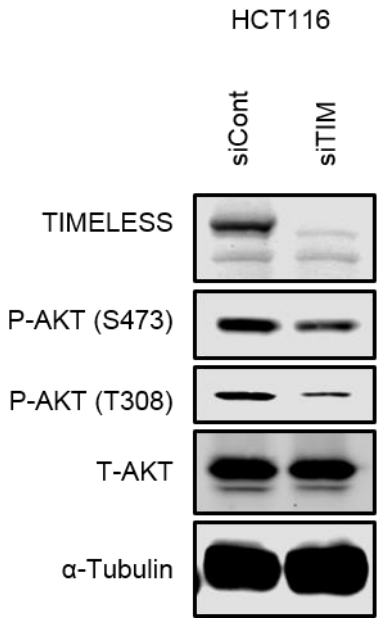

Fig. 4.22: TIMELESS depletion decreases AKT activation. Western blot of phospho- and total-AKT (S473 and T308) following RNAi-mediated TIMELESS depletion for 72 hours in HCT116 cells.

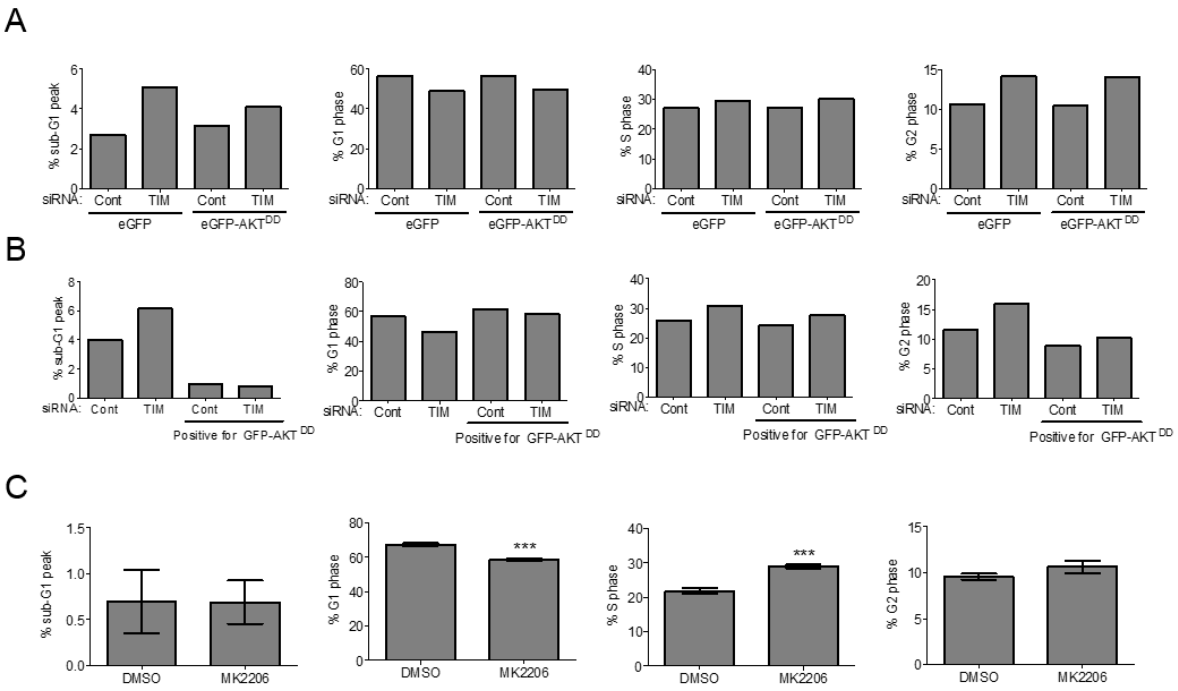

Fig. 4.23: AKT can drive cells through G2/M, but AKT inhibition does not mimic TIMELESS depletion and cause G2/M arrest. (A) Cell cycle analysis by PI stain following TIMELESS depletion for 72 hours and exogenous expression of AKT^{DD} for 48 hours prior to collection. (N=1). (B) Re-evaluation of data from A separating the eGFP-AKT^{DD} based on GFP positivity. (N=1). (C) Cell cycle analysis following inhibition of AKT with 500 nM MK2206 for 48 hours. (GFP-AKT^{DD} and the AKT inhibitor MK2206 were a kind gift from the Black Lab at UNMC).

on GFP positivity revealed that the cells expressing the eGFP-AKT^{DD} no longer underwent G2/M arrest following TIMELESS depletion (Fig. 4.23B). This suggested that activated AKT was able to push the cells through the G2/M cell cycle checkpoint. However, inhibition of AKT with MK2206 did not induce a G2/M arrest, but instead triggered S phase arrest (Fig. 4.23C). This suggests that TIMELESS depletion is not inducing G2/M arrest through AKT despite the potential for activated AKT to rescue cells from this arrest.

TIMELESS depletion causes G2/M arrest through increasing levels of DNA damage and subsequent phosphorylation of CHK1 and CDK1

In normal cells, TIMELESS has been shown to promote DNA synthesis and DNA damage repair [114,160]. In a panel of five colon cancer cell lines, RNAi-mediated TIMELESS depletion for 72 hours ubiquitously caused an increase in γH2AX, a marker of DNA damage (Fig. 4.24). Downstream of γH2AX, all five cancer cell lines demonstrated increased phosphorylation of CHK1 and CDK1 (Fig. 4.24), which provides a mechanism for the G2/M arrest following TIMELESS depletion. The increase in γH2AX, P-CHK1, and P-CDK1 was recapitulated using four individual oligos targeting TIMELESS in HCT116 cells (Fig. 4.25). This mechanism appears to also be present in HCECs, but is triggered to a lesser degree likely as a result of intact DNA repair mechanisms, high fidelity DNA replication, and a slower cell proliferation rate in the normal HCECs compared to colon cancer cells (Fig. 4.26).

ERK inhibition increases γH2AX, which cannot be rescued with exogenous TIMELESS expression

Since ERK inhibition decreases TIMELESS expression, and TIMELESS depletion dramatically increased the level of γH2AX, the effect of ERK inhibition on DNA damage was examined, which demonstrated that ERK inhibition also substantially increased the phosphorylation of H2AX (γH2AX) (Fig. 4.27). To determine if this increase in γH2AX was an effect of decreased TIMELESS levels following ERK inhibition, TIMELESS was transiently

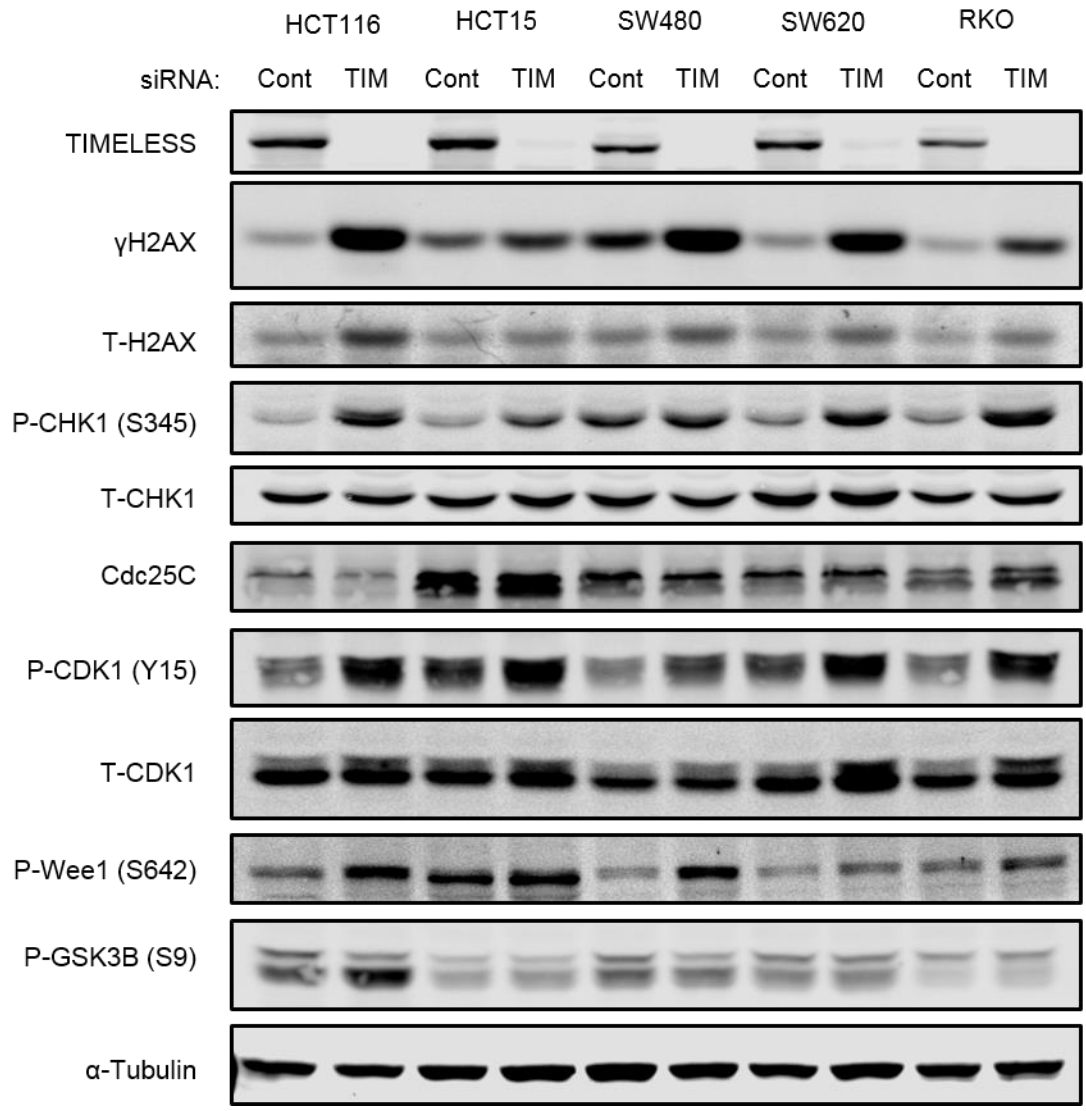

Fig. 4.24: TIMELESS depletion induces G2/M arrest via CHK1 phosphorylation, which leads to Cdk1 phosphorylation and inactivation. Immunoblot of phospho- and total-H2AX, phospho- and total CHK1 (S345), phospho- and total- CDK1 (Y15) and AKT targets phospho-GSK3B (S9) and phospho-Wee1 (S642) following RNAi-mediated TIMELESS depletion for 72 hours in a panel of colon cancer cells. Note: The primary antibody used for the T-CDK1 blot was 77055 cell signaling antibody. All other T-CDK1 blots used the 9112 cell signaling antibody.

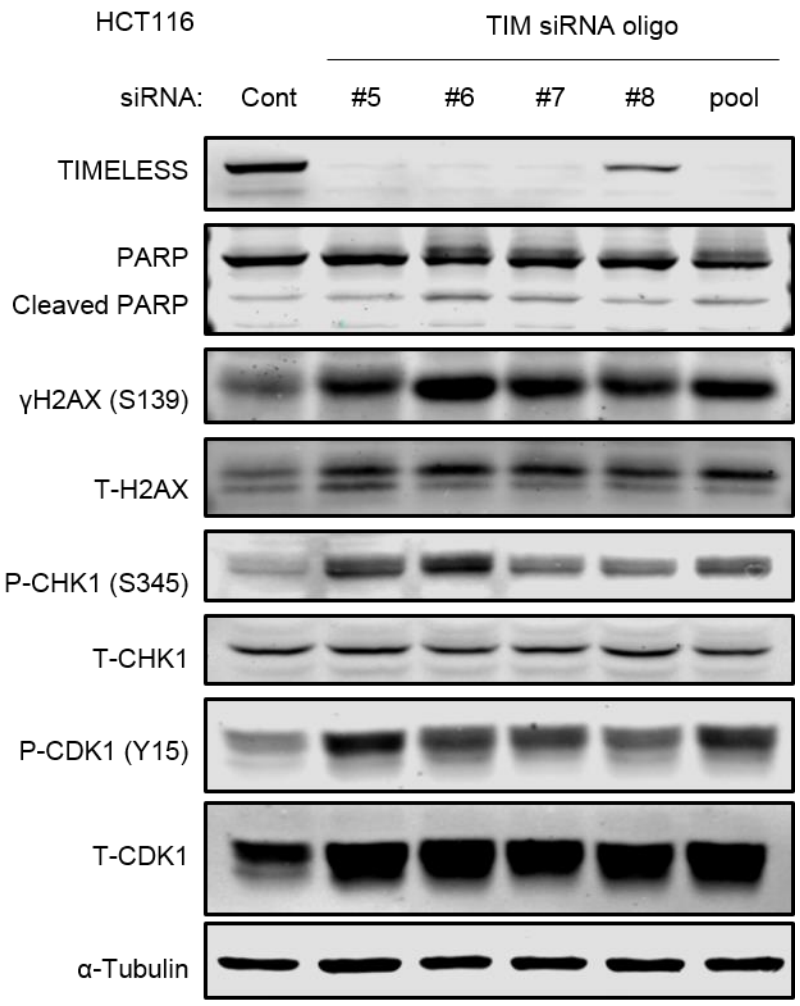

Fig. 4.25: Individual oligos induce TIMELESS depletion, which causes increased γH2AX, CHK1 phosphorylation, and CDK1 phosphorylation in HCT116 cells. Western blot of phospho- and total-H2AX, phospho- and total CHK1 (S345), phospho- and total- CDK1 (Y15) following RNAi-mediated TIMELESS depletion for 72 hours using four individual oligos or a pool of all four oligos in HCT116 cells.

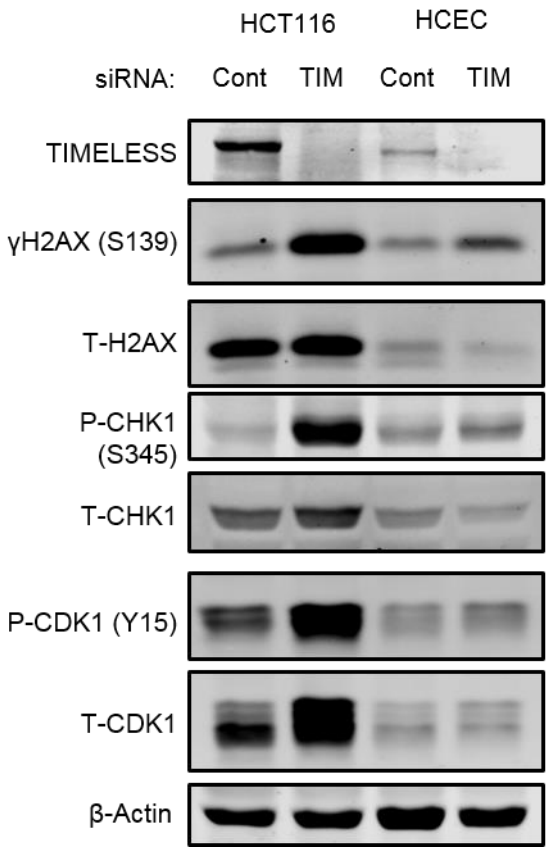

Fig. 4.26: TIMELESS depletion induces increased γH2AX, CHK1 phosphorylation, and CDK1 phosphorylation in HCT116 cells and to a lesser extent in HCECs. Western blot of phospho- and total-H2AX, phospho- and total CHK1 (S345), phospho- and total- CDK1 (Y15) following RNAi-mediated TIMELESS depletion for 72 hours in HCEC and HCT116 cells.

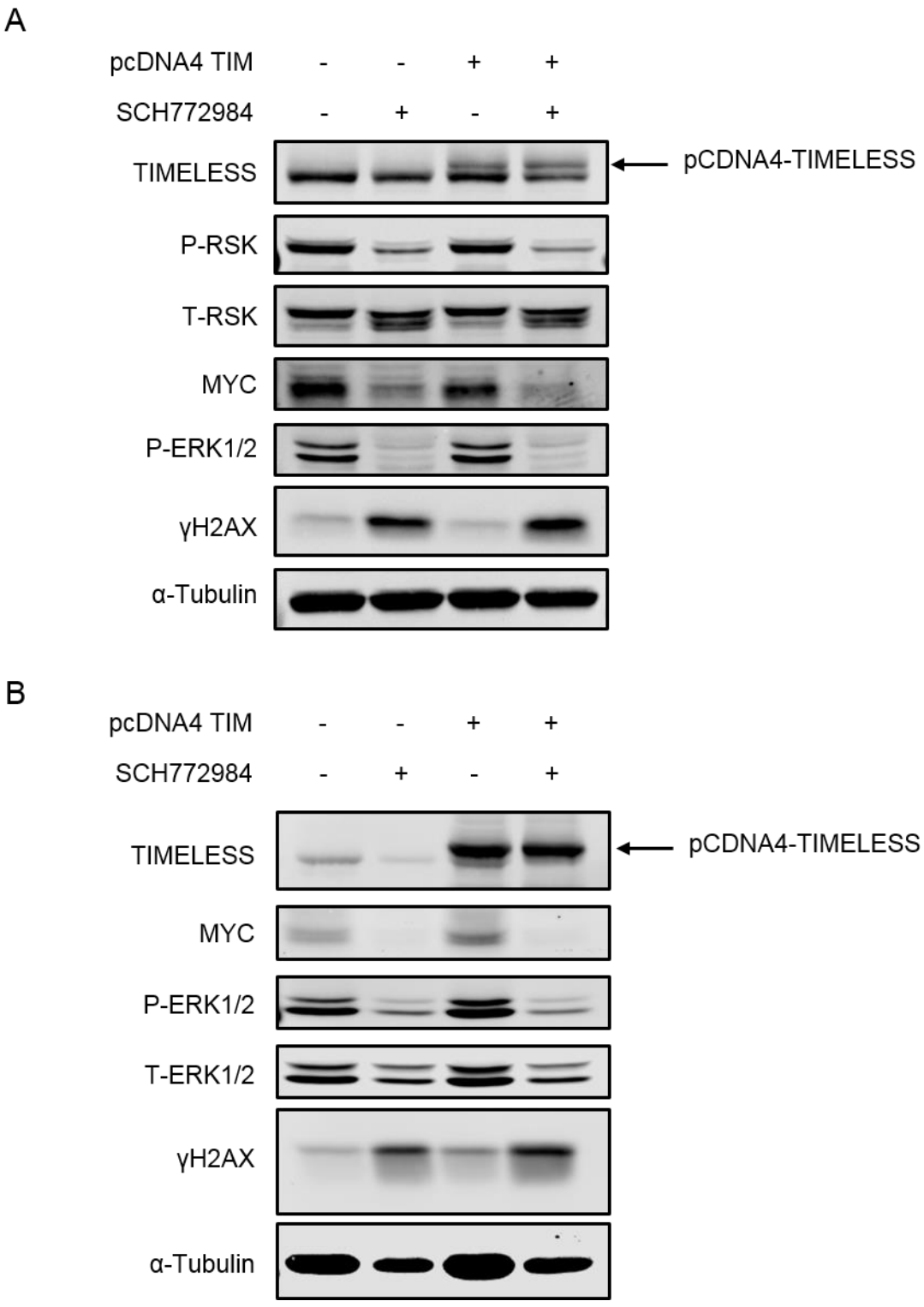

Fig. 4.27: Exogenous TIMELESS expression does not prevent the accumulation of γH2AX following ERK inhibition. (A and B) Western blot of ERK and its downstream targets including γH2AX following moderate (A) or high (B) exogenous expression of TIMELESS for 72 hours with or without ERK inhibition with 1 μM SCH772984 for 48 hours.

exogenously expressed in HCT116 cells prior to treatment with SCH772984 for 48 hours. Low levels (Fig. 4.27A) and high levels (Fig. 4.27B) of exogenous TIMELESS were unable to prevent the increase in γH2AX or restore MYC expression in HCT116 cells following ERK inhibition (Fig. 4.27) suggesting the induction of γH2AX following ERK inhibition is not solely due to a decrease in TIMELESS expression.

Of note, while ERK inhibition decreased endogenous TIMELESS expression, it did not affect the exogenous expression (Fig. 4.27). This demonstrates that ERK does not affect TIMELESS protein stability, and must instead affect either transcription, mRNA stability, or translation.

ERK inhibition prevents the phosphorylation and activation of CHK1 and CDK1 in response to DNA damage.

Paradoxically, ERK inhibition with 1 μM SCH772984 for 24 hours in HCT116 cells dramatically reduces the total and phosphorylated levels of CHK1 and CDK1 despite an increase in γH2AX (Fig. 4.28). This is consistent with previous reports that ERK is activated in response to DNA damage, and this activation contributes to DNA damage-induced cell cycle arrest or apoptosis depending on the level of DNA damage induced [221]. This effect may be coordinated by RSK as RSK has been shown to phosphorylate CHK1 at S280, which is a prerequisite for nuclear localization that is required for DNA-damage induced ATR-mediated phosphorylation of CHK1 at S345 [222]. Thus, Ras signaling ensures high DNA fidelity during DNA replication to allow for increased cell proliferation, which explains the loss of CHK1 and CDK1 phosphorylation with ERK inhibition.

Combination therapy with TIMELESS depletion and DNA-damaging chemotherapies

TIMELESS depletion caused an increase in γH2AX, a marker of DNA damage; however, it is unclear whether this increase is due to an increase in the induction of DNA damage or a reduced capacity to repair DNA damage. Regardless of the mechanism, the potential exists for

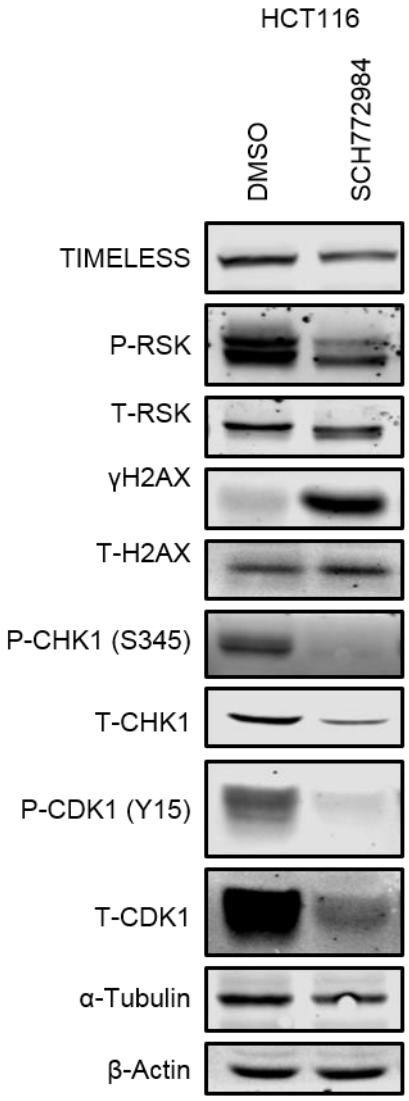

Fig. 4.28: ERK inhibition increases γH2AX, but decreases phospho- and total- CHK1 and CDK1. (A) Western blot of TIMELESS, phospho- and total- RSK, phospho- and total- CHK1, and phospho- and total- CDK1 after ERK inhibition for 24 hours with 1 μM SCH772984.

TIMELESS depletion to synergize with other DNA-damaging therapies as the combination could further induce damage or the increased induction of damage could be amplified by a decreased ability to repair it. Therefore, the effect of TIMELESS depletion with other DNA damaging agents including mitomycin C (MMC), 5-fluoruracil (5-FU), and oxaliplatin (OXAL) was examined. The induction of γH2AX following TIMELESS depletion was modestly increased with the addition of MMC (Fig. 4.29). Treatment with 5-FU further decreased viability compared to TIMELESS depletion alone, but the effect was small and likely was not even additive (Fig. 4.30A). OXAL treatment reduced the effect of TIMELESS depletion (Fig. 4.30A). Interestingly, treatment with 5-FU did not increase and may have in fact reduced the level of γH2AX following TIMELESS depletion, while OXAL treatment caused a slight increase in γH2AX following TIMELESS depletion (Fig. 4.30B). Even though these are largely negative results, they may provide hints towards the mechanism behind the requirement for TIMELESS in cancer cells. The principal mechanism by which 5-FU affects cancer cells is by inhibiting DNA replication through depletion of thymidine that is required for DNA synthesis. If TIMELESS is limiting the induction of DNA damage during DNA synthesis by supporting replication fork stability, slowing DNA synthesis through 5-FU treatment, may, in fact, reduce the level of DNA damage induced by TIMELESS depletion, while serving to reduce cell proliferation. On the other hand, OXAL directly induces double-stranded DNA breaks and blocks DNA replication following the formation of platinum-DNA adducts or cross-linking DNA. This could explain the increased level of γH2AX, while also reducing the effect of TIMELESS depletion by again limiting DNA synthesis.

Combination therapy with TIMELESS depletion and ionizing radiation

Examining TIMELESS depletion in combination with ionizing radiation (IR) treatment in a panel of colon cancer cell lines revealed variable effects with HCT116, SW480, SW620, and T84 cells showing some increased effects with combination treatment, while HCT15, RKO, and LoVo cells did not (Fig. 4.31A). However, even in the cell lines that demonstrated some effect of

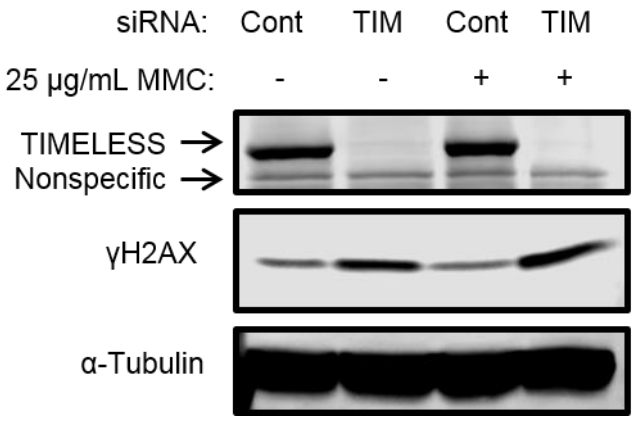

Fig. 4.29: TIMELESS depletion induces DNA damage as evidenced by increased phosphorylation of H2AX. (A) Western blot of phospho- and total H2AX following RNAi-mediated TIMELESS depletion for 72 hours with and without MMC treatment for 48 hours in HCT116 cells. (Fig. 4.26A was completed in collaboration with Danielle Frodyma).

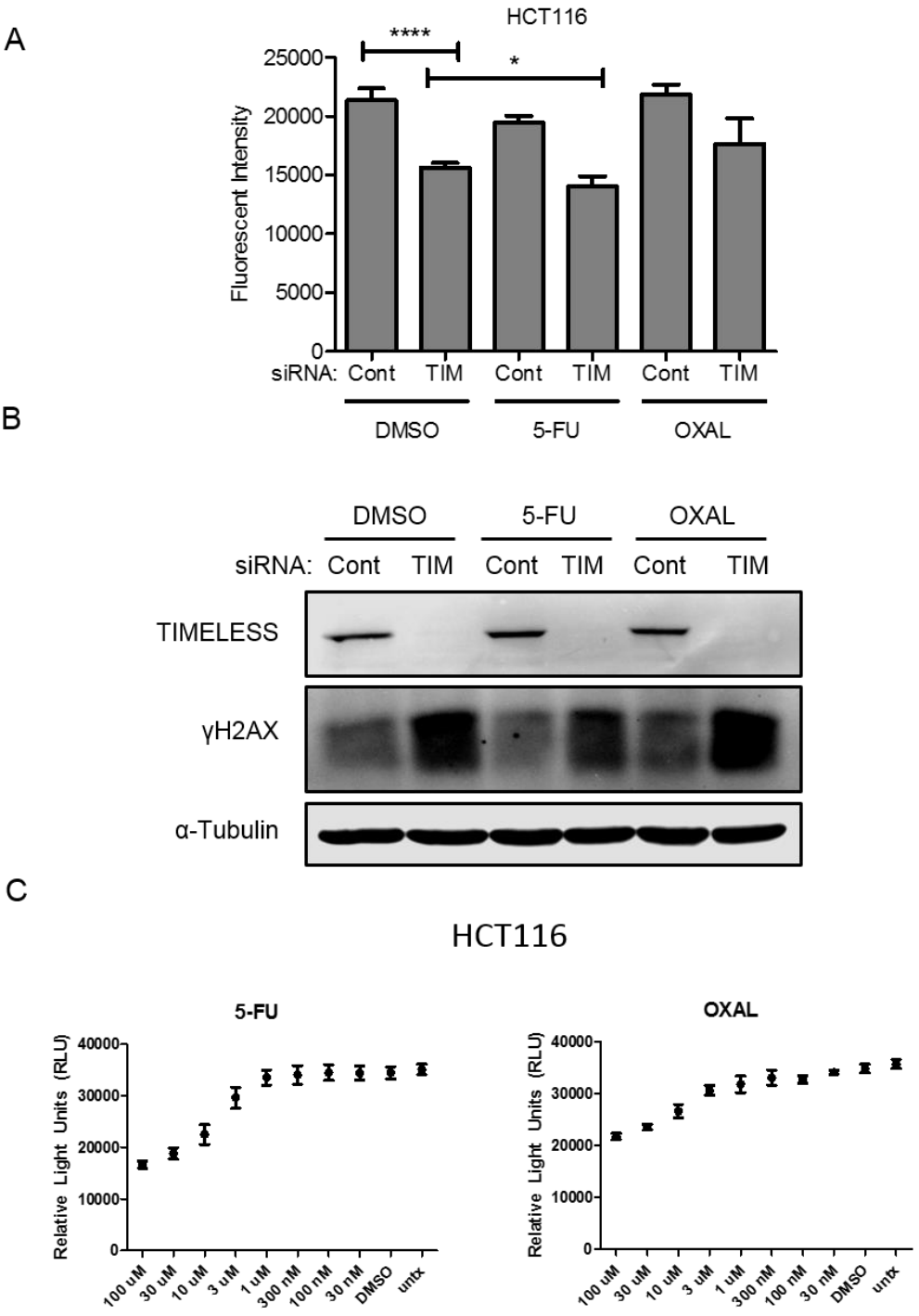

Fig. 4.30: TIMELESS depletion in conjunction with DNA damaging agents (5-FU and oxaliplatin). (A and B) Cell viability (A) as measured by alamarBlue and western blot (B) of γH2AX in HCT116 cells following 72-hour TIMELESS depletion in combination with 1 μM 5-FU or OXAL treatment for 48 hours. (C) Dose-response curves for 5-FU and oxaliplatin (OXAL) in HCT116 cells treated for 48 hours.

combination treatment, the effect of the combination demonstrated less than additive effects. Specifically, in HCT116 cells, both TIMELESS depletion or IR treatment alone dramatically reduced cell viability; however, the combination barely outperformed either of these treatments individually based on viability (Fig. 4.31A). The combination of TIMELESS depletion with IR did increase the level of γH2AX further than either TIMELESS depletion or IR treatment alone (Fig. 4.31B). Taken together these results suggest there may be limiting returns for inducing more and more DNA damage or a longer assay may be needed for the full effects of these combination treatments to be realized.

Combination therapy with TIMELESS depletion and cell cycle checkpoint inhibitors

Since TIMELESS depletion induces G2/M arrest, the potential for TIMELESS depletion to synergize with checkpoint inhibition was examined. With individual drug treatment, CHK1 inhibition was more lethal than Wee1 inhibition in all cell lines except HCT15 cells, which were more sensitive to the Wee1 inhibitor (Fig. 4.32). Cell viability was decreased with TIMELESS depletion in HCECs, but combination treatment with Wee1 or CHK1 inhibitors reduced this effect (Fig. 4.32). In contrast, TIMELESS depletion in combination with Wee1 or CHK1 inhibition further decreased cell viability than either perturbation alone in all the colon cancer cell lines tested except for HCT15 cells (Fig. 4.32). Inhibition of Wee1 or CHK1 actually increased the percentage reduction in viability following TIMELESS depletion suggesting at least additive, if not synergistic, effect with this combination in all of the colon cancer cell lines tested, but an inhibitory effect in HCECs (Fig. 4.32B). Interestingly, TIMELESS depletion has no effect in HCT15 cells with no drug treatment or Wee1 inhibition; however, CHK1 inhibition sensitized HCT15 cells to TIMELESS depletion.

Conclusions

This and previous studies have demonstrated that TIMELESS is highly expressed in multiple types of cancer [204,206,207,210,216,217]. Despite the high prevalence of TIMELESS

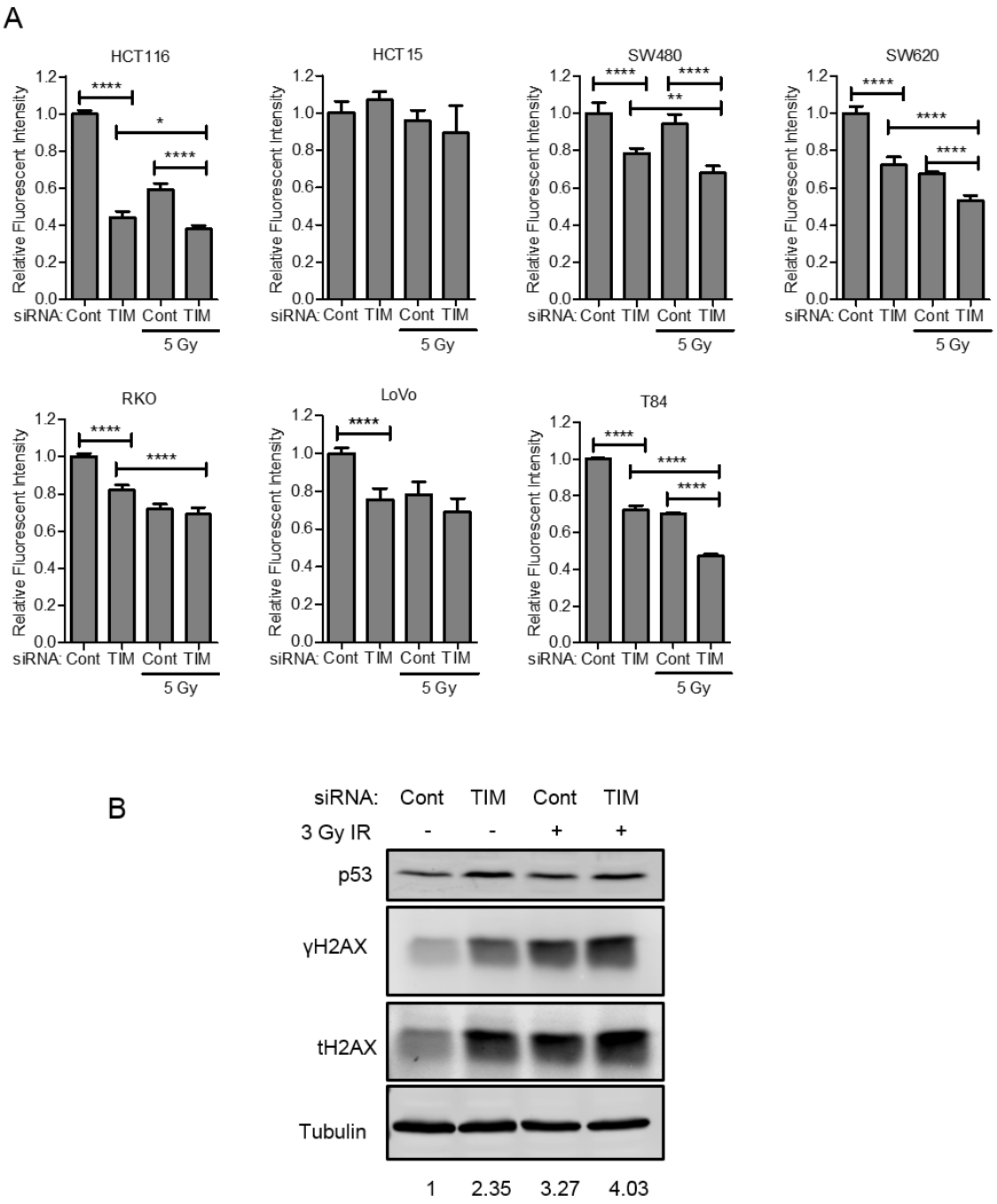

Fig. 4.31: TIMELESS depletion in conjunction with ionizing radiation in a panel of colon cancer cell lines. (A and B) Viability (N=6) (A) and Western blot (B) of p53, phospho- and total-H2AX following RNAi-mediated TIMELESS depletion for 96 hours with and without a single dose treatment of 5 or 3 Gy ionizing radiation 48 hours prior to collection in a panel of colon cancer cells and HCT116 cells, respectively.

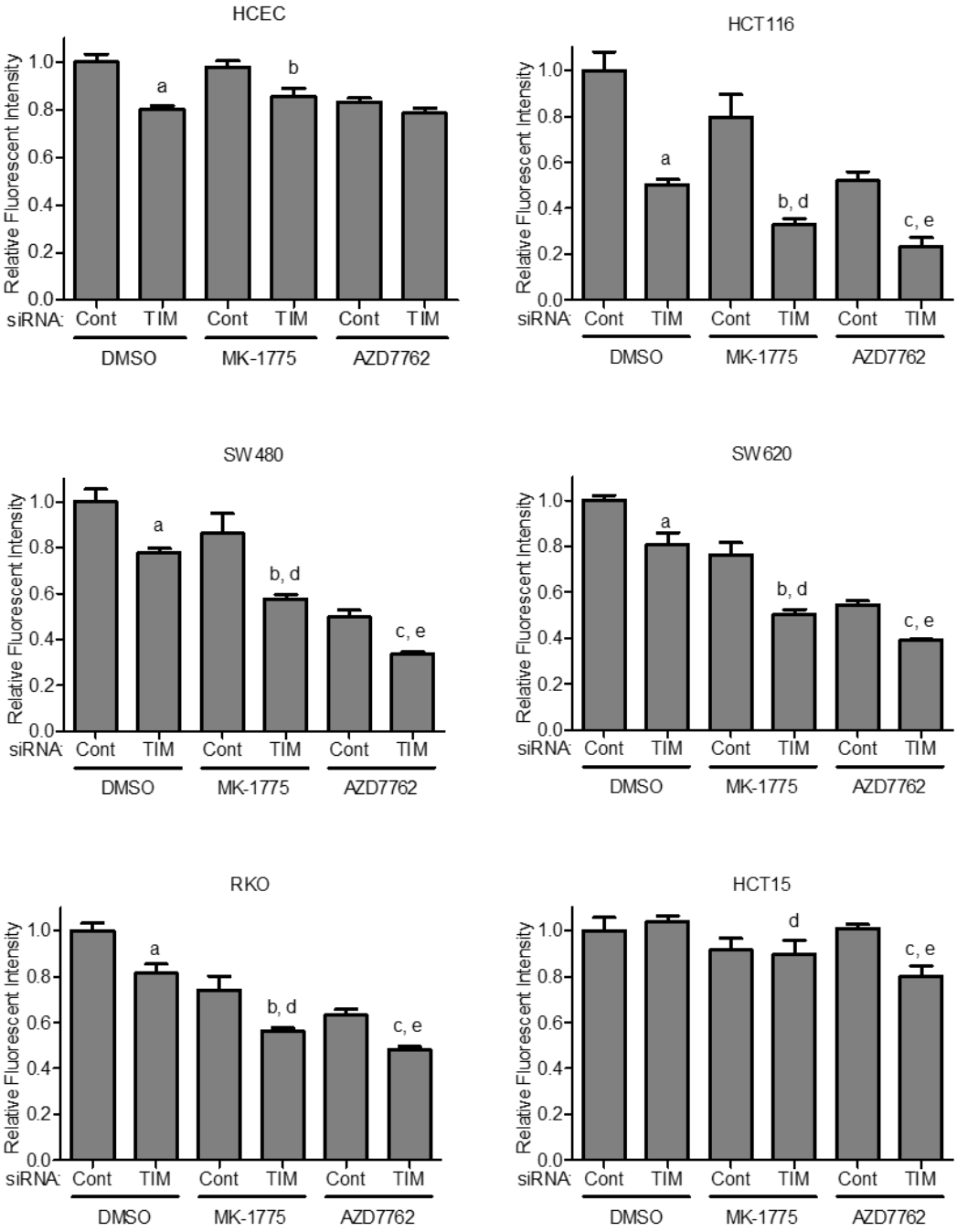

Fig. 4.32: TIMELESS depletion sensitizes colon cancer cells to Wee1 and CHK1 inhibition. (A) Cell viability in a panel of colon cancer cells following RNAi-mediated depletion of TIMELESS with Wee1 inhibition or CHK1 inhibition. Viability was measured by alamarBlue® assays 96 hours after transfection. 300 nM of Wee1 (MK-1775) or CHK1 (AZD7762) inhibitor was added 48 hours after transfection. Data are normalized to the DMSO treated control transfection (far left bar) and are shown as mean ± SD. (N=6). The lower case letters denote a statistical significance (one-way ANOVA with Bonferroni's Multiple Comparison test for the specified comparisons) with a p value less than 0.001 for the following comparisons: a – DMSO-treated siCont vs DMSO-treated siTIM; b – MK-1775-treated siCont vs MK-1775-treated siTIM; c – AZD7762-treated siCont vs AZD7762-treated siTIM; d – DMSO-treated siTIM vs MK-1775-treated siTIM; e – DMSO-treated siTIM vs AZD7762-treated siTIM.

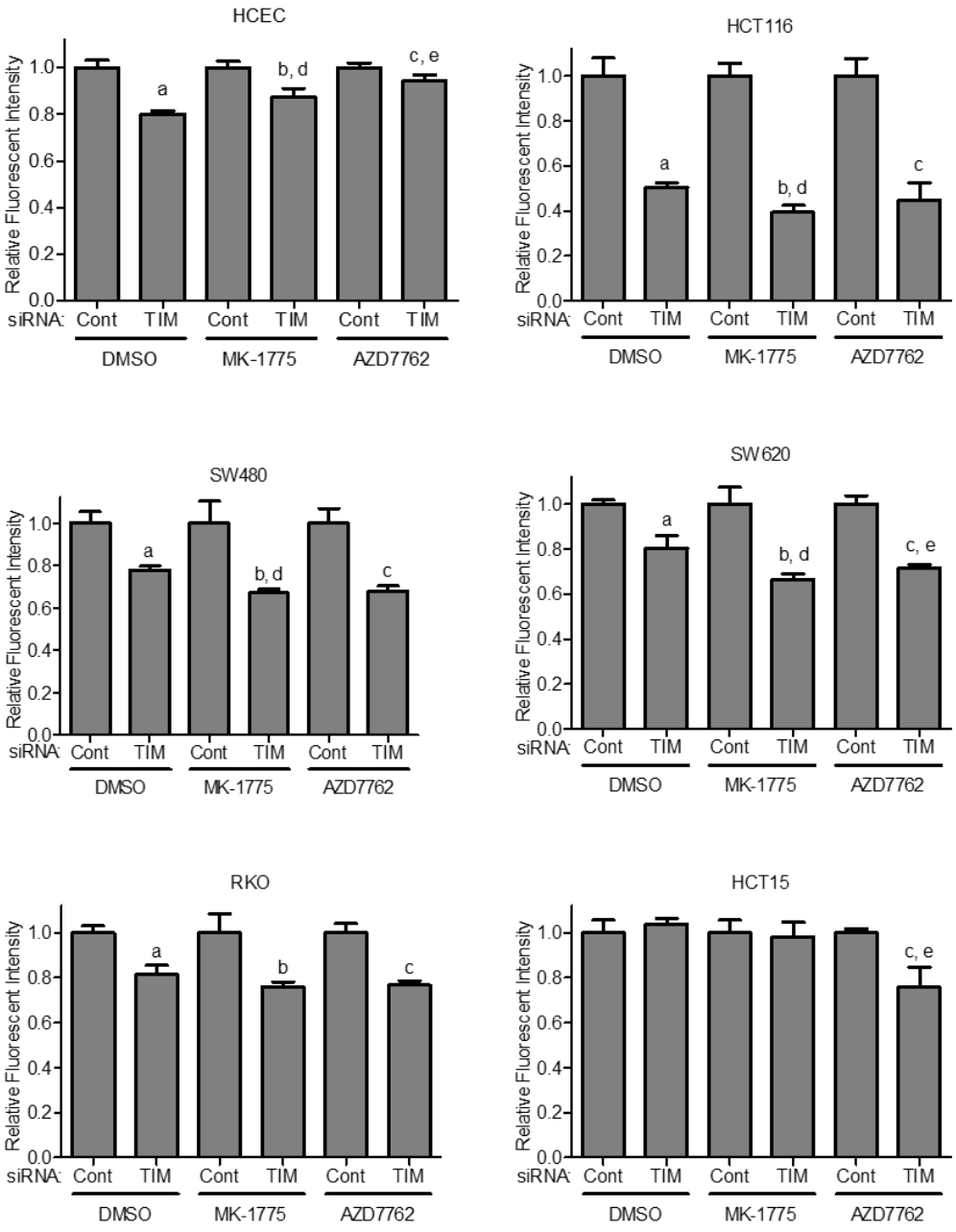

Fig. 4.32 Continued: TIMELESS depletion sensitizes colon cancer cells to Wee1 and CHK1 inhibition. (B) Same data as A, but data are normalized to the control transfection for each drug treatment to isolate the subsequence effect of TIMELESS depletion on top of the drug-mediated effects. (N=6). The lower case letters denote a statistical significance (one-way ANOVA with Bonferroni's Multiple Comparison test for the specified comparisons) with a p value less than 0.001 for the following comparisons: a – DMSO-treated siCont vs DMSO-treated siTIM; b – MK-1775-treated siCont vs MK-1775-treated siTIM; c – AZD7762-treated siCont vs AZD7762-treated siTIM; d – DMSO-treated siTIM vs MK-1775-treated siTIM; e – DMSO-treated siTIM vs AZD7762-treated siTIM.

overexpression, there is a distinct lack of mutations in TIMELESS in cancer [204] suggesting that individual mutations are unlikely to increase TIMELESS activity and instead TIMELESS expression determines its level of activity. These results demonstrate oncogenic Ras promoted TIMELESS overexpression in cancer. Downstream of Ras this effect is mediated by ERK or mTOR depending on the colon cancer cell line and is possibly tied to the ability of ERK or mTOR to modulate translation. However, TIMELESS expression has been shown to vary with cell cycle, with the highest levels being seen in the S and G2 phases [182]. Therefore, it is possible that ERK or mTOR activation promote TIMELESS expression as a side effect of increasing cell proliferation and subsequently increasing the percentage of cells in S and G2 phases. Consistent with the hypothesis that proliferation rate affects TIMELESS expression levels, as HCECs become more confluent, TIMELESS expression decreases; however, in HCT116 cells, TIMELESS expression is constitutively high regardless of confluency. TIMELESS is also aberrantly expressed in colon cancer as it is constitutively expressed in HCT116 cells and has lost the circadian expression that is present in HCECs, which could also be a result of oncogenic signaling overriding the normal regulation of TIMELESS expression to drive its constitutive expression.

It is also likely that TIMELESS expression is increased through other mechanisms since TIMELESS is overexpressed, at least at the mRNA level, in several cancers that are not commonly driven by oncogenic Ras including breast, uterine, ovarian, and cervical cancers (Fig. 4.4A). Additionally, while the exogenous expression of mutant Ras in HCECs increased the level of TIMELESS expression, the colon cancer cell lines still maintained a much higher level of TIMELESS expression. Previous reports have hypothesized TIMELESS expression is increased as a result of decreased DNA methylation in breast cancer [217], but this was not seen in colon cancer. Alternatively, the TIMELESS promoter contains an E-box sequence such that CLOCK and BMAL1, the driving circadian rhythm transcription factors, are likely to promote the transcription of TIMELESS; however, this has not yet been demonstrated in mammalian cells.

Additionally, the presence of this E-box opens the possibility that MYC could drive the expression of TIMELESS as MYC has recently been shown to disrupt the normal circadian-regulated expression of REV-ERBα and promote its constitutive expression by aberrantly binding to the E-box within its promoter [202].

The increase in TIMELESS expression in multiple cancers suggests that TIMELESS may ubiquitously promote cell proliferation by supporting high fidelity DNA synthesis, DNA damage repair, and cell cycle advancement likely through numerous mechanisms as several potentially contributing mechanisms have already been described [114,160,162-165,168,169,173,175,207]. Interestingly, TIMELESS has been shown to be required for the maintenance of cancer-associated viral genomes as well [176,177], which could provide some rationale for its particularly high expression in cervical cancer, which is almost always driven by human papillomavirus (HPV).

While TIMELESS depletion increased γH2AX and triggered the same downstream activation of CHK1 and inhibition of CDK1 in HCT15 cells as it did in the other cell lines examined (Fig. 4.24), TIMELESS depletion did not reduce HCT15 cell viability (Fig. 4.17). This could be due to dramatically disrupted and non-functioning cell cycle checkpoint function in these cells as HCT15 cells have a high basal level of P-CDK1 (Fig. 4.24), yet maintain a high proliferative rate. HCT15 cells have an abundance of genetic alterations that disrupt DNA damage repair and cell cycle checkpoint pathways including mutations in ATM, ATR, BRCA1, BRCA2, CHK2, and FANCA. These or other alterations that promote cell cycle advancement in the presence of DNA damage could allow cells to lose their dependency on TIMELESS. Similarly, SW480 cells had high basal level of P-CHK1 and demonstrated a limited capacity to phosphorylate and inactivate CDK1 even following a robust induction of γH2AX (Fig. 4.24) suggesting these cells may also contain additional alterations that suppress DNA damage checkpoint signaling cascades and subsequent cell cycle arrest. Elucidating the mechanisms by which HCT15 cells promote cell cycle advancement even in the presence of phosphorylated and inactivated CDK1 and SW480 cells limit CDK1 inactivation by CHK1 may reveal novel

mechanisms with potential therapeutic implications.

Despite the potential for some cancer cells to be insensitive or develop insensitivity to TIMELESS depletion, four of the colon cancer cell lines that were tested in this study demonstrated a substantial requirement for TIMELESS in order to maintain a high level of proliferation. G2/M arrest was particularly high in HCT116 and RKO cells, two colon cancer cell lines with wildtype p53. Several previous studies have demonstrated there are both p53-independent and p53-dependent pathways in cell cycle checkpoints following DNA damage. This suggests the p53-wildtype cells may trigger both p53-independent and p53-dependent pathways thereby inducing a more robust cell cycle arrest as compared to the mutant p53 cell lines (HCT15, SW480, and SW620) that only trigger p53-independent pathways.

Interestingly, ERK inhibition increases γH2AX, but downstream CHK1 phosphorylation does not occur. This could be the result of decreased RSK phosphorylation as RSK has previously been shown to phosphorylate CHK1 at S280, which is required for CHK1 nuclear localization, a prerequisite for ATM or ATR mediated phosphorylation at S345 in response to DNA damage. Additionally, ERK inhibition increases γH2AX independent of TIMELESS as exogenous expression of TIMELESS does not reduce γH2AX levels.

TIMELESS appears to have a highly conserved functional role in cells that could make it difficult to target therapeutically with a reasonable therapeutic index. However, HCECs expressed TIMELESS at lower levels and demonstrated less sensitivity to TIMELESS depletion. This could be a result of a slower proliferation rate, a difference that could also be exploited *in vivo* and that is the only means of cancer selectivity for several clinically approved chemotherapeutics. Targeting TIMELESS directly may be particularly efficacious in tumors that possess other defects in DNA damage repair pathways as they may be more dependent on TIMELESS to prevent or repair DNA damage. Unfortunately, combination treatment with TIMELESS depletion and DNA damaging chemotherapeutics or ionizing radiation had only small incremental increases in efficacy over single treatments. This suggests there may be an

upper limit for the efficacy of DNA damaging agents or a minimum amount of DNA damage that is required for cell cycle arrest such that once this level is reached further induction of DNA damage has little or no effect. Alternatively, the combinatory effects of TIMELESS depletion in conjunction with DNA-damaging chemotherapeutics or ionizing radiation might only be seen with longer treatment regimens to allow for the effects of DNA damage accumulation to be fully realized. Additional studies using other DNA damaging agents and/or longer experimental courses may reveal a potential for TIMELESS depletion to complement currently used cancer therapies.

Combination therapy with TIMELESS depletion and either Wee1 or CHK1 inhibition demonstrated at least additive effects in the colon cancer cell lines, but not in HCECs, suggesting this combination may be an efficacious strategy for the treatment of colon cancer. Interestingly, the CHK1 inhibitor AZD7762 did not decrease HCT15 viability alone, but sensitized the HCT15 cells to TIMELESS depletion.

Recent studies have also demonstrated increased efficacy and decreased side effects when chemotherapeutics are dosed in a circadian fashion [195,203,223-225] suggesting a window of time exists when cancer cells, but not normal cells are proliferating and therefore even more sensitive to chemotherapeutics. TIMELESS has been shown to be circadianly expressed in normal tissue; however, it is likely constitutively overexpressed in cancer due to oncogene-driven expression. This opens the possibility that a circadian dosing scheme could increase the therapeutic index of TIMELESS inhibition.

This may not be necessary, however, as TIMELESS has previously been shown to physically interact with PARP at sites of DNA damage and PARP inhibitors trap TIMELESS with PARP at DNA lesions [193] effectively sequestering and possibly preventing TIMELESS from performing its other functions in the cell. Clinical trials with PARP inhibitors have demonstrated favorable side effect profiles such that these inhibitors are clinically approved for the treatment of multiple cancers, which provides optimism that, if developed, direct TIMELESS inhibitors may

also be efficacious and have minimal side effects in patients. However, the effects of PARP inhibitors on TIMELESS have not been evaluated, and the high level of TIMELESS expression in cancer may mitigate any effect from sequestration of TIMELESS with PARP at sites of DNA damage. Additional work is needed to evaluate if PARP inhibitors functionally inhibit TIMELESS and if this mechanism also contributes to their efficacy.

To summarize, oncogenic Ras, through increased ERK activation, contributes to the overexpression of TIMELESS in cancer. TIMELESS reduces the accumulation of DNA damage thereby supporting cell proliferation by preventing cell cycle checkpoint-induced G2/M arrest. These results demonstrate a clear role for TIMELESS in cancer and suggest that further examination of the link between circadian rhythm and cell cycle regulation may reveal novel approaches for the development of cancer therapeutics. TIMELESS represents only one of many therapeutic targets and associated vulnerabilities identified from the FUSION screen. Future work validating and characterizing additional targets will increase our understanding of oncogene-induced vulnerabilities in cancer and provide viable, novel approaches for the development of selective cancer therapeutics.

Chapter 5: WDR5 supports colon cancer cells by promoting methylation of H3K4 and suppressing DNA damage

Portions of the material covered in this chapter are the subject of a manuscript submitted for publication by Neilsen BK *et al*.

Introduction

WDR5 (WD-repeat containing protein 5) is a WD40-repeat containing seven-bladed propeller protein. WDR5 was initially identified as being a BMP2 inducible gene and was originally named BIG-3 (BMP2-induced 3-kb gene protein). Early studies demonstrated that WDR5 dramatically increased osteoblastic differentiation and chondrocyte differentiation downstream of BMP2 [226,227]. Several additional studies have further demonstrated the role WDR5 plays in skeletal development, but the role of WDR5 has been expanded since its identification, and it has been shown to function ubiquitously in human tissues.

COMPASS Complex

Importantly, WDR5 serves as a core component of several complexes within the cell [228]. It has been most well-studied for its role in the SET/MLL COMplex of Proteins ASsociated with Set1 (COMPASS), which serves to mono-, di-, and tri-methylate Histone 3 Lysine 4 (H3K4Me1-3), [229-231]. WDR5 has been shown to contribute to recognition of specific H3K4Me3 targets, which serves to promote increased transcription of select target genes as the H3K4 methylation often occurs within enhancer or promoter regions [232]. WDR5 has a significant role in development as it regulates embryonic stem cell pluripotency, self-renewal, and reprogramming by modulating the transcription of targets that promote stem cell-like states [233-236]. In particular, as part of the COMPASS complex, WDR5 has been shown to regulate several HOX genes as well as SOX9 expression [235,237-239]. Of note, WDR5 can also promote its own expression through a positive feedback loop where increased H3K4Me3 within the WDR5 promoter increases its transcription [239].

The SET/MLL COMPASS Complex consists of one of the KMT2/MLL proteins (KMT2A/MLL1, KMT2B/MLL2 or MLL4, KMT2C/MLL3, KMT2D/MLL4 or MLL2, KMT2F/SETD1A, or KMT2G/SETD1B) in addition to a common subcomplex that includes WDR5, RBBP5, Ash2L, DPY30 (WRAD subcomplex) [240]. Interestingly, the catalytic component

of this complex, the KMT2/MLL proteins, have very little activity outside of the complex, and thus require the common WRAD subcomplex and COMPSS complex formation to be functionally active. COMPASS complex formation serves to dramatically increase the affinity of the KMT2/MLL protein for DNA and increases its catalytic activity [241].

KMT2/MLL family proteins, while highly related, have both distinct and redundant functions [242]. In mammals, these six proteins form three pairs of paralogs: KMT2A/MLL1 and KMT2B/MLL2; KMT2C/MLL3 and KMT2D/MLL4; and KMT2F/SETD1A and KMT2G/SETD1B. While all KMT2/MLL proteins bind to the WRAD subcomplex, each pair also has unique additional complex members, which may contribute to their unique functions and specific target genes [241].

The COMPASS complex primarily functions to add methyl groups to H3K4, which generally promotes transcription by recruiting transcription factors and coactivators to promoters while also interfering with the addition of epigenetic modifications that would repress transcription [241]. However, the location of methylation (in promoters or enhancers) and degree of methylation (mono-, di-, and tri-methylation) varies between KMT2/MLL proteins and can be tissue-specific. In general, monomethylation is most often associated with enhancers and tri-methylation with promoters and transcription start sites in genes that are actively being transcribed [241].

KMT2A/MLL1 and KMT2B/MLL2 have specific or limited methylation activity and are most commonly associated with di- or tri-methylation of H3K4. Specific target genes of KMT2A/MLL1 and KMT2B/MLL2 include the HOX genes where increasing H3K4Me3 increases their transcription [241]. KMT2A/MLL1 is commonly chromosomally translocated or mutated in leukemia. In normal cells, KMT2A/MLL1 is required for hemopoietic stem cell maintenance at least in part by promoting the expression of hemopoietic stem cell transcription factors HOXA9, PRDM16, PBX1 by increasing H3K4Me3 and H4K16Ac in or near these target genes, which increases their transcription. KMT2B/MLL2 is not chromosomally translocated in

leukemia and cannot replace KMT2A/MLL1 in these cancers likely due to its lower affinity for CpG sequences [243,244]. However, a recent report has indicated that maintenance of KMT2B/MLL2, and not KMT2A/MLL1, is required in KMT2A/MLL1-rearranged leukemia [245]. KMT2B/MLL2 is required for H3K4Me3 maintenance at promoters and may limit trimethylation at Histone 3 Lysine 27 (H3K27Me3), which is inhibitory for transcription, thereby modulating the expression of bivalent promoters [241].

KMT2C/MLL3 and KMT2D/MLL4 demonstrate redundancy and both maintain H3K4Me1 levels on enhancers [241,246,247] and recruit CBP/p300 to enhancers [247,248]; however, either knockout alone is embryonic/perinatal lethal in mice suggesting that neither one is able to fully compensate for the loss of the other. Traditionally, KMT2C/MLL3 and KMT2D/MLL4 have been considered tumor suppressors in leukemia and have been implicated as such in solid tumors as well [241]. Knockdown of KMT2C/MLL3 or KMT2D/MLL4 impaired differentiation of hematopoietic stem/multipotent progenitor cells and increased the prevalence of progenitor cells [249 250]. These defects may be caused by increased oxidative stress due to the reduced expression of KMT2D/MLL4-dependent genes that protect cells from oxidative stress [250]. However, deletion of KMT2D/MLL4 in an Acute Myeloid Leukemia (AML) model system, as opposed to most studies that are performed in lymphoma models, demonstrated limited effects suggesting there may be context or tissue-specific effects of KMT2D/MLL4 [250]. Additionally, KMT2C/MLL3 and KMT2D/MLL4 contribute to the mono-methylation of H3K4 in collaboration with hormone receptors, and thus may play a pro-tumorigenic role in hormone-driven tumors [241 251 252-254].

KMT2F/SETD1A and KMT2G/SETD1B are highly related, but phenotypes from KMT2F/SETD1A knockouts demonstrate global decreases in mono-, di-, and tri-methylation on H3K4, while KMT2G/SETD1B knockouts do not suggesting KMT2F/SETD1A may be the dominant allele and capable of compensating for the loss of KMT2G/SETD1B [255]. Alternatively, their functions may not be fully redundant with KMT2F/SETD1A preferentially affecting H3K4 methylation and KMT2G/SETD1B potentially contributing to a different, unrecognized function.

Functionally, changes in methylation on H3K4 downstream of KMT2F/SETD1A affect target gene expression, which has been shown to affect erythroid cell differentiation as KMT2F/SETD1A conditional knockouts demonstrated decreased expression of *Gata1* and *Tal1* corresponding to decreased H3K4Me3 at their promoters [256].

While the significance of KMT2A/MLL1 rearrangements in leukemia has been established for many years [257-259], the specific effects of unique rearrangements and mutations, and the mechanisms behind their pro-tumorigenic behavior are still being elucidated and characterized [259]. Interestingly, examining four specific mutations within the catalytic SET domain of KMT2A/MLL1 that were identified in cancer demonstrated that these mutations can decrease or increase KMT2A/MLL1 baseline activity and can modulate the augmented effect of complex formation on DNA binding affinity and enzymatic activity [260]. However, the H3K4 methyltransferase domain in KMT2A/MLL1 is often excluded from KMT2A/MLL1 fusion proteins, yet the fusion protein still modulates transcriptional elongation. This suggests a broader role for KMT2/MLL proteins in addition to altering specific chromatin modifications [261]. KMT2A/MLL1 and KMT2A/MLL1-fusion proteins have also been shown to have distinct chromatin target sites, which may be a consequence of the KMT2A/MLL1:WDR5 interaction [262]. This highlights the complexity and potentially tumor-specific effect of KTM2/MLL proteins in cancer. More recently, the surprisingly high frequency of KMT2/MLL mutations in solid tumors, including breast, prostate, pancreas, stomach, and colon has been recognized. In addition to being commonly mutated, these proteins are often overexpressed in cancer, and their expression has largely been associated with protumorigenic effects and worse patient outcomes (pancreatic cancer) [263].

In general, within cancer KMT2/MLL proteins have been shown to promote transcriptional reprogramming through increased methylation at H3K4 [264] and through interactions with commonly recognized oncogenic transcription factors. Specific targets of KMT2/MLL epigenetic regulation have been shown to include hTERT (KMT2A/MLL1, in

melanoma) [265] , several HOX genes (KMT2A/MLL1) [266], ERα target genes in breast cancer (KMT2D/MLL4) [254,267], and androgen receptor target genes in prostate cancer (KMT2A/MLL1 and WDR5) [268,269]. Inhibition or depletion of KMT2D/MLL4 in breast cancer or KMT2A/MLL1 in prostate cancer decreased the expression of important transcriptional targets thereby inhibiting cancer cell growth [254,269]. In pancreatic cancer, KMT2C/MLL3 and KMT2D/MLL4 depletion caused downregulation of genes related to cell cycle advancement and proliferation based on microarray and gene set enrichment analysis [263]. The variable effects of individual KMT2/MLL family member inhibition or depletion in various types of cancer supports the idea that KMT2/MLL proteins have distinct roles and targets that are context- and tissue-specific.

In colon cancer, KMT2D and KMT2C mutations are common and are present in 10% of tumors (Table 5.1, [270], COSMIC v83). In contrast, the common components of the COMPASS complex were rarely mutated (Table 5.1). Additionally, many of the commonly used colon cancer cell lines harbor multiple mutations within KMT2/MLL family members (Table 5.2, COSMIC Cell Lines Project,[271]). However, the effects of these mutations are still being debated. While often labelled as tumor suppressors, evidence demonstrating a protumorigenic role for KMT2C and KMT2D in solid tumors has recently been reported. For example, one study demonstrated that KMT2D promoted global K3K4 monomethylation in transcriptional enhancers, and depletion of KMT2D in two colon cancer cell lines (HCT116 and DLD-1) decreased cancer cell proliferation and migration [264].

Recent studies have identified a correlation between H3K4Me3 enrichment, transcriptional fidelity, and enhanced elongation rates [272,273]. This suggests a potential role for the COMPASS complex in promoting DNA synthesis while preventing DNA damage during replication, which could ultimately support cell proliferation. Recent studies have specifically demonstrated that KMT2A/MLL1 as well as WDR5 are required for proper chromosome congression and spindle assembly during mitosis, which may affect chromosomal stability [274], and a KMT2B/MLL2 mutation resulted in genome instability [275]. In another report, AML driven

Gene	Percent Mutated	Samples (Mutated/Tested)
KMT2C/MLL3	13%	323/2478
KMT2D/MLL2	11%	243/2209
KMT2A/MLL	7%	152/2178
KMT2B/MLL4	7%	150/2130
KMT2F/SETD1A	6%	116/2109
KMT2G/SETD1B	3%	67/2098
RBBP5	2%	32/2109
WDR5	1%	28/2109
ASH2L	1%	25/2109
DPY30	<1%	6/2098

Table 5.1: Frequency of KMT2/MLL Mutations in Colon Adenocarcinoma (COSMIC v83).

Cell Line	KMT2A	KMT2B	KMT2C	KMT2D	KMT2F	KMT2G	WDR5
HCT116		D550fs[2] G1881fs[1] L2136fs[2]	Q419R[1] I1344fs[1,2]	V160M[2] R2173fs[1] R2443fs[1,2]		G1578fs[2]	Y260H[1,2]
HCT15	T771fs[2] S1062Y[1,2] V2178A[1]	R226W[2] R1125H[2] A1989T[2]	G3438D[1,2] S3543N[1,2]	P1152H[2] E1244D[1] E1517D[1,2] P1931H[2]		D159N[2] Q780H[2]	
SW480				D1633N[2]			
SW620		G273S[2] G292V[1,2]					
RKO	T771fs[2] S873fs[2] D877fs[1]	A905T[2] R1579H[2] D1819fs[2] P1823fs[1]	G2636C[1] R3853W[2]	R916H[1] R1189H[1,2] L1327P[1] L1600P[1,2] G1960fs[2] P2550fs[2] G3465*[1,2] L4516P[1] R4964fs[2] L5056P[1,2]	A1325T[2]	T1657A[2]	V217Ins[1]
LoVo		R525W[1,2] P2255L[2]	C1013R[1] E1313K[1]	H77fs[1,2] P647fs[1,2] P648fs[1,2] T3548I[2]		V1404I[2]	G277D[1,2]
T84				None[1,2]			

Table 5.2: Frequency of KMT2/MLL and WDR5 Mutations in Colon Cancer Cell Lines.

[1]=COSMIC
[2]=Mouradov *et al*
Note: SW480 are not included in COSMIC

by KMT2A/MLL1 fusions were shown to be proficient in DNA-damage response (DDR) leading PARP inhibitor resistance. However, depleting or inhibiting cells of HOXA9, a downstream target of KMT2A/MLL1, caused DDR impairment and PARP inhibitor sensitization [266]. Together these data suggest a role for this complex in supporting DNA replication and maintaining DNA fidelity thereby promoting cancer cell survival and proliferation. Consistent with this hypothesis, depletion of KMT2D/MLL4 in multiple pancreatic cancer cell lines increased their responsiveness to 5-FU [263] suggesting a possible role for KMT2/MLL or COMPASS complex inhibition in chemotherapy or radiation sensitization.

The role of WDR5 outside of the COMPASS Complex

In addition to serving as a required component of the COMPASS complex, new evidence shows that WDR5 participates in several other protein complexes such as the CH8-containing ATP dependent chromatin remodeling complexes [276], human acetyltransferase complexes such as MOF (Males absent On the First) and ATAC (Ada Two-A Containing) [277-279], and NSL (Non-Specific Lethal) complex in Drosophila [228]. WDR5, as a component of a CHD8-containing complex, regulates the expression of β-catenin target genes [276]. WDR5 has also been shown to regulate genes that are expressed in a circadian manner by supporting PER-mediated transcriptional repression through histone methylation within the promoter region of clock-regulated genes [280]. WDR5 also plays an important role in the self-renewal of embryonic stem cells and the maintenance of active chromatin for pluripotency genes [235,281] and is required to induce pluripotent stem cell generation from differentiated somatic cells [233]. This may be the result of WDR5 binding to RNA as further studies identified a RNA-binding pocket in WDR5 through which WDR5 interacts with more than a thousand RNA including several lncRNAs known to be important for embryonic stem cell gene expression [234].

WDR5 has also been shown to physically interact with MYC and promote transcription of a subset of MYC target genes [282-286] [287]. This synergistic increase in transcription following MYC and WDR5 interaction is thought to contribute to tumorigenesis, particularly in

neuroblastoma and other MYC-driven tumors. Interestingly, a study using patient-derived xenografts of pancreatic cancer demonstrated the WDR5:Myc interaction *in vivo* and showed this interaction prevented DNA damage accumulation [287]. Additional reports have shown that WDR5 regulated DNA replication and chromosomal polyploidy [288] as well as abscission through localization to the midbody [289]. The induction of DNA damage following loss of WDR5 could be independent of or a result of its role in the COMPASS complex as there are multiple reports suggesting that depletion of KMT2A/MLL1 or KMT2B/MLL2 induce DNA damage [263,266,272-275]. WDR5 has also been shown to increase transcription of cyclins, which serve to promote cell cycle progression and increase cell proliferation [290,291].

Cancer

Recent studies have also demonstrated a role for WDR5 in cancer based on its increased expression and requirement for cancer cell survival. Specifically, expression of WDR5 is increased in prostate cancer tissues [268], leukemia [292], and bladder cancer [293]. WDR5 promotes survival, proliferation, and chemoresistance in bladder cancer [293]. WDR5 overexpression is associated with worse patient outcomes in breast cancer and hepatocellular carcinoma [291,294]. In breast cancer, WDR5 promotes cell survival [295] and tamoxifen resistance [296]. WDR5 has also been shown to physically interact with MYC and promote target recognition contributing to tumorigenesis [282,284]. In pancreatic cancer, WDR5 promotes cell proliferation, survival, and migration [297]. As expected, WDR5 appears to play a role in leukemia as it is overexpressed, promotes H3K4Me3, and depletion of WDR5 decreases cell proliferation, increases cell death, and reduces H3K4Me3 on target gene promoters [292].

In general, the mechanism by which WDR5 supports cancer cells has been shown to be through increased target gene expression. For example, WDR5 has been shown to promote epithelial to mesenchymal transition (EMT) by interacting with HDA3 to promote hypoxia-induced EMT by promoting mesenchymal gene activation [298]. WDR5 promotes colon cancer metastasis by binding to ZNF407 [299]. WDR5 has also been shown to promote both ErbB2 and

NOTCH expression and signaling through a H3K4Me3-dependent manner to promote mammary tumorigenesis [295,300], and depletion of WDR5 reduced ErbB2 expression and cooperated with trastuzumab or chemotherapy to reduce ErbB2-positive breast cancer cell growth [295]. WDR5 has been shown to cooperate with HOTTIP to promote HOXA9 in prostate and pancreatic cancer [301,302] and HOXA13 expression in esophageal and gastric cancer cells by increasing H3K4Me3 on their promoters [303,304]. Increased HOX protein expression promoted aggressive cellular phenotypes as cells demonstrated increased invasion and migration [301]. In bladder cancer, WDR5 promotes global transcription by increasing H2A.Z incorporation [305] and increases the transcription of cyclin B1, cyclin E1, cyclin E2, UHMK1, MCL1, BIRC3 and Nanog via increased histone H3 lysine 4 trimethylation [306] [293,306]. WDR5 promotes gastric tumorigenesis through multiple mechanisms including upregulation of cyclin D1 [290,307]. Based on its widespread overexpression and pro-tumorigenic role in cancer, inhibition of WDR5 has therapeutic potential in multiple cancers.

Therapeutic Targeting of WDR5

After multiple reports characterizing the structure and binding domains of WDR5 that included the crystal structure of WDR5 in complex with KMT2A/MLL1 Win motifs [308,309], MYC Mb111b peptide [284], and histone H3K4 peptides [310], numerous groups have designed inhibitors of WDR5. Successful inhibitors have largely targeted the WDR5:MLL protein:protein interaction [260,311-320] with some groups demonstrating selective targeting of KMT2A/MLL1:WDR5 [318] interactions or KMT2F/SETD1A:WDR5 [314] interactions. Further, use of a WDR5:MLL inhibitor, OICR-9429 in C/EBPα N-terminal acute myeloid leukemia cells inhibited proliferation and induced differentiation [321]. More recent attempts have largely focused on targeting other WDR5 protein interactions with the WDR5:MYC interaction being a primary target, but these have not yet been successful.

Results

Preliminary Biological Validation of WDR5

Based on the screen results, the seven-bladed beta propeller protein WDR5B was identified as a hit. Unfortunately, there is very little known about WDR5B. In contrast, the highly-related protein WDR5 is well-established in the literature, has validated reagents, and several inhibitors targeting this protein have been developed.

Initial biological validation of targets identified using FUSION was performed by assessing cancer cell growth or viability in anchorage-independent conditions following RNAi-mediated target depletion by measuring cell growth on a polyHEMA-coated plate [214,215] using CellTiter-Glo® Luminescent Cell Viability Assay, as previously described [3]. The smartPool of four siRNA oligos (Dharmacon) targeting KSR1, WDR5, or WDR5B was used to deplete cells of the target. Growth in anchorage-independent conditions was reduced substantially with KSR1 or WDR5 depletion, but not WDR5B depletion in HCT116 colon cancer cells (Fig. 5.1A). Repeating the WDR5 knockdown in two colon cancer cell lines, HCT116 and HCT15, demonstrated a robust decrease in HCT116 cell viability, but a relatively small decrease in viability in HCT15 cells (Fig. 5.1B). HCECs are unable to proliferate in an anchorage-independent environment and were therefore not assayed in this manner. To compare the effects of WDR5 depletion in colon cancer cells to immortalized, yet non-transformed HCECs, RNAi-mediated depletion of WDR5 was completed under normal plating conditions and viability was measured using alamarBlue. WDR5 depletion in HCECs, HCT116, and HCT15 cells for 72 hours reduced viability in all three cell lines, but did so to varying degrees with the HCT116 cells decreasing viability by more than 80% and HCEC and HCT15 cells decreasing by 20% and 25%, respectively (Fig. 5.1C). Additionally, apoptosis was significantly upregulated in HCT116 cells depleted of WDR5 where nearly 40% of the cells resided in the sub-G1 peak following propidium iodide staining and flow cytometry analysis (Fig. 5.1D). In contrast, the HCEC and HCT15 cells demonstrated no increase in sub-G1 peak following loss of WDR5. HCT15 cells did demonstrate a robust increase in G1 peak; however, representing a cell cycle arrest (Fig. 5.1E).

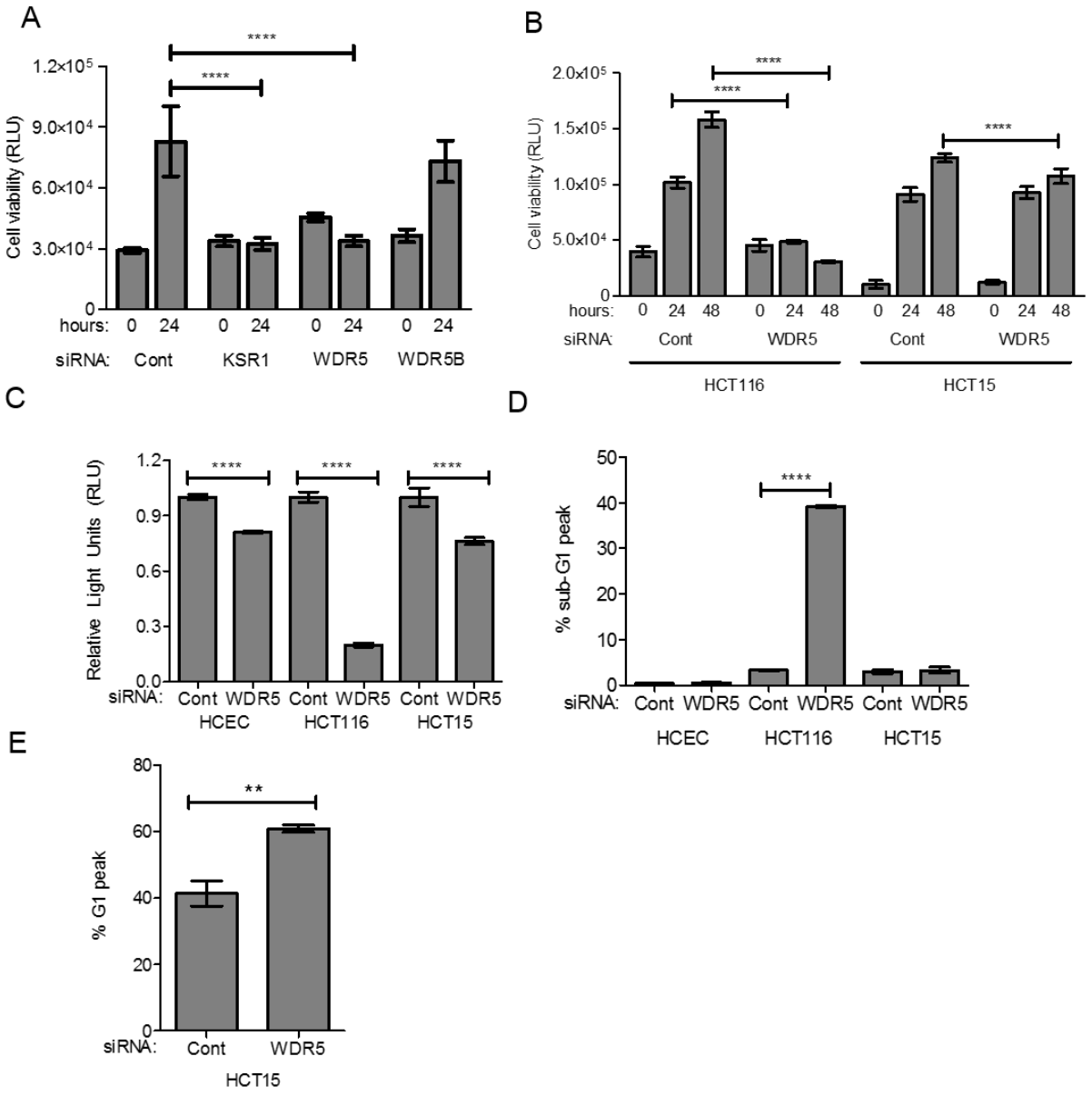

Fig. 5.1: Preliminary biological validation of WDR5. (A) Viability of HCT116 colon cancer cells measured using CellTiter-Glo® following RNAi of KSR1, WDR5, or WDR5B that were re-plated on polyHEMA-coated plates 48 hours following transfection to simulate anchorage-independent conditions. (N=6). (B) Viability of HCT116 and HCT15 colon cancer cells measured using CellTiter-Glo® following RNAi of WDR5 that were replated on polyHEMA-coated plates 48 hours following transfection to simulate anchorage-independent conditions. (N=6). (C) Viability of HCECs, HCT116, and HCT15 cells measured using alamarBlue® following RNAi-mediated WDR5 depletion for 72 hours in normal culture conditions. (N=6). (D) Apoptosis (percent of cells in the sub-G1 peak) in HCEC, HCT116, and HCT15 cells after WDR5 depletion by RNAi for 72 hours. (N=3). (E) G1 arrest (percent of cells in the G1 peak) in HCT15 cells after WDR5 depletion by RNAi for 72 hours. Apoptosis and cell cycle were evaluated using propidium iodide staining followed by flow cytometry analysis. Data are shown as mean ± SD. (N=3).

A single oligo targeting WDR5 increases p53 stability in HCT116 cells

To elucidate the mechanism behind the massive increase in apoptosis in HCT116 cells following WDR5 depletion that is not seen in HCECs or HCT15 cells, cells were depleted of WDR5 using the smartPool oligos for 72 hours and assessed for expression of pro-apoptotic proteins. PARP cleavage, p53, and downstream p53 effectors (p21, MDM2, PUMA) were increased following WDR5 depletion in HCT116 cells, but not HCECs or HCT15 cells (Fig. 5.2). Of note, HCEC and HCT116 cells have wild-type p53, but HCT15 cells have mutated p53, which explains the constitutively high level of p53 expression in HCT15 cells and could explain why WDR5 depletion in HCT15 cells does not reduce their viability.

A common mechanism by which p53 expression is increased in cells is by increasing protein stability following DNA damage. Therefore, the effect of WDR5 depletion on p53 protein stability was examined in HCT116 cells. Preliminary studies found the half-life of p53 was approximately 2 hours in these cells in stable conditions, therefore cells were treated with cycloheximide for four hours to allow for approximately 75% p53 protein degradation. HCT116 cells depleted of WDR5 using the smartPool oligos and treated with cycloheximide (100 μg/mL) to prevent translation of new proteins, demonstrate p53 is significantly stabilized with WDR5 depletion (Fig. 5.3A). To confirm the effect of WDR5 on viability is p53 mediated, HCT116 cells that lack p53 (HCT116 $p53^{-/-}$) were utilized. HCT116 cells without p53 were less sensitive to WDR5 depletion suggesting the effects of WDR5 knockdown in HCT116 cells are, at least in part, p53-mediated (Fig. 5.3B-D).

Based on previous studies, known mechanisms by which WDR5 could be acting include serving as part of the COMPASS complex to facilitate histone modifications that support tumor maintenance or physically interacting with MYC to promote tumorigenesis. However, MYC depletion decreased p53 expression (Fig. 5.4A) and OICR-9429, an inhibitor of WDR5:KMT2/MLL interaction and COMPASS complex formation, had no effect on p53 (Fig. 5.4B).

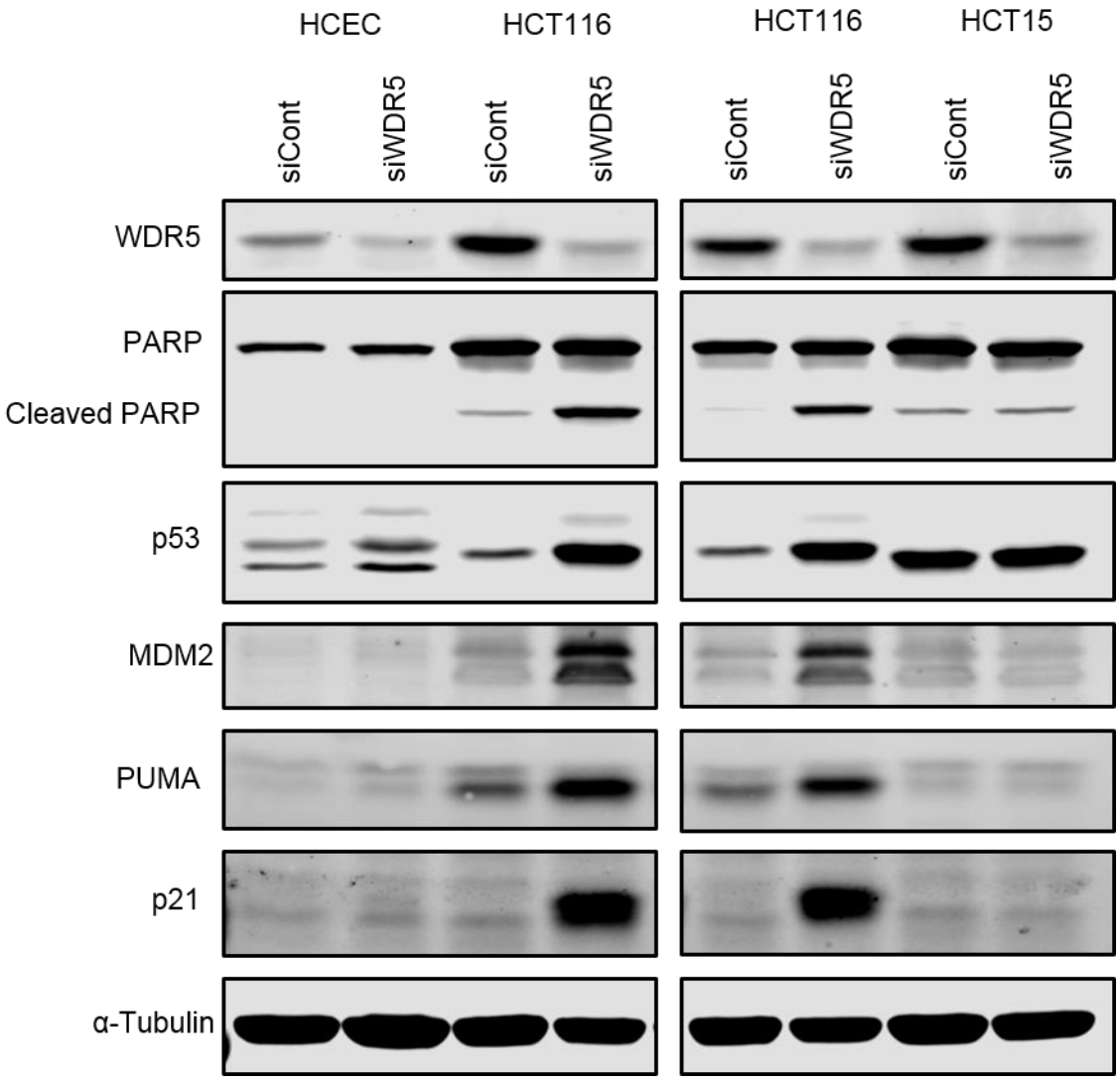

Fig. 5.2: WDR5 depletion Induces p53 expression and PARP cleavage in HCT116 colon cancer cells. (A) Immunoblot of WDR5, PARP, p53, and downstream p53 targets (MDM2, PUMA, and p21) following RNAi-mediated WDR5 depletion for 72 hours in HCECs, HCT116, and HCT15 cells.

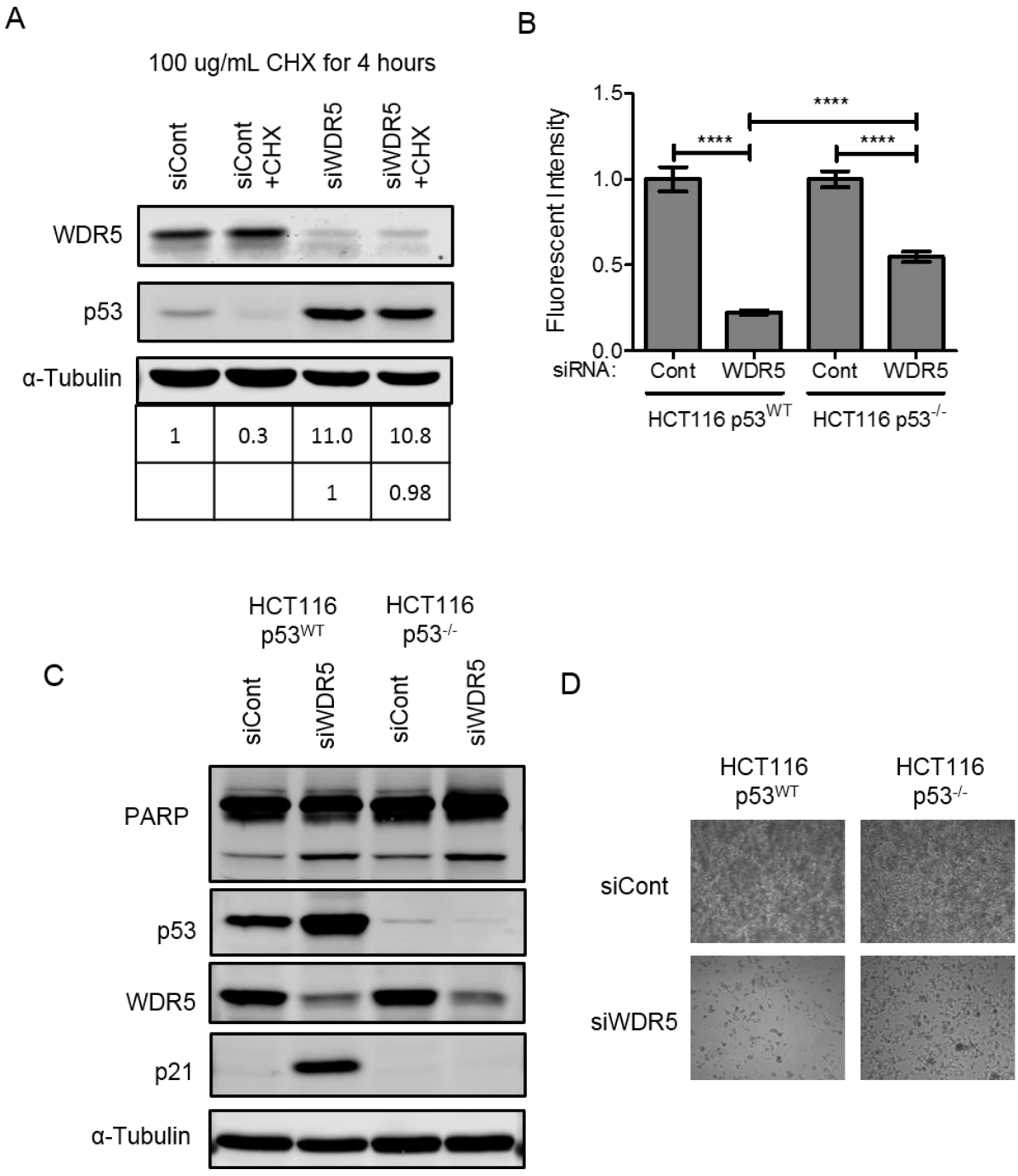

Fig. 5.3: WDR5 depletion induces cell death in HCT116 colon cancer cells by stabilizing p53. (A) Immunoblot and relative densitometry-based quantification (below) of p53 following RNAi-mediated WDR5 depletion for 72 hours and 100 µg/mL CHX treatment for 4 hours prior to collection to inhibit new protein translation. (B-D) Viability as measured with alamarBlue® (N=6) (B), immunoblot of PARP, WDR5, p53, and p21 (C), and photomicrographs (D) of $p53^{WT}$ and $p53^{-/-}$ HCT116 cells following RNAi-mediated WDR5 depletion for 72 hours.

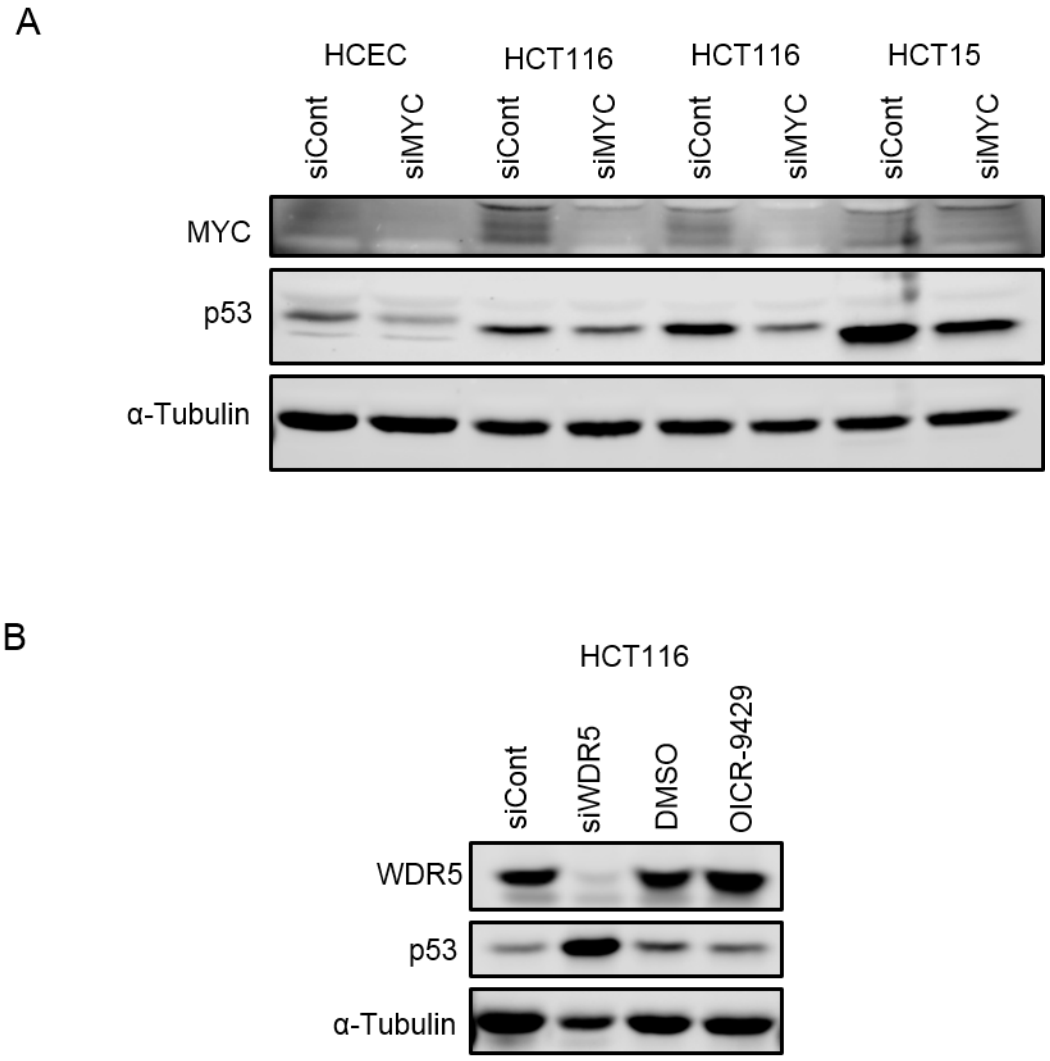

Fig. 5.4: MYC depletion or OICR-9429 treatment does not induce p53 expression. (A) Immunoblot of p53 following RNAi-mediated MYC depletion for 72 hours in HCECs, HCT116, and HCT15 cells. (B) Immunoblot of p53 following WDR5 depletion (smartPool) or OICR-9429 treatment for 72 hours in HCT116 cells.

Concerningly, WDR5 depletion in other colon cancer cell lines did not induce p53 expression (Fig. 5.5) even in another other cell lines with wildtype p53 (LoVo). Examining the individual oligos from the smartPool of four oligos targeting WDR5 revealed that even though all four dramatically decreased WDR5 levels, in HCT116 cells, oligo #6, the smartPool (a pre-mixed pool of all four oligos in an undisclosed ratio), and 1:1:1:1 pool of all four oligos dramatically decreased viability to a level substantially lower than the other three individual oligos (#5, #7, and #8) even though the level of WDR5 depletion was comparable (Fig. 5.6A). Comparing oligo #6 with #8, both oligos induced DNA damage, as evidenced by increased phosphorylation of H2AX (γH2AX), yet only oligo #6 increased p53 expression and induced PARP cleavage in HCT116 cells (Fig. 5.6B). This was concerning for the possibility of an off-target effect for oligo #6. A blast search using the oligo #6 sequence demonstrated an 100% match to WDR5, but also shared a high degree of similarity to ME1 sharing a 14-nucleotide substring within the 19-nucleotide siRNA oligo: G**UGGAAGAGUGACUG**CUAA (large, bold letters were matches). A substantial, previous publication demonstrated ME1 depletion induced p53 [322], suggesting this off-target could likely be causing the p53 induction in HCT116 cells. Reassuringly, all four individual oligos and both pools reduced HCT116 viability as measured by alamarBlue following WDR5 depletion by more than 30% in 72 hours suggesting WDR5 itself is playing a role supporting colon cancer cells, but the mechanism of action remains to be revealed.

WDR5 is required for colon cancer cell survival

To determine whether WDR5 is required for cell survival in more than just HCT116 cells, cell viability in a panel of colon cancer cell lines and HCECs following transient depletion of WDR5 by RNAi was measured. A pool containing all four oligos was used for all cell lines except HCECs and HCT116s where oligo #6 was shown to induce p53. In HCECs and HCT116 cells a pool of oligos #7 and #8 was used. Cell viability was measured using CellTiter-Glo® Luminescent Cell Viability Assay 72 hours after WDR5 depletion. WDR5 depletion reduced

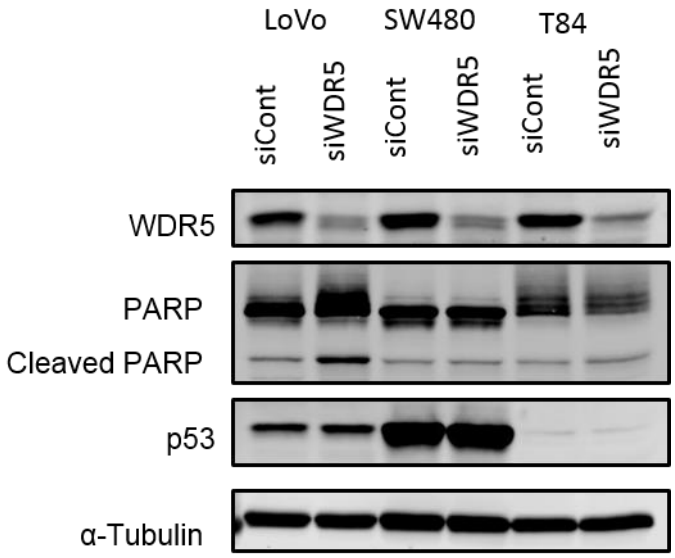

Fig. 5.5: WDR5 depletion does not induce p53 in other colon cancer cell lines. (A) Immunoblot of WDR5, PARP, and p53 following RNAi-mediated WDR5 depletion for 72 hours in LoVo ($p53^{WT}$), SW480 ($p53^{MUT}$), and T84 cells ($p53^{NULL}$).

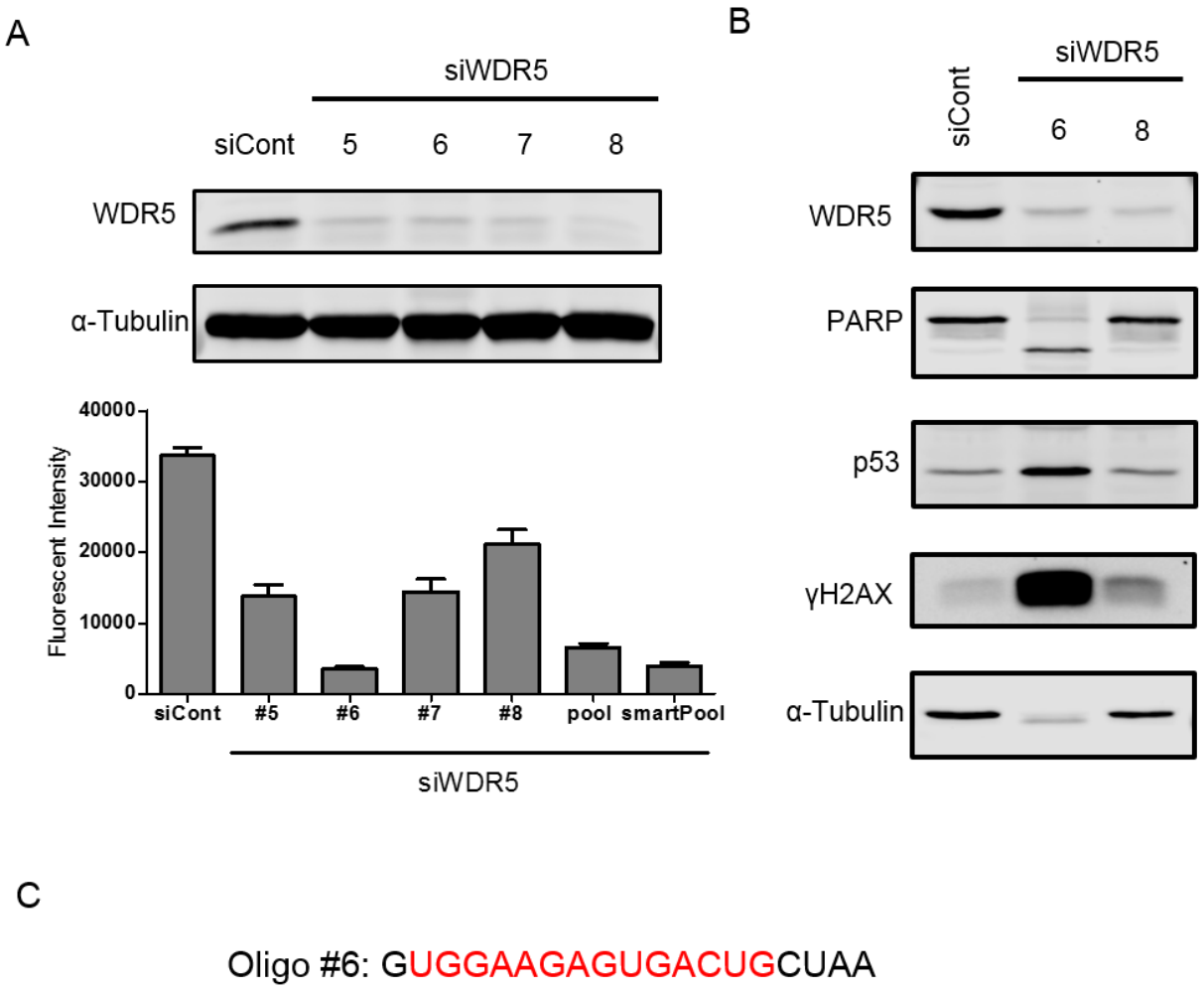

Fig. 5.6: Evaluation of individual WDR5 siRNA. (A) Immunoblot of WDR5 and viability as measured by alamarBlue® following RNAi-mediated knockdown with individual siRNA oligos in HCT116 colon cancer cells. (N=6). (B) Immunoblot of WDR5, PARP, p53, and γH2AX following RNAi-mediated WDR5 depletion using either oligo #6 or #8. (C) WDR5 #6 oligo sequence with nucleotides that match the ME1 sequence shown in red.

cell ATP levels by 15-30 percent in six colon cancer cell lines (Fig. 5.7A). These results were largely confirmed using the alamarBlue® Cell Viability Assay after 96 hours of WDR5 depletion (Fig. 5.7B) with the only change being WDR5 depletion having no effect on viability in LoVo cells as measured by alamarBlue. In contrast, HCECs demonstrated only a 5% decrease in cell ATP levels (Fig. 5.7A) and no difference in viability following WDR5 depletion as measured using the alamarBlue assay (Fig. 5.7B).

COMPASS complex inhibition is detrimental to colon cancer cells

To evaluate the effect of WDR5 inhibition, the effect of OICR-9429 on colon cancer cells and HCECs was examined. OICR-9429 is an antagonist of the interaction of WDR5 with peptide regions of MLL and Histone 3, and disrupts COMPASS complex formation by blocking the interaction between WDR5 and MLL1 and RBBP5 [319,321]. Treatment with 10 μM OICR-9429 for 72 hours also decreased cell viability (alamarBlue® Cell Viability Assay), but to a lesser extent than seen with WDR5 depletion in some cell lines (Fig. 5.7C). Interestingly, OICR-9429 treatment had less of an effect in RKO and HCT116 cells, two cell lines that harbor WDR5 mutations that may reduce the affinity of OICR-9429 for WDR5. Two cell lines with wildtype WDR5 and relatively few or no mutations in any COMPASS components (Table 5.2), SW620 and T84 cells, were more sensitive to both WDR5 depletion as well as OICR-9429 treatment with approximately a 50% decrease in cells over 72 hours.

WDR5 is overexpressed in colon cancer cells

To evaluate the expression of the components of the required WRAD subcomplex within the COMPASS complex in cancer, the mRNA levels of WDR5, RBBP5, ASH2L, and DPY30 in tumors compared to solid tissue normal samples were examined based on RNASeq from the colon adenocarcinoma (COAD) dataset within The Cancer Genome Atlas (Fig. 5.8A). WDR5, RBBP5, and DPY30 are increased in tumors relative to normal tissue; however, WDR5 was expressed at the highest level and showed the most dramatic increase in expression between

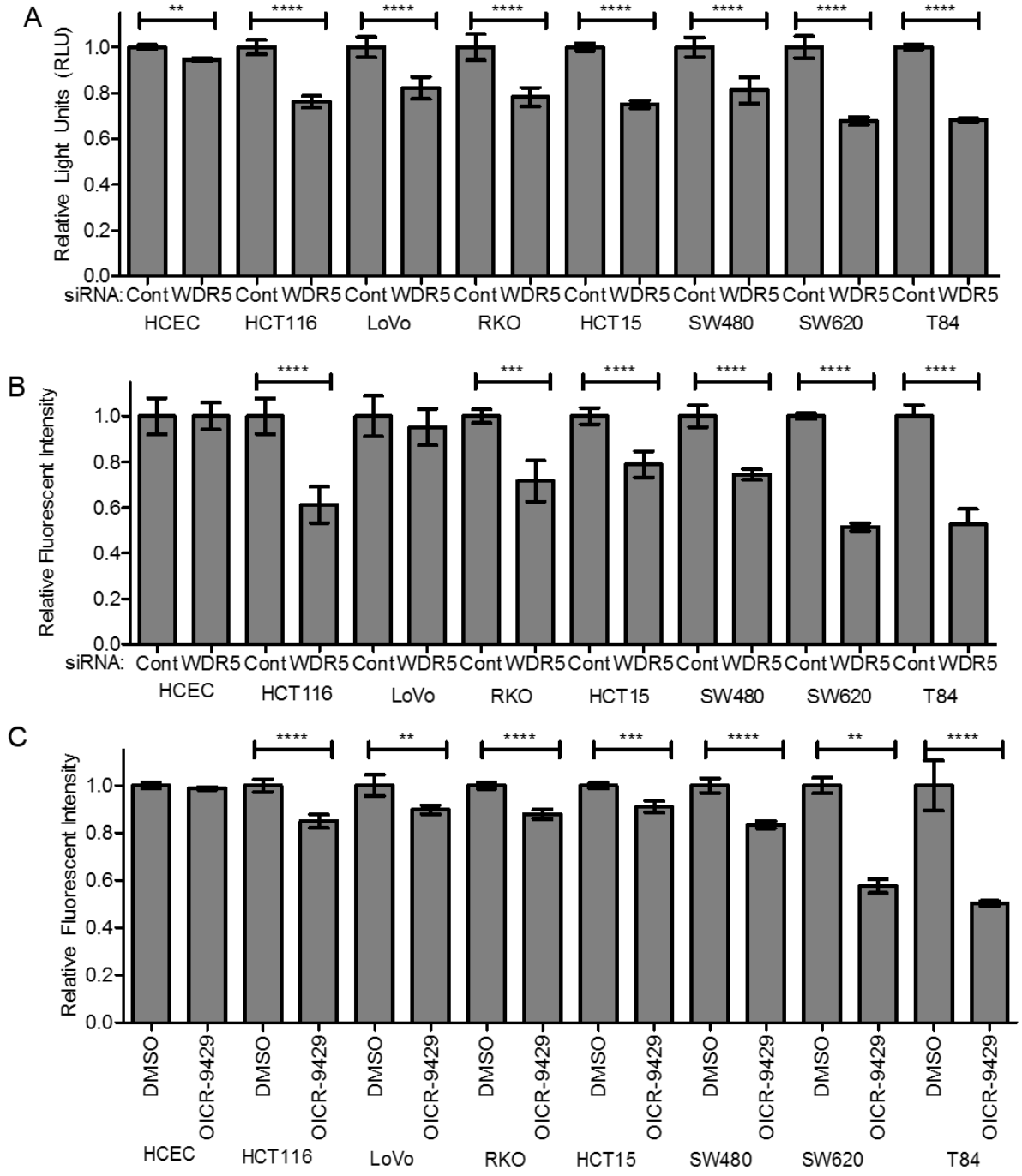

Fig. 5.7: WDR5 depletion or disruption of the COMPASS complex limits cell proliferation or viability in colon cancer cells. (A and B) Cell viability in a panel of colon cancer cells as compared to HCECs following RNAi-mediated depletion of WDR5. Viability was measured by CellTiter-Glo® (A) and alamarBlue® (B) assays 72 hours and 96 hours after transfection, respectively. (C) Cell viability in a panel of colon cancer cells as compared to HCECs following 72 hour treatment with 10 uM OICR-9429 as measured by alamarBlue®. Data are shown as mean relative light units or relative fluorescent intensity ± SD. (N=6). ** $p < 0.01$ *** $p < 0.001$ **** $p < 0.0001$

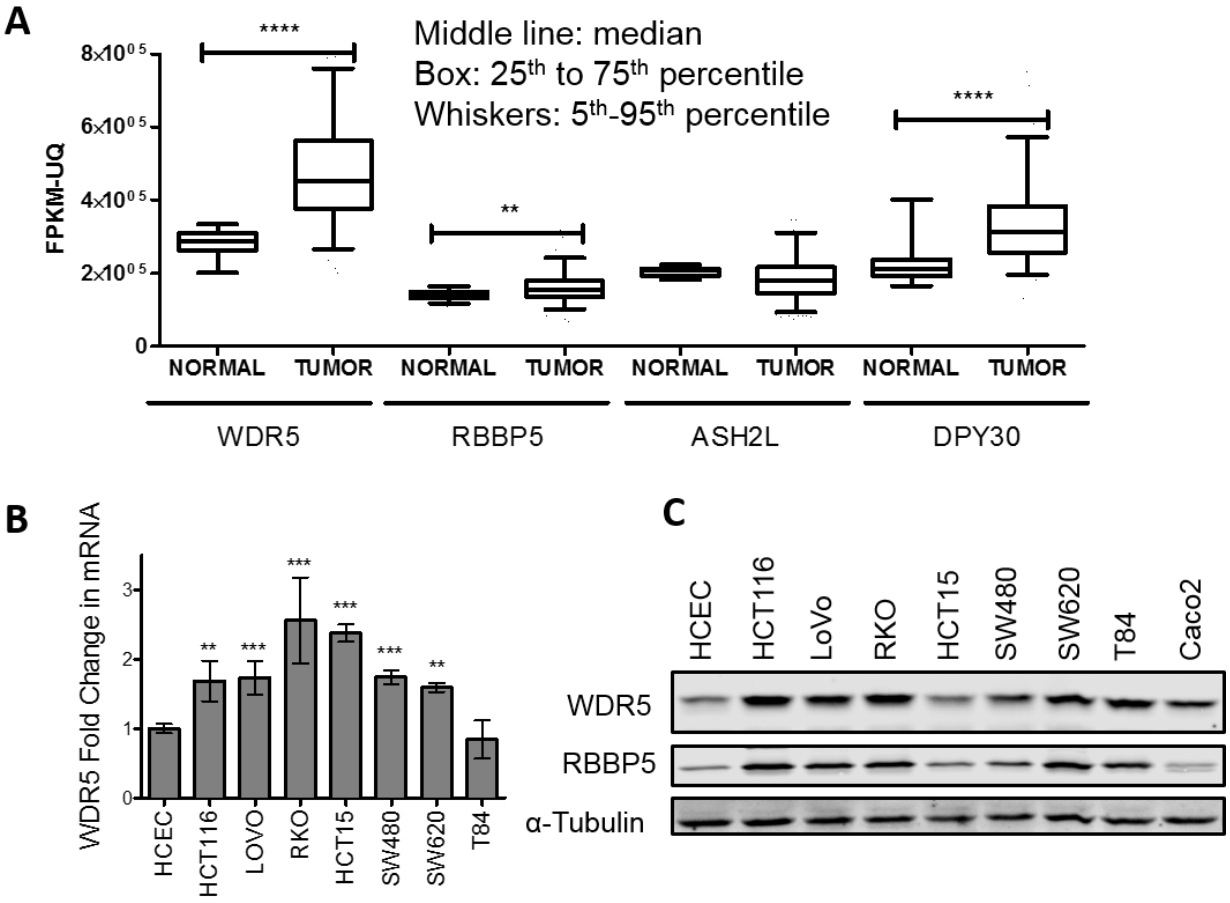

Fig. 5.8: WDR5 is overexpressed in colon cancer cells. (A) WDR5, RBBP5, ASH2L, and DPY30 gene expression (RNASeq) data from the Colon Adenocarcinoma (COAD) dataset within TCGA for unpaired primary colon tumors and normal solid tissue samples. Tumor includes 478 samples from 456 patients for each gene. Normal includes 41 samples from 41 patients for each gene. The results published here are in whole or part based upon data generated by the TCGA Research Network: http://cancergenome.nih.gov/. (B) RT-qPCR of WDR5 and (C) western blot of WDR5 and RBBP5 in a panel of colon tumor cell lines as compared to immortalized, non-transformed HCECs. RT-qPCR data is shown as mean ± SD. (N=3).** $p < 0.01$ *** $p < 0.001$ **** $p < 0.0001$ (Figure 5.8B was performed by Danielle Frodyma and Jamie McCall).

normal tissue and colon tumor tissue. WDR5 is also overexpressed at the mRNA (Fig. 5.8B) and protein level (Fig. 5.8C) in a panel of colon cancer cells as compared to immortalized, yet non-transformed human colon epithelial cells (HCECs) [102]. RBBP5 is similarly overexpressed at the protein level (Fig. 5.8C) in a panel of colon cancer cells as compared to the HCECs.

OICR-9429 treatment dramatically decreases colony growth in colon cancer cell lines

Based on the assumption that WDR5 depletion or COMPASS complex inhibition is altering histone modifications, it would be expected that the effects on proliferation would increase with a longer treatment. Therefore, drug treatment with OICR-9429 for 10-14 days in a colony forming assay was performed in a panel of colon cancer cell lines. Interestingly, OICR-9429 treatment had variable effects between colon cancer cell lines. RKO, LoVo, SW480, SW620, and T84 cell lines demonstrated dramatic decreases in colony formation; however, HCT15 and HCT116 cell lines demonstrated no effect (Fig. 5.9) even after an effect in viability was seen after 72 hours of treatment (Fig. 5.7C).

WDR5 depletion does not decrease AKT phosphorylation and activation

Preliminary data in the lab demonstrated that WDR5 depletion (pool of all four oligos) decreased AKT phosphorylation at both S473 and T308 (Fig. 5.10A); however, later analysis demonstrated the opposite effect (Fig. 5.10B). The misinterpretation of the preliminary results could have been a result of uneven loading. Regardless, if a relationship exists between WDR5 and AKT activation, this relationship is likely indirect and context-specific. Therefore, the mechanism or relationship between WDR5 and AKT phosphorylation was not pursued further.

WDR5 depletion increases DNA damage and decreases trimethylation of H3K4

To further examine the role WDR5 plays in cancer, the effect of WDR5 depletion (oligos #7 and #8 only) and OICR-9429 treatment on H3K4Me3, H3K4Me1, and phosphorylation of H2A.X (γH2AX) was examined in HCT116, SW620, and RKO cells. These cell lines were chosen because HCT116 cells were highly sensitive to WDR5 depletion, but not OICR-9429

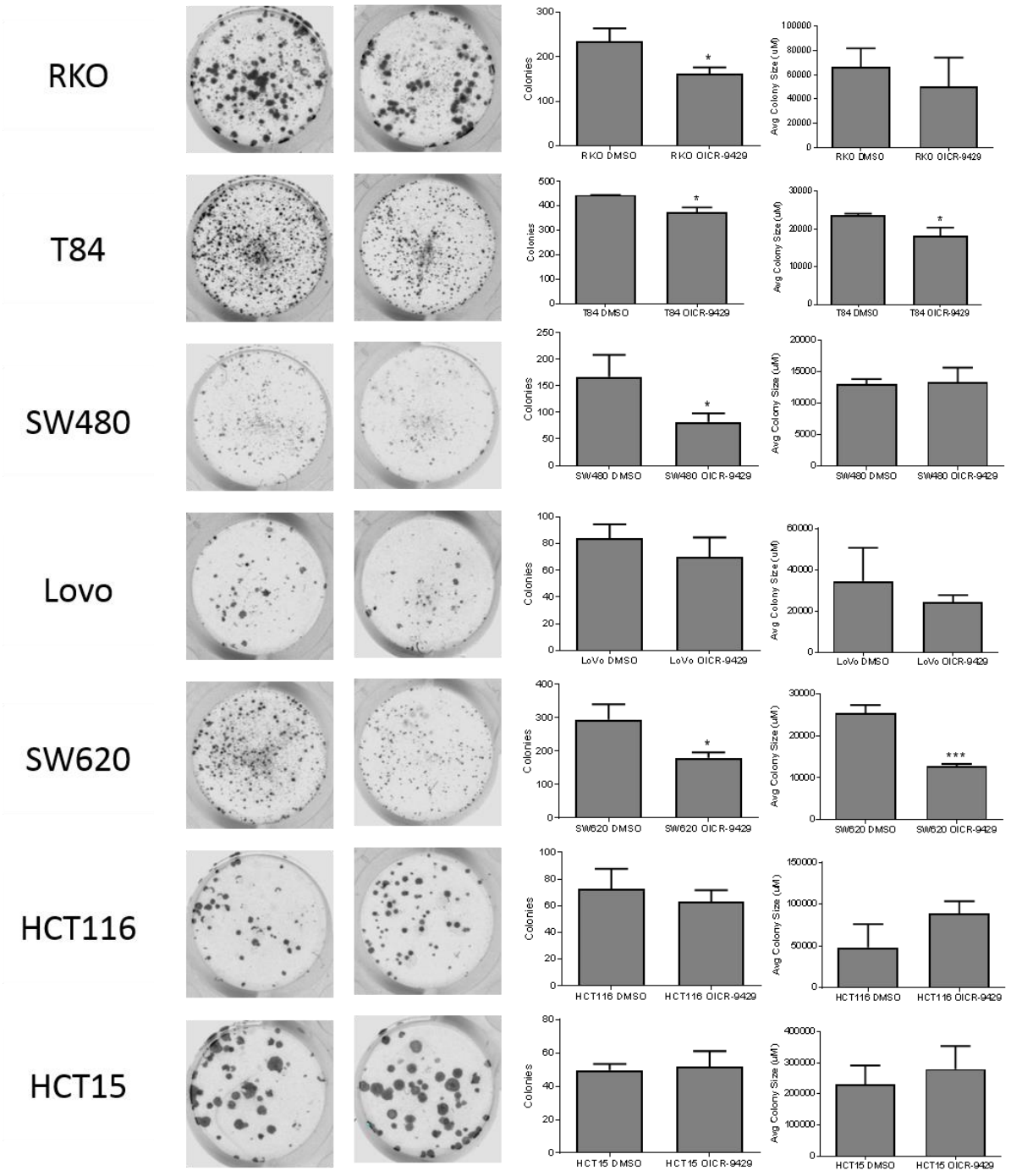

Fig. 5.9: Disruption of the COMPASS complex decreases cell colonies in colon cancer cells. (A and B) Representative pictures (A) and quantification of number and average size of colonies (B) formed on 24-well plates in colon cancer cell lines following treatment with OICR-9429 treatment for 10-14 days. (N=3).

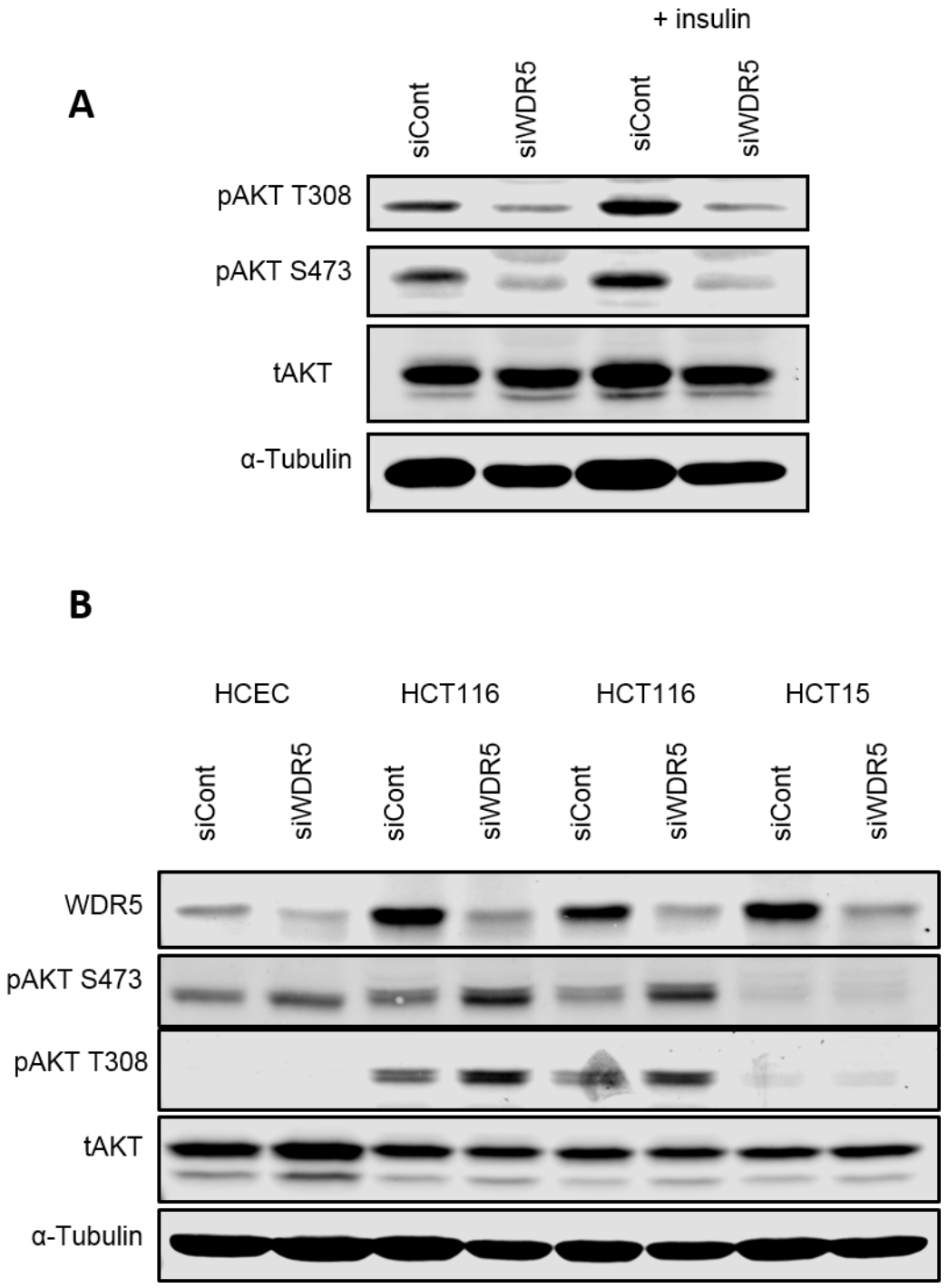

Fig. 5.10: The relationship between WDR5 and AKT may be context dependent. (A) Immunoblot of pAKT (S473), pAKT (T308), and tAKT following RNAi-mediated WDR5 depletion (smartPool of all four oligos) for 72 hours with insulin stimulation for 30 minutes prior to collection in HCT116 cells. (B) Immunoblot of WDR5, pAKT (S473), pAKT (T308), and tAKT following RNAi-mediated WDR5 depletion (smartPool of all four oligos) for 72 hours in HCECs, HCT116 (two independent replicates), and HCT15 cells.

treatment; RKO cells were sensitive to both WDR5 depletion and OICR-9429 treatment, but to a lesser extent; SW620 cells were highly sensitive to both WDR5 depletion and OICR-9429 treatment; and HCT15 cells were mildly sensitive to both WDR5 depletion and OICR-9429 treatment. In all four cell lines, WDR5 depletion induced γH2AX formation and decreased H3K4Me3 (Fig. 5.11). In SW620 cells, WDR5 depletion also decreased H3K4Me1. OICR-9429 treatment was able to induce γH2AX in SW620 cells, but did not affect γH2AX in the other two cell lines. OICR-9429 treatment decreased H3K4Me3 levels in HCT116 cells and to a less extent in RKO and SW620 cells (Fig. 5.11).

These results suggest that WDR5 depletion induces damage in colon cancer, but the OICR-9429 treatment is unable to fully replicate this effect in HCT116 and RKO colon cancer cells. This could be due to the presence of WDR5 mutations in these cell lines that render them less sensitive to OICR-9429 treatment. In contrast, SW620 cells that harbor wildtype WDR5 appear to be equally sensitive to WDR5 RNAi-mediated depletion and OICR-9429 treatment and demonstrate increased γH2AX with either manipulation. The effect on H3K4 methylation appears to be more consistently affected by OICR-9429 treatment. This could be due to the drugs ability to not only directly interact with WDR5, but could be the result of generalized COMPASS complex disruption. This leads one to wonder if the effect of WDR5 on γH2AX is a function of its role within the COMPASS complex or another mechanism. In fact, RBBP5 depletion did not affect cell viability suggesting that WDR5 may function outside of the COMPASS complex to promote tumorigenesis (Fig. 5.12).

WDR5 depletion sensitizes colon cancer cells to IR-induced DNA damage

The increase in γH2AX with WDR5 depletion (Fig 5.11) and previous literature demonstrating that WDR5 depletion induces DNA damage suggests that WDR5 depletion may be able to sensitize cancer cells to DNA damage. To evaluate the potential that loss of WDR5 sensitizes cells to DNA damage, the effect of WDR5 depletion (oligos #7 and #8 only) on IR-induced γH2AX formation and PARP cleavage was assessed. HCT116, HCT15, SW620, and

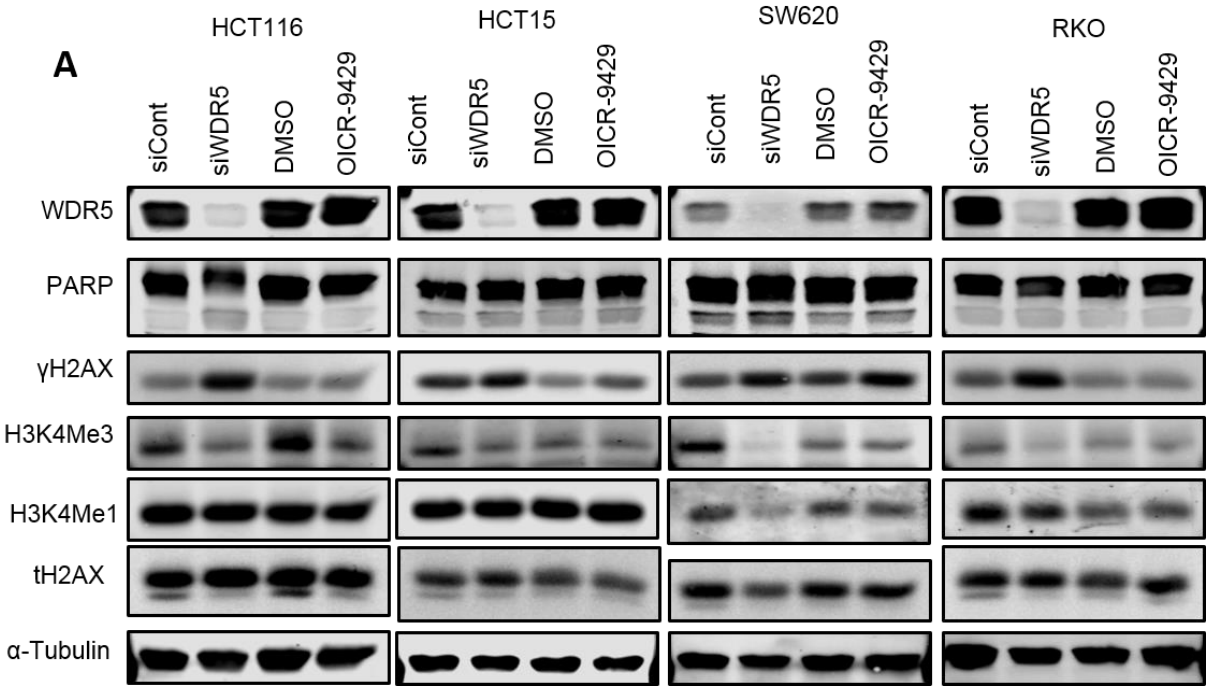

Fig. 5.11: WDR5 depletion increases DNA damage and reduces H3K4Me3. (A) Immunoblot of γH2AX, H3K4Me1, and H3K4Me3 following 96-hour RNAi-mediated WDR5 depletion (oligo pool of #7 and #8 only) or 72 hour OICR-9429 treatment in HCT116, HCT15, SW620, and RKO colon cancer cells.

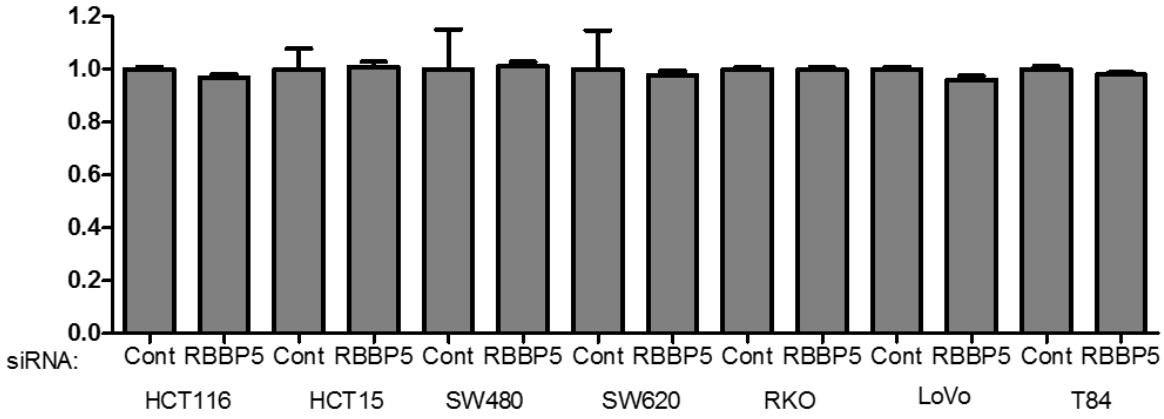

Fig. 5.12: RBBP5 depletion does not affect cell viability in a panel of colon cancer cell lines. (N=3).

RKO cells were depleted of WDR5 for 48 hours prior to a single dose of irradiation (3 Gy). Cells were allowed to recover for 48 hours after IR prior to collection and then were assessed for γH2AX expression and PARP cleavage. In control cells, radiation increased γH2AX levels, which were further increased with the loss of WDR5 in all cell lines tested (Fig. 5.13). SW620 and RKO cells demonstrated a step-wise increase in γH2AX levels with WDR5 depletion, irradiation in control cells, with maximal γH2AX in the cells that received irradiation in conjunction with WDR5 depletion (Fig. 5.13). In contrast, HCT116 and HCT15 cells demonstrated substantial increased in γH2AX with WDR5 depletion that was not further increased with the addition of IR (Fig. 5.13). This could be a consequence of the high level of endogenous genomic instability and defects in DNA damage repair present in these cells. Regardless, in all conditions, WDR5 depletion further increased γH2AX levels indicating increased DNA damage.

Conclusions

The data presented clearly demonstrate that WDR5 is overexpressed and preferentially required in colon cancer cells more so than in immortalized, yet non-transformed human colon epithelial cells (HCECs); however, the mechanism behind its overexpression and requirement for survival has not been fully revealed. WDR5 has previously been shown to promote its own expression through a positive feedback loop where increased H3K4Me3 at the WDR5 promoter increases its transcription [239]. It is possible this positive feedback loop could be contributing to the maintenance of the overexpression of WDR5 demonstrated here in both colon cancer cell lines and human colon tumors, yet this cannot explain the initial increase in WDR5 expression and is difficult to demonstrate experimentally. The overexpression of WDR5 is not unique to colon cancer as several recent studies have demonstrated WDR5 is overexpressed in several cancer types including breast, prostate, bladder, and pancreatic cancer. Of importance, WDR5 overexpression has been clinically associated with worse patient outcomes in breast cancer and

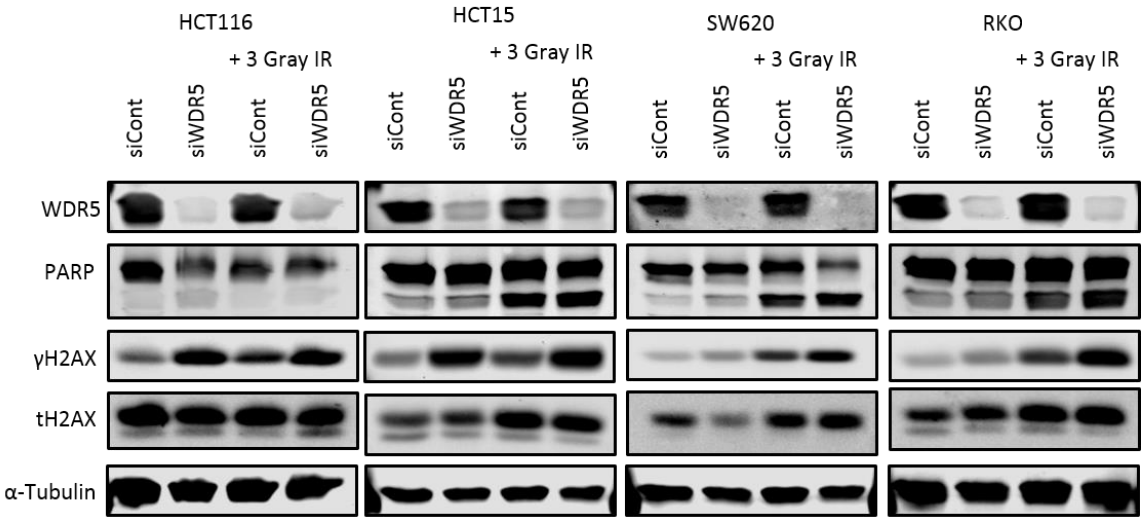

Fig. 5.13: WDR5 depletion increases sensitivity to ionizing radiation. Immunoblot of γH2AX and PARP following 96-hour RNAi-mediate WDR5 depletion (oligo pool with #7 and #8 only) with 3 Gy gamma IR for 48 hours prior to collection.

hepatocellular carcinoma [291,294]. Our data demonstrate that colon cancer cells rely on WDR5 for increased proliferation and cell survival as depletion of WDR5 reduces cell viability, but does not substantially increase apoptosis. Other groups have demonstrated similar findings and demonstrated that WDR5 is similarly required for cell survival and proliferation in various other types of cancer including leukemia [292], prostate[268], bladder [293] breast [295], and pancreatic cancer [297].

In general, the mechanism by which WDR5 supports cancer cells has largely been shown to be through increased target gene expression. Consistent with these findings, our data demonstrate that WDR5 depletion caused a decrease in global H3K4Me3 levels likely suppressing target gene expression. However, our data demonstrated that WDR5 depletion induced a robust increase in γH2AX levels representative of an increase in DNA damage that was highly associated with decreased viability in colon cancer cells following WDR5 depletion. Recently, WDR5 has been shown to physically interact with MYC to promote transcription of a subset of MYC target genes. In addition, this interaction also prevented DNA damage accumulation in patient-derived xenografts of pancreatic cancer [287]. Other mechanisms by which WDR5 may suppress the accumulation of DNA include regulating DNA replication, chromosomal polyploidy [323] and abscission through localization to the midbody [289]. Based on our data demonstrating WDR5 depletion increases DNA damage accumulation, it is likely that WDR5 is contributing to DNA fidelity possibly through one of the previously described mechanisms thereby supporting cancer cell viability. The contribution of WDR5 to DNA fidelity may or may not be independent of its role in the WRAD subcomplex, as RBBP5 did not affect viability in a panel of colon cancer cells. However, there are multiple reports suggesting that depletion of KMT2A/MLL1 and KMT2B/MLL2 induce DNA damage as well as WDR5 suggesting a potential connection between the increased DNA damage following WDR5 depletion and its role in the COMPASS complex [263,266,272-275].

Resolution of γH2AX is thought to occur through exchange of γH2AX with dephosphorylated H2AX with subsequent dephosphorylation of the removed γH2AX by

phosphatases. One mechanism that facilitates the dephosphorylation of γH2AX is through H3K4 and H3K36 methylation by metnase, a protein that contains a SET domain and is a potential binding partner of WDR5. Metnase also promoted non-homologous end-joining, restart of stalled replication forks, resolution of γH2AX, and knockdown increased sensitivity to ionizing radiation [324]. Alternatively, WDR5 could contribute to K3K4 methylation through the COMPASS complex to facilitate γH2AX resolution. WDR5 itself has been shown to promote the incorporation of H2A.Z to promote global transcription [305] suggesting a potential mechanism where WDR5 regulates cell cycle progression through increased transcription (H2A.Z incorporation) and release of cell cycle checkpoints (removal of γH2AX). Future studies are needed to further elucidate the individual contributions each of the multitude of functions WDR5 has on the induction of DNA damage, and more importantly, on cancer cell viability.

Our data demonstrated increased sensitivity to radiation, particularly in SW620 and RKO colon cancer cells. While the HCT116 cells demonstrated increased γH2AX following WDR5 depletion, WDR5 depletion alone was sufficient to increase γH2AX to the same level seen with IR. Relative to the other cell lines, HCT116 cells demonstrated the highest induction of γH2AX with WDR5 depletion alone. This could be a result of the high level of genomic instability in these cells. This, in combination with the additive effect of WDR5 depletion following IR-induced DNA damage, suggests WDR5 is particularly required in cells following DNA damage.

Overall, WDR5 depletion demonstrated a more robust phenotype than OICR-9429 treatment. Several factors could contribute to this disparity, but likely either WDR5 plays a role independent of the COMPASS complex that is not inhibited by OICR-9429 treatment or mutations in WDR5 or other COMPASS components limited the affinity and therefore efficacy of OICR-9429. Consistent with the second possibility, cells with limited mutations in WDR5 and KMT2/MLL proteins had increased sensitivity to both WDR5 depletion and OICR-9429. This could be because that without mutations in KMT2/MLL components, the KMT2/MLL have a significant requirement for WDR5 in order to function to methylate H3K4 as they have very little

enzymatic activity outside of the COMPASS complex. Cells containing WDR5 mutations could be less sensitive to OICR-9429 as mutations could reduce the affinity of the drug for WDR5. These results also suggest that it is unlikely that the reduced effect on cells following OICR-9429 treatment as compared to WDR5 depletion is simply due to the drug being unable to inhibit WDR5 as some cell lines showed a similar response to WDR5 depletion and OICR-9429 treatment.

Additional studies on the effect of mutations in KMT2/MLL proteins and WDR5 will provide further understanding of the role of WDR5 and the COMPASS complex in cancer and will help delineate whether these proteins have tumor suppressive, oncogenic, or a combination of both roles. Further studies are also needed to fully distinguish if the role of WDR5 is a result of its contribution to the COMPASS complex, is due to an alternative mechanism, or a combination of multiple mechanisms. Regardless, WDR5 is required for colon cancer cell proliferation and sensitized cells to ionizing radiation demonstrating a clear role for WDR5 in cancer and revealing its potential as a therapeutic target in cancer.

Chapter 6: FUSION identified 5'-hydroxy-staurosporine as an AMPK inhibitor that is selectively toxic in colon cancer cells

Portions of the material covered in this chapter are the subject of a manuscript published in *Scientific Reports* by Das B*, Neilsen BK* *et al*. [1]

* Denotes equal contribution

Introduction

The Ras oncogene is activated in more than 40% of colon tumors [325] and 25%-30% of human cancers overall [6,7]. Despite substantial efforts to develop therapeutics targeting this pathway [18,326], significant challenges still exist. We previously demonstrated that Kinase Suppressor of Ras 1 (KSR1), a molecular scaffold for the Raf/MEK/ERK kinase cascade, is required to maintain the transformed phenotype of Ras-driven colon cancer cell lines, but is dispensable for the survival and proliferation of non-transformed human colon epithelial cells[3]. Using KSR1 as a reference standard in a RNAi-based gene expression high-throughput screen termed Functional Signature Ontology (FUSION) [101], we identified and validated the γ1 subunit of AMP-activated protein kinase (AMPK) as a contributor to the survival of human colon tumor cells [3].

AMPK belongs to a family of serine/threonine kinases that are highly conserved from yeast to humans [327]. AMPK functions as a heterotrimeric complex consisting of a catalytic α and regulatory β and γ subunits [328]. Mammalian AMPK acts as an energy sensing kinase that is activated by an increasing AMP/ATP ratio and by metabolic alterations, such as hypoxia, glucose deprivation, decreased ATP production, or increased energy consumption. AMPK is a substrate for kinases such as LKB1 and CAMKK2, which modulate its activity by phosphorylation of the activation loop on both alpha subunits at threonine 172. During severe stress, AMP binding to the γ subunit allosterically activates AMPK, promoting phosphorylation of the α subunit at threonine 172, and protects it from dephosphorylation [329].

The role of AMPK in cancer is controversial and has been shown to both support and inhibit tumor growth [3,328,330-340]. Retrospective population-based studies suggest that AMPK may act as a tumor suppressor because metformin, an inhibitor of mitochondrial electron transport complex 1 and an indirect AMPK activator, appears to decrease the risk for cancer [341,342]. While the mechanism through which metformin lowers cancer risk is not fully understood, numerous

studies demonstrate the value of metformin as an anti-cancer agent *in vitro,* in preclinical *in vivo* models, and in patients [332,333,338,341,342]. However, the link implicating AMPK as a contributor to the metformin-induced anti-cancer effect is controversial.

One recent study demonstrated that some cancer cells have upregulated cancer-specific ubiquitin ligases (MAGE-A3/6) that promote the degradation of AMPK to allow for increased mTORC1 signaling [339]. Peutz-Jeghers Syndrome, which is characterized by the formation of numerous benign and malignant tumors, is characterized by loss of LKB1 kinase activity, a known upstream kinase and activator of AMPK [343]. However, LKB1 is not the only kinase that phosphorylates AMPK, and LKB1 phosphorylates numerous additional downstream targets that may contribute to its tumor suppressive role.

In contrast, AMPK activation was seen in early stages of glioblastoma tumor formation [344], and AMPK activation was found to be critical for pancreatic cancer cell growth in anchorage-independent conditions [345]. Moreover, both AMPK$\alpha 1^{-/-}$ and AMPK$\alpha 2^{-/-}$ MEFs are resistant to Ras-induced oncogenic transformation, arguing that Ras-driven transformation requires AMPK [334,337]. Based on the conflicting evidence, AMPK has been described as a "conditional tumor suppressor and contextual oncogene" [338]. The cause of these conflicting reports may be due to the role of AMPK in stress response. In non-transformed cells, AMPK likely contributes to the maintenance of a non-transformed phenotype by promoting a controlled stress response. However, in transformed cells the stress response function of AMPK may promote survival in a suboptimal environment. While AMPK$\gamma 1$ is required for colon cancer cell survival [3], the contribution of other subunit isoforms on cancer cell survival has not been examined. We examined the expression and function of the AMPK$\alpha 2$ subunit in colon cancer cells and used FUSION to detect a competitive inhibitor of AMPK within a natural product library. This study highlights the potential of evaluating and targeting specific AMPK isoforms and serves as a proof-of-concept for FUSION-based detection of small molecule inhibitors of therapeutic targets.

Results

AMPKγ1 depletion is preferentially toxic to HCT116 colon cancer cells, but not to HCECs.

To demonstrate that the γ1 subunit of AMPK (AMPKγ1) is required for tumor cell survival, the metabolic capacity of cells (alamarBlue® Cell Viability Assay) and PARP cleavage (marker of apoptosis) was examined in immortalized, non-transformed human colon epithelial cells (HCECs) and HCT116 colon cancer cells following RNAi-mediated depletion of AMPKγ1 for 72 hours. AMPKγ1 depletion substantially reduced the metabolic capacity of HCT116 cancer cells, but did not decrease the metabolic capacity of HCECs (Fig 6.1A). AMPKγ1 depletion for the previous assay was verified and PARP cleavage was assessed by immunoblot. AMPKγ1 protein expression was reduced following RNAi-mediated depletion in both cell lines assessed, but PARP cleavage was only increased in the HCT116 colon cancer cell lines following AMPKγ1 depletion (Fig 6.1B).

AMPKγ1 depletion caused variable levels of toxicity in colon cancer cell lines, which correlated with its ability to inhibit autophagy.

AMPK is known to regulate autophagy in cells through phosphorylation of ULK1 (Fig. 6.2A), and this function could contribute to its specific requirement in cancer cells where autophagy is known to be upregulated. To evaluate whether this known function of AMPK is contributing to its requirement in colon cancer cells, we examined beclin 1 levels following AMPKγ1 depletion. In HCT116 cells, beclin 1 levels were decreased, suggesting a decrease in autophagy, following AMPKγ1 depletion. In contrast, there was no induction of PARP cleavage or decrease in beclin 1 levels in SW480 colon cancer cells with AMPKγ1 depletion (Fig. 6.2B-C), which suggests the regulation of autophagy may mediate the detrimental effect AMPKγ1 depletion has on HCT116 colon cancer cells (Fig 6.2B). When HCT116 cells were starved of serum for 16 hours prior to collection to induce autophagy, AMPKγ1 depletion resulted in an even more robust decrease in beclin 1 levels and decreased phosphorylation of ULK1 (Fig. 6.2C).

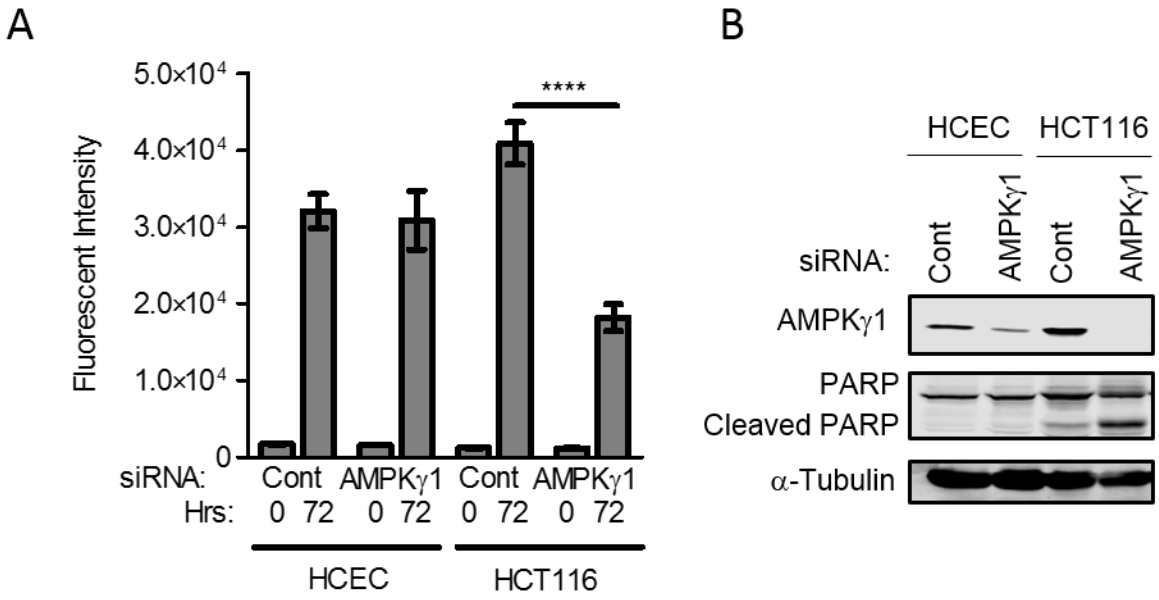

Fig. 6.1: AMPKγ1 depletion is preferentially toxic to HCT116 colon cancer cells, but not to HCECs. (A and B) Cell viability assay (N=6) (A) and immunoblot (B) of AMPKγ1 and PARP following RNAi-mediated AMPKγ1 depletion for 72 hours in HCECs and HCT116 cells.

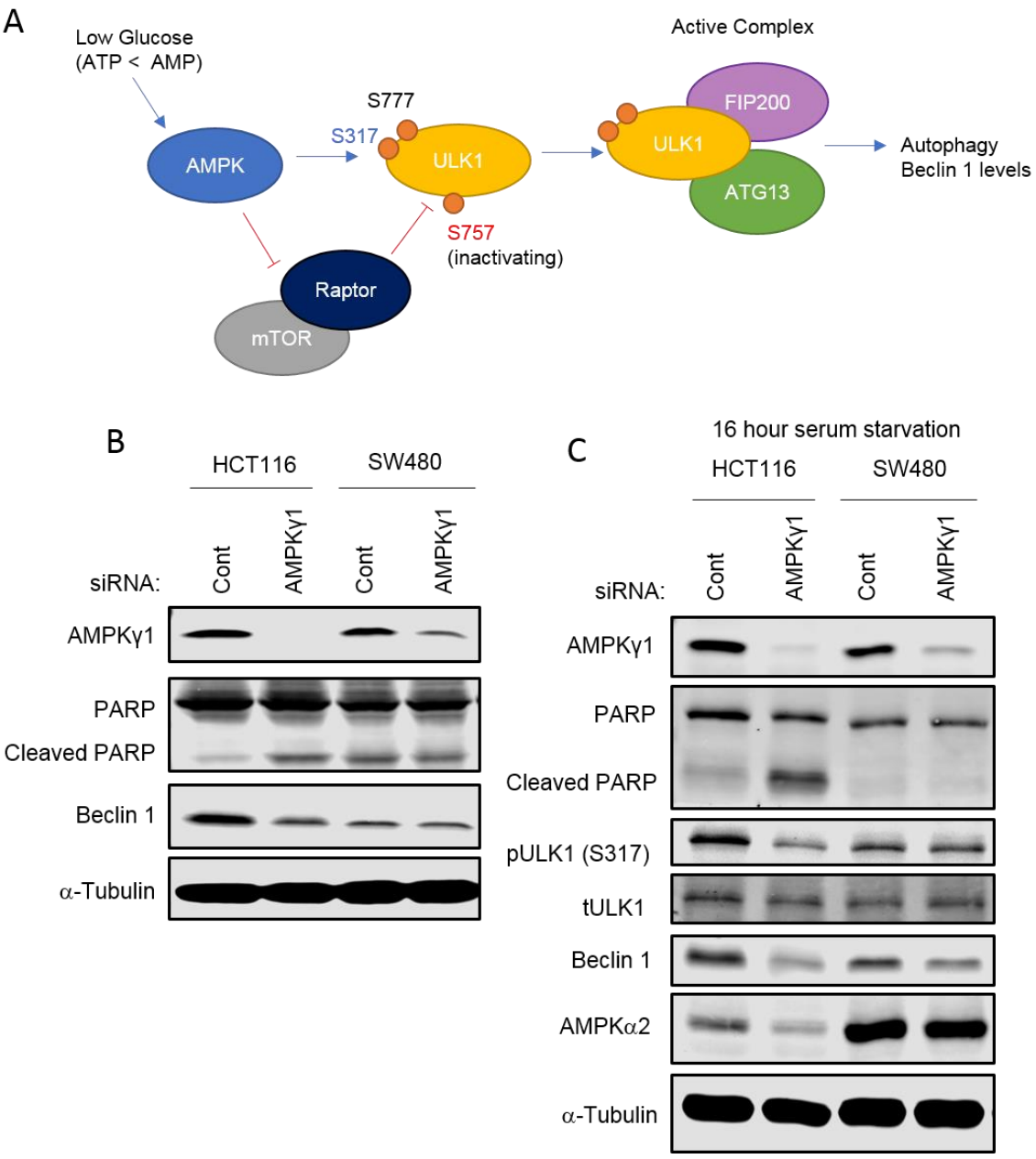

Fig. 6.2: AMPKγ1 depletion induces apoptosis and blocks autophagy in HCT116 colon cancer cells, but not SW480 colon cancer cells. (A) Cartoon of AMPK in autophagy. (B) Immunoblot of AMPK subunits, PARP, and an autophagy marker (beclin 1) following RNAi-mediated AMPKγ1 depletion for 72 hours in HCT116 and SW480 cells. (C) Immunoblot of AMPK subunits, PARP, and autophagy markers (beclin 1, pULK1) following RNAi-mediated AMPKγ1 depletion for 72 hours in HCT116 and SW480 cells with serum starvation for the 16 hours prior to collection.

In contrast, AMPKγ1 depletion did not affect beclin 1 levels or ULK1 phosphorylation in SW480 colon cancer cells even with serum starvation; however, the level of knockdown was not as robust in the SW480 cells as compared to the HCT116 cells, which could also be limiting its effects. Interestingly, AMPKγ1 depletion also resulted in a decrease in AMPKα2 in HCT116 cells, but did not affect AMPKα2 levels in SW480s. This observation raises the possibility that AMPKγ1 is required for the formation and stabilization of the AMPK heterotrimer in HCT116 cells, but not SW480s, and that stabilization of the holoenzyme is required for HCT116 cell survival.

AMPKα2 is differentially expressed in colon cancer cell lines.

AMPK functions as a heterotrimeric complex consisting of a catalytic α subunit that possesses kinase activity and regulatory β and γ subunits[328]. The α2, β2, and γ1 AMPK subunits, but not the α1 and β1 subunits, promoted the survival of HCT116 colon cancer cells[3]. However, AMPKγ1 was not required for survival in SW480 colon cancer cells (Fig. 6.2B-C). To further evaluate the importance of the individual AMPK subunits, the expression of various AMPK subunits in a panel of colon cancer cell lines was examined. AMPKα1, AMPKγ1, and AMPKβ1 expression was relatively consistent across cancer cells lines and was comparable to immortalized, non-transformed human colon epithelial cells (HCEC) expression (Fig. 6.3). However, the expression of AMPKα2 and AMPKβ2 was variable between cancer cell lines. Of note, the highest expression of AMPKα2 was observed in the SW480 and SW620 cancer cells. HCECs, as well as the LoVo and HCT116 cancer cells had moderate expression. While, HCT15, DLD1 and SK-CO-1 cells demonstrated very low AMPKα2 expression (Fig. 6.3).

AMPKα2, but not AMPKα1, is required for colon cancer cell survival.

To evaluate the role the kinase activity of AMPK plays in promoting colon cancer cell survival, the effect of AMPKα1 or AMPKα2 depletion on colon cancer cells was examined. Cell lines with moderate (HCT116) and high (SW480) AMPKα1 and AMPKα2 expression were selected for analysis, and propidium iodide staining followed by flow cytometry analysis and

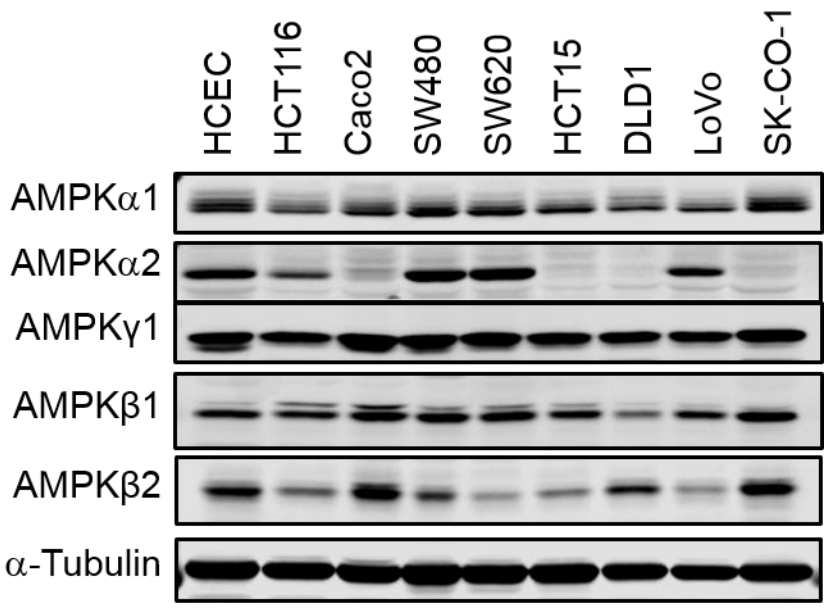

Fig. 6.3: AMPK subunit expression in a panel of colon cancer cell lines as compared to immortalized, non-transformed human colon epithelial cells (HCEC).
(Part of Fig. 6.3 has been previously published in [1]**).**

PARP cleavage assessment were used to evaluate cell death after AMPKα1 or AMPKα2 depletion by RNAi for 72 hours. AMPKα2 depletion increased cell death in both HCT116 and SW480 colon cancer cell lines, while AMPKα1 depletion did not (Fig. 6.4A-C). These data indicate that AMPKα2, and therefore AMPK activity, is required for colon cancer cell survival even though individual AMPK subunits (AMPKα1) may be dispensable. These data suggest that while individual AMPK subunits likely have overlapping roles in cells, they also have unique, non-redundant functions. Of note, individual AMPKα1 or AMPKα2 depletion or combination depletion of AMPKα1/α2 does not induce apoptosis in HCECs (Fig 6.4D), suggesting that colon cancer cells have developed a unique dependence upon AMPK activity. Thus, identifying a compound that selectively inhibits the functional AMPK heterotrimer may be an efficacious therapeutic strategy to selectively target cancer cells regardless of their preference or requirement for specific AMPK subunits.

AMPKα2 is required for autophagy and increased metabolic capacity.

To evaluate the effects of AMPKα2 depletion in cancer cells, phosphorylation of ULK-1 and beclin 1 expression, a marker of autophagy, was examined. Following AMPKα2 depletion for 72 hours, ULK1 phosphorylation and beclin-1 levels decreased; however, these changes were modest and more robustly seen in HCT116 cells and to a lesser extent seen in SW480 cells (Fig 6.5A). In HCT116 cells, AMPKα2 depletion, but not AMPKα1 depletion, caused a decrease in PGC1β and ERRα expression, two proteins that have previously been shown to be required for HCT116 colon cancer cell survival (Fig 6.5B), which opens the possibility that AMPKα2 has multiple mechanisms by which it promotes colon cancer cell survival.

FUSION identifies a natural product that inhibits AMPK kinase activity.

Functional Signature Ontology (FUSION) detects functional relationships between genes and microRNAs based on changes to a gene expression-based functional signature[3,101,346]. Previously, FUSION identified AMPKγ1 as a genetic functional analog of KSR1 based on

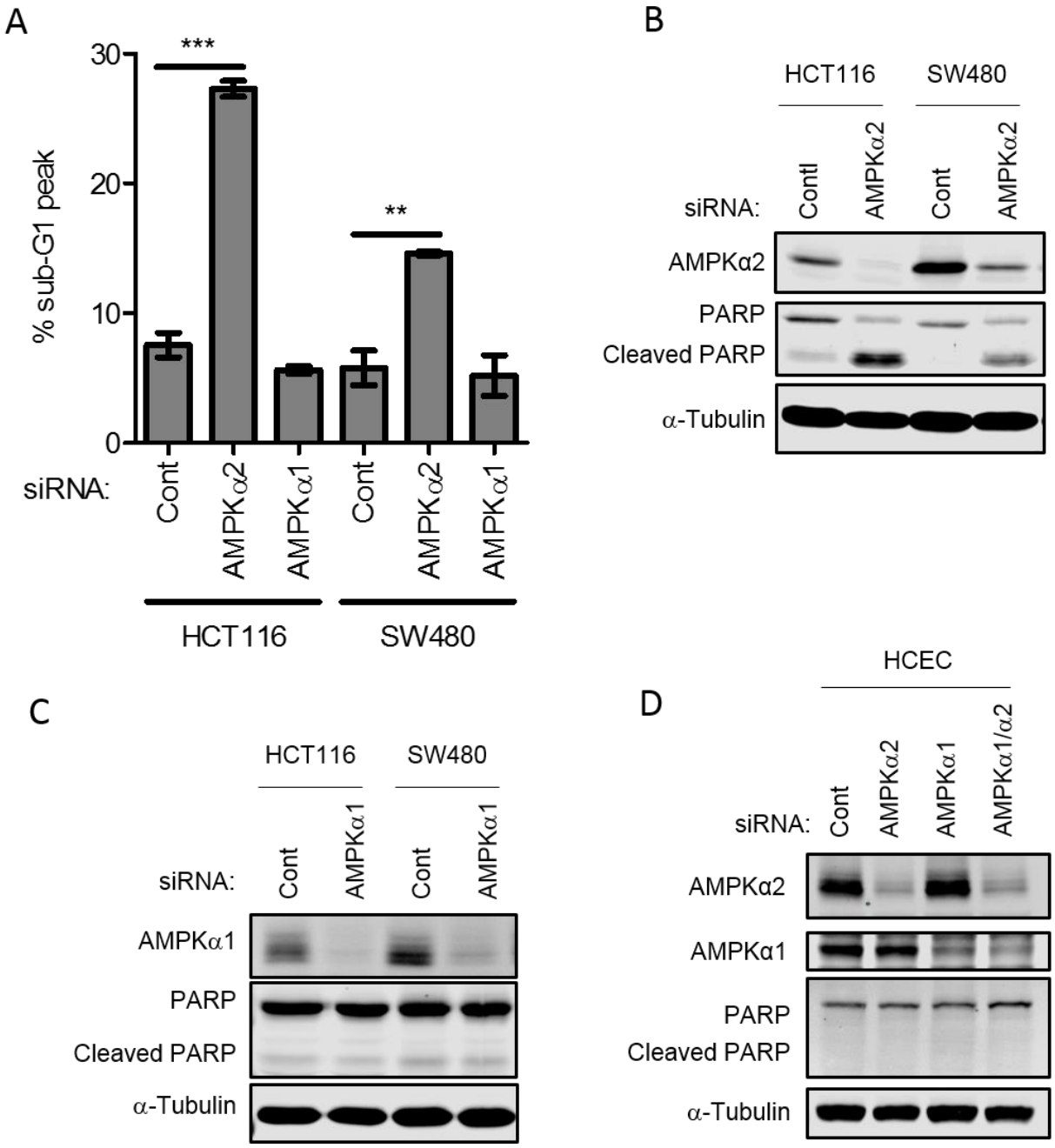

Fig. 6.4: AMPKα2 is selectively required for colon cancer cell survival, but not HCEC survival. (A) Apoptosis (percent of cells in the sub-G1 peak) in HCT116 and SW480 cells after AMPKα1 or AMPKα2 depletion by RNAi for 72 hours. Apoptosis was evaluated using propidium iodide staining followed by flow cytometry analysis. (N=3). (B) Immunoblot of AMPKα2 expression and PARP cleavage in HCT116 and SW480 cells following RNAi-mediated AMPKα2 depletion for 72 hours. (C) Immunoblot of AMPKα1 expression and PARP cleavage in HCT116 and SW480 cells following RNAi-mediated AMPKα1 depletion for 72 hours. (D) Immunoblot of AMPKα1, AMPKα2, and PARP cleavage in HCECs following RNAi-mediated AMPKα1 or AMPKα2 depletion for 72 hours. (Part of Fig. 6.4 has been previously published in [1]).

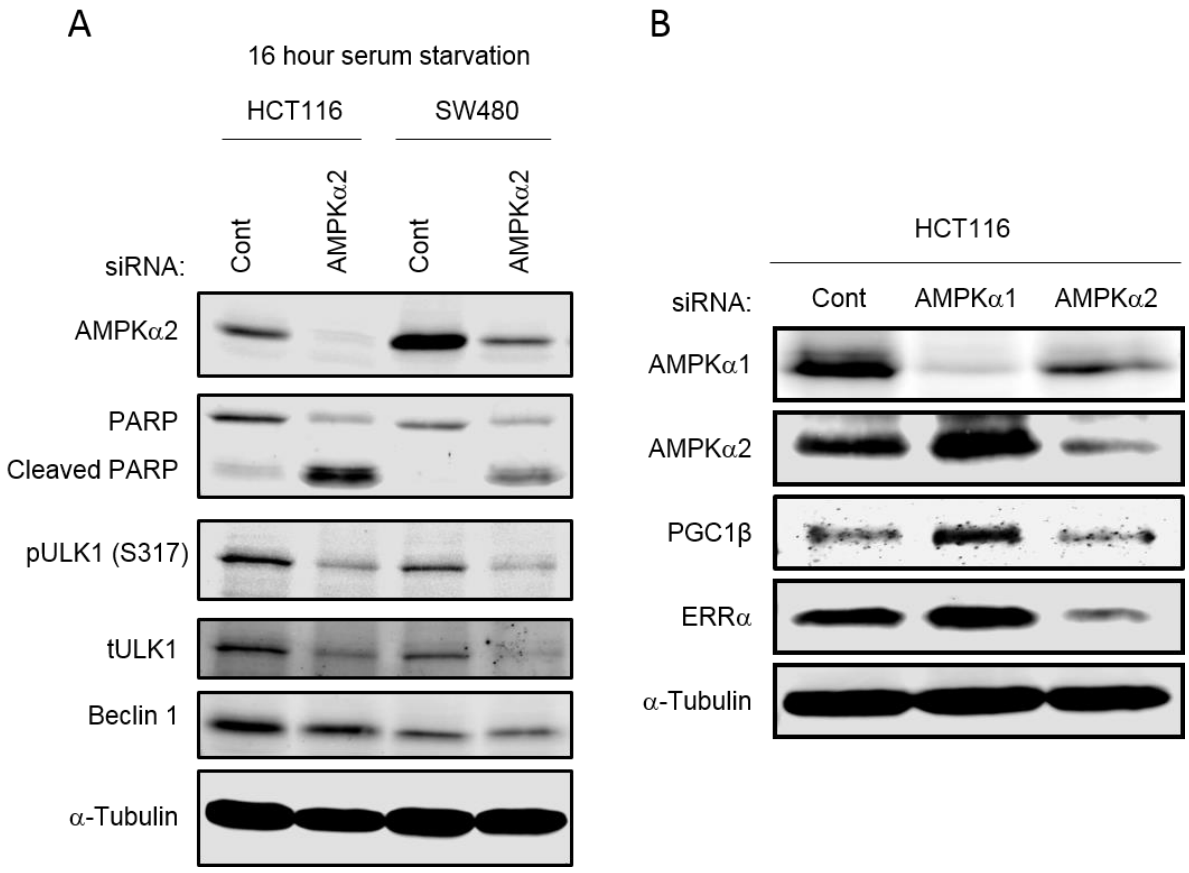

Fig. 6.5: AMPKα2 depletion reduces phosphorylation of ULK-1 and expression of beclin 1, PGC1β, and ERRα. (A) Immunoblot of AMPKα2, PARP, total- and phospho-ULK1, and beclin 1 following RNAi-mediated depletion of AMPKα2 for 72 hours in HCT116 and SW480 cells. (B) Immunoblot of AMPKα1, AMPKα2, PGC1β, and ERRα following AMPKα1 or AMPKα2 depletion for 72 hours in HCT116 cells. (Experiment 6.5B was done in collaboration with Binita Das and is published in [3]. Part of Fig. 6.5A has been previously published in [1]).

unsupervised hierarchical clustering and quantification of similarity metrics (Euclidean distance and Pearson correlation) based on reporter gene expression following RNAi-mediated depletion of individual genes from a genome-scale human siRNA library. Biological validation demonstrated AMPKγ1 is also required for the survival of colon tumor cells, but not immortalized, non-transformed colon epithelial cells[3]. We hypothesized this approach could be used to identify small molecule inhibitors that mimic the effects of AMPK inhibition and be preferentially toxic to human colon tumor cells. As a proof-of-concept experiment, reporter gene expression signatures were generated for 1,186 unique chemical fractions isolated from a natural product library derived from a diverse selection of marine bacteria [101]. Comparing the gene expression signature of Compound C (also known as Dorsomorphin), a drug known to inhibit AMPK[333], with fractions isolated from the natural product library, FUSION identified several fractions whose biologic activity was similar to Compound C treatment [101,347].

Several fractions isolated from the *Streptomyces bacillaris* strain SN-B-004 clustered with Compound C (Fig. 6.6A). Based on this observation, we hypothesized that the SN-B-004 fractions that clustered with Compound C contained an inhibitor of AMPK. Treatment with SN-B-004 fractions 13-17 decreased viability of colon tumor cell line HCT116 (Fig. 6.6B) and SN-B-004 fractions 13-16 decreased phosphorylation of two AMPK substrates acetyl-CoA carboxylase (ACC) at Ser79 and RAPTOR at Ser792 (Fig. 6.6C). In contrast, SN-B-004 fraction 12, which clustered further away from Compound C, but was collected in series with fractions 13-16, did not affect cell viability or phosphorylation of AMPK downstream targets (Fig. 6.6B-C).

SN-B-004 fractions 13-17 appeared pharmacologically and mechanistically distinct from Compound C because they demonstrate a limited ability to prevent the phosphorylation of AMPKα at Thr172 (Fig. 6.6C), which is critical for AMPK activity[348], while Compound C was able to decrease phosphorylation at Thr172. While Compound C has been shown to inhibit AMPK activity by decreasing phosphorylation on downstream targets, the mechanism behind its inhibition has not been fully elucidated. Increasing activating AMPK signals (AICAR or

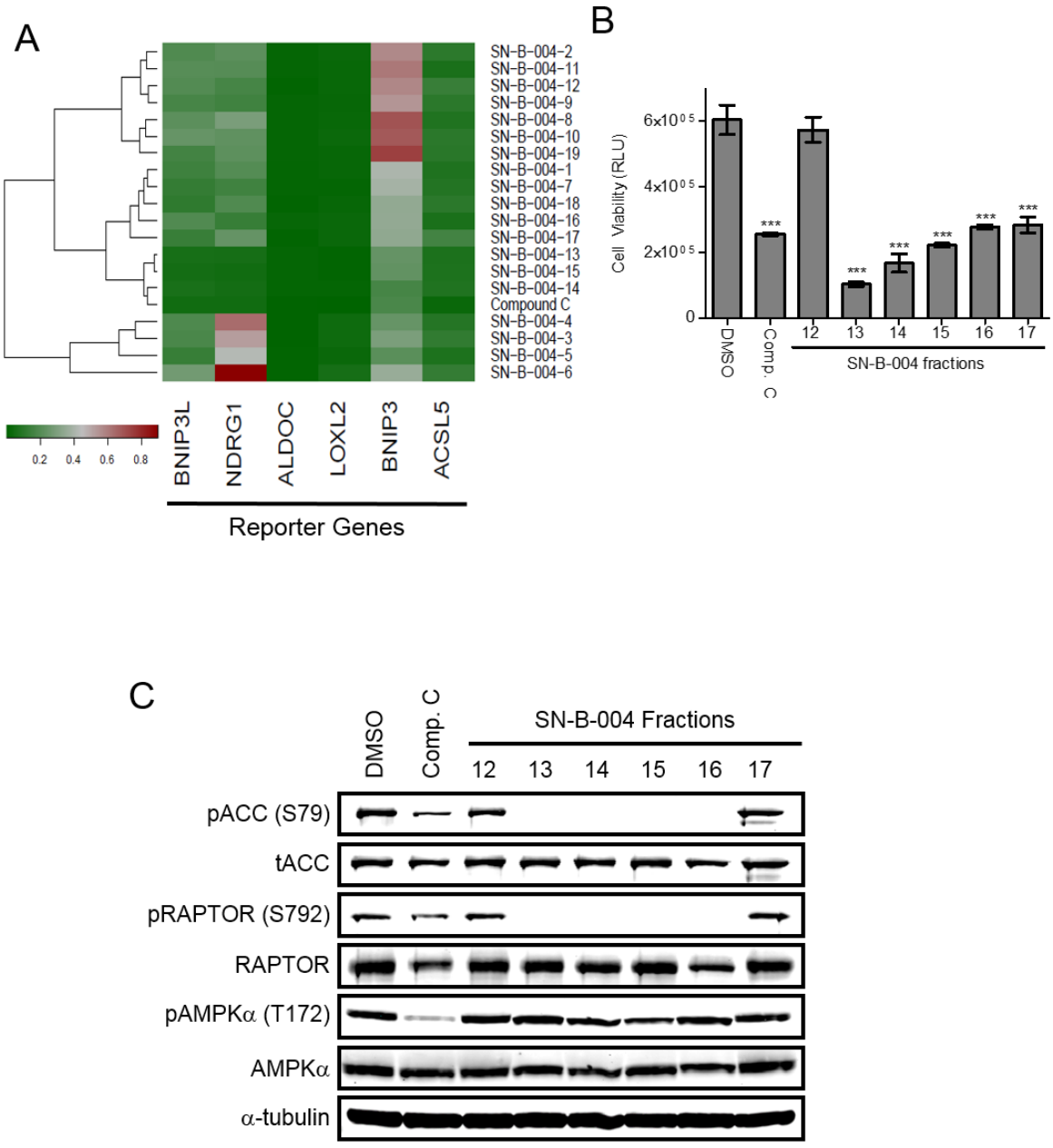

Fig. 6.6: FUSION identified natural product fractions that inhibit AMPK. (A) Unsupervised hierarchical clustering of fractions isolated from the *Streptomyces bacillaris* strain SN-B-004 with Compound C. (B) Cell viability assay in HCT116 cells treated for 24 hours with the indicated natural product fractions. Data are shown as mean relative light units (RLU) ± SD. ***p<0.001 (N=3). (C) Immunoblots of total and phosphorylated ACC (Ser79), RAPTOR (Ser792) and AMPK (Thr172) in HCT116 cells treated for 48 hours with the indicated natural product fractions. (Experiment 6.6A was completed in collaboration with Hyun Seok Kim and Michael White. Experiments 6.6B-C were completed by Kurt Fisher and Binita Das. Fig. 6.6 has been previously published in [1]).

metformin treatment) is sufficient to overcome inhibition of Compound C suggesting that it does not directly inhibit the kinase activity of AMPK, but instead may act by regulating the activation of AMPK itself, which is likely based on its detrimental effect on AMPK phosphorylation[333]. In contrast, direct inhibition of the kinase activity of AMPK would lead to decreased phosphorylation of downstream targets of AMPK without directly affecting AMPK phosphorylation, though it may paradoxically increase the phosphorylation of AMPK itself due to loss of negative feedback loops.

The active compound within the impure fraction SN-B-004-16 was isolated and the structure was determined using mass spectrometry and nuclear magnetic resonance spectroscopy to be 5´-hydroxy-staurosporine[349] (5-OH-S, Fig. 6.7A), a derivative of the well-known, non-specific kinase inhibitor staurosporine [350]. To date, 5-OH-S has only been described in one other report in the literature in which it was isolated from another marine bacterium *Micromonospora* sp. strain L-31-CLCO-002[349]. To determine if 5-OH-S directly inhibits AMPK kinase activity, we performed *in vitro* kinase assays of AMPK using SAMS peptide as a substrate, in the presence or absence of 5-OH-S. The IC_{50} of 5-OH-S for recombinant AMPKα1β1γ1 and AMPKα2β1γ1 was similar at 517.5 nM and 583.3 nM, respectively (Fig. 6.7B). The K_i for 5-OH-S inhibition of ATP binding to recombinant AMPK α1β1γ1 was 347 nM (Fig. 6.7C).

AMPK inhibition via 5-OH-S treatment is selectively toxic to colon cancer cells.

AMPKγ1 and AMPKα2 were selectively required for colon cancer cell survival, but not HCECs survival (Fig 6.1 and 6.4) [3], which led to the prediction that tumor cells would also be selectively sensitive to 5-OH-S as an inhibitor of AMPK. Treatment with 5-OH-S inhibited anchorage independent growth of HCT116 cells in a soft agar assay (Fig. 6.8A), and 5-OH-S was preferentially toxic to the colon cancer cells lines (HCT116 and SW480) as compared to the HCECs (Fig. 6.8B). The induction of cell death following 5-OH-S treatment was verified in HCT116 and SW480 cells by analyzing PARP cleavage (Fig. 6.8C), which demonstrated

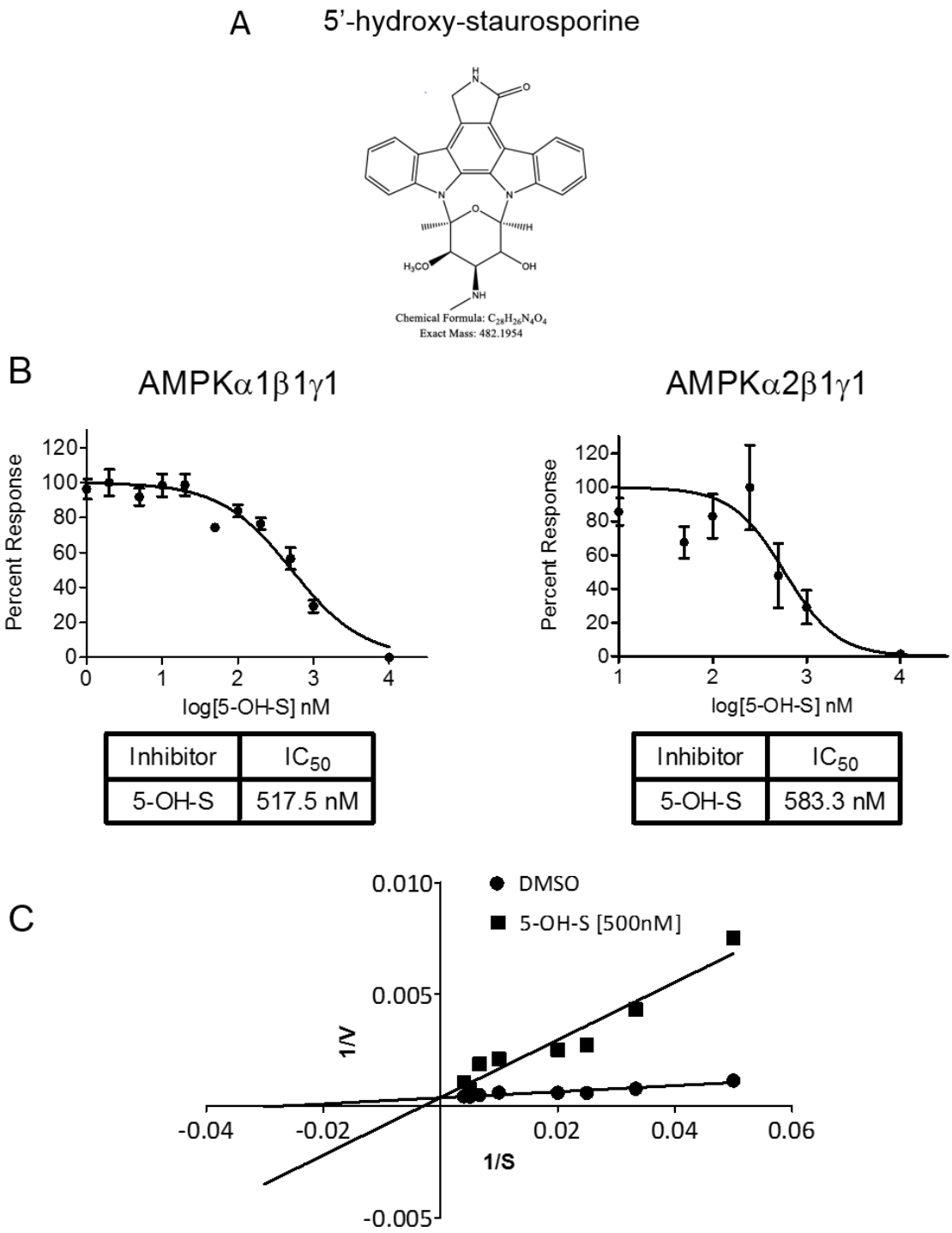

Fig. 6.7. The identified active molecule, 5-OH-S, inhibits AMPK kinase activity. (A) Structure of 5-OH-S. (B) Dose-dependent inhibition of recombinant AMPKα1β1γ1 and recombinant AMPKα2β1γ1 kinase activity by 5-OH-S. (C) Lineweaver-Burke plots of AMPK substrate phosphorylation in the presence of DMSO or 500 nM 5-OH-S. (Natural product identification in 6.7A was completed by our collaborator Youcai Hu and John MacMillan. Experiments 6.7B-C were completed by Binita Das and Dee Volle. Fig. 6.7 has been previously published in [1]).

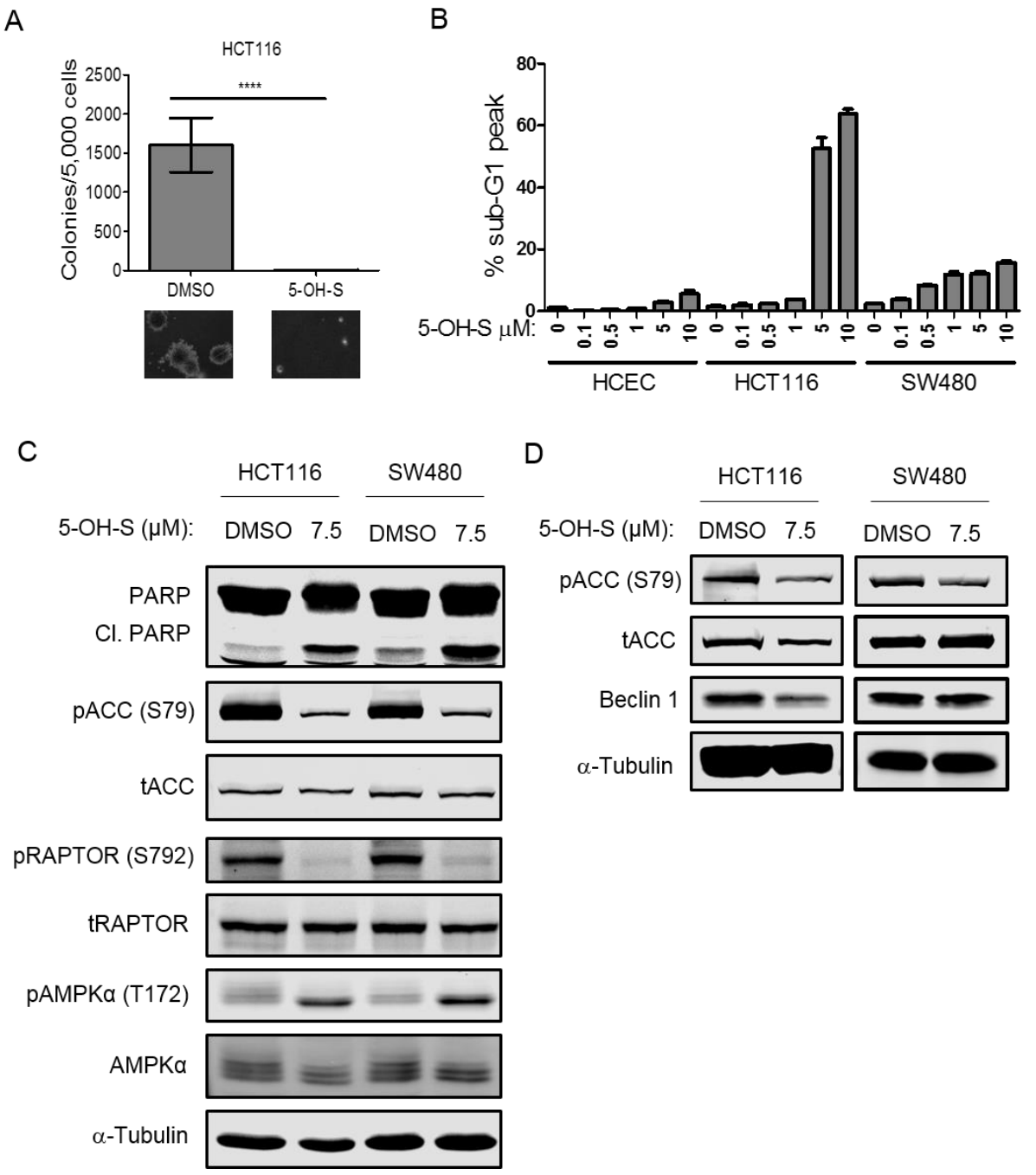

Fig. 6.8. 5-OH-S treatment preferentially inhibits colon cancer cell survival by reducing phosphorylation of known downstream AMPK targets. (A) Colony formation following treatment with 7.5 μM 5-OH-S. **** $p < 0.0001$ (B) Dose-dependent apoptosis in HCT116 and SW480 colon cancer cells and HCECs following treatment with 5-OH-S. (N=3). (C) Immunoblots of total and phosphorylated ACC (Ser79), RAPTOR (Ser792) and AMPK (Thr172) after 48-hour treatment with 7.5 μM 5-OH-S in HCT116 and SW480 cells. (D) Immunoblot of total and phosphorylated ACC (Ser79) and beclin 1 after 48-hour treatment with 7.5 μM 5-OH-S in HCT116 and SW480 cells. (Experiment 6.8A was completed by Binita Das. Experiment 6.8B was completed by Drew Gehring. Part of Fig. 6.8 has been previously published in [1]).

increased PARP cleavage with 5-OH-S treatment. Similar to the SN-B-004 fractions, 5-OH-S decreased the phosphorylation of ACC at Ser79 and of RAPTOR at Ser792, known AMPK downstream targets, without decreasing the phosphorylation of AMPK at Thr172 in colon cancer cell lines HCT116 and SW480 (Fig. 6.8C). Treatment with 5-OH-S decreased AMPK kinase activity in all cell lines tested as illustrated by reduced phosphorylation of ACC and RAPTOR (Fig. 6.8C); however, 5-OH-S treatment only decreased beclin-1 levels in HCT116s, but not SW480s. This correlated with the much higher level of cell death in HCT116 cells following 5-OH-S treatment. Similarly, 5-OH-S treatment inhibited AMPK activity in HCECs as evidenced by reduced phosphorylation of ACC and RAPTOR (unpublished data, Binita Das), but did not cause cell death in these cells (Fig. 6.8B). This suggests therapeutic targeting of AMPK could lead to efficacious cancer therapeutics as the cancer cells have either developed a generalized increased dependence on AMPK activity or depend on AMPK to perform functions that it does not normally perform in normal cells.

In Ras-driven cancer, disruption of ERK signaling increased AMPK dependence.

Tumor cells evolve in ways such that they develop vulnerabilities. Clinically, these are taken advantage of when inhibitors are developed that target characteristics only present in cancer cells such as mutations, aberrantly expressed genes, or uniquely required pathways. These are called targeted therapies. Unfortunately, however, cells often find ways to develop resistance and evade these therapies by further adapting and shedding these targetable characteristics. Ras mutations commonly activate the Ras/Raf/MEK/ERK signaling cascade, and a multitude of drugs targeting multiple levels of this pathway have been developed. Even though these inhibitors have demonstrated selective inhibition on the desired targets, most have shown limited efficacy. This suggests cells are able to evolve to avoid the detrimental effects of the inhibitor.

As described earlier, KSR1 is required for full ERK activation downstream of activated Ras. To evaluate the adaptations that cells undergo when ERK signaling is limited as a result of KSR1 depletion, gene expression changes were evaluated using an Affymetrix Human Genome

U133 Plus 2.0 Array in HCT116 cells with and without KSR1. In HCT116 cells that are stably depleted of KSR1, AMPKα2 expression is dramatically increased based on an online GEO2R analysis (default settings) of the GEO dataset GSE65351[3] (Fig 6.9A). In fact, probes for the a2 subunit of AMPK were the top two results of targets that demonstrated altered expression between the control (no transfection and shCont) and experimental conditions (shKSR1 #1 and #2). This relationship was further confirmed as transient knockdown of ERK in HCT116 and SW480 cells caused an increase in AMPK activation based on increased phosphorylation at T172 and increase in beclin 1 (HCT116 only) (Fig 6.9B). MEK depletion had less of an effect on AMPK phosphorylation and beclin 1 levels, which could be due to residual ERK activation being sufficient for the cells as phospho-ERK levels are maintained at a level similar to that seen in control cells (Fig 6.9B). These results suggested that combination ERK and AMPK inhibition could be synergistic and/or prevent the development of resistance to either agent alone.

Therefore, the effects of ERK inhibition alone and in combination with Compound C, a known, non-specific AMPK inhibitor, were evaluated using the linear isobol model [351] to investigate the possibility of synergy between ERK and AMPK inhibition. The linear isobol model is based on the idea that if a drug has additive effects with another drug, one could plot the dose required for one drug to reach the ED_{50} on the x axis and the other on the y axis. Drawing a line between these points would represent the combination doses that would also achieve the same ED_{50} effect. This is called an isobologram. This intuitively makes sense if one considers the possibility that treatment actually includes a combination of two agents that in reality contained the same active ingredient. Regardless of differing formulations or dilutions, a given percentage of the ED_{50} would still be expected to provide a given amount of effect. For example, if given half of the ED_{50} dose for each of the two drug formulations, one would have received a full ED_{50} dose and therefore a response equivalent to the ED_{50} would be expected. Plotting this point on the isobologram would place the point on the line between the ED_{50} points for each drug. Any other fractional combination would also be plotted on this same line provided the fractional doses fit

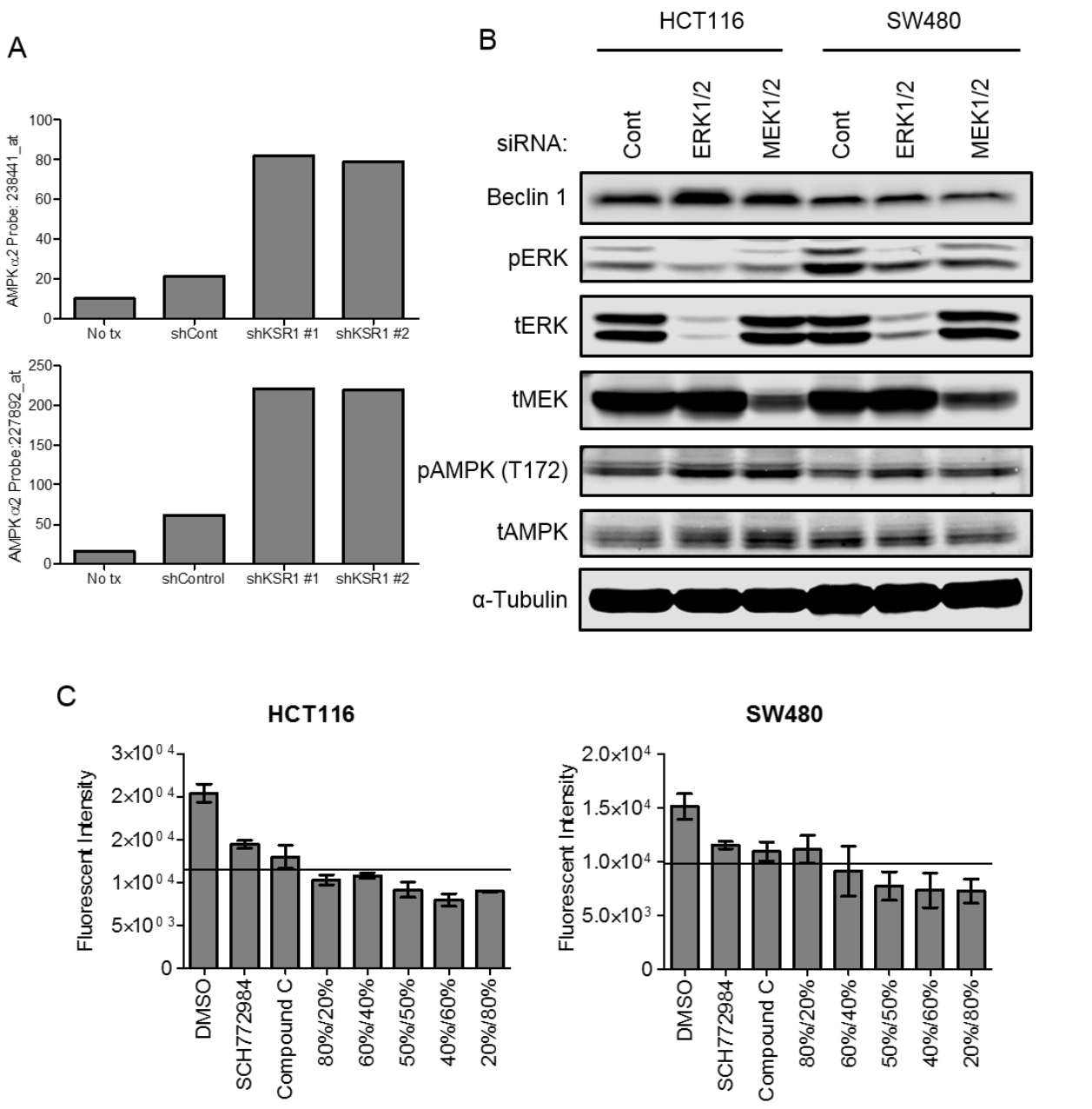

Fig. 6.9 Disruption of ERK signaling upregulated AMPKa2 activation, and ERK and AMPK inhibition were synergistic. (A) AMPKα2 expression from probes 227892_at and 238441_at on an Affymetrix Human Genome U133 Plus 2.0 Array in HCT116 cells stably-depleted of KSR1 using shRNA (N=1). (Data is available on Geo: GSE65351). (HCT116 shKSR1 cells were developed and gene expression was assessed by microarray by Kurt Fisher). (B) Immunoblot of ERK, total and phosho-AMPK, and beclin 1 following RNAi-mediated depletion of ERK for 72 hours. (C) Viability of HCT116 and SW480 cells following treatment with 1 μM of SCH772984, 20 μM of Compound C, or a combination of both SCH772984 and Compound C such that the doses fulfill the following criteria $Dose_{sch772984}$/1 μM SCH772984 + $Dose_{Compound\ C}$/20 μM Compound C = 1 to evaluate synergy between the two compounds. The horizontal line represents the lower edge of the predicted range of expected drug additivity (i.e. 500 nM SCH772984 and 10 μM Compound C (50%/50%), 400 nM SCH772984 and 12 μM Compound C (40%/60%), 200 nM SCH772984 and 16 μM Compound C (20%/80%), etc.) (N=3).

the following formula $Dose_A/ ED_{50\_A} + Dose_B/ ED_{50\_B} = 1$ (i.e., 0.25 of the ED_{50} of drug A given in combination with 0.75 of the ED_{50} of drug B). If any of these combinations demonstrate increased efficacy relative to both individual agents given at the ED_{50}, this suggests a super-additive effect or synergism in both HCT116 and SW480 colon cancer cells (Fig. 6.9C). Combination treatment with SCH772984 (ERK inhibitor) and Compound C (AMPK inhibitor) showed super-additive or synergistic results for various doses of combination drug treatments.

Conclusions

Our data show that AMPK promotes the survival of multiple human colon cancer cell lines and that variable levels of AMPK alpha subunits may contribute to or predict the cells' relative sensitivity to AMPK depletion. Interestingly, human colon epithelial cells (HCECs) do no share this dependence on AMPK. This could be exploited for the development of therapeutics targeting AMPK that will be selectively detrimental to cancer cells, but less so or not at all lethal to normal cells. However, cancer cells that have increased or altered AMPK subunit expression or have employed alternative mechanisms to circumvent AMPK-regulated pathways, may overcome or lose sensitivity to AMPK depletion or inhibition.

These data also suggest a role for AMPK isoforms with specific subunit composition and expression level in determining the contribution of AMPK toward tumor cell viability. This study provides additional evidence that cancer cells evolve diverse mechanisms to overcome obstacles limiting survival and proliferation. Cancer cells develop defined dependencies and vulnerabilities that offer a basis for their characterization and specific therapeutic intervention. This may reflect differing responses to environmental stresses that directed the tumor's evolution and suggests that at least a subset of colon tumors may be highly susceptible to AMPK inhibition. In this study, we showed that colon cancer cells have an increased, but variable, requirement for the AMPK $\alpha 2$ subunit isoform for their survival, more so than a requirement for the $\alpha 1$ subunit. This suggests that the individual subunits likely have unique, non-redundant functions that add another layer to

the complexity surrounding the role of AMPK in cancer. This phenomenon is not likely to be limited to colon cancer as several other groups have demonstrated a requirement for AMPK or its downstream effects in both prostate and breast cancer and have shown that inhibition of AMPK is detrimental to cancer cells [352-356].

In this study, we describe a novel, direct kinase AMPK inhibitor, 5´-hydroxy-staurosporine (5-OH-S) that has been isolated only from marine bacteria and has yet to be widely synthesized or made commercially available[349]. The effects of 5-OH-S appear to exceed those seen with individual AMPK subunit depletion. This is not surprising as 5-OH-S treatment inhibits AMPK isoforms containing either α subunit and likely all AMPK trimer complexes. However, a detailed kinase inhibitor profiling to assess the effects of 5-OH-S on other targets has not been completed. Therefore, the possibility exists that 5-OH-S may have off-target effects that contribute to its anticancer effects. A structurally similar compound, 7´-hydroxy-staurosporine (also known as UCN-01[357]), has also previously demonstrated significant anti-cancer effects. Like other staurosporine derivatives, 7´-hydroxy-staurosporine has broad intracellular effects and inhibits multiple kinases, notably Protein Kinase C[358,359]. Regardless, 7´-hydroxy-staurosporine (7-OH-S) has been examined in numerous phase I and phase II trials for multiple types of cancer including T-cell lymphomas, leukemia, breast cancer, small cell lung cancer, melanoma, pancreatic cancer, kidney cancer, ovarian/fallopian tube cancer, and many other solid tumors[360-372]; however, its use has been constrained due to limited single agent efficacy, in conjunction with a less than optimal pharmacokinetic profile, and undesirable side effects. However, comparing 7-OH-S directly to 5-OH-S demonstrated less toxicity in HCECs and increased lethality in HCT116 cells (unpublished data, Das and Lewis) suggesting that further evaluation of 5-OH-S is likely to reveal its superiority to 7-OH-S. Our data suggest that staurosporine derivatives can act as lead compounds for the development of more specific AMPK kinase domain inhibitors with the goal of improved target specificity, anti-cancer efficacy, and reduced treatment complications.

The current study expands upon previous work that used FUSION to identify microRNAs

and individual genes as potential therapeutic targets in cancer[3,101,346]. This study demonstrates the ability of FUSION to identify novel small molecules from an unbiased screen of crude natural product fractions that inhibit a specific target important for cancer cell survival. In this instance, FUSION identified 5-OH-S as an inhibitor of AMPK, which can serve as a lead compound that can be used to understand AMPK activity and could be further developed using medicinal chemistry for use as a cancer therapeutic.

These results also demonstrate a connection between KSR1 and AMPK signaling based on the increased dependence on AMPK following disruption of KSR1 or ERK. These data provide rationale for further studies examining the interconnectedness of these two pathways and highlight the potential for synergism or the ability to prevent the development of resistance with this combination of targeted therapies. This potential is unfortunately hampered by the lack of a specific, high affinity AMPK inhibitor, which further highlights the value of the development of FUSION as a novel method that can distinguish genes and compounds with particular cellular functions or phenotypes in an unbiased manner. This proof-of-concept study suggests that applying FUSION to a larger, more diverse library of small molecules and/or crude natural product fractions could identify numerous lead compounds that are more specific inhibitors of AMPK or other promising therapeutic targets, leading to the discovery of new, efficacious targeted therapies.

Chapter 7: Discussion/Conclusions

FUSION

These results demonstrate the value of FUSION as an unbiased function-based screen that can be applied to identify functionally-related genes and reveal inhibitors of target genes. This study expands upon previous work by Stegmaier *et al.* that applied a gene expression-based signature to identify compounds that induced differentiation in leukemia [103]. This original study revealed the potential to use a gene expression-based signature as a proxy for a phenotype of interest by evaluating approximately 1700 compounds using PCR and mass spectrometry to evaluate the expression of five genes that composed the differentiation signature. FUSION further developed this concept by applying the Affymetrix Quantigene 2.0 Assay to measure gene expression. This allowed for the gene expression of multiple genes to be measured simultaneously using a Luminex machine so the screen could be expanded tenfold to evaluate more than 17,000 perturbations (individual gene depletions and treatments with microRNA, natural product fractions, and drugs). This method has successfully identified several promising genetic targets including three genes (TIMELESSS, WDR5, and AMPKγ1) and one natural product (5-OH-S) that are the subject of several manuscripts and this dissertation [3,42,101].

However, the current application of FUSION is limited by several confounding features in its implementation that could be eliminated in the future to realize the full potential of this approach. First, all of the screens were performed in a single Ras-mutated colon cancer cell line, HCT116. HCT116 colon cancer cells have wildtype p53, an unstable genome, and a high level of sensitivity to commonly used cancer therapies. This creates the potential of identifying targets in the genome-scale RNAi screen that are preferentially toxic to HCT116 cells, but potentially less so to other cancer cells. Based on the results contained herein, this appears to be the case as HCT116 cells were generally more sensitive to the identified gene depletions (TIMELESS, WDR5, and AMPK/5-OH-S) than other cell lines. Importantly, the FUSION screen was successful in identifying targets that were preferentially required in cancer as the cancer cell lines were more sensitive to the gene depletions than immortalized, but non-transformed human colon

epithelial cells. Expanding the FUSION screen to test multiple cell lines, preferably from additional cancer types or with different tumor characteristics, is likely to reveal common targets that are ubiquitously required for cancer cell survival, but dispensable for normal cell survival. At the very least, as new genetic targets or therapeutics are identified that are predicted to be selectively required for cancer cell survival, it is extremely important to evaluate their effect in a panel of cancer cells early in biological validation in order to focus research efforts on studying targets that are not specific to HCT116 cells.

Based on the issues with off-target effects identified with the individual siRNA oligos targeting WDR5 (Fig. 5.6), an additional follow-up screen evaluating the consistency of the gene depletion effects using individual oligos could have further helped to prioritize the hits and eliminated targets that were likely only hits due to off-target effects. This is a common practice where four individual oligos targeting the genes identified as being hits in the initial screen are individually tested to evaluate the consistency of the gene depletion effect. However, this follow-up screen can substantially increase the cost of a screen, even if a more cost-effective assay is used in the follow-up screen. Additionally, it is not uncommon for individual oligos to fail to decrease target expression despite having sequences that match the target gene such that the expected phenotype may not be seen and true positives may inadvertently be excluded from further evaluation.

While two algorithms were applied to identify the potential of off-target seed sequence effects, both of these algorithms are based on seed sequences starting with the first nucleotide in the siRNA oligo. The experimentally identified likely off-target effects in the WDR5 oligo #6 are the result of the oligo almost completely matching another gene, ME1; however, the matching sequence actually starts with the second nucleotide in the siRNA sequence providing rationale for why both of the seed sequence off-target effect algorithms failed to recognize this potential off-target effect.

Finally, when undertaking an experiment of this scale that will require substantial

computational analysis to evaluate the results, ideally the individuals that will be performing the analysis should be included in the experimental planning from the beginning. This allows them to understand the experiment prior to planning their computational approach and provides the opportunity for them to contribute to the experimental design to simplify the subsequent computational analysis. In this screen, the non-random plating of control wells and grouping of functionally related genes on the same plate limited the options for robust normalization. This precludes the use of plate-position normalization, and therefore any effects that were caused by plate positioning, if present, could not be taken into account. While completely random plating is likely impossible, and increasing the randomness of plating would increase the biological experiment complexity, the benefits for subsequent computational analysis may have outweighed the increased experimental requirements. Therefore, the effort required to complete the biological experiment and computational evaluation needs to be balanced and discussed to ensure the most appropriate biological and computational approaches are applied to generate the most robust and easily interpretable results.

Finally, FUSION was initially designed based upon a gene expression signature of KSR1 depletion making it particularly suited to identify targets that are KSR1-like. However, a modified FUSION screen has the potential to reveal genes that are functionally similar to any specified gene of interest. Ultimately, the success of such a screen would be dependent upon the quality of the set of genes used for the gene expression-based signature. Therefore, designing a modified FUSION screen that could be used to evaluate the functional similarity between any two genes would require the establishment of an expanded or revised panel of genes to be used in the gene expression-base signature. Ideally, these genes would be independent and not covary, and reveal effects of different downstream pathways. This would include avoiding the inclusion of multiple genes with the same or highly similar functions as these would have a high likelihood of covarying and would be less likely to provide additional resolving power in the screen. One method to identify potential genes would be to individually deplete cells of known key regulators,

particularly targets that are implicated in cancer (e.g. Ras, MYC, p53, PI3K, AMPK, ATM/ATR, β-catenin, PKCs, hexokinase, BCL-2, TGFβ, NFκB, etc.) and evaluate gene expression using microarrays or RNASeq to identify genes whose expression either increases or decreases following each perturbation. Identifying changes that are specific to a limited number of perturbations and that demonstrate independence would provide a good starting point for a gene panel. Genes that would provide additional refinement could be identified by treating with drugs known to activate various pathways as an additional mechanism to increase the delineating power of the FUSION screen. In the current application of FUSION, all of the genes from the gene expression-based signature were decreased following KSR1 depletion. Therefore, selecting genes that decrease as well as genes that increase in expression following a given perturbation may increase the resolving power of the screen.

After the identification of a gene set for the gene expression-based signatures, several additional factors would need to be considered in order for an experiment on this scale to be fruitful. Multiple cell lines would need to be selected for the screen in order for the results to be generalizable. Additionally, performing a screen on this scale would be technically difficult. An alternative would be to simulate this analysis bioinformatically.

Instead of experimentally screening multiple cells lines for similarities in gene expression for a panel of genes, one could analyze publicly available microarray or RNASeq data to simulate a similar analysis. In this situation, the gene expression of thousands of genes could be evaluated for a given genetic or drug-induced perturbation of interest to identify a subset of genes whose expression changed in response to the given manipulation. This could then be used to screen for other genetic manipulations or drug treatments that had a similar effect. This computational analysis would be limited by the availability of applicable data (i.e. the cell lines or models used may not match, the timing may be different for each dataset, the specific assay performed or microarray used is likely to be different, and the experiments would have been performed by different groups), but this method would benefit from being able to compare a huge number of

gene expression changes. Computational screening would also be substantially cheaper than biological screening, but would require substantial expertise in bioinformatic analysis, which is currently a substantial limiting factor in re-use of data in medical research.

TIMELESS

This work expands upon the preliminary studies that have indicated TIMELESS is overexpressed in cancer and correlates with poorer patient outcomes and reveals a common mechanism by which loss of TIMELESS induces G2/M arrest and slows cancer cell proliferation. This work demonstrates that TIMELESS is overexpressed in multiple types of cancer and is likely required for increased DNA synthesis and cell proliferation. TIMELESS is overexpressed at the mRNA and protein level in cancer. In colon cancer, TIMELESS mRNA overexpression is not due to changes in promoter methylation. Transcriptionally, TIMELESS is thought to be regulated via transcription factor binding to E-box elements in its promoter in conjunction with chromatin modifications including acetylation of K3-K9 and trimethylation of H3K4 (H3K4Me3) [122,123,373]. H3K4Me3 is added by the histone methyltransferase KMT2A/MLL1, which permits circadian oscillation [374]. This suggests the possibility that WDR5 overexpression in cancer could facilitate, if not promote, circadian dysregulation in cancer.

Independent of a mechanism that upregulates TIMELESS mRNA, oncogenic Ras increases ERK activation, which subsequently increases TIMELESS expression. However, ERK inhibition did not globally reduce TIMELESS expression in colon cancer cells. In cells that were resistant to ERK inhibition-induced changes in TIMELESS expression, mTOR inhibition decreased TIMELESS expression. ERK and mTOR are known to regulate translation, which is likely the mechanism by which they regulate TIMELESS expression in colon cancer.

Likely as a result of oncogenic signaling aberrantly driving its expression, TIMELESS expression is constitutively high, is no longer circadianly regulated, and is not decreased with increasing cell confluency. In contrast, in immortalized, yet non-transformed human colon

epithelial cells (HCECs), TIMELESS expression follows a circadian pattern after circadian synchronization and is inversely related to cell confluency. TIMELESS expression is known to vary based on cell cycle phase and is highest in the S and G2 phases of the cell cycle. Therefore, the changes in TIMELESS expression in HCECs relative to their confluency could be the result of an accumulation of cells in the G0/G1 phase. Interestingly, this change in expression mirrored changes in ERK phosphorylation. Considering this in conjunction with data demonstrating that ERK inhibition decreased TIMELESS levels even in HCECs suggests that ERK activation downstream of Ras promotes TIMELESS expression even in normal cells. Importantly, Ras/ERK and AKT/mTOR signaling has been shown to affect circadian rhythms [375,376]. Circadian oscillations of ERK phosphorylation have been seen, and AKT/TOR regulates Sgg/GSK3 to affect the nuclear accumulation of TIMELESS [376].

In colon cancer, TIMELESS depletion did not affect ERK phosphorylation as was previously predicted [205] or reduce MYC expression in colon cancer as was previously shown in breast cancer [207]. Instead, TIMELESS depletion decreased cell proliferation and induced G2/M arrest in HCT116, SW480, SW620, and RKO colon cancer cells as a result of increased γH2AX and downstream CHK1 and CDK1 phosphorylation. This mechanism is preserved in HCECs, but is seen to a lesser extent than in the colon cancer cells.

ERK inhibition induces an increase in γH2AX that cannot be rescued by exogenous TIMELESS expression, yet fails to induce CHK1 and CDK1 phosphorylation. ERK inhibition may also indirectly inhibit CHK1 phosphorylation as previous studies have shown that CHK1 nuclear localization is dependent upon p90RSK phosphorylation of CHK1 at S280. This phosphorylation by p90RSK and subsequent nuclear localization is a prerequisite for DNA-damage induced ATR-mediated phosphorylation of CHK1 at S345 [222].

The increased and aberrant expression of TIMELESS represents a unique vulnerability downstream of oncogenic Ras signaling and reveals a novel mechanism cancer cells employ to circumvent normal proliferative constraints. This suggests circadian dysregulation may be

essential within cancer cells for increased cell cycle advancement and implies that the development of therapeutics targeting this pathway may be efficacious in the treatment of cancer.

This work is limited by the lack of an *in vivo* model to substantiate that TIMELESS is playing a vital role for the proliferation of cancer cells, and future work should be applied to evaluate the *in vivo* utility of targeting TIMELESS. This is particularly important as cells lose their organism-wide circadian entrainment *in vitro*. Even though intracellular circadian cycles are intact in this context, the potential exists that TIMELESS functions differently or is subject to additional regulation *in vivo* in the presence of constant organism-wide circadian entrainment. Additionally, TIMELESS has also been shown to be required for transcriptional upregulation of steroid hormone-producing enzymes [377] and regulates bacteria phagocytosis in *Drosophila* as *Drosophila* lacking TIMELESS are more sensitive to infection by *S. pneumoniae* [378]. Phagocytosis is circadianly regulated with a higher level of phagocytosis at night. Loss of PER, another circadian gene, has a similar phenotype, and normal *Drosophila* demonstrate oscillating resistance to *S. pneumoniae* that is absent in TIMELESS mutants. Therefore, the effect of TIMELESS depletion on phagocytosis is likely a result of defective circadian cycle, which opens the possibility that circadian disruption in cancer may also affect immune system function. Based on these observations regarding other cellular functions of TIMELESS, additional mechanisms might exist *in vivo* that either contribute to its requirement for cancer cell survival and proliferation or preclude its use as a therapeutic target due to currently unforeseen side effects of inhibiting TIMELESS.

Clearly, TIMELESS represents a novel vulnerability that is present in cancer cells, but not normal cells, that can be used to selectively target cancer cells and may be particularly effective if paired with a circadian dosing regimen; however, future work is needed to evaluate TIMELESS *in vivo.*

WDR5

KMT2/MLL proteins are commonly mutated in colon cancer, but their role in tumor development and maintenance is still being debated. In contrast, WDR5 is rarely mutated in colon tumors, and preliminary studies have shown it is pro-tumorigenic. Several colon cancer cell lines including HCT116, RKO, and LoVo cells have WDR5 mutations, but their functional impact is unknown. WDR5 is also ubiquitously overexpressed in colon cancer cells. This overexpression could be the result of oncogenic signaling, but this has yet to be shown. WDR5 depletion or inhibition is selectively, but variably, toxic in colon cancer cells, more so than in HCECs. WDR5 depletion induces γH2AX in HCT116, SW620, and RKO cells and decreases H3K4Me3 in HCT116, HCT15, SW620, and RKO cells. WDR5 inhibition with OICR-9429 treatment only induced γH2AX in the two cell lines with wildtype WDR5, HCT15 and SW620, and decreased H3K4Me3 in HCT116. Combination of WDR5 with ionizing radiation further increased the level of γH2AX. Future work is required to evaluate the role of WDR5 within *in vivo* tumors.

Interestingly, both TIMELESS and WDR5 depletion induced γH2AX. Two additional hits from FUSION were MAP2K7 and MAP4K4, two kinases that phosphorylate JNK1. One study demonstrated that JNK1 may also contribute to increased H2AX phosphorylation (γH2AX) and DNA damage repair [379]. The fact that this common mechanism is shared between multiple hits from FUSION suggests that DNA damage repair may be a pathway that is highly required in cancer. While this may be true, the genes within the KSR1-depletion gene expression-based signature may also have been primed or more likely to identify targets that share this specific mechanism of action and/or this pathway could be preferentially necessary in HCT116 cells.

Further work to evaluate if KSR1 depletion also induces an increase in γH2AX may reveal additional mechanisms by which KSR1 promotes Ras-driven tumor formation and maintenance. KSR1 is known to be required for cell cycle restart following DNA damage repair, but further elucidating the downstream effects of KSR1 depletion on CHK1 and CDK1 phosphorylation and the mechanism behind the cell cycle arrest could reveal additional functional similarities between KSR1 and other hits identified by FUSION.

AMPK/5-OH-S

The gamma 1 subunit of AMPK is selectively required for HCT116 colon cancer cell survival, but not HCEC cell survival. In HCT116 cells, AMPKγ1 depletion causes a decrease in AMPKα2 expression, which likely mediates this effect as AMPKα2, but not AMPKα1 is required for HCT116 and SW480 colon cancer cell survival. AMPKα1, AMPKα2, or combination AMPKα1/α2 depletion does not cause apoptosis in HCECs.

AMPKα2 depletion decreases P-ULK1 and beclin 1 expression suggesting AMPKα2 depletion decreases autophagy. AMPKα2, but not AMPKα1 depletion reduced PGC1β and ERRα expression. FUSION discovered a natural product fraction that inhibited AMPK. The active compound was identified as 5-OH-S and was shown to directly inhibit AMPK kinase activity. 5-OH-S was preferentially required for HCT116 and SW480 cell survival, but was largely dispensable for HCEC survival. A related 7'-hydroxy-staurosporine, aka UCN-01, has been examined intensively for its anticancer properties and has been the subject of several clinical trials. UCN-01 is known to inhibit several kinases including AKT, PKC, several CDKs, CHK1, and AMPK. UCN-01 induces G1/S arrest and prevents DNA damage repair, which is thought to be the result of CHK1 inhibition. This suggests that in addition to inhibiting AMPK, 5-OH-S may also disrupt DNA damage repair and/or induce cell cycle arrest in addition to inducing apoptosis.

Disruption of ERK signaling, through KSR1, ERK1/2, or MEK1/2 depletion, caused an increase in AMPK expression and/or activation suggesting cells may have an increased dependence on AMPK following disruption of Ras signaling. Combination treatment with SCH772984 and Compound C demonstrated synergy.

Synergistic Interactions

Previous reports indicated that combination inhibition with Torin-2, an ATP-competitive inhibitor of mTOR, ATM, and ATR, and AZD6244, a MEK inhibitor, yielded significant growth inhibition [380]. Another group demonstrated that treatment with UCN-01 (7'-

hydroxystaurosporine) induces MEK1/2 and ERK1/2 in malignant hematopoietic cells, while combination UCN-01 and MEK1/2 or Ras inhibition prevented the ERK activation and induced apoptosis [381-384]. These reports demonstrate the potential benefit of treating cells with multiple targeted therapies to prevent the development of resistance. UCN-01 is structurally similar to the FUSION-identified AMPK inhibitor, 5-OH-S. Therefore, considering the previous reports that UCN-01 prevented the development of resistance to MEK or Ras inhibition in conjunction with results herein that KSR1 or ERK depletion induced AMPKα2 expression and phosphorylation, the interplay between these two pathways is clearly demonstrated. Further, ERK and AMPK inhibition demonstrated additive to synergistic effects on colon cancer cell viability revealing the benefit of simultaneously targeting these pathways.

Combination treatment with TIMELESS depletion and DNA damaging agents or ionizing radiation showed little if any increase in efficacy. The effect was most promising with the combination of TIMELESS depletion with ionizing radiation. HCT116 cells may not be the best cell line to test the potential for synergistic effects either as they have an intrinsically unstable genome. Therefore, if TIMELESS is required for DNA damage repair, HCT116 cells would be likely to be more dependent upon TIMELESS expression than other more genomically stable cell lines, and the addition of a DNA-damaging agent to these cells may not increase their dependence on TIMELESS further.

However, combination treatment with TIMELESS depletion in conjunction with Wee1 or CHK1 inhibition had at least additive, if not synergistic, effects on efficacy suggesting this combination may be a viable approach for the treatment of colon cancer.

Final Thoughts

These results have revealed the importance of genes that sit in between multiple regulatory pathways and coordinate communication or signal between these pathways to regulate their execution. Clearly, TIMELESS sits at the cross-roads and regulates the balance and

coordinated execution of the DNA synthesis, DNA damage repair, circadian rhythm and cell cycle pathways. This regulation forces these pathways to be inextricably linked such that cells undergo coordinated regulation to ensure balance is maintained. Unfortunately, in cancer, oncogenes disrupt the balance by forcing cells to pursue unregulated proliferation. In order to maintain some semblance of order and prevent cell suicide, oncogenes simultaneously alter the regulation of a subset of genes that are required to allow the cancer cells to survive and thrive despite all of the external and internal signals to the contrary. Revealing the key players that are required for cancer cells to survive and maintain their transformed phenotype will lay the groundwork for the development of selective, efficacious therapeutics to treat cancer.

Our results demonstrate the ability of FUSION to identify oncogene-induced changes in cancer that promote proliferation and cell survival, but also leave the cancer cell vulnerable to selective targeting that disrupts these co-opted pathways. The potential exists for all of the identified genes, TIMELESS, WDR5, and AMPK, to be required in other types of cancer as their identified mechanisms of action are likely to be present in other tissues and favorable for cancer regardless of the tissue of origin. Further characterizing these vulnerabilities and demonstrating their presence *in vivo* will determine their potential to serve as selective therapeutic targets for the development of targeted therapies for the treatment of cancer.

Appendix A: Biological validation of other FUSION hits: ECE2, HAS2, DYRK1A, and BMP4

Rationale:

FUSION identified 788 genes that are predicted to be required for colon cancer cell survival, but not normal cell survival. Preliminary biological validation was performed for several of these targets including ECE2, HAS2, DYRK1A, and BMP4.

Results/Discussion:

RNAi-mediated ECE2 depletion decreased cell viability in HCT116 colon cancer cells, but not in HCECs (Fig. A.1A). Cell count was also decreased in HCT116 cells following ECE2 depletion (Fig. A.1B). ECE2 mRNA expression, but not ECE1 mRNA expression, is increased in colon cancer based on RNASeq evaluation of data from the COAD dataset within TCGA (Fig. A.1C). RNAi-mediated HAS2 depletion decreased cell viability similar to KSR1 depletion in anchorage-independent conditions when replated on polyHEMA-coated plates (Fig. A.2A). RNAi-mediated HAS2 depletion decreased cell viability in HCT116 cells, but not HCT15 colon cancer cells in normal culture conditions (Fig. A.2B). Unfortunately, due to a lack of quality reagents (particularly a lack of antibodies that could be validated) for ECE2 and HAS2 these targets were not pursued further.

RNAi-mediated depletion of DYRK1A decreased cell counts in HCT116 colon cancer cells (Fig. A.3A). However, DYRK1A is known to serve as a scaffold for Ras/Raf/MEK kinase cascade. Therefore, DYRK1A was not pursued further.

RNAi-mediated depletion of BMP4 decreased cell viability in HCT116, but not in HCT15 colon cancer cells (Fig. A.4A). The mRNA expression of BMP4, BMP2, BMP7, GREM2, and BMP3 in human tumors was evaluated in the COAD TCGA dataset. BMP4 and

BMP7 were increased in colon tumors compared to normal tissue, whereas BMP2, GREM2, and BMP3 were decreased in colon tumors (Fig. A.4B). BMP4 and BMP7 mRNA expression was increased in a panel of colon cancer cells as compared to human colon epithelial cells (Fig. A.4C and D).

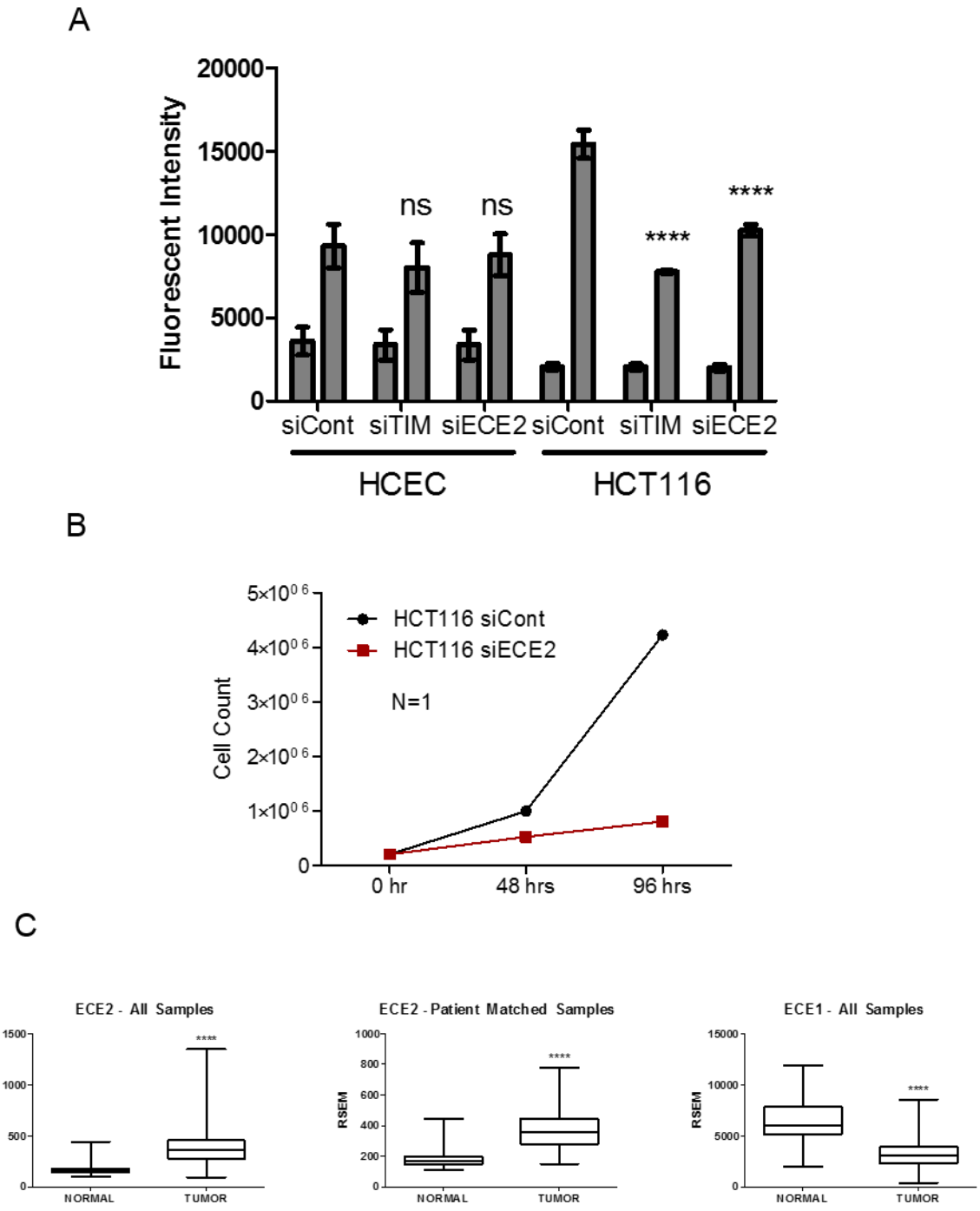

Fig. A.1: Biological validation of ECE2. (A) Viability of HCECs and HCT116 colon cancer cells measured using alamarBlue following RNAi-mediated depletion of KSR1, TIMELESS, or ECE2 for 72 hours. (B) Cell counts in HCT116 cells following RNAi-mediated ECE2 depletion. (C) ECE2 and ECE1 gene expression (RNA-Seq) data from the Colon Adenocarcinoma (COAD) dataset within TCGA for unpaired and paired primary colon tumors and normal solid tissue samples. The results published here are in whole or part based upon data generated by the TCGA Research Network: http://cancergenome.nih.gov/. (Fig. A.1B was completed in collaboration with Eyerusalem Lemma).

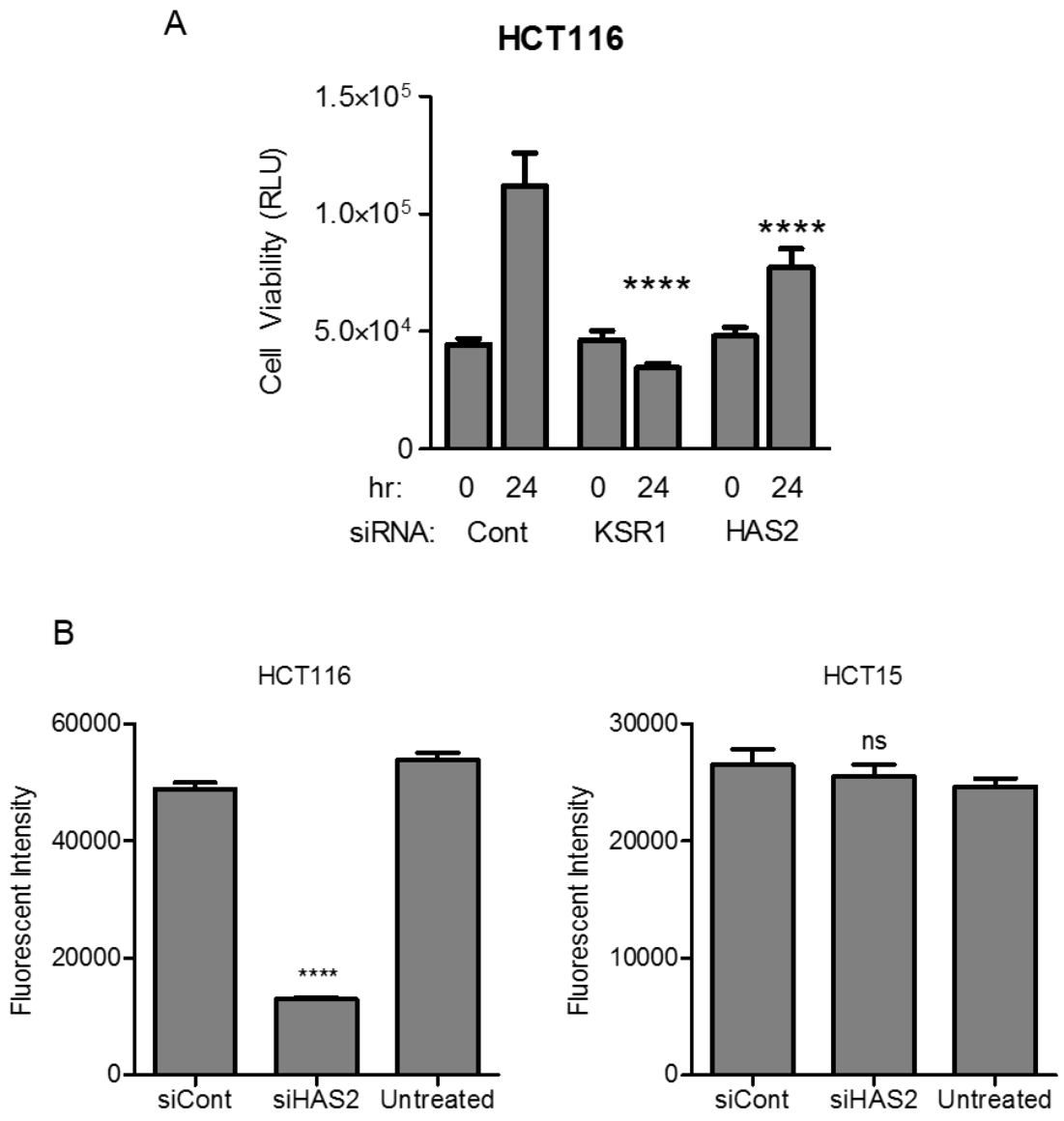

Fig. A.2: Biological validation of HAS2. (A) Viability of HCT116 colon cancer cells measured using CellTiter-Glo® following RNAi-mediated depletion of KSR1 or HAS2 that were replated on polyHEMA-coated plates 48 hours following transfection to simulate anchorage-independent conditions. Cell viability is measured immediately after replating (Hrs: 0) and 24 hours later. (B) Viability of HCT116 and HCT15 colon cancer cells measured using alamarBlue following RNAi-mediated depletion of HAS2 for 72 hours. (Experiments A.2 were done in collaboration with Danielle Frodyma).

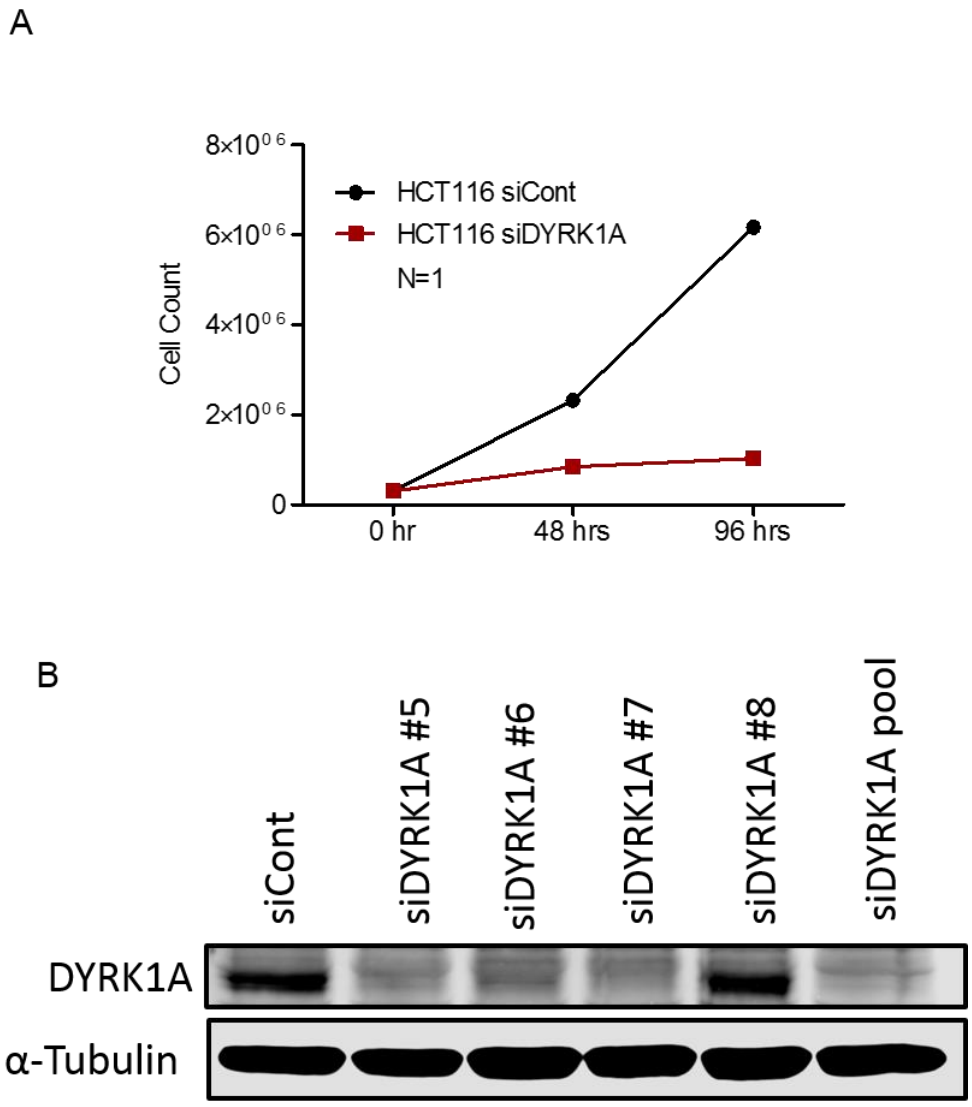

Fig. A.3: Biological validation of DYRK1A. (A) Cell counts in HCT116 cells following RNAi-mediated ECE2 depletion. (B) Western blot of DYRK1A after RNAi-mediated depletion of DYRK1A with individual siRNA oligos.

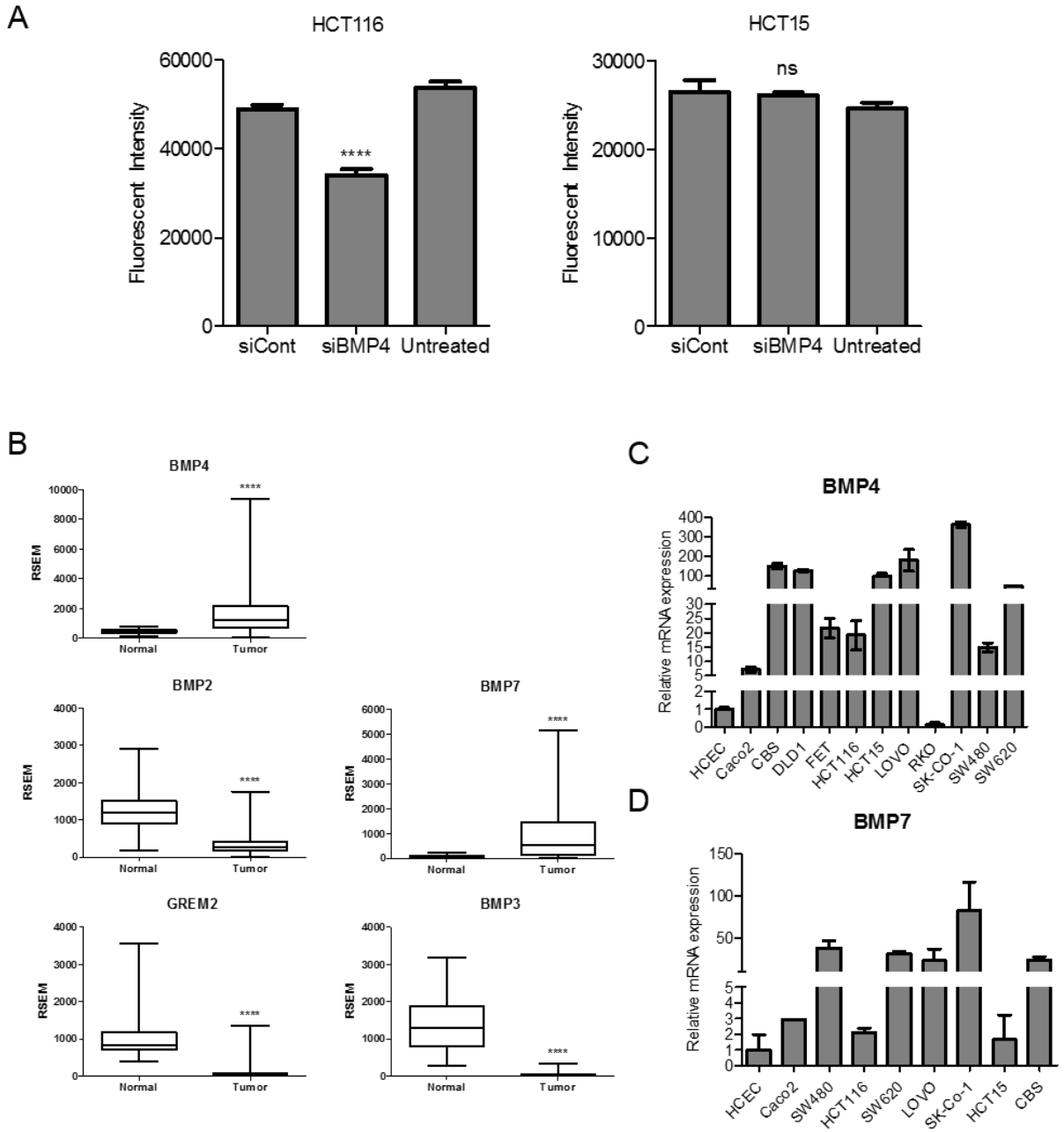

Fig. A.4: Biological Validation of BMP4. (A) Viability of HCT116 and HCT15 colon cancer cells measured using alamarBlue following RNAi-mediated depletion of BMP4 for 72 hours. (B) BMP4, BMP2, BMP7, GREM2, and BMP3 gene expression (RNA-Seq) data from the Colon Adenocarcinoma (COAD) dataset within TCGA for unpaired primary colon tumors and normal solid tissue samples. The results published here are in whole or part based upon data generated by the TCGA Research Network: http://cancergenome.nih.gov/. (C and D) RT-qPCR of BMP4 (C) and BMP7 (D) in a panel of colon tumor cell lines as compared to immortalized, non-transformed HCECs. RT-qPCR data is shown as mean ± SD. ** $p < 0.01$ *** $p < 0.001$ **** $p < 0.0001$ (Experiments A.4C-D were done in collaboration with Danielle Frodyma).

Appendix B: Other mechanisms regulating TIMELESS expression

Rationale:

TIMELESS expression appears to be regulated through several mechanisms. The most prominent mechanism regulating TIMELESS expression in colon cancer discovered thus far appears to be via translation regulation by ERK or mTOR as described in Chapter 4: TIMELESS; however, even these mechanisms cannot completely explain the increased level of TIMELESS expression. Evaluating the effect of genetic depletions on TIMELESS expression is complicated because TIMELESS expression varies with cell cycle with the highest expression being seen in S and G2 phases. Therefore, any manipulation that affects the percentage of cells in each phase of the cell cycle could indirectly affect TIMELESS expression.

Results/Discussion:

RNAi-mediated depletion of MYC in HCEC and HCT116 cells decreased TIMELESS expression (Fig. B.1A). RNAi-mediated depletion of WDR5 with individual siRNA oligos in HCT116 also decreased TIMELESS expression, but oligos #5 and #6 had a much more dramatic effect (Fig. B.1B).

RNAi-mediated depletion of BMP4 decreased TIMELESS expression at the protein (Fig. B.2A). RNAi-mediated depletion of BMP4, but not BMP7, decreased TIMELESS expression at the mRNA level (Fig. B.2B and C). RNAi-mediated depletion of CRY1 decreased TIMELESS expression at the mRNA level (Fig. B.2D).

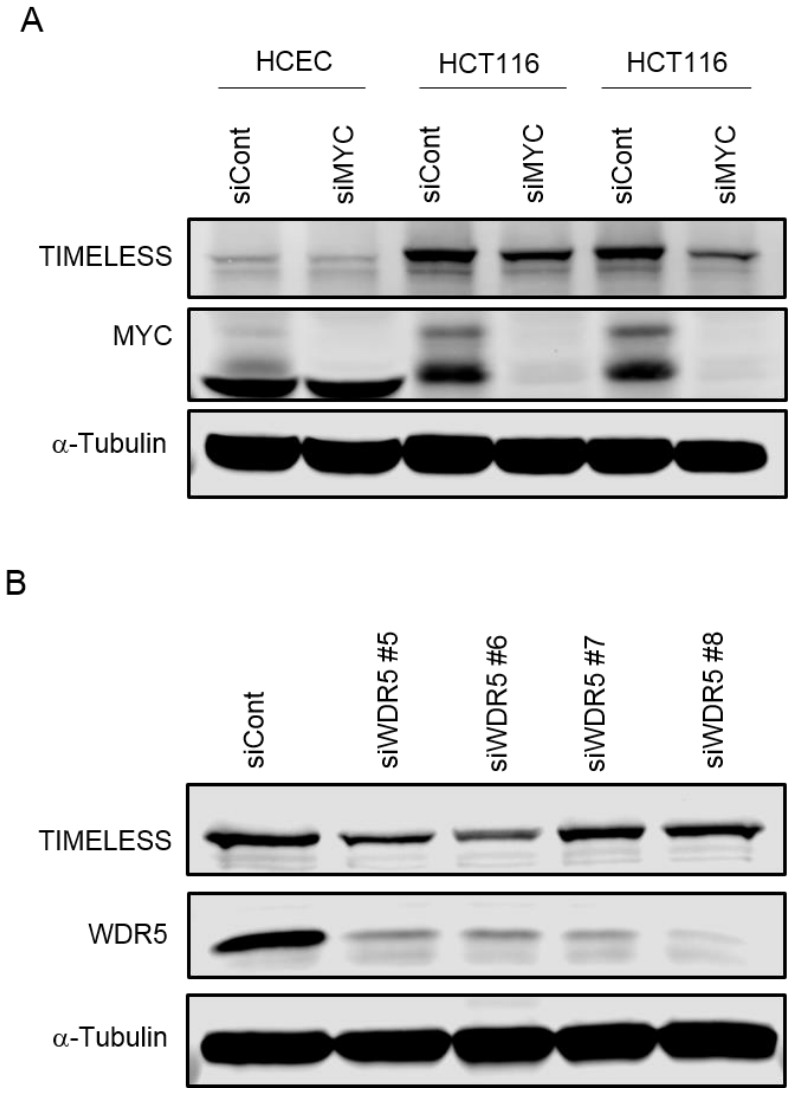

Fig. B.1: MYC and WDR5 may promote TIMELESS expression. (A) Western blot of TIMELESS and MYC following RNAi-mediated MYC depletion for 72 hours in HCEC and HCT116 cells. (B) Western blot of TIMELESS and WDR5 following RNAi-mediated WDR5 depletion with individual siRNA oligos for 72 hours.

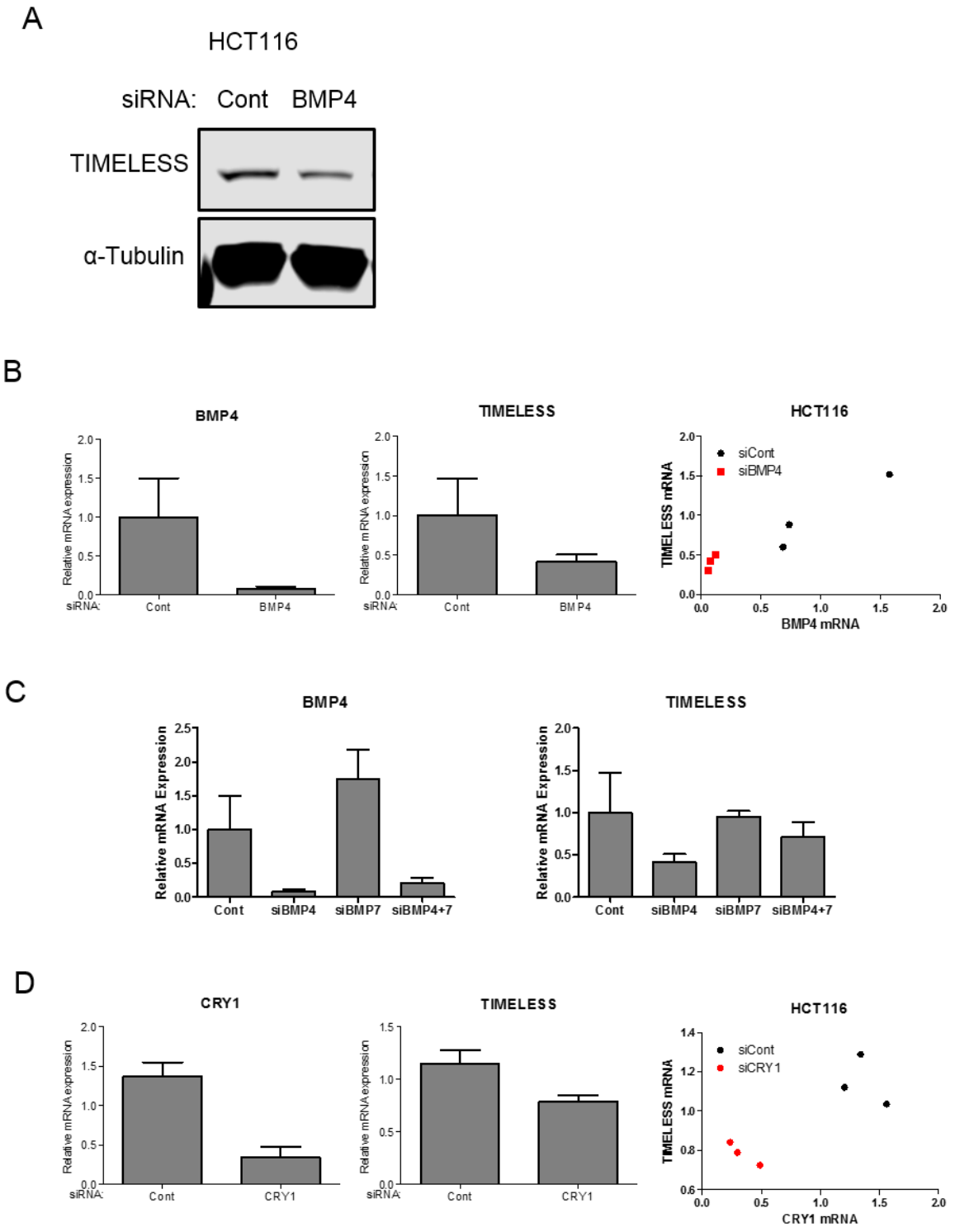

Fig. B.2: BMP4 and CRY1 may promote TIMELESS expression. (A-C) Western blot (A) and RT-qPCR (B and C) of TIMELESS following RNAi-mediated depletion of BMP4 and/or BMP7 for 72 hours in HCT116 cells. (D) RT-qPCR of CRY1 and TIMELESS following RNAi-mediated depletion of CRY1 for 72 hours in HCT116 cells. (Experiments B.2 were completed in collaboration with Danielle Frodyma).

Appendix C: Cross-referencing the results from FUSION with other datasets

Rationale:

Hits identified from the FUSION screen are predicted to be selectively required for colon cancer cell survival, but not normal cell survival. Cross referencing these hits with screens performed by other groups can reveal additional features or characteristics of the FUSION hits.

Results/Discussion:

Cross referencing the 788 FUSION hits with results from ERRα ChIP-Seq in A549 cells revealed a subset of probably ERRα genetic targets that are also predicted to be required for colon cancer cell survival. Further limiting this list to targets that have increased mRNA expression in colon cancer based on RNASeq analysis in the COAD dataset within TCGA identified eleven genes (Fig. C.1).

Cross referencing the 788 FUSION hits with genes that whose expression was increased via increased translation downstream of oncogenic Ras and MYC revealed a subset of genes that were predicted to be selectively required for colon cancer cell survival and overexpressed in cancer through oncogene-driven increases in translation (Fig. C.2)

A

	Euclidean Distance	Pearson Correlation
PIGL	1.532	0.923
NUDT4	1.370	0.916
TCFL5	0.927	0.911
EPHB4	1.440	0.878
DDX47	1.988	0.850
MAP4K4	0.792	0.817
PODXL	0.786	0.798
FUBP3	0.836	0.787
PLCB4	1.273	0.73
LTBP2	1.696	0.714
TAZ	2.746	0.709

B

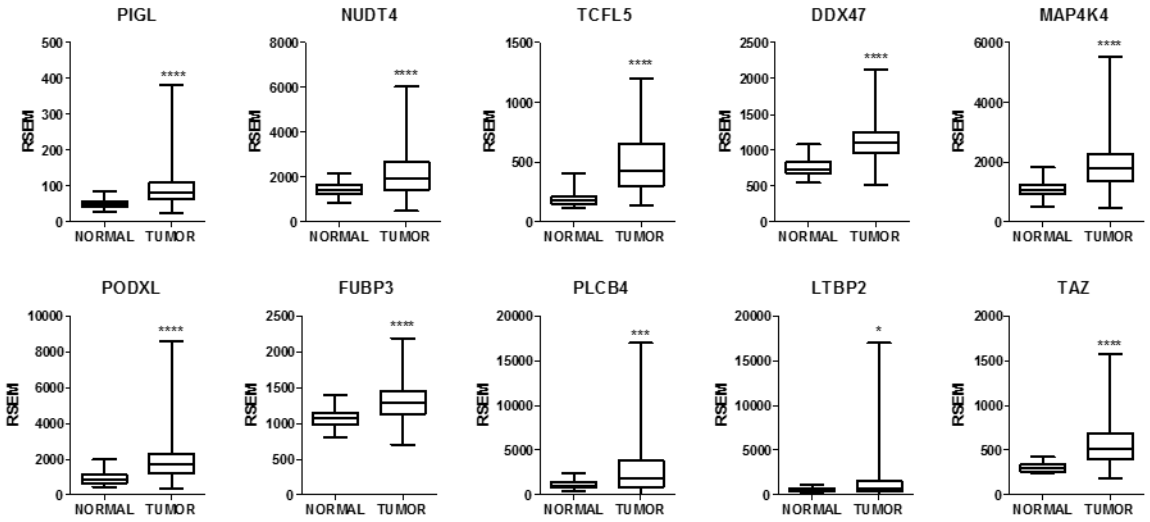

Fig. C.1: FUSION hits predicted to be regulated by ERRα and upregulated in colon cancer. (A)Table with a list of FUSION hits that are also predicted to be targets of ERRα based on publically available ChipSeq data that was performed in A549 cells (GSE91793). (B) PIGL, NUDT4, TCFL5, DDX47, MAP4K4, PODXL, FUBP3, PLCB4, LTBP2, and TAZ gene expression (RNASeq) data from the Colon Adenocarcinoma (COAD) dataset within TCGA for unpaired primary colon tumors and normal solid tissue samples. The results published here are in whole or part based upon data generated by the TCGA Research Network: http://cancergenome.nih.gov/. Note: EPHB4 is not included in B because those results were previously published.

	Euclidean Distance	Pearson Correlation	Translation Effect
BMP2	1.096	0.767	Decreased
BMP4	**1.109**	**0.757**	**Increased**
CDH5	0.897	0.702	Decreased
CDKN1B	**1.563**	**0.725**	**Increased**
CUGBP1	**1.928**	**0.718**	**Increased**
DEDD	**0.649**	**0.884**	**Increased**
DHRS9	1.497	0.836	Decreased
EMR1	**1.101**	**0.718**	**Increased**
ETV4	**4.327**	**0.802**	**Increased**
FNDC1	**1.443**	**0.715**	**Increased**
GPR82	1.570	0.730	Decreased
HAS2	**0.774**	**0.788**	**Increased**
HSPB8	**1.738**	**0.744**	**Increased**
IGFBP5	**1.063**	**0.745**	**Increased**
LTBP2	**1.696**	**0.714**	**Increased**
LUM	0.672	0.704	Decreased
MYH11	**0.845**	**0.739**	**Increased**
PODXL	0.786	0.798	Decreased
PTPRJ	2.248	0.729	Decreased
RGS4	**1.244**	**0.843**	**Increased**
SELE	1.534	0.794	Decreased
SPARC	0.909	0.721	Decreased
ST5	**1.439**	**0.798**	**Increased**
VBP1	**2.467**	**0.748**	**Increased**
VCAM1	**0.664**	**0.889**	**Increased**

Table C.1: FUSION hits that are also predicted to be regulated by Ras- or MYC-driven translation.

Appendix D: Sequences of qPCR primers and siRNA duplexes

Target	Item #	siRNA	Target Sequence
CRY1	J-015421	5	CAGCAGCUUUCACGAUAUA
		6	GGAGUAGAAGUCAUUGUAA
		7	UAUAUGACCUAGACAAGAU
		8	CAACUGUUAUGGCGUGAAU
ECE2	J-005858	6	CAAGCAUCCUGAACAAUUA
		7	CCUACUACCUUCCAACUAA
		8	GGAUGACGCCCUUGGCUUU
		9	GCAUUCGAGUGGCUGGAAA
HAS2	J-012053	19	GGGUGUGUUCAGUGCAUUA
		20	GGAUUAAAGUUGUCAUGGU
		21	CCAAACGGAUAAUUACUAU
		22	GGUUUGUGAUUCAGACACU
ERK1	J-003592	7	GACCGGAUGUUAACCUUUA
		8	CCUGCGACCUUAAGAUUUG
		9	CCAAUAAACGGAUCACAGU
		10	AGACUGACCUGUACAAGUU
ERK2	J-003555	11	UCGAGUAGCUAUCAAGAAA
		12	CACCAACCAUCGAGCAAAU
		13	GGUGUGCUCUGCUUAUGAU
		14	ACACCAACCUCUCGUACAU
AMPKa1	J-005027	6	CCAUACCCUUGAUGAAUUA
		7	GCCCAGAGGUAGAUAUAUG
		8	GAGGAUCCAUCAUAUAGUU
		9	ACAAUUGGAUUAUGAAUGG
AMPKa2	J-005361	6	CGACUAGCCCAAAUCUUU
		7	GAGCAUGUACCUACGUUAU
		8	GACAGAAGAUUCGCAGUUU
		9	GUCUGGAGGUGAAUUAUUU
WDR5b	LU-013375	5	CAUCGCAUCAGCAGCAUUA
		6	AAACAUACACUGGUCAUAA
		7	CAAACUAUGCUCUCAAAUG
		8	GGACAACACUCUUAAACUA

Table D.1: siRNA Sequences

Target	Item #	siRNA	Target Sequence
WDR5	L-013383	5	GACGAAAGCGUGAGGAUAU
		6	GUGGAAGAGUGACUGCUAA
		7	GACGUGAGCUCGGGCAAGU
		8	GAUGGAUCCUUGAUAGUUU
TIMELESS	J-019488	5	UCAAUCGUCUGCUUAGUGA
		6	CAGGGUAGCUUAGUCCUUU
		7	GAGGGAGACACUUACCAUA
		8	CUACUGCUGGUCAGAAAUA
BMP4	J-011221	5	GAGCCAUGCUAGUUUGAUA
		6	UAGCAAGAGUGCCGUCAUU
		7	CGACACUUCUGCAGAUGUU
		8	CAGGAUUAGCCGAUCGUUA
BMP7	J-011592	5	GAGGUGCACUCGAGCUUCA
		6	CAUCGAGAGUUCCGGUUUG
		7	GAUCAGCGUUUAUCAGGUG
		8	GCACAACUCGGCACCCAUG
KSR1	J-003570	7	GAGCAAGUCCCAUGAGUCU
		8	GGAAUGAAGCGUGUCCUGA
		9	AGAAAGAGGUGAUGAACUA
PRKAG1	J-009056	5	GAGGUUCACCGACUUGUAG
		6	UCAAUAUCCUGCACCGCUA
		7	GGAACAAGAUCCACAGGCU
MAP2K1	L-003571	6	CCAUGCUGCUGGCGUCUAA
		7	GAGGUUCUCUGGAUCAAGU
		8	CGACGGCUCUGCAGUUAAC
		9	GCACAAGGUCCUACAUGUC
MAP2K2	J-003573	8	CGACAGCGCAUGCAGGAAC
		9	GAUCAGCAUUUGCAUGGAA
		10	GGUCCGAGGUGGAAGAAGU
		11	UCUUUGAACUCCUGGACUA
RBBP5	LU-012008	5	UAACACGGCAGAUCGAAUA
		6	UAUAGAACUUCAAGGAGUA
		7	GCAAUACCACAGCCAUUAA
		8	GAUGGAACUUUGGAUUGUA
Non-targeting	D-001810		UGGUUUACAUGUCGACUAA

Table D.1 Continued: siRNA Sequences

Target	Accession #	Amplicon size (bp)	Exons	T_m (°C)	F primer 5' -> 3'	R primer 5' -> 3'
TIMELESS	NM_003920	120	10-11	62	GAGACTTCTGCTCTGAGTTCC	CCAAGGCCCACATATAATAGGT
WDR5	NM_052821	135	8-10	58	ATGCGACAGAGACCATCATAG	CGTGAGGATATGGGATGTGAA
BMP4	NM_001202	111	3-4	61	GAGCCTTTCCAGCAAGTTTG	CCATCAGCATTCGGTTACCA
BMP7	NM_001719	121	1-2	61	ATCAAACCGGAACTCTCGATG	CAGCCTGCAAGATAGCCATT
Myc	NM_002467.4	119	3	58	GGCTCCTGGCAAAAGGTCA	CTGCGTAGTTGTGCTGATGT
GAPDH	NM_002046.1	111	2-3	58	GGTGAAGGTCGGAGTCAACGG	GAGGTCAATGAAGGGGTCATTG
HPRT1	NM_000194	128	6-8	60	GTATTCATTATAGTCAAGGGCATATCC	AGATGGTCAAGGTCGCAAG

Table D.2 Sequences of qPCR Primers

Literature Cited:

1 Das, B. *et al.* A Functional Signature Ontology (FUSION) screen detects an AMPK inhibitor with selective toxicity toward human colon tumor cells. *Scientific reports* **8**, 3770, doi:10.1038/s41598-018-22090-6 (2018).

2 Neilsen, B. K., Frodyma, D. E., Lewis, R. E. & Fisher, K. W. KSR as a therapeutic target for Ras-dependent cancers. *Expert opinion on therapeutic targets* **21**, 499-509, doi:10.1080/14728222.2017.1311325 (2017).

3 Fisher, K. W. *et al.* AMPK Promotes Aberrant PGC1beta Expression To Support Human Colon Tumor Cell Survival. *Molecular and cellular biology* **35**, 3866-3879, doi:10.1128/MCB.00528-15 (2015).

4 American Cancer Society. Cancer Facts and Figures 2018. (2018).

5 Murphy SL, X. J., Kochanek KD, Curtin SC, Arias E. Deaths: Final data for 2015 *National Vital Statistics Reports. Hyattsville, MD: National Center for Health Statistics.* **66** (2017).

6 Forbes, S. A. *et al.* COSMIC: mining complete cancer genomes in the Catalogue of Somatic Mutations in Cancer. *Nucleic acids research* **39**, D945-950, doi:10.1093/nar/gkq929 (2011).

7 Fernandez-Medarde, A. & Santos, E. Ras in cancer and developmental diseases. *Genes & cancer* **2**, 344-358, doi:10.1177/1947601911411084 (2011).

8 Prior, I. A., Lewis, P. D. & Mattos, C. A comprehensive survey of Ras mutations in cancer. *Cancer research* **72**, 2457-2467, doi:10.1158/0008-5472.CAN-11-2612 (2012).

9 Ostrem, J. M. & Shokat, K. M. Direct small-molecule inhibitors of KRAS: from structural insights to mechanism-based design. *Nature reviews. Drug discovery* **15**, 771-785, doi:10.1038/nrd.2016.139 (2016).

10 Young, A. *et al.* Ras signaling and therapies. *Advances in cancer research* **102**, 1-17, doi:10.1016/S0065-230X(09)02001-6 (2009).

11 Maurer, T. *et al.* Small-molecule ligands bind to a distinct pocket in Ras and inhibit SOS-mediated nucleotide exchange activity. *Proceedings of the National Academy of Sciences of the United States of America* **109**, 5299-5304, doi:10.1073/pnas.1116510109 (2012).

12 Ostrem, J. M., Peters, U., Sos, M. L., Wells, J. A. & Shokat, K. M. K-Ras(G12C) inhibitors allosterically control GTP affinity and effector interactions. *Nature* **503**, 548-551, doi:10.1038/nature12796 (2013).

13 Sun, Q. *et al.* Discovery of small molecules that bind to K-Ras and inhibit Sos-mediated activation. *Angewandte Chemie* **51**, 6140-6143, doi:10.1002/anie.201201358 (2012).

14 Welsch, M. E. *et al.* Multivalent Small-Molecule Pan-RAS Inhibitors. *Cell* **168**, 878-889 e829, doi:10.1016/j.cell.2017.02.006 (2017).

15 James, G., Goldstein, J. L. & Brown, M. S. Resistance of K-RasBV12 proteins to farnesyltransferase inhibitors in Rat1 cells. *Proceedings of the National Academy of Sciences of the United States of America* **93**, 4454-4458 (1996).

16 Whyte, D. B. *et al.* K- and N-Ras are geranylgeranylated in cells treated with farnesyl protein transferase inhibitors. *The Journal of biological chemistry* **272**, 14459-14464 (1997).

17 Shima, F. *et al.* In silico discovery of small-molecule Ras inhibitors that display antitumor activity by blocking the Ras-effector interaction. *Proceedings of the National Academy of Sciences of the United States of America* **110**, 8182-8187, doi:10.1073/pnas.1217730110 (2013).

18 Samatar, A. A. & Poulikakos, P. I. Targeting RAS-ERK signalling in cancer: promises and challenges. *Nature reviews. Drug discovery* **13**, 928-942, doi:10.1038/nrd4281 (2014).

19 Kornfeld, K., Hom, D. B. & Horvitz, H. R. The ksr-1 gene encodes a novel protein kinase involved in Ras-mediated signaling in C. elegans. *Cell* **83**, 903-913 (1995).

20 Sundaram, M. & Han, M. The C. elegans ksr-1 gene encodes a novel Raf-related kinase involved in Ras-mediated signal transduction. *Cell* **83**, 889-901 (1995).

21 Therrien, M. *et al.* KSR, a novel protein kinase required for RAS signal transduction. *Cell* **83**, 879-888 (1995).

22 Downward, J. KSR: a novel player in the RAS pathway. *Cell* **83**, 831-834 (1995).

23 Morrison, D. K. KSR: a MAPK scaffold of the Ras pathway? *Journal of cell science* **114**, 1609-1612 (2001).

24 Nguyen, A. *et al.* Kinase suppressor of Ras (KSR) is a scaffold which facilitates mitogen-activated

protein kinase activation in vivo. *Molecular and cellular biology* **22**, 3035-3045 (2002).
25 Ritt, D. A., Daar, I. O. & Morrison, D. K. KSR regulation of the Raf-MEK-ERK cascade. *Methods in enzymology* **407**, 224-237, doi:10.1016/S0076-6879(05)07019-9 (2006).
26 Brennan, D. F. *et al.* A Raf-induced allosteric transition of KSR stimulates phosphorylation of MEK. *Nature* **472**, 366-369, doi:10.1038/nature09860 (2011).
27 McKay, M. M., Freeman, A. K. & Morrison, D. K. Complexity in KSR function revealed by Raf inhibitor and KSR structure studies. *Small GTPases* **2**, 276-281, doi:10.4161/sgtp.2.5.17740 (2011).
28 Kolch, W. Coordinating ERK/MAPK signalling through scaffolds and inhibitors. *Nature reviews. Molecular cell biology* **6**, 827-837, doi:10.1038/nrm1743 (2005).
29 Claperon, A. & Therrien, M. KSR and CNK: two scaffolds regulating RAS-mediated RAF activation. *Oncogene* **26**, 3143-3158, doi:10.1038/sj.onc.1210408 (2007).
30 Raabe, T. & Rapp, U. R. KSR--a regulator and scaffold protein of the MAPK pathway. *Science's STKE : signal transduction knowledge environment* **2002**, pe28, doi:10.1126/stke.2002.136.pe28 (2002).
31 Roy, F., Laberge, G., Douziech, M., Ferland-McCollough, D. & Therrien, M. KSR is a scaffold required for activation of the ERK/MAPK module. *Genes & development* **16**, 427-438, doi:10.1101/gad.962902 (2002).
32 Kortum, R. L. & Lewis, R. E. The molecular scaffold KSR1 regulates the proliferative and oncogenic potential of cells. *Molecular and cellular biology* **24**, 4407-4416 (2004).
33 Kortum, R. L. *et al.* The molecular scaffold kinase suppressor of Ras 1 (KSR1) regulates adipogenesis. *Molecular and cellular biology* **25**, 7592-7604, doi:10.1128/MCB.25.17.7592-7604.2005 (2005).
34 Liu, L. *et al.* Proteomic characterization of the dynamic KSR-2 interactome, a signaling scaffold complex in MAPK pathway. *Biochimica et biophysica acta* **1794**, 1485-1495, doi:10.1016/j.bbapap.2009.06.016 (2009).
35 Huang, L. *et al.* Simulating EGFR-ERK signaling control by scaffold proteins KSR and MP1 reveals differential ligand-sensitivity co-regulated by Cbl-CIN85 and endophilin. *PloS one* **6**, e22933, doi:10.1371/journal.pone.0022933 (2011).
36 Kortum, R. L. *et al.* Caveolin-1 is required for kinase suppressor of Ras 1 (KSR1)-mediated extracellular signal-regulated kinase 1/2 activation, H-RasV12-induced senescence, and transformation. *Molecular and cellular biology* **34**, 3461-3472, doi:10.1128/MCB.01633-13 (2014).
37 Karthik, D., Majumder, P., Palanisamy, S., Khairunnisa, K. & Venugopal, V. Targeting cysteine rich C1 domain of Scaffold protein Kinase Suppressor of Ras (KSR) with anthocyanidins and flavonoids - a binding affinity characterization study. *Bioinformation* **10**, 580-585, doi:10.6026/97320630010580 (2014).
38 Razidlo, G. L., Kortum, R. L., Haferbier, J. L. & Lewis, R. E. Phosphorylation regulates KSR1 stability, ERK activation, and cell proliferation. *The Journal of biological chemistry* **279**, 47808-47814, doi:10.1074/jbc.M406395200 (2004).
39 Razidlo, G. L. *et al.* KSR1 is required for cell cycle reinitiation following DNA damage. *The Journal of biological chemistry* **284**, 6705-6715, doi:10.1074/jbc.M806457200 (2009).
40 Klutho, P. J., Costanzo-Garvey, D. L. & Lewis, R. E. Regulation of glucose homeostasis by KSR1 and MARK2. *PloS one* **6**, e29304, doi:10.1371/journal.pone.0029304 (2011).
41 Fisher, K. W., Das, B., Kortum, R. L., Chaika, O. V. & Lewis, R. E. Kinase suppressor of ras 1 (KSR1) regulates PGC1alpha and estrogen-related receptor alpha to promote oncogenic Ras-dependent anchorage-independent growth. *Molecular and cellular biology* **31**, 2453-2461, doi:10.1128/MCB.05255-11 (2011).
42 McCall, J. L. *et al.* KSR1 and EPHB4 Regulate Myc and PGC1beta To Promote Survival of Human Colon Tumors. *Molecular and cellular biology* **36**, 2246-2261, doi:10.1128/MCB.00087-16 (2016).
43 Ohmachi, M. *et al.* C. elegans ksr-1 and ksr-2 have both unique and redundant functions and are required for MPK-1 ERK phosphorylation. *Current biology : CB* **12**, 427-433 (2002).
44 Hansen, L. A. *et al.* Genetically null mice reveal a central role for epidermal growth factor receptor in the differentiation of the hair follicle and normal hair development. *The American journal of pathology* **150**, 1959-1975 (1997).

45 Lozano, J. *et al.* Deficiency of kinase suppressor of Ras1 prevents oncogenic ras signaling in mice. *Cancer research* **63**, 4232-4238 (2003).
46 Fusello, A. M. *et al.* The MAPK scaffold kinase suppressor of Ras is involved in ERK activation by stress and proinflammatory cytokines and induction of arthritis. *Journal of immunology* **177**, 6152-6158 (2006).
47 Le Borgne, M., Filbert, E. L. & Shaw, A. S. Kinase suppressor of Ras 1 is not required for the generation of regulatory and memory T cells. *PloS one* **8**, e57137, doi:10.1371/journal.pone.0057137 (2013).
48 Revelli, J. P. *et al.* Profound obesity secondary to hyperphagia in mice lacking kinase suppressor of ras 2. *Obesity* **19**, 1010-1018, doi:10.1038/oby.2010.282 (2011).
49 Henry, M. D., Costanzo-Garvey, D. L., Klutho, P. J. & Lewis, R. E. Obesity-dependent dysregulation of glucose homeostasis in kinase suppressor of ras 2-/- mice. *Physiological reports* **2**, doi:10.14814/phy2.12053 (2014).
50 Costanzo-Garvey, D. L. *et al.* KSR2 is an essential regulator of AMP kinase, energy expenditure, and insulin sensitivity. *Cell metabolism* **10**, 366-378, doi:10.1016/j.cmet.2009.09.010 (2009).
51 Guo, L. *et al.* Cell non-autonomous regulation of hepatic IGF-1 and neonatal growth by Kinase Suppressor of Ras 2 (KSR2). *Scientific reports* **6**, 32093, doi:10.1038/srep32093 (2016).
52 Fernandez, M. R., Henry, M. D. & Lewis, R. E. Kinase suppressor of Ras 2 (KSR2) regulates tumor cell transformation via AMPK. *Molecular and cellular biology* **32**, 3718-3731, doi:10.1128/MCB.06754-11 (2012).
53 Dougherty, M. K. *et al.* KSR2 is a calcineurin substrate that promotes ERK cascade activation in response to calcium signals. *Molecular cell* **34**, 652-662, doi:10.1016/j.molcel.2009.06.001 (2009).
54 Dhawan, N. S., Scopton, A. P. & Dar, A. C. Small molecule stabilization of the KSR inactive state antagonizes oncogenic Ras signalling. *Nature* **537**, 112-116, doi:10.1038/nature19327 (2016).
55 Joneson, T. *et al.* Kinase suppressor of Ras inhibits the activation of extracellular ligand-regulated (ERK) mitogen-activated protein (MAP) kinase by growth factors, activated Ras, and Ras effectors. *The Journal of biological chemistry* **273**, 7743-7748 (1998).
56 Kortum, R. L. *et al.* The molecular scaffold kinase suppressor of Ras 1 is a modifier of RasV12-induced and replicative senescence. *Molecular and cellular biology* **26**, 2202-2214, doi:10.1128/MCB.26.6.2202-2214.2006 (2006).
57 Stewart, S. *et al.* Kinase suppressor of Ras forms a multiprotein signaling complex and modulates MEK localization. *Molecular and cellular biology* **19**, 5523-5534 (1999).
58 McKay, M. M., Ritt, D. A. & Morrison, D. K. Signaling dynamics of the KSR1 scaffold complex. *Proceedings of the National Academy of Sciences of the United States of America* **106**, 11022-11027, doi:10.1073/pnas.0901590106 (2009).
59 Udell, C. M., Rajakulendran, T., Sicheri, F. & Therrien, M. Mechanistic principles of RAF kinase signaling. *Cellular and molecular life sciences : CMLS* **68**, 553-565, doi:10.1007/s00018-010-0520-6 (2011).
60 Koveal, D. *et al.* A CC-SAM, for coiled coil-sterile alpha motif, domain targets the scaffold KSR-1 to specific sites in the plasma membrane. *Science signaling* **5**, ra94, doi:10.1126/scisignal.2003289 (2012).
61 Michaud, N. R. *et al.* KSR stimulates Raf-1 activity in a kinase-independent manner. *Proceedings of the National Academy of Sciences of the United States of America* **94**, 12792-12796 (1997).
62 Zhou, M., Horita, D. A., Waugh, D. S., Byrd, R. A. & Morrison, D. K. Solution structure and functional analysis of the cysteine-rich C1 domain of kinase suppressor of Ras (KSR). *Journal of molecular biology* **315**, 435-446, doi:10.1006/jmbi.2001.5263 (2002).
63 Therrien, M., Michaud, N. R., Rubin, G. M. & Morrison, D. K. KSR modulates signal propagation within the MAPK cascade. *Genes & development* **10**, 2684-2695 (1996).
64 Jacobs, D., Glossip, D., Xing, H., Muslin, A. J. & Kornfeld, K. Multiple docking sites on substrate proteins form a modular system that mediates recognition by ERK MAP kinase. *Genes & development* **13**, 163-175 (1999).
65 Cacace, A. M. *et al.* Identification of constitutive and ras-inducible phosphorylation sites of KSR: implications for 14-3-3 binding, mitogen-activated protein kinase binding, and KSR overexpression. *Molecular and cellular biology* **19**, 229-240 (1999).
66 Muller, J., Cacace, A. M., Lyons, W. E., McGill, C. B. & Morrison, D. K. Identification of B-

KSR1, a novel brain-specific isoform of KSR1 that functions in neuronal signaling. *Molecular and cellular biology* **20**, 5529-5539 (2000).

67 Pearce, L. R. *et al.* KSR2 mutations are associated with obesity, insulin resistance, and impaired cellular fuel oxidation. *Cell* **155**, 765-777, doi:10.1016/j.cell.2013.09.058 (2013).

68 Guo, L., Volle, D. J. & Lewis, R. E. Identification of a truncated kinase suppressor of Ras 2 mRNA in sperm. *FEBS open bio* **4**, 420-425, doi:10.1016/j.fob.2014.04.004 (2014).

69 Yu, W., Fantl, W. J., Harrowe, G. & Williams, L. T. Regulation of the MAP kinase pathway by mammalian Ksr through direct interaction with MEK and ERK. *Current biology : CB* **8**, 56-64 (1998).

70 Volle, D. J. *et al.* Phosphorylation of the kinase suppressor of ras by associated kinases. *Biochemistry* **38**, 5130-5137, doi:10.1021/bi983050d (1999).

71 Fantz, D. A., Jacobs, D., Glossip, D. & Kornfeld, K. Docking sites on substrate proteins direct extracellular signal-regulated kinase to phosphorylate specific residues. *The Journal of biological chemistry* **276**, 27256-27265, doi:10.1074/jbc.M102512200 (2001).

72 Muller, J., Ory, S., Copeland, T., Piwnica-Worms, H. & Morrison, D. K. C-TAK1 regulates Ras signaling by phosphorylating the MAPK scaffold, KSR1. *Molecular cell* **8**, 983-993 (2001).

73 McKay, M. M., Ritt, D. A. & Morrison, D. K. RAF inhibitor-induced KSR1/B-RAF binding and its effects on ERK cascade signaling. *Current biology : CB* **21**, 563-568, doi:10.1016/j.cub.2011.02.033 (2011).

74 Ritt, D. A. *et al.* CK2 Is a component of the KSR1 scaffold complex that contributes to Raf kinase activation. *Current biology : CB* **17**, 179-184, doi:10.1016/j.cub.2006.11.061 (2007).

75 McKay, M. M. & Morrison, D. K. Caspase-dependent cleavage disrupts the ERK cascade scaffolding function of KSR1. *The Journal of biological chemistry* **282**, 26225-26234, doi:10.1074/jbc.M702692200 (2007).

76 Frodyma, D., Neilsen, B., Costanzo-Garvey, D., Fisher, K. & Lewis, R. Coordinating ERK signaling via the molecular scaffold Kinase Suppressor of Ras. *F1000Research* **6**, 1621, doi:10.12688/f1000research.11895.1 (2017).

77 Denouel-Galy, A. *et al.* Murine Ksr interacts with MEK and inhibits Ras-induced transformation. *Current biology : CB* **8**, 46-55 (1998).

78 Sugimoto, T., Stewart, S., Han, M. & Guan, K. L. The kinase suppressor of Ras (KSR) modulates growth factor and Ras signaling by uncoupling Elk-1 phosphorylation from MAP kinase activation. *The EMBO journal* **17**, 1717-1727, doi:10.1093/emboj/17.6.1717 (1998).

79 Levchenko, A., Bruck, J. & Sternberg, P. W. Scaffold proteins may biphasically affect the levels of mitogen-activated protein kinase signaling and reduce its threshold properties. *Proceedings of the National Academy of Sciences of the United States of America* **97**, 5818-5823 (2000).

80 Morrison, D. K. & Davis, R. J. Regulation of MAP kinase signaling modules by scaffold proteins in mammals. *Annual review of cell and developmental biology* **19**, 91-118, doi:10.1146/annurev.cellbio.19.111401.091942 (2003).

81 Matheny, S. A. *et al.* Ras regulates assembly of mitogenic signalling complexes through the effector protein IMP. *Nature* **427**, 256-260, doi:10.1038/nature02237 (2004).

82 Ory, S., Zhou, M., Conrads, T. P., Veenstra, T. D. & Morrison, D. K. Protein phosphatase 2A positively regulates Ras signaling by dephosphorylating KSR1 and Raf-1 on critical 14-3-3 binding sites. *Current biology : CB* **13**, 1356-1364 (2003).

83 Rajakulendran, T., Sahmi, M., Lefrancois, M., Sicheri, F. & Therrien, M. A dimerization-dependent mechanism drives RAF catalytic activation. *Nature* **461**, 542-545, doi:10.1038/nature08314 (2009).

84 Lavoie, H. & Therrien, M. Regulation of RAF protein kinases in ERK signalling. *Nature reviews. Molecular cell biology* **16**, 281-298, doi:10.1038/nrm3979 (2015).

85 Casar, B., Pinto, A. & Crespo, P. ERK dimers and scaffold proteins: unexpected partners for a forgotten (cytoplasmic) task. *Cell cycle* **8**, 1007-1013, doi:10.4161/cc.8.7.8078 (2009).

86 Casar, B., Pinto, A. & Crespo, P. Essential role of ERK dimers in the activation of cytoplasmic but not nuclear substrates by ERK-scaffold complexes. *Molecular cell* **31**, 708-721, doi:10.1016/j.molcel.2008.07.024 (2008).

87 Lin, W. C. *et al.* H-Ras forms dimers on membrane surfaces via a protein-protein interface. *Proceedings of the National Academy of Sciences of the United States of America* **111**, 2996-3001, doi:10.1073/pnas.1321155111 (2014).

88 Nan, X. *et al.* Ras-GTP dimers activate the Mitogen-Activated Protein Kinase (MAPK) pathway. *Proceedings of the National Academy of Sciences of the United States of America* **112**, 7996-8001, doi:10.1073/pnas.1509123112 (2015).

89 Santos, E. Dimerization opens new avenues into Ras signaling research. *Science signaling* **7**, pe12, doi:10.1126/scisignal.2005318 (2014).

90 Kortum, R. L. & Morrison, D. K. Path Forward for RAF Therapies: Inhibition of Monomers and Dimers. *Cancer cell* **28**, 279-281, doi:10.1016/j.ccell.2015.08.006 (2015).

91 Gibney, G. T., Messina, J. L., Fedorenko, I. V., Sondak, V. K. & Smalley, K. S. Paradoxical oncogenesis--the long-term effects of BRAF inhibition in melanoma. *Nature reviews. Clinical oncology* **10**, 390-399, doi:10.1038/nrclinonc.2013.83 (2013).

92 Freeman, A. K., Ritt, D. A. & Morrison, D. K. Effects of Raf dimerization and its inhibition on normal and disease-associated Raf signaling. *Molecular cell* **49**, 751-758, doi:10.1016/j.molcel.2012.12.018 (2013).

93 Freeman, A. K., Ritt, D. A. & Morrison, D. K. The importance of Raf dimerization in cell signaling. *Small GTPases* **4**, 180-185, doi:10.4161/sgtp.26117 (2013).

94 Lavoie, H. *et al.* Inhibitors that stabilize a closed RAF kinase domain conformation induce dimerization. *Nature chemical biology* **9**, 428-436, doi:10.1038/nchembio.1257 (2013).

95 Yao, Z. *et al.* BRAF Mutants Evade ERK-Dependent Feedback by Different Mechanisms that Determine Their Sensitivity to Pharmacologic Inhibition. *Cancer cell* **28**, 370-383, doi:10.1016/j.ccell.2015.08.001 (2015).

96 Kholodenko, B. N. Drug Resistance Resulting from Kinase Dimerization Is Rationalized by Thermodynamic Factors Describing Allosteric Inhibitor Effects. *Cell reports* **12**, 1939-1949, doi:10.1016/j.celrep.2015.08.014 (2015).

97 Zhang, Y. *et al.* Kinase suppressor of Ras is ceramide-activated protein kinase. *Cell* **89**, 63-72 (1997).

98 Brennan, J. A., Volle, D. J., Chaika, O. V. & Lewis, R. E. Phosphorylation regulates the nucleocytoplasmic distribution of kinase suppressor of Ras. *The Journal of biological chemistry* **277**, 5369-5377, doi:10.1074/jbc.M109875200 (2002).

99 Zhang, J. *et al.* Downregulation of KSR1 in pancreatic cancer xenografts by antisense oligonucleotide correlates with tumor drug uptake. *Cancer biology & therapy* **7**, 1490-1495 (2008).

100 Brown, M. D. & Sacks, D. B. Protein scaffolds in MAP kinase signalling. *Cellular signalling* **21**, 462-469, doi:10.1016/j.cellsig.2008.11.013 (2009).

101 Potts, M. B. *et al.* Using functional signature ontology (FUSION) to identify mechanisms of action for natural products. *Science signaling* **6**, ra90, doi:10.1126/scisignal.2004657 (2013).

102 Roig, A. I. *et al.* Immortalized epithelial cells derived from human colon biopsies express stem cell markers and differentiate in vitro. *Gastroenterology* **138**, 1012-1021 e1011-1015, doi:10.1053/j.gastro.2009.11.052 (2010).

103 Stegmaier, K. *et al.* Gene expression-based high-throughput screening(GE-HTS) and application to leukemia differentiation. *Nature genetics* **36**, 257-263, doi:10.1038/ng1305 (2004).

104 Sigoillot, F. D. *et al.* A bioinformatics method identifies prominent off-targeted transcripts in RNAi screens. *Nature methods* **9**, 363-366, doi:10.1038/nmeth.1898 (2012).

105 Yilmazel, B. *et al.* Online GESS: prediction of miRNA-like off-target effects in large-scale RNAi screen data by seed region analysis. *BMC bioinformatics* **15**, 192, doi:10.1186/1471-2105-15-192 (2014).

106 Mootha, V. K. *et al.* PGC-1alpha-responsive genes involved in oxidative phosphorylation are coordinately downregulated in human diabetes. *Nature genetics* **34**, 267-273, doi:10.1038/ng1180 (2003).

107 Subramanian, A., Kuehn, H., Gould, J., Tamayo, P. & Mesirov, J. P. GSEA-P: a desktop application for Gene Set Enrichment Analysis. *Bioinformatics* **23**, 3251-3253, doi:10.1093/bioinformatics/btm369 (2007).

108 Subramanian, A. *et al.* Gene set enrichment analysis: a knowledge-based approach for interpreting genome-wide expression profiles. *Proceedings of the National Academy of Sciences of the United States of America* **102**, 15545-15550, doi:10.1073/pnas.0506580102 (2005).

109 Croft, D. *et al.* The Reactome pathway knowledgebase. *Nucleic acids research* **42**, D472-477, doi:10.1093/nar/gkt1102 (2014).

110 Fabregat, A. *et al.* The Reactome Pathway Knowledgebase. *Nucleic acids research* **46**, D649-D655, doi:10.1093/nar/gkx1132 (2018).

111 Sangoram, A. M. *et al.* Mammalian circadian autoregulatory loop: a timeless ortholog and mPer1 interact and negatively regulate CLOCK-BMAL1-induced transcription. *Neuron* **21**, 1101-1113 (1998).

112 Zylka, M. J. *et al.* Molecular analysis of mammalian timeless. *Neuron* **21**, 1115-1122 (1998).

113 Benna, C. *et al.* A second timeless gene in Drosophila shares greater sequence similarity with mammalian tim. *Current biology : CB* **10**, R512-513 (2000).

114 Gotter, A. L., Suppa, C. & Emanuel, B. S. Mammalian TIMELESS and Tipin are evolutionarily conserved replication fork-associated factors. *Journal of molecular biology* **366**, 36-52, doi:10.1016/j.jmb.2006.10.097 (2007).

115 Gotter, A. L. A Timeless debate: resolving TIM's noncircadian roles with possible clock function. *Neuroreport* **17**, 1229-1233, doi:10.1097/01.wnr.0000233092.90160.92 (2006).

116 Koike, N. *et al.* Identification of the mammalian homologues of the Drosophila timeless gene, Timeless1. *FEBS letters* **441**, 427-431 (1998).

117 Holzer, S. *et al.* Crystal structure of the N-terminal domain of human Timeless and its interaction with Tipin. *Nucleic acids research* **45**, 5555-5563, doi:10.1093/nar/gkx139 (2017).

118 Gotter, A. L. *et al.* A time-less function for mouse timeless. *Nature neuroscience* **3**, 755-756, doi:10.1038/77653 (2000).

119 Takumi, T. *et al.* A mammalian ortholog of Drosophila timeless, highly expressed in SCN and retina, forms a complex with mPER1. *Genes to cells : devoted to molecular & cellular mechanisms* **4**, 67-75 (1999).

120 Tischkau, S. A. *et al.* Oscillation and light induction of timeless mRNA in the mammalian circadian clock. *The Journal of neuroscience : the official journal of the Society for Neuroscience* **19**, RC15 (1999).

121 Barnes, J. W. *et al.* Requirement of mammalian Timeless for circadian rhythmicity. *Science* **302**, 439-442, doi:10.1126/science.1086593 (2003).

122 McDonald, M. J., Rosbash, M. & Emery, P. Wild-type circadian rhythmicity is dependent on closely spaced E boxes in the Drosophila timeless promoter. *Molecular and cellular biology* **21**, 1207-1217, doi:10.1128/MCB.21.4.1207-1217.2001 (2001).

123 Wang, G. K. *et al.* Regulation of the cycling of timeless (tim) RNA. *Journal of neurobiology* **47**, 161-175 (2001).

124 Gekakis, N. *et al.* Isolation of timeless by PER protein interaction: defective interaction between timeless protein and long-period mutant PERL. *Science* **270**, 811-815 (1995).

125 Myers, M. P., Wager-Smith, K., Wesley, C. S., Young, M. W. & Sehgal, A. Positional cloning and sequence analysis of the Drosophila clock gene, timeless. *Science* **270**, 805-808 (1995).

126 Sehgal, A. *et al.* Rhythmic expression of timeless: a basis for promoting circadian cycles in period gene autoregulation. *Science* **270**, 808-810 (1995).

127 Hunter-Ensor, M., Ousley, A. & Sehgal, A. Regulation of the Drosophila protein timeless suggests a mechanism for resetting the circadian clock by light. *Cell* **84**, 677-685 (1996).

128 Lee, C., Parikh, V., Itsukaichi, T., Bae, K. & Edery, I. Resetting the Drosophila clock by photic regulation of PER and a PER-TIM complex. *Science* **271**, 1740-1744 (1996).

129 Darlington, T. K. *et al.* Closing the circadian loop: CLOCK-induced transcription of its own inhibitors per and tim. *Science* **280**, 1599-1603 (1998).

130 Darlington, T. K., Lyons, L. C., Hardin, P. E. & Kay, S. A. The period E-box is sufficient to drive circadian oscillation of transcription in vivo. *Journal of biological rhythms* **15**, 462-471, doi:10.1177/074873040001500603 (2000).

131 Lee, C., Bae, K. & Edery, I. PER and TIM inhibit the DNA binding activity of a Drosophila CLOCK-CYC/dBMAL1 heterodimer without disrupting formation of the heterodimer: a basis for circadian transcription. *Molecular and cellular biology* **19**, 5316-5325 (1999).

132 Glossop, N. R., Lyons, L. C. & Hardin, P. E. Interlocked feedback loops within the Drosophila circadian oscillator. *Science* **286**, 766-768 (1999).

133 Yu, W., Zheng, H., Houl, J. H., Dauwalder, B. & Hardin, P. E. PER-dependent rhythms in CLK phosphorylation and E-box binding regulate circadian transcription. *Genes & development* **20**, 723-733, doi:10.1101/gad.1404406 (2006).

134 Griffin, E. A., Jr., Staknis, D. & Weitz, C. J. Light-independent role of CRY1 and CRY2 in the

mammalian circadian clock. *Science* **286**, 768-771 (1999).
135 Kloss, B. *et al.* The Drosophila clock gene double-time encodes a protein closely related to human casein kinase Iepsilon. *Cell* **94**, 97-107 (1998).
136 Kloss, B., Rothenfluh, A., Young, M. W. & Saez, L. Phosphorylation of period is influenced by cycling physical associations of double-time, period, and timeless in the Drosophila clock. *Neuron* **30**, 699-706 (2001).
137 Lin, J. M. *et al.* A role for casein kinase 2alpha in the Drosophila circadian clock. *Nature* **420**, 816-820, doi:10.1038/nature01235 (2002).
138 Akten, B. *et al.* A role for CK2 in the Drosophila circadian oscillator. *Nature neuroscience* **6**, 251-257, doi:10.1038/nn1007 (2003).
139 Harms, E., Young, M. W. & Saez, L. CK1 and GSK3 in the Drosophila and mammalian circadian clock. *Novartis Foundation symposium* **253**, 267-277; discussion 102-269, 277-284 (2003).
140 Meissner, R. A., Kilman, V. L., Lin, J. M. & Allada, R. TIMELESS is an important mediator of CK2 effects on circadian clock function in vivo. *The Journal of neuroscience : the official journal of the Society for Neuroscience* **28**, 9732-9740, doi:10.1523/JNEUROSCI.0840-08.2008 (2008).
141 Bae, K. & Edery, I. Regulating a circadian clock's period, phase and amplitude by phosphorylation: insights from Drosophila. *Journal of biochemistry* **140**, 609-617, doi:10.1093/jb/mvj198 (2006).
142 Zheng, X., Sowcik, M., Chen, D. & Sehgal, A. Casein kinase 1 promotes synchrony of the circadian clock network. *Molecular and cellular biology* **34**, 2682-2694, doi:10.1128/MCB.01571-13 (2014).
143 Hara, T., Koh, K., Combs, D. J. & Sehgal, A. Post-translational regulation and nuclear entry of TIMELESS and PERIOD are affected in new timeless mutant. *The Journal of neuroscience : the official journal of the Society for Neuroscience* **31**, 9982-9990, doi:10.1523/JNEUROSCI.0993-11.2011 (2011).
144 Jang, A. R., Moravcevic, K., Saez, L., Young, M. W. & Sehgal, A. Drosophila TIM binds importin alpha1, and acts as an adapter to transport PER to the nucleus. *PLoS genetics* **11**, e1004974, doi:10.1371/journal.pgen.1004974 (2015).
145 Top, D., Harms, E., Syed, S., Adams, E. L. & Saez, L. GSK-3 and CK2 Kinases Converge on Timeless to Regulate the Master Clock. *Cell reports* **16**, 357-367, doi:10.1016/j.celrep.2016.06.005 (2016).
146 Price, J. L. *et al.* double-time is a novel Drosophila clock gene that regulates PERIOD protein accumulation. *Cell* **94**, 83-95 (1998).
147 Naidoo, N., Song, W., Hunter-Ensor, M. & Sehgal, A. A role for the proteasome in the light response of the timeless clock protein. *Science* **285**, 1737-1741 (1999).
148 Myers, M. P., Wager-Smith, K., Rothenfluh-Hilfiker, A. & Young, M. W. Light-induced degradation of TIMELESS and entrainment of the Drosophila circadian clock. *Science* **271**, 1736-1740 (1996).
149 Koh, K., Zheng, X. & Sehgal, A. JETLAG resets the Drosophila circadian clock by promoting light-induced degradation of TIMELESS. *Science* **312**, 1809-1812, doi:10.1126/science.1124951 (2006).
150 Lamaze, A. *et al.* The E3 ubiquitin ligase CTRIP controls CLOCK levels and PERIOD oscillations in Drosophila. *EMBO reports* **12**, 549-557, doi:10.1038/embor.2011.64 (2011).
151 Grima, B., Dognon, A., Lamouroux, A., Chelot, E. & Rouyer, F. CULLIN-3 controls TIMELESS oscillations in the Drosophila circadian clock. *PLoS biology* **10**, e1001367, doi:10.1371/journal.pbio.1001367 (2012).
152 Grima, B. *et al.* The F-box protein slimb controls the levels of clock proteins period and timeless. *Nature* **420**, 178-182, doi:10.1038/nature01122 (2002).
153 O'Reilly, L. P., Zhang, X. & Smithgall, T. E. Individual Src-family tyrosine kinases direct the degradation or protection of the clock protein Timeless via differential ubiquitylation. *Cellular signalling* **25**, 860-866, doi:10.1016/j.cellsig.2012.12.009 (2013).
154 Agrawal, P. & Hardin, P. E. An RNAi Screen To Identify Protein Phosphatases That Function Within the Drosophila Circadian Clock. *G3* **6**, 4227-4238, doi:10.1534/g3.116.035345 (2016).
155 Gotter, A. L. Tipin, a novel timeless-interacting protein, is developmentally co-expressed with timeless and disrupts its self-association. *Journal of molecular biology* **331**, 167-176 (2003).
156 Li, Z. *et al.* A role for Timeless in epithelial morphogenesis during kidney development.

Proceedings of the National Academy of Sciences of the United States of America **97**, 10038-10043 (2000).

157 Xiao, J., Li, C., Zhu, N. L., Borok, Z. & Minoo, P. Timeless in lung morphogenesis. *Developmental dynamics : an official publication of the American Association of Anatomists* **228**, 82-94, doi:10.1002/dvdy.10346 (2003).

158 Inaguma, Y. *et al.* Morphological characterization of mammalian timeless in the mouse brain development. *Neuroscience research* **92**, 21-28, doi:10.1016/j.neures.2014.10.017 (2015).

159 O'Reilly, L. P., Watkins, S. C. & Smithgall, T. E. An unexpected role for the clock protein timeless in developmental apoptosis. *PloS one* **6**, e17157, doi:10.1371/journal.pone.0017157 (2011).

160 Urtishak, K. A. *et al.* Timeless Maintains Genomic Stability and Suppresses Sister Chromatid Exchange during Unperturbed DNA Replication. *The Journal of biological chemistry* **284**, 8777-8785, doi:10.1074/jbc.M806103200 (2009).

161 Schalbetter, S. A., Mansoubi, S., Chambers, A. L., Downs, J. A. & Baxter, J. Fork rotation and DNA precatenation are restricted during DNA replication to prevent chromosomal instability. *Proceedings of the National Academy of Sciences of the United States of America* **112**, E4565-4570, doi:10.1073/pnas.1505356112 (2015).

162 Smith, K. D., Fu, M. A. & Brown, E. J. Tim-Tipin dysfunction creates an indispensible reliance on the ATR-Chk1 pathway for continued DNA synthesis. *The Journal of cell biology* **187**, 15-23, doi:10.1083/jcb.200905006 (2009).

163 Leman, A. R., Noguchi, C., Lee, C. Y. & Noguchi, E. Human Timeless and Tipin stabilize replication forks and facilitate sister-chromatid cohesion. *Journal of cell science* **123**, 660-670, doi:10.1242/jcs.057984 (2010).

164 Smith-Roe, S. L. *et al.* Separation of intra-S checkpoint protein contributions to DNA replication fork protection and genomic stability in normal human fibroblasts. *Cell cycle* **12**, 332-345, doi:10.4161/cc.23177 (2013).

165 Dheekollu, J. *et al.* Timeless links replication termination to mitotic kinase activation. *PloS one* **6**, e19596, doi:10.1371/journal.pone.0019596 (2011).

166 Leman, A. R. *et al.* Timeless preserves telomere length by promoting efficient DNA replication through human telomeres. *Cell cycle* **11**, 2337-2347, doi:10.4161/cc.20810 (2012).

167 Akamatsu, Y. & Kobayashi, T. The Human RNA Polymerase I Transcription Terminator Complex Acts as a Replication Fork Barrier That Coordinates the Progress of Replication with rRNA Transcription Activity. *Molecular and cellular biology* **35**, 1871-1881, doi:10.1128/MCB.01521-14 (2015).

168 Chou, D. M. & Elledge, S. J. Tipin and Timeless form a mutually protective complex required for genotoxic stress resistance and checkpoint function. *Proceedings of the National Academy of Sciences of the United States of America* **103**, 18143-18147, doi:10.1073/pnas.0609251103 (2006).

169 Cho, W. H. *et al.* Human Tim-Tipin complex affects the biochemical properties of the replicative DNA helicase and DNA polymerases. *Proceedings of the National Academy of Sciences of the United States of America* **110**, 2523-2527, doi:10.1073/pnas.1222494110 (2013).

170 Numata, Y., Ishihara, S., Hasegawa, N., Nozaki, N. & Ishimi, Y. Interaction of human MCM2-7 proteins with TIM, TIPIN and Rb. *Journal of biochemistry* **147**, 917-927, doi:10.1093/jb/mvq028 (2010).

171 Cali, F., Bharti, S. K., Di Perna, R., Brosh, R. M., Jr. & Pisani, F. M. Tim/Timeless, a member of the replication fork protection complex, operates with the Warsaw breakage syndrome DNA helicase DDX11 in the same fork recovery pathway. *Nucleic acids research* **44**, 705-717, doi:10.1093/nar/gkv1112 (2016).

172 Xu, X., Wang, J. T., Li, M. & Liu, Y. TIMELESS Suppresses the Accumulation of Aberrant CDC45.MCM2-7.GINS Replicative Helicase Complexes on Human Chromatin. *The Journal of biological chemistry* **291**, 22544-22558, doi:10.1074/jbc.M116.719963 (2016).

173 Unsal-Kacmaz, K. *et al.* The human Tim/Tipin complex coordinates an Intra-S checkpoint response to UV that slows replication fork displacement. *Molecular and cellular biology* **27**, 3131-3142, doi:10.1128/MCB.02190-06 (2007).

174 Smith-Roe, S. L. *et al.* Timeless functions independently of the Tim-Tipin complex to promote sister chromatid cohesion in normal human fibroblasts. *Cell cycle* **10**, 1618-1624,

doi:10.4161/cc.10.10.15613 (2011).
175 Chan, R. C. *et al.* Chromosome cohesion is regulated by a clock gene paralogue TIM-1. *Nature* **423**, 1002-1009, doi:10.1038/nature01697 (2003).
176 Dheekollu, J., Chen, H. S., Kaye, K. M. & Lieberman, P. M. Timeless-dependent DNA replication-coupled recombination promotes Kaposi's Sarcoma-associated herpesvirus episome maintenance and terminal repeat stability. *Journal of virology* **87**, 3699-3709, doi:10.1128/JVI.02211-12 (2013).
177 Dheekollu, J. & Lieberman, P. M. The replisome pausing factor Timeless is required for episomal maintenance of latent Epstein-Barr virus. *Journal of virology* **85**, 5853-5863, doi:10.1128/JVI.02425-10 (2011).
178 Matsuo, T. *et al.* Control mechanism of the circadian clock for timing of cell division in vivo. *Science* **302**, 255-259, doi:10.1126/science.1086271 (2003).
179 Dekens, M. P. *et al.* Light regulates the cell cycle in zebrafish. *Current biology : CB* **13**, 2051-2057 (2003).
180 Nagoshi, E. *et al.* Circadian gene expression in individual fibroblasts: cell-autonomous and self-sustained oscillators pass time to daughter cells. *Cell* **119**, 693-705, doi:10.1016/j.cell.2004.11.015 (2004).
181 You, S. *et al.* Daily coordination of cancer growth and circadian clock gene expression. *Breast cancer research and treatment* **91**, 47-60, doi:10.1007/s10549-004-6603-z (2005).
182 Unsal-Kacmaz, K., Mullen, T. E., Kaufmann, W. K. & Sancar, A. Coupling of human circadian and cell cycles by the timeless protein. *Molecular and cellular biology* **25**, 3109-3116, doi:10.1128/MCB.25.8.3109-3116.2005 (2005).
183 Yang, X., Wood, P. A. & Hrushesky, W. J. Mammalian TIMELESS is required for ATM-dependent CHK2 activation and G2/M checkpoint control. *The Journal of biological chemistry* **285**, 3030-3034, doi:10.1074/jbc.M109.050237 (2010).
184 Liu, Q. *et al.* Chk1 is an essential kinase that is regulated by Atr and required for the G(2)/M DNA damage checkpoint. *Genes & development* **14**, 1448-1459 (2000).
185 Niida, H., Katsuno, Y., Banerjee, B., Hande, M. P. & Nakanishi, M. Specific role of Chk1 phosphorylations in cell survival and checkpoint activation. *Molecular and cellular biology* **27**, 2572-2581, doi:10.1128/MCB.01611-06 (2007).
186 Yoshizawa-Sugata, N. & Masai, H. Human Tim/Timeless-interacting protein, Tipin, is required for efficient progression of S phase and DNA replication checkpoint. *The Journal of biological chemistry* **282**, 2729-2740, doi:10.1074/jbc.M605596200 (2007).
187 Witosch, J., Wolf, E. & Mizuno, N. Architecture and ssDNA interaction of the Timeless-Tipin-RPA complex. *Nucleic acids research* **42**, 12912-12927, doi:10.1093/nar/gku960 (2014).
188 Engelen, E. *et al.* Mammalian TIMELESS is involved in period determination and DNA damage-dependent phase advancing of the circadian clock. *PloS one* **8**, e56623, doi:10.1371/journal.pone.0056623 (2013).
189 Kemp, M. G. *et al.* Tipin-replication protein A interaction mediates Chk1 phosphorylation by ATR in response to genotoxic stress. *The Journal of biological chemistry* **285**, 16562-16571, doi:10.1074/jbc.M110.110304 (2010).
190 Sercin, O. & Kemp, M. G. Characterization of functional domains in human Claspin. *Cell cycle* **10**, 1599-1606, doi:10.4161/cc.10.10.15562 (2011).
191 Yang, X. H., Shiotani, B., Classon, M. & Zou, L. Chk1 and Claspin potentiate PCNA ubiquitination. *Genes & development* **22**, 1147-1152, doi:10.1101/gad.1632808 (2008).
192 Yang, X. H. & Zou, L. Dual functions of DNA replication forks in checkpoint signaling and PCNA ubiquitination. *Cell cycle* **8**, 191-194, doi:10.4161/cc.8.2.7357 (2009).
193 Xie, S. *et al.* Timeless Interacts with PARP-1 to Promote Homologous Recombination Repair. *Molecular cell* **60**, 163-176, doi:10.1016/j.molcel.2015.07.031 (2015).
194 Young, L. M. *et al.* TIMELESS Forms a Complex with PARP1 Distinct from Its Complex with TIPIN and Plays a Role in the DNA Damage Response. *Cell reports* **13**, 451-459, doi:10.1016/j.celrep.2015.09.017 (2015).
195 Fu, L. & Lee, C. C. The circadian clock: pacemaker and tumour suppressor. *Nature reviews. Cancer* **3**, 350-361, doi:10.1038/nrc1072 (2003).
196 Lamont, E. W., James, F. O., Boivin, D. B. & Cermakian, N. From circadian clock gene expression to pathologies. *Sleep medicine* **8**, 547-556, doi:10.1016/j.sleep.2006.11.002 (2007).

197 Hansen, J. Increased breast cancer risk among women who work predominantly at night. *Epidemiology* **12**, 74-77 (2001).
198 Buja, A. *et al.* Cancer incidence among female flight attendants: a meta-analysis of published data. *Journal of women's health* **15**, 98-105, doi:10.1089/jwh.2006.15.98 (2006).
199 Mormont, M. C. *et al.* Marked 24-h rest/activity rhythms are associated with better quality of life, better response, and longer survival in patients with metastatic colorectal cancer and good performance status. *Clinical cancer research : an official journal of the American Association for Cancer Research* **6**, 3038-3045 (2000).
200 Sephton, S. E., Sapolsky, R. M., Kraemer, H. C. & Spiegel, D. Diurnal cortisol rhythm as a predictor of breast cancer survival. *Journal of the National Cancer Institute* **92**, 994-1000 (2000).
201 Rafnsson, V., Tulinius, H., Jonasson, J. G. & Hrafnkelsson, J. Risk of breast cancer in female flight attendants: a population-based study (Iceland). *Cancer causes & control : CCC* **12**, 95-101 (2001).
202 Altman, B. J. *et al.* MYC Disrupts the Circadian Clock and Metabolism in Cancer Cells. *Cell metabolism* **22**, 1009-1019, doi:10.1016/j.cmet.2015.09.003 (2015).
203 Kiessling, S. *et al.* Enhancing circadian clock function in cancer cells inhibits tumor growth. *BMC biology* **15**, 13, doi:10.1186/s12915-017-0349-7 (2017).
204 Yoshida, K. *et al.* TIMELESS is overexpressed in lung cancer and its expression correlates with poor patient survival. *Cancer science* **104**, 171-177, doi:10.1111/cas.12068 (2013).
205 Mao, Y. *et al.* Potential cancer-related role of circadian gene TIMELESS suggested by expression profiling and in vitro analyses. *BMC cancer* **13**, 498, doi:10.1186/1471-2407-13-498 (2013).
206 Zhang, W. *et al.* Aberrant TIMELESS expression is associated with poor clinical survival and lymph node metastasis in early-stage cervical carcinoma. *International journal of oncology* **50**, 173-184, doi:10.3892/ijo.2016.3784 (2017).
207 Chi, L. *et al.* TIMELESS contributes to the progression of breast cancer through activation of MYC. *Breast cancer research : BCR* **19**, 53, doi:10.1186/s13058-017-0838-1 (2017).
208 Elgohary, N. *et al.* Protumorigenic role of Timeless in hepatocellular carcinoma. *International journal of oncology* **46**, 597-606, doi:10.3892/ijo.2014.2751 (2015).
209 Yang, M. Y. *et al.* Up-regulation of PER3 Expression Is Correlated with Better Clinical Outcome in Acute Leukemia. *Anticancer research* **35**, 6615-6622 (2015).
210 Mazzoccoli, G. *et al.* Clock gene expression levels and relationship with clinical and pathological features in colorectal cancer patients. *Chronobiology international* **28**, 841-851, doi:10.3109/07420528.2011.615182 (2011).
211 Liu, S. L. *et al.* TIMELESS confers cisplatin resistance in nasopharyngeal carcinoma by activating the Wnt/beta-catenin signaling pathway and promoting the epithelial mesenchymal transition. *Cancer letters* **402**, 117-130, doi:10.1016/j.canlet.2017.05.022 (2017).
212 Tozlu-Kara, S. *et al.* Oligonucleotide microarray analysis of estrogen receptor alpha-positive postmenopausal breast carcinomas: identification of HRPAP20 and TIMELESS as outstanding candidate markers to predict the response to tamoxifen. *Journal of molecular endocrinology* **39**, 305-318, doi:10.1677/JME-07-0001 (2007).
213 Schepeler, T. *et al.* A high resolution genomic portrait of bladder cancer: correlation between genomic aberrations and the DNA damage response. *Oncogene* **32**, 3577-3586, doi:10.1038/onc.2012.381 (2013).
214 Kawada, M., Fukazawa, H., Mizuno, S. & Uehara, Y. Inhibition of anchorage-independent growth of ras-transformed cells on polyHEMA surface by antisense oligodeoxynucleotides directed against K-ras. *Biochemical and biophysical research communications* **231**, 735-737, doi:10.1006/bbrc.1997.6179 (1997).
215 Xu, L. H. *et al.* The focal adhesion kinase suppresses transformation-associated, anchorage-independent apoptosis in human breast cancer cells. Involvement of death receptor-related signaling pathways. *The Journal of biological chemistry* **275**, 30597-30604, doi:10.1074/jbc.M910027199 (2000).
216 Reszka, E. & Przybek, M. Circadian Genes in Breast Cancer. *Advances in clinical chemistry* **75**, 53-70, doi:10.1016/bs.acc.2016.03.005 (2016).
217 Fu, A. *et al.* Genetic and epigenetic associations of circadian gene TIMELESS and breast cancer risk. *Molecular carcinogenesis* **51**, 923-929, doi:10.1002/mc.20862 (2012).
218 Wiegering, A. *et al.* Targeting Translation Initiation Bypasses Signaling Crosstalk Mechanisms

That Maintain High MYC Levels in Colorectal Cancer. *Cancer discovery* **5**, 768-781, doi:10.1158/2159-8290.CD-14-1040 (2015).

219 Kandel, E. S. *et al.* Activation of Akt/protein kinase B overcomes a G(2)/m cell cycle checkpoint induced by DNA damage. *Molecular and cellular biology* **22**, 7831-7841 (2002).

220 Katayama, K., Fujita, N. & Tsuruo, T. Akt/protein kinase B-dependent phosphorylation and inactivation of WEE1Hu promote cell cycle progression at G2/M transition. *Molecular and cellular biology* **25**, 5725-5737, doi:10.1128/MCB.25.13.5725-5737.2005 (2005).

221 Tang, D. *et al.* ERK activation mediates cell cycle arrest and apoptosis after DNA damage independently of p53. *The Journal of biological chemistry* **277**, 12710-12717, doi:10.1074/jbc.M111598200 (2002).

222 Li, P. *et al.* P90 RSK arranges Chk1 in the nucleus for monitoring of genomic integrity during cell proliferation. *Molecular biology of the cell* **23**, 1582-1592, doi:10.1091/mbc.E11-10-0883 (2012).

223 Green, C. B. Time for chronotherapy? Clock genes dictate sensitivity to cyclophosphamide. *Proceedings of the National Academy of Sciences of the United States of America* **102**, 3529-3530, doi:10.1073/pnas.0500552102 (2005).

224 Mormont, M. C. & Levi, F. Cancer chronotherapy: principles, applications, and perspectives. *Cancer* **97**, 155-169, doi:10.1002/cncr.11040 (2003).

225 Vincenzi, B., Santini, D., La Cesa, A. & Tonini, G. Cancer chronotherapy: principles, applications, and perspectives. *Cancer* **98**, 881-882; author reply 882-883, doi:10.1002/cncr.11600 (2003).

226 Gori, F. & Demay, M. B. BIG-3, a novel WD-40 repeat protein, is expressed in the developing growth plate and accelerates chondrocyte differentiation in vitro. *Endocrinology* **145**, 1050-1054, doi:10.1210/en.2003-1314 (2004).

227 Gori, F., Divieti, P. & Demay, M. B. Cloning and characterization of a novel WD-40 repeat protein that dramatically accelerates osteoblastic differentiation. *The Journal of biological chemistry* **276**, 46515-46522, doi:10.1074/jbc.M105757200 (2001).

228 Dias, J. *et al.* Structural analysis of the KANSL1/WDR5/KANSL2 complex reveals that WDR5 is required for efficient assembly and chromatin targeting of the NSL complex. *Genes & development* **28**, 929-942, doi:10.1101/gad.240200.114 (2014).

229 Ruthenburg, A. J. *et al.* Histone H3 recognition and presentation by the WDR5 module of the MLL1 complex. *Nature structural & molecular biology* **13**, 704-712, doi:10.1038/nsmb1119 (2006).

230 Dou, Y. *et al.* Regulation of MLL1 H3K4 methyltransferase activity by its core components. *Nature structural & molecular biology* **13**, 713-719, doi:10.1038/nsmb1128 (2006).

231 Couture, J. F., Collazo, E. & Trievel, R. C. Molecular recognition of histone H3 by the WD40 protein WDR5. *Nature structural & molecular biology* **13**, 698-703, doi:10.1038/nsmb1116 (2006).

232 Han, Z. *et al.* Structural basis for the specific recognition of methylated histone H3 lysine 4 by the WD-40 protein WDR5. *Molecular cell* **22**, 137-144, doi:10.1016/j.molcel.2006.03.018 (2006).

233 Ang, Y. S. *et al.* Wdr5 mediates self-renewal and reprogramming via the embryonic stem cell core transcriptional network. *Cell* **145**, 183-197, doi:10.1016/j.cell.2011.03.003 (2011).

234 Yang, Y. W. *et al.* Essential role of lncRNA binding for WDR5 maintenance of active chromatin and embryonic stem cell pluripotency. *eLife* **3**, e02046, doi:10.7554/eLife.02046 (2014).

235 Wysocka, J. *et al.* WDR5 associates with histone H3 methylated at K4 and is essential for H3 K4 methylation and vertebrate development. *Cell* **121**, 859-872, doi:10.1016/j.cell.2005.03.036 (2005).

236 Migliori, V., Mapelli, M. & Guccione, E. On WD40 proteins: propelling our knowledge of transcriptional control? *Epigenetics* **7**, 815-822, doi:10.4161/epi.21140 (2012).

237 Wysocka, J. *et al.* A PHD finger of NURF couples histone H3 lysine 4 trimethylation with chromatin remodelling. *Nature* **442**, 86-90, doi:10.1038/nature04815 (2006).

238 Wang, K. C. *et al.* A long noncoding RNA maintains active chromatin to coordinate homeotic gene expression. *Nature* **472**, 120-124, doi:10.1038/nature09819 (2011).

239 Xu, Z. *et al.* Synergistic effect of SRY and its direct target, WDR5, on Sox9 expression. *PloS one* **7**, e34327, doi:10.1371/journal.pone.0034327 (2012).

240 Shilatifard, A. The COMPASS family of histone H3K4 methylases: mechanisms of regulation in development and disease pathogenesis. *Annual review of biochemistry* **81**, 65-95,

doi:10.1146/annurev-biochem-051710-134100 (2012).
241 Ford, D. J. & Dingwall, A. K. The cancer COMPASS: navigating the functions of MLL complexes in cancer. *Cancer genetics* **208**, 178-191, doi:10.1016/j.cancergen.2015.01.005 (2015).
242 Yang, W. & Ernst, P. Distinct functions of histone H3, lysine 4 methyltransferases in normal and malignant hematopoiesis. *Current opinion in hematology* **24**, 322-328, doi:10.1097/MOH.0000000000000346 (2017).
243 Risner, L. E. *et al.* Functional specificity of CpG DNA-binding CXXC domains in mixed lineage leukemia. *The Journal of biological chemistry* **288**, 29901-29910, doi:10.1074/jbc.M113.474858 (2013).
244 Bach, C., Mueller, D., Buhl, S., Garcia-Cuellar, M. P. & Slany, R. K. Alterations of the CxxC domain preclude oncogenic activation of mixed-lineage leukemia 2. *Oncogene* **28**, 815-823, doi:10.1038/onc.2008.443 (2009).
245 Chen, Y. *et al.* MLL2, Not MLL1, Plays a Major Role in Sustaining MLL-Rearranged Acute Myeloid Leukemia. *Cancer cell* **31**, 755-770 e756, doi:10.1016/j.ccell.2017.05.002 (2017).
246 Lee, J. E. *et al.* H3K4 mono- and di-methyltransferase MLL4 is required for enhancer activation during cell differentiation. *eLife* **2**, e01503, doi:10.7554/eLife.01503 (2013).
247 Hu, D. *et al.* The MLL3/MLL4 branches of the COMPASS family function as major histone H3K4 monomethylases at enhancers. *Molecular and cellular biology* **33**, 4745-4754, doi:10.1128/MCB.01181-13 (2013).
248 Wang, C. *et al.* Enhancer priming by H3K4 methyltransferase MLL4 controls cell fate transition. *Proceedings of the National Academy of Sciences of the United States of America* **113**, 11871-11876, doi:10.1073/pnas.1606857113 (2016).
249 Chen, C. *et al.* MLL3 is a haploinsufficient 7q tumor suppressor in acute myeloid leukemia. *Cancer cell* **25**, 652-665, doi:10.1016/j.ccr.2014.03.016 (2014).
250 Santos, M. A. *et al.* DNA-damage-induced differentiation of leukaemic cells as an anti-cancer barrier. *Nature* **514**, 107-111, doi:10.1038/nature13483 (2014).
251 Chauhan, C., Zraly, C. B. & Dingwall, A. K. The Drosophila COMPASS-like Cmi-Trr coactivator complex regulates dpp/BMP signaling in pattern formation. *Developmental biology* **380**, 185-198, doi:10.1016/j.ydbio.2013.05.018 (2013).
252 Kanda, H., Nguyen, A., Chen, L., Okano, H. & Hariharan, I. K. The Drosophila ortholog of MLL3 and MLL4, trithorax related, functions as a negative regulator of tissue growth. *Molecular and cellular biology* **33**, 1702-1710, doi:10.1128/MCB.01585-12 (2013).
253 Goo, Y. H. *et al.* Activating signal cointegrator 2 belongs to a novel steady-state complex that contains a subset of trithorax group proteins. *Molecular and cellular biology* **23**, 140-149 (2003).
254 Mo, R., Rao, S. M. & Zhu, Y. J. Identification of the MLL2 complex as a coactivator for estrogen receptor alpha. *The Journal of biological chemistry* **281**, 15714-15720, doi:10.1074/jbc.M513245200 (2006).
255 Bledau, A. S. *et al.* The H3K4 methyltransferase Setd1a is first required at the epiblast stage, whereas Setd1b becomes essential after gastrulation. *Development* **141**, 1022-1035, doi:10.1242/dev.098152 (2014).
256 Li, Y. *et al.* Setd1a and NURF mediate chromatin dynamics and gene regulation during erythroid lineage commitment and differentiation. *Nucleic acids research* **44**, 7173-7188, doi:10.1093/nar/gkw327 (2016).
257 Ziemin-van der Poel, S. *et al.* Identification of a gene, MLL, that spans the breakpoint in 11q23 translocations associated with human leukemias. *Proceedings of the National Academy of Sciences of the United States of America* **88**, 10735-10739 (1991).
258 Bolouri, H. *et al.* The molecular landscape of pediatric acute myeloid leukemia reveals recurrent structural alterations and age-specific mutational interactions. *Nature medicine*, doi:10.1038/nm.4439 (2017).
259 Meyer, C. *et al.* The MLL recombinome of acute leukemias in 2017. *Leukemia*, doi:10.1038/leu.2017.213 (2017).
260 Weirich, S., Kudithipudi, S. & Jeltsch, A. Somatic cancer mutations in the MLL1 histone methyltransferase modulate its enzymatic activity and dependence on the WDR5/RBBP5/ASH2L complex. *Molecular oncology* **11**, 373-387, doi:10.1002/1878-0261.12041 (2017).
261 de Boer, J., Walf-Vorderwulbecke, V. & Williams, O. In focus: MLL-rearranged leukemia. *Leukemia* **27**, 1224-1228, doi:10.1038/leu.2013.78 (2013).

262 Xu, J. *et al.* MLL1 and MLL1 fusion proteins have distinct functions in regulating leukemic transcription program. *Cell discovery* **2**, 16008, doi:10.1038/celldisc.2016.8 (2016).

263 Dawkins, J. B. *et al.* Reduced Expression of Histone Methyltransferases KMT2C and KMT2D Correlates with Improved Outcome in Pancreatic Ductal Adenocarcinoma. *Cancer research* **76**, 4861-4871, doi:10.1158/0008-5472.CAN-16-0481 (2016).

264 Guo, C. *et al.* KMT2D maintains neoplastic cell proliferation and global histone H3 lysine 4 monomethylation. *Oncotarget* **4**, 2144-2153, doi:10.18632/oncotarget.1555 (2013).

265 Zhang, C. *et al.* KMT2A promotes melanoma cell growth by targeting hTERT signaling pathway. *Cell death & disease* **8**, e2940, doi:10.1038/cddis.2017.285 (2017).

266 Esposito, M. T. *et al.* Synthetic lethal targeting of oncogenic transcription factors in acute leukemia by PARP inhibitors. *Nature medicine* **21**, 1481-1490, doi:10.1038/nm.3993 (2015).

267 Toska, E. *et al.* PI3K pathway regulates ER-dependent transcription in breast cancer through the epigenetic regulator KMT2D. *Science* **355**, 1324-1330, doi:10.1126/science.aah6893 (2017).

268 Kim, J. Y. *et al.* A role for WDR5 in integrating threonine 11 phosphorylation to lysine 4 methylation on histone H3 during androgen signaling and in prostate cancer. *Molecular cell* **54**, 613-625, doi:10.1016/j.molcel.2014.03.043 (2014).

269 Malik, R. *et al.* Targeting the MLL complex in castration-resistant prostate cancer. *Nature medicine* **21**, 344-352, doi:10.1038/nm.3830 (2015).

270 Lu, Y. W. *et al.* Colorectal Cancer Genetic Heterogeneity Delineated by Multi-Region Sequencing. *PloS one* **11**, e0152673, doi:10.1371/journal.pone.0152673 (2016).

271 Mouradov, D. *et al.* Colorectal cancer cell lines are representative models of the main molecular subtypes of primary cancer. *Cancer research* **74**, 3238-3247, doi:10.1158/0008-5472.CAN-14-0013 (2014).

272 Benayoun, B. A. *et al.* H3K4me3 breadth is linked to cell identity and transcriptional consistency. *Cell* **158**, 673-688, doi:10.1016/j.cell.2014.06.027 (2014).

273 Chen, K. *et al.* Broad H3K4me3 is associated with increased transcription elongation and enhancer activity at tumor-suppressor genes. *Nature genetics* **47**, 1149-1157, doi:10.1038/ng.3385 (2015).

274 Ali, A., Veeranki, S. N., Chinchole, A. & Tyagi, S. MLL/WDR5 Complex Regulates Kif2A Localization to Ensure Chromosome Congression and Proper Spindle Assembly during Mitosis. *Developmental cell* **41**, 605-622 e607, doi:10.1016/j.devcel.2017.05.023 (2017).

275 Kantidakis, T. *et al.* Mutation of cancer driver MLL2 results in transcription stress and genome instability. *Genes & development* **30**, 408-420, doi:10.1101/gad.275453.115 (2016).

276 Thompson, B. A., Tremblay, V., Lin, G. & Bochar, D. A. CHD8 is an ATP-dependent chromatin remodeling factor that regulates beta-catenin target genes. *Molecular and cellular biology* **28**, 3894-3904, doi:10.1128/MCB.00322-08 (2008).

277 Suganuma, T. *et al.* ATAC is a double histone acetyltransferase complex that stimulates nucleosome sliding. *Nature structural & molecular biology* **15**, 364-372, doi:10.1038/nsmb.1397 (2008).

278 Wang, Y. L., Faiola, F., Xu, M., Pan, S. & Martinez, E. Human ATAC Is a GCN5/PCAF-containing acetylase complex with a novel NC2-like histone fold module that interacts with the TATA-binding protein. *The Journal of biological chemistry* **283**, 33808-33815, doi:10.1074/jbc.M806936200 (2008).

279 Mendjan, S. *et al.* Nuclear pore components are involved in the transcriptional regulation of dosage compensation in Drosophila. *Molecular cell* **21**, 811-823, doi:10.1016/j.molcel.2006.02.007 (2006).

280 Brown, S. A. *et al.* PERIOD1-associated proteins modulate the negative limb of the mammalian circadian oscillator. *Science* **308**, 693-696, doi:10.1126/science.1107373 (2005).

281 Migliori, V. *et al.* Symmetric dimethylation of H3R2 is a newly identified histone mark that supports euchromatin maintenance. *Nature structural & molecular biology* **19**, 136-144, doi:10.1038/nsmb.2209 (2012).

282 Thomas, L. R. *et al.* Interaction with WDR5 promotes target gene recognition and tumorigenesis by MYC. *Molecular cell* **58**, 440-452, doi:10.1016/j.molcel.2015.02.028 (2015).

283 Thomas, L. R., Foshage, A. M., Weissmiller, A. M. & Tansey, W. P. The MYC-WDR5 Nexus and Cancer. *Cancer research* **75**, 4012-4015, doi:10.1158/0008-5472.CAN-15-1216 (2015).

284 Sun, Y. *et al.* WDR5 Supports an N-Myc Transcriptional Complex That Drives a Protumorigenic Gene Expression Signature in Neuroblastoma. *Cancer research* **75**, 5143-5154, doi:10.1158/0008-

5472.CAN-15-0423 (2015).
285 Ullius, A. *et al.* The interaction of MYC with the trithorax protein ASH2L promotes gene transcription by regulating H3K27 modification. *Nucleic acids research* **42**, 6901-6920, doi:10.1093/nar/gku312 (2014).
286 Lorenzin, F. *et al.* Different promoter affinities account for specificity in MYC-dependent gene regulation. *eLife* **5**, doi:10.7554/eLife.15161 (2016).
287 Carugo, A. *et al.* In Vivo Functional Platform Targeting Patient-Derived Xenografts Identifies WDR5-Myc Association as a Critical Determinant of Pancreatic Cancer. *Cell reports* **16**, 133-147, doi:10.1016/j.celrep.2016.05.063 (2016).
288 Blumenthal, D. T. *et al.* Clinical utility and treatment outcome of comprehensive genomic profiling in high grade glioma patients. *Journal of neuro-oncology* **130**, 211-219, doi:10.1007/s11060-016-2237-3 (2016).
289 Bailey, J. K. *et al.* WD repeat-containing protein 5 (WDR5) localizes to the midbody and regulates abscission. *The Journal of biological chemistry* **290**, 8987-9001, doi:10.1074/jbc.M114.623611 (2015).
290 Sun, W., Guo, F. & Liu, M. Up-regulated WDR5 promotes gastric cancer formation by induced cyclin D1 expression. *Journal of cellular biochemistry*, doi:10.1002/jcb.26491 (2017).
291 Dai, X. *et al.* WDR5 Expression Is Prognostic of Breast Cancer Outcome. *PloS one* **10**, e0124964, doi:10.1371/journal.pone.0124964 (2015).
292 Ge, Z. *et al.* WDR5 high expression and its effect on tumorigenesis in leukemia. *Oncotarget* **7**, 37740-37754, doi:10.18632/oncotarget.9312 (2016).
293 Chen, X. *et al.* Upregulated WDR5 promotes proliferation, self-renewal and chemoresistance in bladder cancer via mediating H3K4 trimethylation. *Scientific reports* **5**, 8293, doi:10.1038/srep08293 (2015).
294 Quagliata, L. *et al.* Long noncoding RNA HOTTIP/HOXA13 expression is associated with disease progression and predicts outcome in hepatocellular carcinoma patients. *Hepatology* **59**, 911-923, doi:10.1002/hep.26740 (2014).
295 Mungamuri, S. K., Murk, W., Grumolato, L., Bernstein, E. & Aaronson, S. A. Chromatin modifications sequentially enhance ErbB2 expression in ErbB2-positive breast cancers. *Cell reports* **5**, 302-313, doi:10.1016/j.celrep.2013.09.009 (2013).
296 Yoshimaru, T. *et al.* Targeting BIG3-PHB2 interaction to overcome tamoxifen resistance in breast cancer cells. *Nature communications* **4**, 2443, doi:10.1038/ncomms3443 (2013).
297 Cheng, Y., Jutooru, I., Chadalapaka, G., Corton, J. C. & Safe, S. The long non-coding RNA HOTTIP enhances pancreatic cancer cell proliferation, survival and migration. *Oncotarget* **6**, 10840-10852, doi:10.18632/oncotarget.3450 (2015).
298 Wu, M. Z. *et al.* Interplay between HDAC3 and WDR5 is essential for hypoxia-induced epithelial-mesenchymal transition. *Molecular cell* **43**, 811-822, doi:10.1016/j.molcel.2011.07.012 (2011).
299 Tan, X. *et al.* PI3K/AKT-mediated upregulation of WDR5 promotes colorectal cancer metastasis by directly targeting ZNF407. *Cell death & disease* **8**, e2686, doi:10.1038/cddis.2017.111 (2017).
300 Chung, C. Y. *et al.* Cbx8 Acts Non-canonically with Wdr5 to Promote Mammary Tumorigenesis. *Cell reports* **16**, 472-486, doi:10.1016/j.celrep.2016.06.002 (2016).
301 Malek, R. *et al.* TWIST1-WDR5-Hottip Regulates Hoxa9 Chromatin to Facilitate Prostate Cancer Metastasis. *Cancer research* **77**, 3181-3193, doi:10.1158/0008-5472.CAN-16-2797 (2017).
302 Fu, Z. *et al.* LncRNA HOTTIP modulates cancer stem cell properties in human pancreatic cancer by regulating HOXA9. *Cancer letters* **410**, 68-81, doi:10.1016/j.canlet.2017.09.019 (2017).
303 Lin, C. *et al.* Transcriptional and posttranscriptional regulation of HOXA13 by lncRNA HOTTIP facilitates tumorigenesis and metastasis in esophageal squamous carcinoma cells. *Oncogene* **36**, 5392-5406, doi:10.1038/onc.2017.133 (2017).
304 Chang, S. *et al.* HOTTIP and HOXA13 are oncogenes associated with gastric cancer progression. *Oncology reports* **35**, 3577-3585, doi:10.3892/or.2016.4743 (2016).
305 Kim, K. *et al.* Gene dysregulation by histone variant H2A.Z in bladder cancer. *Epigenetics & chromatin* **6**, 34, doi:10.1186/1756-8935-6-34 (2013).
306 Chen, X. *et al.* Gene expression profiling of WDR5 regulated genes in bladder cancer. *Genomics data* **5**, 27-29, doi:10.1016/j.gdata.2015.05.003 (2015).
307 Sun, T. T. *et al.* LncRNA GClnc1 Promotes Gastric Carcinogenesis and May Act as a Modular Scaffold of WDR5 and KAT2A Complexes to Specify the Histone Modification Pattern. *Cancer*

discovery **6**, 784-801, doi:10.1158/2159-8290.CD-15-0921 (2016).
308 Dharmarajan, V., Lee, J. H., Patel, A., Skalnik, D. G. & Cosgrove, M. S. Structural basis for WDR5 interaction (Win) motif recognition in human SET1 family histone methyltransferases. *The Journal of biological chemistry* **287**, 27275-27289, doi:10.1074/jbc.M112.364125 (2012).
309 Patel, A., Dharmarajan, V. & Cosgrove, M. S. Structure of WDR5 bound to mixed lineage leukemia protein-1 peptide. *The Journal of biological chemistry* **283**, 32158-32161, doi:10.1074/jbc.C800164200 (2008).
310 Schuetz, A. *et al.* Structural basis for molecular recognition and presentation of histone H3 by WDR5. *The EMBO journal* **25**, 4245-4252, doi:10.1038/sj.emboj.7601316 (2006).
311 Karatas, H. *et al.* Discovery of a Highly Potent, Cell-Permeable Macrocyclic Peptidomimetic (MM-589) Targeting the WD Repeat Domain 5 Protein (WDR5)-Mixed Lineage Leukemia (MLL) Protein-Protein Interaction. *Journal of medicinal chemistry* **60**, 4818-4839, doi:10.1021/acs.jmedchem.6b01796 (2017).
312 Karatas, H., Townsend, E. C., Bernard, D., Dou, Y. & Wang, S. Analysis of the binding of mixed lineage leukemia 1 (MLL1) and histone 3 peptides to WD repeat domain 5 (WDR5) for the design of inhibitors of the MLL1-WDR5 interaction. *Journal of medicinal chemistry* **53**, 5179-5185, doi:10.1021/jm100139b (2010).
313 Karatas, H. *et al.* High-affinity, small-molecule peptidomimetic inhibitors of MLL1/WDR5 protein-protein interaction. *Journal of the American Chemical Society* **135**, 669-682, doi:10.1021/ja306028q (2013).
314 Alicea-Velazquez, N. L. *et al.* Targeted Disruption of the Interaction between WD-40 Repeat Protein 5 (WDR5) and Mixed Lineage Leukemia (MLL)/SET1 Family Proteins Specifically Inhibits MLL1 and SETd1A Methyltransferase Complexes. *The Journal of biological chemistry* **291**, 22357-22372, doi:10.1074/jbc.M116.752626 (2016).
315 Li, D. D. *et al.* Structure-based design of ester compounds to inhibit MLL complex catalytic activity by targeting mixed lineage leukemia 1 (MLL1)-WDR5 interaction. *Bioorganic & medicinal chemistry* **24**, 6109-6118, doi:10.1016/j.bmc.2016.09.073 (2016).
316 Senisterra, G. *et al.* Small-molecule inhibition of MLL activity by disruption of its interaction with WDR5. *The Biochemical journal* **449**, 151-159, doi:10.1042/BJ20121280 (2013).
317 Bolshan, Y. *et al.* Synthesis, Optimization, and Evaluation of Novel Small Molecules as Antagonists of WDR5-MLL Interaction. *ACS medicinal chemistry letters* **4**, 353-357, doi:10.1021/ml300467n (2013).
318 Cao, F. *et al.* Targeting MLL1 H3K4 methyltransferase activity in mixed-lineage leukemia. *Molecular cell* **53**, 247-261, doi:10.1016/j.molcel.2013.12.001 (2014).
319 Getlik, M. *et al.* Structure-Based Optimization of a Small Molecule Antagonist of the Interaction Between WD Repeat-Containing Protein 5 (WDR5) and Mixed-Lineage Leukemia 1 (MLL1). *Journal of medicinal chemistry* **59**, 2478-2496, doi:10.1021/acs.jmedchem.5b01630 (2016).
320 Li, D. D. *et al.* Structure-based design and synthesis of small molecular inhibitors disturbing the interaction of MLL1-WDR5. *European journal of medicinal chemistry* **118**, 1-8, doi:10.1016/j.ejmech.2016.04.032 (2016).
321 Grebien, F. *et al.* Pharmacological targeting of the Wdr5-MLL interaction in C/EBPalpha N-terminal leukemia. *Nature chemical biology* **11**, 571-578, doi:10.1038/nchembio.1859 (2015).
322 Jiang, P., Du, W., Mancuso, A., Wellen, K. E. & Yang, X. Reciprocal regulation of p53 and malic enzymes modulates metabolism and senescence. *Nature* **493**, 689-693, doi:10.1038/nature11776 (2013).
323 Lu, F. *et al.* Regulation of DNA replication and chromosomal polyploidy by the MLL-WDR5-RBBP5 methyltransferases. *Biology open* **5**, 1449-1460, doi:10.1242/bio.019729 (2016).
324 De Haro, L. P. *et al.* Metnase promotes restart and repair of stalled and collapsed replication forks. *Nucleic acids research* **38**, 5681-5691, doi:10.1093/nar/gkq339 (2010).
325 Vaughn, C. P., Zobell, S. D., Furtado, L. V., Baker, C. L. & Samowitz, W. S. Frequency of KRAS, BRAF, and NRAS mutations in colorectal cancer. *Genes Chromosomes Cancer* **50**, 307-312, doi:10.1002/gcc.20854 (2011).
326 Ciombor, K. K., Wu, C. & Goldberg, R. M. Recent therapeutic advances in the treatment of colorectal cancer. *Annual review of medicine* **66**, 83-95, doi:10.1146/annurev-med-051513-102539 (2015).
327 Dolinski, K. & Botstein, D. Orthology and functional conservation in eukaryotes. *Annual review*

of genetics **41**, 465-507, doi:10.1146/annurev.genet.40.110405.090439 (2007).
328 Chuang, H. C., Chou, C. C., Kulp, S. K. & Chen, C. S. AMPK as a potential anticancer target - friend or foe? *Current pharmaceutical design* **20**, 2607-2618 (2014).
329 Hardie, D. G., Carling, D. & Gamblin, S. J. AMP-activated protein kinase: also regulated by ADP? *Trends in biochemical sciences* **36**, 470-477, doi:10.1016/j.tibs.2011.06.004 (2011).
330 Jeon, S. M., Chandel, N. S. & Hay, N. AMPK regulates NADPH homeostasis to promote tumour cell survival during energy stress. *Nature* **485**, 661-665, doi:10.1038/nature11066 (2012).
331 Faubert, B. *et al.* AMPK is a negative regulator of the Warburg effect and suppresses tumor growth in vivo. *Cell metabolism* **17**, 113-124, doi:10.1016/j.cmet.2012.12.001 (2013).
332 Hardie, D. G. The LKB1-AMPK pathway-friend or foe in cancer? *Cancer cell* **23**, 131-132, doi:10.1016/j.ccr.2013.01.009 (2013).
333 Zhou, G. *et al.* Role of AMP-activated protein kinase in mechanism of metformin action. *The Journal of clinical investigation* **108**, 1167-1174, doi:10.1172/JCI13505 (2001).
334 Laderoute, K. R. *et al.* 5'-AMP-activated protein kinase (AMPK) is induced by low-oxygen and glucose deprivation conditions found in solid-tumor microenvironments. *Molecular and cellular biology* **26**, 5336-5347, doi:10.1128/MCB.00166-06 (2006).
335 Gwinn, D. M. *et al.* AMPK phosphorylation of raptor mediates a metabolic checkpoint. *Molecular cell* **30**, 214-226, doi:10.1016/j.molcel.2008.03.003 (2008).
336 Kim, J., Kundu, M., Viollet, B. & Guan, K. L. AMPK and mTOR regulate autophagy through direct phosphorylation of Ulk1. *Nature cell biology* **13**, 132-141, doi:10.1038/ncb2152 (2011).
337 Ng, T. L. *et al.* The AMPK stress response pathway mediates anoikis resistance through inhibition of mTOR and suppression of protein synthesis. *Cell death and differentiation* **19**, 501-510, doi:10.1038/cdd.2011.119 (2012).
338 Zadra, G., Batista, J. L. & Loda, M. Dissecting the Dual Role of AMPK in Cancer: From Experimental to Human Studies. *Molecular cancer research : MCR* **13**, 1059-1072, doi:10.1158/1541-7786.MCR-15-0068 (2015).
339 Pineda, C. T. *et al.* Degradation of AMPK by a cancer-specific ubiquitin ligase. *Cell* **160**, 715-728, doi:10.1016/j.cell.2015.01.034 (2015).
340 Sanduja, S. *et al.* AMPK promotes tolerance to Ras pathway inhibition by activating autophagy. *Oncogene*, doi:10.1038/onc.2016.70 (2016).
341 Decensi, A. *et al.* Metformin and cancer risk in diabetic patients: a systematic review and meta-analysis. *Cancer prevention research* **3**, 1451-1461, doi:10.1158/1940-6207.CAPR-10-0157 (2010).
342 Evans, J. M., Donnelly, L. A., Emslie-Smith, A. M., Alessi, D. R. & Morris, A. D. Metformin and reduced risk of cancer in diabetic patients. *Bmj* **330**, 1304-1305, doi:10.1136/bmj.38415.708634.F7 (2005).
343 Mehenni, H. *et al.* Loss of LKB1 kinase activity in Peutz-Jeghers syndrome, and evidence for allelic and locus heterogeneity. *American journal of human genetics* **63**, 1641-1650 (1998).
344 Jang, T. *et al.* 5'-AMP-activated protein kinase activity is elevated early during primary brain tumor development in the rat. *International journal of cancer. Journal international du cancer* **128**, 2230-2239, doi:10.1002/ijc.25558 (2011).
345 Kato, K. *et al.* Critical roles of AMP-activated protein kinase in constitutive tolerance of cancer cells to nutrient deprivation and tumor formation. *Oncogene* **21**, 6082-6090, doi:10.1038/sj.onc.1205737 (2002).
346 McCall, J. L. *et al.* KSR1 and EPHB4 regulate Myc and PGC1beta to promote survival of human colon tumor cells. *Molecular and cellular biology*, doi:10.1128/MCB.00087-16 (2016).
347 Yu, P. B. *et al.* Dorsomorphin inhibits BMP signals required for embryogenesis and iron metabolism. *Nature chemical biology* **4**, 33-41, doi:10.1038/nchembio.2007.54 (2008).
348 Stein, S. C., Woods, A., Jones, N. A., Davison, M. D. & Carling, D. The regulation of AMP-activated protein kinase by phosphorylation. *The Biochemical journal* **345 Pt 3**, 437-443 (2000).
349 Hernandez, L. M. *et al.* 4'-N-methyl-5'-hydroxystaurosporine and 5'-hydroxystaurosporine, new indolocarbazole alkaloids from a marine Micromonospora sp. strain. *The Journal of antibiotics* **53**, 895-902 (2000).
350 Tanramluk, D., Schreyer, A., Pitt, W. R. & Blundell, T. L. On the Origins of Enzyme Inhibitor Selectivity and Promiscuity: A Case Study of Protein Kinase Binding to Staurosporine. *Chemical Biology & Drug Design* **74**, 16-24, doi:10.1111/j.1747-0285.2009.00832.x (2009).

351 Gessner, P. K. Isobolographic analysis of interactions: an update on applications and utility. *Toxicology* **105**, 161-179 (1995).
352 Tennakoon, J. B. *et al.* Androgens regulate prostate cancer cell growth via an AMPK-PGC-1alpha-mediated metabolic switch. *Oncogene* **33**, 5251-5261, doi:10.1038/onc.2013.463 (2014).
353 Park, H. U. *et al.* AMP-activated protein kinase promotes human prostate cancer cell growth and survival. *Molecular cancer therapeutics* **8**, 733-741, doi:10.1158/1535-7163.MCT-08-0631 (2009).
354 Hindupur, S. K. *et al.* Identification of a novel AMPK-PEA15 axis in the anoikis-resistant growth of mammary cells. *Breast cancer research : BCR* **16**, 420, doi:10.1186/s13058-014-0420-z (2014).
355 Chen, E. I. *et al.* Adaptation of energy metabolism in breast cancer brain metastases. *Cancer research* **67**, 1472-1486, doi:10.1158/0008-5472.CAN-06-3137 (2007).
356 Frigo, D. E. *et al.* CaM kinase kinase beta-mediated activation of the growth regulatory kinase AMPK is required for androgen-dependent migration of prostate cancer cells. *Cancer research* **71**, 528-537, doi:10.1158/0008-5472.CAN-10-2581 (2011).
357 Takahashi, I., Kobayashi, E., Asano, K., Yoshida, M. & Nakano, H. UCN-01, a selective inhibitor of protein kinase C from Streptomyces. *The Journal of antibiotics* **40**, 1782-1784 (1987).
358 Takahashi, I., Asano, K., Kawamoto, I., Tamaoki, T. & Nakano, H. UCN-01 and UCN-02, new selective inhibitors of protein kinase C. I. Screening, producing organism and fermentation. *The Journal of antibiotics* **42**, 564-570 (1989).
359 Takahashi, I. *et al.* UCN-01 and UCN-02, new selective inhibitors of protein kinase C. II. Purification, physico-chemical properties, structural determination and biological activities. *The Journal of antibiotics* **42**, 571-576 (1989).
360 Sugiyama, K. *et al.* UCN-01 selectively enhances mitomycin C cytotoxicity in p53 defective cells which is mediated through S and/or G(2) checkpoint abrogation. *International journal of cancer. Journal international du cancer* **85**, 703-709 (2000).
361 Kortmansky, J. *et al.* Phase I trial of the cyclin-dependent kinase inhibitor and protein kinase C inhibitor 7-hydroxystaurosporine in combination with Fluorouracil in patients with advanced solid tumors. *Journal of clinical oncology : official journal of the American Society of Clinical Oncology* **23**, 1875-1884, doi:10.1200/JCO.2005.03.116 (2005).
362 Lara, P. N., Jr. *et al.* The cyclin-dependent kinase inhibitor UCN-01 plus cisplatin in advanced solid tumors: a California cancer consortium phase I pharmacokinetic and molecular correlative trial. *Clinical cancer research : an official journal of the American Association for Cancer Research* **11**, 4444-4450, doi:10.1158/1078-0432.CCR-04-2602 (2005).
363 Sampath, D. *et al.* Pharmacodynamics of cytarabine alone and in combination with 7-hydroxystaurosporine (UCN-01) in AML blasts in vitro and during a clinical trial. *Blood* **107**, 2517-2524, doi:10.1182/blood-2005-08-3351 (2006).
364 Edelman, M. J. *et al.* Phase I and pharmacokinetic study of 7-hydroxystaurosporine and carboplatin in advanced solid tumors. *Clinical cancer research : an official journal of the American Association for Cancer Research* **13**, 2667-2674, doi:10.1158/1078-0432.CCR-06-1832 (2007).
365 Marti, G. E. *et al.* Phase I trial of 7-hydroxystaurosporine and fludararbine phosphate: in vivo evidence of 7-hydroxystaurosporine induced apoptosis in chronic lymphocytic leukemia. *Leukemia & lymphoma* **52**, 2284-2292, doi:10.3109/10428194.2011.589547 (2011).
366 Fracasso, P. M. *et al.* A Phase 1 study of UCN-01 in combination with irinotecan in patients with resistant solid tumor malignancies. *Cancer chemotherapy and pharmacology* **67**, 1225-1237, doi:10.1007/s00280-010-1410-1 (2011).
367 Li, T. *et al.* A phase II study of cell cycle inhibitor UCN-01 in patients with metastatic melanoma: a California Cancer Consortium trial. *Investigational new drugs* **30**, 741-748, doi:10.1007/s10637-010-9562-8 (2012).
368 Ma, C. X. *et al.* A phase II study of UCN-01 in combination with irinotecan in patients with metastatic triple negative breast cancer. *Breast cancer research and treatment* **137**, 483-492, doi:10.1007/s10549-012-2378-9 (2013).
369 Bloy, N. *et al.* Trial Watch: Radioimmunotherapy for oncological indications. *Oncoimmunology* **3**, e954929, doi:10.4161/21624011.2014.954929 (2014).
370 Manic, G., Obrist, F., Sistigu, A. & Vitale, I. Trial Watch: Targeting ATM-CHK2 and ATR-

CHK1 pathways for anticancer therapy. *Molecular & cellular oncology* **2**, e1012976, doi:10.1080/23723556.2015.1012976 (2015).

371 Obrist, F., Manic, G., Kroemer, G., Vitale, I. & Galluzzi, L. Trial Watch: Proteasomal inhibitors for anticancer therapy. *Molecular & cellular oncology* **2**, e974463, doi:10.4161/23723556.2014.974463 (2015).

372 Sistigu, A., Manic, G., Obrist, F. & Vitale, I. Trial watch - inhibiting PARP enzymes for anticancer therapy. *Molecular & cellular oncology* **3**, e1053594, doi:10.1080/23723556.2015.1053594 (2016).

373 Taylor, P. & Hardin, P. E. Rhythmic E-box binding by CLK-CYC controls daily cycles in per and tim transcription and chromatin modifications. *Molecular and cellular biology* **28**, 4642-4652, doi:10.1128/MCB.01612-07 (2008).

374 Katada, S. & Sassone-Corsi, P. The histone methyltransferase MLL1 permits the oscillation of circadian gene expression. *Nature structural & molecular biology* **17**, 1414-1421, doi:10.1038/nsmb.1961 (2010).

375 Williams, J. A., Su, H. S., Bernards, A., Field, J. & Sehgal, A. A circadian output in Drosophila mediated by neurofibromatosis-1 and Ras/MAPK. *Science* **293**, 2251-2256, doi:10.1126/science.1063097 (2001).

376 Zheng, X. & Sehgal, A. AKT and TOR signaling set the pace of the circadian pacemaker. *Current biology : CB* **20**, 1203-1208, doi:10.1016/j.cub.2010.05.027 (2010).

377 Di Cara, F. & King-Jones, K. The Circadian Clock Is a Key Driver of Steroid Hormone Production in Drosophila. *Current biology : CB* **26**, 2469-2477, doi:10.1016/j.cub.2016.07.004 (2016).

378 Stone, E. F. *et al.* The circadian clock protein timeless regulates phagocytosis of bacteria in Drosophila. *PLoS pathogens* **8**, e1002445, doi:10.1371/journal.ppat.1002445 (2012).

379 Benzina, S. *et al.* A kinome-targeted RNAi-based screen links FGF signaling to H2AX phosphorylation in response to radiation. *Cellular and molecular life sciences : CMLS* **72**, 3559-3573, doi:10.1007/s00018-015-1901-7 (2015).

380 Liu, Q. *et al.* Characterization of Torin2, an ATP-competitive inhibitor of mTOR, ATM, and ATR. *Cancer research* **73**, 2574-2586, doi:10.1158/0008-5472.CAN-12-1702 (2013).

381 Dai, Y. *et al.* Pharmacological inhibitors of the mitogen-activated protein kinase (MAPK) kinase/MAPK cascade interact synergistically with UCN-01 to induce mitochondrial dysfunction and apoptosis in human leukemia cells. *Cancer research* **61**, 5106-5115 (2001).

382 Dai, Y. *et al.* Interruption of the Ras/MEK/ERK signaling cascade enhances Chk1 inhibitor-induced DNA damage in vitro and in vivo in human multiple myeloma cells. *Blood* **112**, 2439-2449, doi:10.1182/blood-2008-05-159392 (2008).

383 Dai, Y. *et al.* Statins synergistically potentiate 7-hydroxystaurosporine (UCN-01) lethality in human leukemia and myeloma cells by disrupting Ras farnesylation and activation. *Blood* **109**, 4415-4423, doi:10.1182/blood-2006-09-047076 (2007).

384 Hamed, H. *et al.* Transient exposure of carcinoma cells to RAS/MEK inhibitors and UCN-01 causes cell death in vitro and in vivo. *Molecular cancer therapeutics* **7**, 616-629, doi:10.1158/1535-7163.MCT-07-2376 (2008).